# Evaluation of fibres recycled from fishing nets and methods for quantifying plastic shrinkage cracking

**imgber**

# Evaluation of fibres recycled from fishing nets and methods for quantifying plastic shrinkage cracking

Ida Maria Gieysztor Bertelsen

PhD Thesis

Department of Civil Engineering

Technical University of Denmark

Kgs. Lyngby

February, 2019

**Supervisors**

Professor Lisbeth M. Ottosen, DTU Byg, Denmark

Associate Professor Gregor Fischer, DTU Byg, Denmark

Associate Professor Gunvor Marie Kirkelund, DTU Byg, Denmark

Associate Professor Jacob Wittrup Schmidt, DTU Byg, Denmark


**Assessment Committee**

Associate Professor Marianne Tange Hasholt, DTU Byg, Denmark

Assistant Professor Eduardo Nuno Borges Pereira, University of Minho, Portugal

Professor Nina Štirmer, University of Zagreb, Croatia

# Preface

This PhD thesis compiles the findings during my research, which was conducted as an employee at the Section for Arctic Technology and Sustainable Solutions (2015-2017) and later at the Section of Materials and Durability (2018-2019), Department of Civil Engineering at the Technical University of Denmark (DTU). The main supervisor of the project was Lisbeth M. Ottosen, and my co-supervisors were Gregor Fischer, Gunvor Marie Kirkelund and Jacob Wittrup Schmidt.

The PhD study was part of the international project, Circular Ocean, which was funded through the ERDF Interreg VB Northern Periphery and Arctic (NPA) Programme 2014-2020 (Grant no. 21) and DTU Civil Engineering. The Artic Technology Centre (Artek), DTU, acted as the Greenlandic partner in the Circular Ocean project with partners from NTNU, Norway, UHI, ERI, Scotland, Cfsd, England and MacroomE, Ireland. The overall aim of the Circular Ocean project was to identify new solutions for reusing discarded fishing gear. Project website: http://www.circularocean.eu/.

Most of the experimental work, writing tasks and co-supervision of Bachelor and Master Students was carried out at the facilities at DTU Civil Engineering in Kgs. Lyngby, Denmark. Shorter research stays in Sisimiut, Greenland, were spent during the PhD project. From February to June 2018, an external research stay was accomplished at the University of British Columbia, Vancouver, Canada hosted by Assistant Professor, Cristina Zanotti.

Kgs. Lyngby, February 2019

# Acknowledgement

# Abstract

Polymeric waste materials were investigated with the aim of being recycled as fibre reinforcement in construction materials. The type of waste fibres studied was made of recycled polyethylene (R-PE) obtained by mechanical cutting of discarded fishing nets. The characterisation of the R-PE fibres showed a relatively low tensile strength and stiffness, which indicated that the fibres for example could be beneficial in controlling plastic shrinkage cracking in fresh cement-based materials. This type of cracking can be detrimental for the durability and overall lifetime of concrete structures. A well-established technique for preventing these cracks is the addition of randomly distributed fibres of synthetic materials.

When studying the formation of plastic shrinkage cracking at laboratory-scale, the use of techniques enabling objective quantification of cracking and its evolution is essential for a more comprehensive understanding of the material behaviour. However, such a detailed quantification of the degree of cracking has only been reached to a limited extent. To overcome this, an optical digital image correlation (DIC) technique was applied in the present study for monitoring the crack development. The DIC technique was subsequently used to evaluate the influence of the addition of randomly distributed R-PE and commercial polypropylene (PP) fibres.

In addition, an experimental program on the use of R-PE fibres in different types of construction materials with the aim of improving the mechanical performance was carried out for achieving a better understanding of the fibre influence.

The application of the DIC technique for quantification of plastic shrinkage cracking and an approach developed for further analysis of the DIC data by numerical post-processing revealed the following advancements:

- Data obtained by the DIC technique can display the formation of displacements and strains on a specimen surface and their continuous development over time. This provides very detailed information on the behaviour of the fresh cement-based material.

- A numerical post-processing approach for further analysis of the DIC data was developed. This enabled a quantitative measure of the degree of surface cracking presented as crack width distributions over the entire specimen surface. The approach facilitated an objective comparison of cement-based mixtures with the addition of different types of fibres.

- Generally, it was found that the DIC technique is highly efficient for monitoring shrinkage-induced deformations and cracking. Results obtained by post-processing of the DIC data showed good correlation with manual measurements using optical microscope.

The major conclusions obtained in this project regarding the performance of R-PE fibres are:

- The addition of R-PE fibres was found to have a positive influence on the formation of plastic shrinkage cracking: An almost crack free surface was achieved when adding the R-PE fibres in volume fractions of 2.0%. However, significantly lower fibre additions were required to obtain similar results with commercially available PP fibres.

- The fibre performance on the mechanical post-crack performance and ductility of different types of construction materials was found to increase with the addition of R-PE fibres. However, the effect was observed to be rather poor, especially for high-modulus materials such as cement-based mortars. Hence, the combined material-fibre performance was found to be better for low-modulus construction materials.

# Resume

Plastikaffald er undersøgt med det formål at genanvende affaldsmaterialet som fiberarmering i byggematerialer. Den specifikke affaldsfraktion består af fibre af genanvendt polyethylen (R-PE) fremstillet ved hjælp af mekanisk nedklipning. Karakteriseringen af fibre af R-PE viste en forholdsvis lav trækstyrke og stivhed, hvilket antyder, at fibrene for eksempel kan anvendes til at kontrollere plastiske svindrevner i cement-baserede materialer. Denne form for revnedannelse kan være skyld i nedsat holdbarhed af betonstrukturen samt kortere overordnet levetid. En anerkendt teknik til forebyggelse af disse revner er at tilføje fibre af syntetiske materialer til betonen.

Når man undersøger udviklingen af plastiske svindrevner på laboratorie-skala, er objektive måleteknikker til kvantitativ evaluering af revnedannelsen afgørende for en bedre forståelse af materialets opførsel over tid. En sådan detaljeret kvantificering af revnedannelsen er dog stadig kun blevet anvendt i et begrænset omfang i tidligere studier om plastisk svind. Derfor blev en optisk teknik (Digital Image Correlation (DIC)) anvendt i dette projekt til at evaluere udviklingen i revnedannelsen. DIC teknikken blev ligeledes anvendt til at evaluere indflydelsen af tilsatte fibre af R-PE- og polypropylen (PP) materialer for kontrol af plastiske svindrevner.

Derudover blev et eksperimentelt program vedr. brugen af R-PE fibre i forskellige typer byggematerialer udført for at opnå en bredere forståelse af fiberpåvirkningen på materialernes mekaniske ydeevne.

Anvendelsen af DIC-teknikken til undersøgelse af plastiske svindrevner samt en metode til at analysere DIC-data ved numerisk efterbehandling viste følgende fremskridt:

- Data fra DIC-teknikken kan anvendes til at vise dannelsen af flytninger og tøjninger på en prøveoverflade og deres udvikling over tid, hvilket giver detaljerede informationer om opførelsen af det friske cementbaserede materiale.
- En numerisk metode til efterbehandling af DIC-dataen blev udviklet, hvilket muliggør en kvantitativ analyse af graden af revnedannelse samt automatisk måling af revnevidder. Fordelingen af revnevidder over hele prøveoverfladen blev præsenteret i histogrammer. Denne fremgangsmåde fremmer en objektiv sammenligning af cementbaserede blandinger og kan bruges til at evaluere effekten af tilsætning af forskellige fibertyper.
- Generelt blev det konstateret at DIC-teknikken er yderst effektiv til at monitorere udviklingen af plastiske svindrevner og deformationer. Resultaterne for revneviddemålinger baseret på efterbehandling af DIC-data viste god korrelation med målinger i optisk mikroskop.

De væsentligste konklusioner opnået i dette projekt vedrørende effekten af R-PE fibre er:

- Tilsætningen af R-PE fibre viste sig at have en positiv indflydelse på dannelsen af plastiske svindrevner: En næsten revnefri prøveoverflade blev opnået ved tilsætning af R-PE-fibre i volumenfraktioner på 2.0%. En signifikant lavere fibertilsætning var dog nødvendig for at opnå lignende resultater med kommercielt producerede PP fibre.

- Effekten af tilsatte R-PE fibre til forskellige typer af byggematerialer viste sig at have en positiv indflydelse på materialets mekaniske opførsel efter selve materialet var brudt og den første revnedannelse er opstået. Dog var effekten relativt lille, især ift. de cement-baserede mørtelprøver med høj stivhed. Det mest effektive ift. forbedring af byggematerialers mekaniske egenskaber, var at anvende R-PE fibrene i materialer med lavere stivhed.

# Table of contents

# List of abbreviations

| | |
|---|---|
| CEB | Compressed earth blocks |
| CRR | Crack reduction ratio |
| CWD | Crack width distribution |
| DIC | Digital image correlation |
| DIP | Digital image processing |
| FEF | Fibre efficiency factor |
| FOV | Field of view |
| MCL | Maximum crack length |
| MCW | Maximum crack width |
| NPA | Northern Periphery and Arctic |
| PA | Polyamide |
| PE | Polyethylene |
| PES | Polystyrene |
| PET | Polyethylene Terephthalate |
| PP | Polypropylene |
| R-PE | Recycled polyethylene |
| REF | Reference |
| SEM | Scanning electron microscope |
| TCA | Total crack area |
| W/C | Water/cement |

# Structure of thesis

The thesis consists of two parts: A first part that gives an overview of this PhD project and a second part, which contains the appended papers (Appendix I-VII). The second part is composed of four journal papers (two published and two submitted), three conference papers and one paper which has not yet been submitted. I am the first author of all the included papers.

The structure of the first part of the thesis is as follows:

- **Chapter 1 - Introduction**: This chapter gives a general introduction to the topics of the thesis. It covers the environmental problems related to discarded fishing nets, possible applications for recycled fibres in construction materials, the use of fibres for controlling plastic shrinkage cracking in cement-based materials and the application of a digital image correlation (DIC) technique for studying the crack formation.

- **Chapter 2 - Identification of knowledge gaps:** Knowledge gaps in relation to the present study are identified and described in this chapter.

- **Chapter 3 - Research methodology**: This chapter gives a brief overview of the research methodology and the experimental techniques used during the present PhD study. The methods are more thoroughly described in Chapter 4-6 and in the appended papers.

- **Chapter 4 - R-PE fibres from fishing nets and their influence in construction materials:** Fibres of recycled polyethylene (R-PE) obtained from discarded fishing nets are characterised in this chapter. In addition, a test program on the mechanical performance of different types of construction materials for evaluation of the influence of R-PE fibres was done.

- **Chapter 5 - Plastic shrinkage cracking in cement-based materials:** A test setup for experimental testing of the formation plastic shrinkage cracking in fresh cement-based materials was designed to enable the application of a DIC technique. A numerical post-processing approach of DIC data developed for quantification of surface cracking is also presented in this chapter. Additionally, a test program on plastic shrinkage cracking and the influence of R-PE fibres was employed and evaluated on the basis of the post-procession approach.

- **Chapter 6 - Overall conclusions:** The overall conclusions from the PhD project are summarized in this final chapter of the first part of the thesis.

# 1   Introduction

As a result of the global increase in the production of plastic, there is a scarcity of space for landfilling and environmental problems due to the disposal are arising. The utilization of plastic waste materials has therefore become an attractive alternative to disposal or incineration [1]. In Europe, approximately 26 million tonnes (2015) of plastic waste are generated yearly. According to a report by the European Commission [2], ~31% ends up at landfill sites, ~39% is used for energy recovery and less than 30% is collected for recycling. In 2018, the European Commission has published a strategy for including plastics in a circular economy and the Danish Government has published a national strategy for circular economy [3]. As a consequence of the Danish national strategy [3], there will be an increased focus on circular economy in the construction sector.

The application of various forms of recycled plastic in construction materials has gained increasing attention in the recent decades [4,5]. Several studies on the topic have shown that it is possible to improve different durability-related or mechanical properties of construction materials by adding waste plastics in the forms of fibres [6–10] or aggregates to the material [11,12]. The gain is two-sided: 1) the sustainable aspects achieved by re-establishing value to a waste material; and 2) the possible material improvements and prolonged lifetime gained by adding the plastic waste material to some types of construction materials [4,5].

The international project, Circular Ocean, which this PhD project is part of, has the main aim of discovering new applications for discarded fishing gear. Artek, DTU, participated in the project as the Greenlandic partner in the Circular Ocean project. Thus, the starting point was based on the situation in Greenland, i.e. the focus was on the accessible types of waste fishing gear, which were present in large quantities at local landfill sites in towns along the Greenlandic coastline. However, it was quickly realised that the types of fishing nets and trawls used in the entire northern periphery and Arctic (NPA) region was relatively homogeneous. Hence, the encountered solutions for recycling could as well be implemented in other regions. The idea of the project was to investigate the use of recycled plastic fibres from discarded fishing nets as fibre reinforcement in construction materials, which is in accordance with the above mentioned agendas concerning circular economy. However, when incorporating various types of (waste) fractions into construction materials, there is simultaneously created a need for better waste management for construction demolition waste [13]. This will be an important topic for future studies.

## 1.1   Discarded fishing nets and recycling opportunities

Approximately 8 million tonnes of plastic enter the ocean each year [14]. Of this enormous fraction, fishing nets constitute an important part because of the amount of lost or otherwise discarded nets and their physical

size and shape. Discarded fishing nets are not only a problem when disposed into the ocean, but they are also often difficult to dispose of, costly to transport, and take up a lot of space in landfill sites. Improved waste management and recycling strategies are therefore crucial. Historically, fishing gear was made of natural materials such as hemp, cotton, sisal that would decompose relatively quickly making them less detrimental to the marine wildlife [15,16]. Nowadays, nets are typically made of synthetic materials such as polyethylene (PE), polypropylene (PP), polyester (PES) or polyamide/nylon (PA), which can persist in the marine environment for long periods [16,17]. Still, plastic degradation, which refers to the chemical change of the polymer, can drastically influence the properties of the polymer and occurs while the nets are in the marine environment or when stored at e.g. landfill sites. The main reasons for degradation under marine conditions or when stored at landfill sites are photo degradation (due to sun light exposure) [18,19], hydrolysis (reaction with water), and thermooxidative degradation (although very slow at moderate temperatures) [20]. Besides the environmental degradation mechanisms, the fishing operations and associated mechanical damage such as continuous load impacts and abrasion with the sea bed during the fishing operations, also lead to impairment of the material properties [21]. Figure 2 shows examples on the preparation (a) and use (b) of large fishing trawls.



|          (a)          |          (b)          |
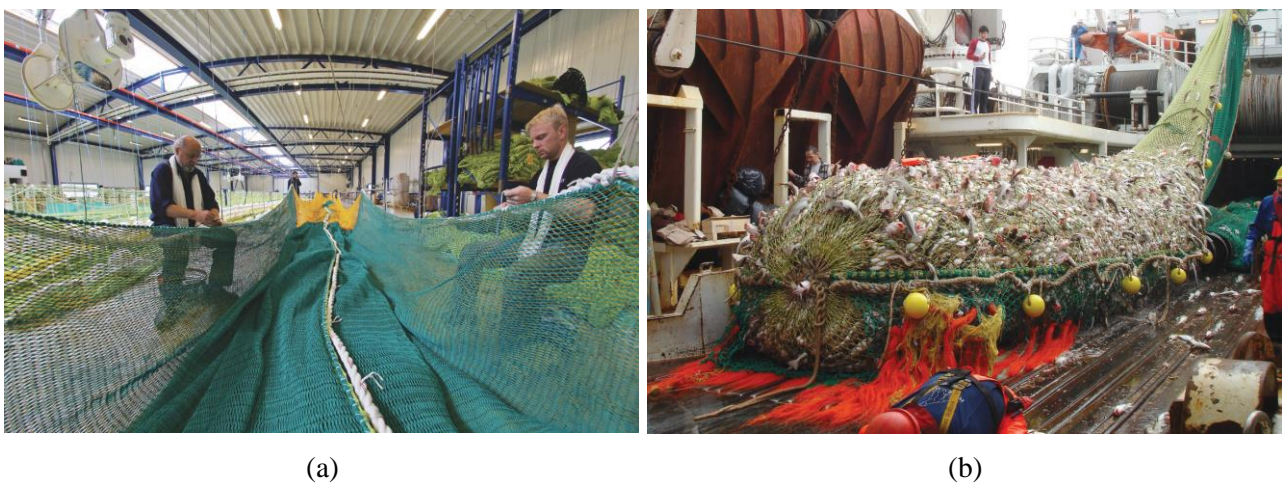
*Figure 1. a) Preparation of trawl of polyethylene (PE) materials* [22]*; b) Fishing operations* [22]*.*

Several companies have increased the focus on the potential of recycling discarded fishing nets. One of them is the Danish recycling company Plastix A/S who transforms fishing nets and other types of plastic waste fractions into high quality raw materials, and there are several companies and initiatives in smaller or larger scales globally. For an overview of some of these companies, organisations and initiatives, please see [23,24].

|              |              |
| :----------: | :----------: |
|     (a)      |     (b)      |

*Figure 2. a) Discarded fishing nets piled up at the landfill site in Sisimiut, Greenland; b) Monofilament R-PE fibres from discarded fishing nets processed by a mechanical cutting operation by Plastix A/S*

Figure 2 illustrates the storage of fishing nets and trawls at a landfill site in Sisimiut, Greenland (a), and fibres of recycled polyethylene (R-PE) obtained from discarded fishing nets by mechanical cutting operations at Plastix A/S (b). The fishing net lines often consist of monofilament fibres with a shape corresponding to those used as synthetic fibre reinforcement in construction materials such as concrete. This observation led to the idea of investigating the use of fibres obtained from discarded fishing nets as fibre reinforcement with the aim of identifying possible reuse options.

## 1.2    The use of synthetic fibres in cement-based materials

The addition of synthetic plastic fibres in cement-based materials is a commonly used technique for improving different material properties. These include enhancements in post-crack performance by increased ductility, impact resistance and other mechanical properties of quasi-brittle materials [25,26], for mitigating shrinkage cracking in cement-based materials [27,28], and for improving the fire safety by preventing spalling in concrete structures such as tunnel linings under fire exposure [29,30]. Specific applications for concrete reinforced with synthetic fibres are e.g. in the shotcrete industries, floor slabs, slabs on grade, tunnel linings and other underground structures [31,32]. Some of the advantages are the combined effect for possible applications, the reduced labour time and ease of construction [33]. Commonly, for load-bearing applications, plastic fibres are added together with traditional steel reinforcement [34,35].

Depending on the specific application of the material, the fibre characteristics play a significant role. Some of the relevant fibre properties include the geometry and shape, chemical/geometrical bonding to the matrix, mechanical properties, and thermal properties. Various types of synthetic fibres are used in cement-based materials to mitigate cracking in structures susceptible to large plastic shrinkage deformations during very early-age setting or drying [31,36]. Since plastic shrinkage cracking occur while the material fresh and has a

low strength and stiffness, fibres of low-modulus materials, such as fine polypropylene (PP) fibres, added in low volume fractions of ~0.1-0.2%, have been found to effectively reduce the formation of this type of cracking [27,28]. The fibre effects on the formation of plastic shrinkage in cement-based materials will be more thoroughly discussed in Section 1.3.

Quasi-brittle cement-based materials have brittle failure modes when exposed to tensile stress. By adding randomly distributed fibres, the composite material can achieve significant improvements in the post-crack performance. Inside the quasi-brittle matrix, the fibres have the ability to absorb energy beyond matrix cracking. Hence, improving the ductility of the composite material and the resistance to crack propagation [29,34]. After the brittle material fails, the fibres can bridge the cracks by transferring tensile stresses from the matrix to the fibres, and provide resistance to the crack propagation [31]. Depending on the fibre properties, there are different ways for stress transfer from the matrix to fibres, and failure modes for the fibres inside the matrix can occur. These modes are schematically demonstrated in Figure 3 [31,36].
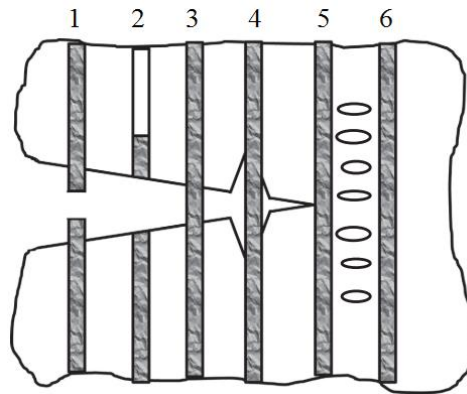


*Figure 3. Failure mechanisms in fibre reinforced concrete: (1) Fibre failure; (2) fibre pull-out; (3) fibre bridging; (4) fibre-to-matrix debonding; (5) fibre preventing crack propagation; (6) matrix micro cracking. Figure from Yin et al.* [31,36]

Besides the addition of fibres to cement-based materials, similar fibre types have also been used to improve the performance of other types of construction materials such as gypsum plaster, bitumen, earth-based materials (adobe, CEB) etc. [37–39].

### 1.2.1 Recycled fibres of plastic waste

The use of different fractions of plastic waste materials as fibre reinforcement in both cement-based materials and other types of construction materials has already been investigated. The application has gained recognition in the construction industry due to their broad applicability, low price and sustainability aspects [1,4,5]. Several studies have focused on the performance of plastic waste fibres for various applications; e.g. for mitigating plastic shrinkage cracking [6–8,40–42] or for improving the mechanical performance in

cement-based materials [9,10,43–45] and in gypsum-based materials [46,47]. These recent studies have shown that several types of plastic waste materials can be profitably employed to create low-cost reinforcement techniques for applications similarly to commercial fibres. Two previous studies have found that the addition of nylon fibres cut down from discarded fishing nets can improve the post-crack performance of cement-based mortars [10,43]. Besides using fibres from discarded fishing nets, other researchers suggested to produce fibres from waste fractions such as bottles of polyethylene terephthalate (PET) [6,8,9,44,48,49], car tyres [41,50,51], textile carpets [52,53], driving belts in cars [54] and different types of mixed industrial or post-consumer waste [7,42,55,56]. Fibres obtained from fractions of plastic waste can be processed by either mechanical recycling such as mechanical cutting or shredding operations, or by thermal reprocessing, where the material is heated so that new products can be processed by e.g. extrusion [1]. Although some recycled fibres have been produced by thermal reprocessing [6,7,40], it is considered more energy-efficient to produce them by mechanical operations [8–10,43–45].

Some of the benefits of using recycled fibres in construction materials are:
- The improvements of some material properties to which the fibres are added (e.g. mechanical performance, durability, design).
- The use of local waste fractions as resources can reduce the need for production and transportation of fibres of virgin materials, which would probably also lead to reduced costs of the final product.
- The reuse or recycling of a waste material could potentially solve disposal problems.

## 1.3 Plastic shrinkage cracking in cement-based materials and the influence of fibre reinforcement

Concrete structures with a large surface area to volume ratio, such as slabs bridge decks, industrial floors, tunnel linings and thin concrete surface repairs, can commonly be susceptible to plastic shrinkage cracking [27]. A typical crack pattern induced by plastic shrinkage deformations in a concrete slab can be seen in Figure 4a [57]. These types of cracks are not only aesthetically undesirable, but can also affect the long-term durability, especially considering steel reinforced concrete structures [58]. The cracks may propagate further during drying and allow the ingress of aggressive agents such as water and chlorides leading to corrosion of the steel rebars and premature deterioration of the structure [28]. Plastic shrinkage in cement-based materials occurs while the material is still in a plastic state and is due to the volumetric contraction in the first few hours after casting [58]. A well-established technique for mitigating the formation of plastic shrinkage cracking is the addition of randomly distributed fibres [27].

|  (a)  |  (b)  |
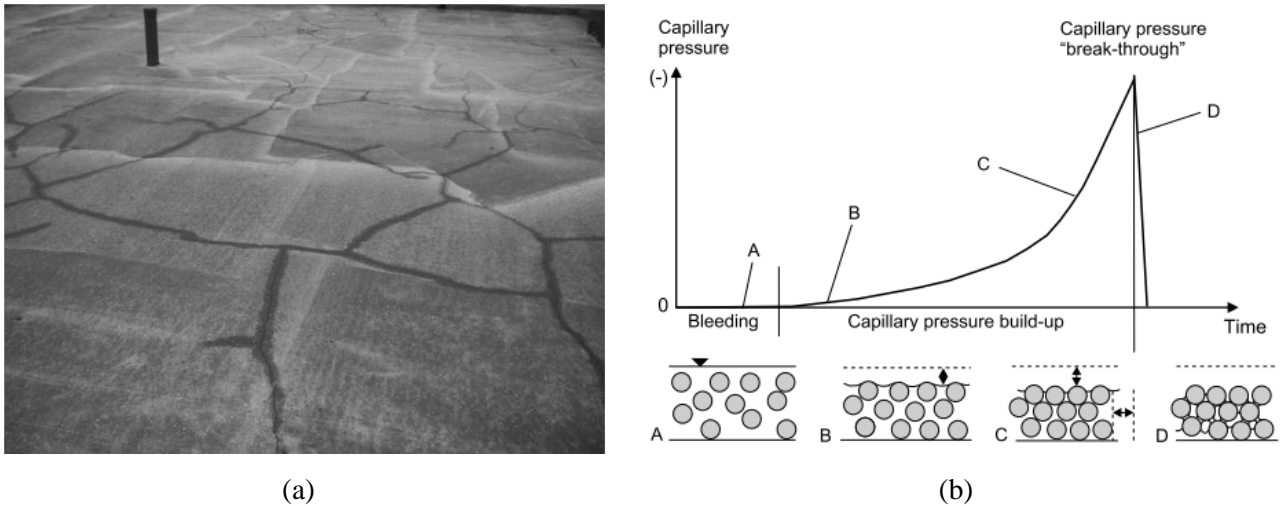
*Figure 4. a) Plastic shrinkage cracking in concrete slab 4 h after casting; b) Capillary pressure build-up. Figures from Slowik et al.* [57]

The process of plastic shrinkage cracking is schematically illustrated in Figure 4b, and can briefly be described as the increase in capillary pressure between the solid particles, which occurs while the specimen surface dries out [57]. When the capillary pressure exceeds the relatively low tensile strength of the fresh concrete, cracking can start to occur.

Unrestrained plastic shrinkage does normally not lead to any crack formation because the material is allowed to deform freely. However, concrete structures are almost always restrained either internally or externally, with the restraints arising from e.g. steel rebars, large aggregates, an underlying surface, support conditions, non-uniform drying or differential shrinkage [25,58,59]. The formation of these early-age cracks is also highly dependent on the environmental conditions during the first few hours after casting, the material composition, the geometry of the structure and the on-site building practices [60]. Specific environmental conditions such as low relative humidity, elevated temperatures and exposure to high wind flows, which induce a high rate of evaporation of mixing water from the surface, are known to make the cement-based material more susceptible to plastic shrinkage cracking [61]. According to Sayahi [60], plastic shrinkage cracking is not only a challenge in southern countries with warmer and dryer climates, but also in Scandinavia as a consequence of new types of concretes, which shrink more than traditional concretes.

## 1.3.1    Fibre mechanisms in controlling plastic shrinkage cracking

The addition of fibres to a cement-based matrix is a widely accepted and studied technique for mitigating plastic shrinkage cracking [25]. The role of the fibres is explained more thoroughly in the literature review presented in Appendix I. The fibres are reported not to eliminate crack formation, but to disperse the cracks so that many micro cracks appear instead of fewer larger ones [59]. Thus, the fibres mitigate the propagation of micro cracks from developing into larger cracks by creating bridging forces across the cracks and

improving the strain capacity of the fresh mixture [6,25,59,62]. These bridging forces are dependent on several fibre characteristics, e.g. the fibre-to-matrix bonding, the stiffness and geometrical parameters. Depending on the fibre characteristics, some types of fibres have also been shown to increase the early-age tensile strength of the material [63], thereby lowering the possibilities for stresses exceeding the low tensile strength of the plastic material [58]. Fibres added to fresh concrete have also been found to reduce segregation of coarser aggregates, which therefore tend to remain closer to the surface and ease plastic settlement [59,62].

### 1.3.2  Performance of macro fibres for mitigating plastic shrinkage cracking

The performance of fibres for mitigating plastic shrinkage cracking is highly related to the fibre characteristics. Micro fibres (d ≤ 100 µm per definition by Yin et al. [31]) are generally found to perform better than coarser fibres with all other parameters being the same (length, volume fraction, material, shape etc.). However, several studies on the use of macro fibres (d > 100 µm) of virgin or waste materials have also shown promising results. Because of the relatively coarse nature of the R-PE fibres investigated in this PhD project (d = 280 ± 15 µm, L = 15 ± 9 mm), this section focuses on the performance of fibres with similar coarse diameter (macro fibres) investigated in other studies. Table 1 gives an overview of selected studies on plastic shrinkage cracking in cement-based materials and the influence of the addition of macro fibres of virgin or recycled synthetic materials. The performance of fibres or other preventative measures is often measured by the crack reduction ratio (CRR) [64] based on basic crack parameters such as the total crack area (TCA) or the maximum crack width (MCW). The CRR is calculated as the ratio of a fibre reinforced specimen and the control specimen:

$$CRR = \left(1 - \frac{TCA_{fib}}{TCA_{ctr}}\right) \times 100\% \qquad \text{(Eq. 1)}$$

*Table 1. Selected studies investigating the influence of synthetic macro fibres on plastic shrinkage cracking.*

| Ref. | Fibre type and processing | Short summary and major findings |
|---|---|---|
| Kim et al. [6] | Fibres of different shapes and geometries (straight, crimped, and embossed) were obtained by thermal reprocessing of waste PET bottles.<br>d = 0.2-0.5 x 1.0-1.3 mm<br>L = 50 mm<br>Vol% = 0.1-1.0% | Restrained plastic shrinkage cracking of cement-based mortars was studied on thin slab-like specimens with edge restraints in accordance with the Kraai method [65]. No information on the crack measuring technique.<br>The deformed fibre shapes were especially beneficial in controlling plastic shrinkage cracking. A CRR for the total crack area of ~90% was achieved with fibre additions of 0.5% for all fibre types. |
| Borg et al. [8] | Fibres of straight and deformed shapes were obtained by mechanical shredding of waste PET bottles.<br>d = 0.7-0.9 mm<br>L = 30-50 mm<br>Vol% = 0.5-1.5% (ASTM C1579) | Restrained plastic shrinkage of concrete was studied using the ASTM C1579 method [64]. Cracks were measured using a DIP technique. The deformed fibres performed slightly better than straight fibres and longer fibres performed better than shorter fibres. A CRR for the maximum crack width of 70% was obtained for long (L = 50 mm), deformed fibres added in 1.5%.<br><br>Restrained plastic shrinkage was studied on mortars using the Kraai method |

| | | |
|---|---|---|
| | Vol% = 0.25-1.0% (Kraai panel) | [65]. A CRR for total crack area of ~90% was obtained for the addition of 1.0% of long, deformed fibres. App. similar results were obtained for straight and deformed fibres as well as for longer and shorter fibres. |
| Pešic, et al. [7] | Fibres with straight shape were obtained by extrusion of recycled HDPE material from mixed post-consumer waste.<br>d = 0.25-0.4 mm<br>L = 23-30 mm<br>Vol% = 0.4-1.25% | Restrained plastic shrinkage of concrete was studied using the ASTM C1579 method [64]. Cracks were measured using a DIP technique.<br>A CRR for the average crack width of 75-84% was obtained with the addition of 1.25% of fibres. No clear indications on whether shorter and finer fibres performed better than longer and coarser fibres. |
| Al-Tulaian et al. [40] | Fibres with straight shapes were obtained by thermal reprocessing of plastic waste materials into thin sheets, of which fibres were cut.<br>b x t = 0.5 x 2.0 mm<br>L = 20-50 mm<br>Vol% = 0.5-1.5% | Restrained plastic shrinkage of mortar was studied using the Kraai method [65]. Cracks were measured using microscopic measurements.<br>A CRR for the total crack area of 100% was obtained with the addition of 1.5% of longer fibres (L = 50 mm). The specimens with the addition of shorter fibres (L = 20 mm) in similar volume fractions obtained a CRR of 80%. |
| Najm & Balaguru [66] | Polyolefin fibres with a straight shape of virgin materials.<br>d = 0.15-0.64 mm<br>L = 25.4-50.8 mm<br>Vol% = 0.5-3.0% | Restrained plastic shrinkage of mortar was studied using the Kraai method [65]. No information on the crack measuring technique.<br>The finest fibres (d = 0.15 mm) with the highest aspect ratio were able to completely reduce the surface cracking when added in 1.0%. It was necessary with fibre additions of 2.0% for obtaining similar results for other fibre diameters. |
| Banthia & Yan [67] | Polyolefin fibres with a straight shape of virgin materials (comparison with PP and steel fibres)<br>d = 0.15-0.63 mm<br>L = 19-50 mm<br>Vol% = 0.1-0.7% | Restrained plastic shrinkage was studied on restrained mortar overlays cast on top of concrete substrates with a rough surface. Cracks were measured using microscopic measurements.<br>The performance of fibres with similar diameter was found not to be influenced by an increase in fibre length. A CRR for the total crack area of 90% was obtained for the fibres with the finest diameter (d = 0.15 mm) when added in 0.5%. The coarsest fibres (d = 0.63 mm) showed the worst performance, with a CRR of ~80% when added in 0.7%. |
| Mazzoli et al. [68] | PP, PVA and PET fibres of virgin materials in various geometries, shapes and stiffness's.<br>d = 0.43-0.82 mm<br>L = 40-54 mm<br>Vol% = 0.3% | Restrained plastic shrinkage of mortar was studied using the Kraai method [65]. Cracks were measured using microscopic measurements and a DIP technique.<br>The fibres with the highest aspect ratio (PP and PET fibres) showed the best performance with a CRR for the total crack area of ~80%. However, because of large variations in dimensions, material and stiffness of the studied fibres, no clear conclusions could be drawn from this study. |

The results given in Table 1 illustrate that most of the studied macro fibres can be highly effective for mitigating plastic shrinkage cracking. All the recycled fibres besides the fibres obtained from waste PET bottles studied by Borg et al. [8], were thermally reprocessed, which enabled production of fibres with the desired shapes and geometries. To the downside, the thermal reprocessing is more energy consuming than the pure mechanical processing. This observation was an encouragement for studying the R-PE fibres as preventative measure for plastic shrinkage cracking, since these were produced solely by mechanical cutting.

### 1.3.3 Detection and quantification of shrinkage cracking

In order to study the formation of shrinkage cracking at laboratory-scale conditions, quantitative crack measuring techniques are essential for obtaining objective and comparative measures of the degree of cracking. This can be challenging because of the unknown time of crack initiation, location, growth rate, and

the often scattered nature of the crack pattern. This is especially the case when considering plastic shrinkage cracking, because the crack initiation and growth can happen rapidly [67]. The experimental evaluation of plastic shrinkage cracking is often done by visual inspection and monitoring of the specimens and subsequent measurement of crack parameters such as crack width, length, and area with the use of either manual measuring techniques or more sophisticated image-based techniques. Figure 5 shows a typical scattered crack pattern obtained by the test method initially proposed by Kraai in 1985 [65], where a thin test specimen is restrained along the perimeter of the slab. The scattered nature of such crack patterns is common for specimens exposed to evenly distributed restraining conditions as by Kraai [65] and specimens with other types of bottom-restraints [27,28,69–71]. Obviously, this type of crack pattern is challenging to instrument and objectively quantify with the use of manual measuring techniques, which rely on various operator-dependent factors such as experience and expertise and is therefore prone to human error [72]. Hence, more advanced techniques would be preferable for the quantification of such crack patterns.



*Figure 5. Typical scattered crack pattern obtained for the Kraai panels (15 x 600 x 900 mm³ with perimeter restraints). Figure from Lee & Won* [73]

More advanced image-based techniques, such as digital image processing (DIP) [68,72,74–78] and digital image correlation (DIC) [71,79–87], have recently been successfully applied for shrinkage-induced crack detection. These are non-contact optical techniques and work by capturing high-resolution images of the cracked surface. This makes it possible to track the evolution in crack growth in a series of pictures taken almost directly after casting. A schematic presentation of a test setup using DIC is shown in Figure 6. Despite the manual application of a high-contrast surface pattern, the DIC technique does not rely on operator-dependent factors. Hence, their accuracy simply depends on the setup, e.g. the resolution of the images, the constant light source and the quality of the investigated surface [88]. The DIC technique works by tracking surface deformations based on a reference (undeformed) stage and a deformed stage as shown in Figure 7. A high-contrast surface pattern should be applied on the tested specimen surface for enabling the

computation of these displacement fields. Therefore, it is especially valued for monitoring crack formations, because the technique enables a more detailed crack characterization and understanding of the early-age behaviour of the specimen surface [89,90].
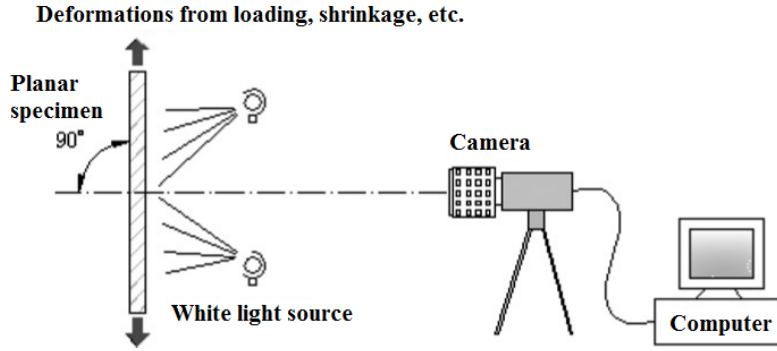


*Figure 6. Schematic illustration of a 2D-DIC test setup. Figure from Pan et al.* [89]
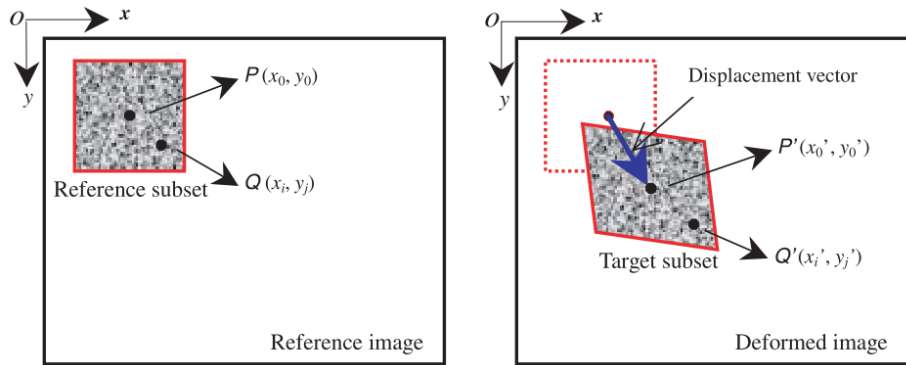


*Figure 7. Basic principles of DIC showing a reference (undeformed) subset element and the target (deformed) subset. Figure from Pan et al.* [89]

The DIC technique has been widely accepted as an effective tool for studying surface deformations in hardened cement-based materials [83,91–94]. However, it has only been used in a few studies on early-age cement-based materials because of difficulties related to the creation of a high-contrast surface pattern when the material still is plastic and possibly has bleeding water on the surface [79,95]. The quality of the high-contrast surface pattern is known to be closely related to the correlation precision of the image. The surface pattern must allow the specimens to evaporate freely, without sealing the surface, which would otherwise slow down the shrinkage deformations. The process of creating this pattern is therefore essential for the quality of the DIC post-processing [96,97] and is usually achieved by applying a white-coloured base layer and a black speckle pattern using spray bottles or air brushes [97]. Other studies on the topic are presented in Table 2 and have used different strategies to overcome these challenges. The table gives an overview of the

selected studies and contains a brief description of the test method, material and type of DIC method (2D or 3D-DIC) and strategies used to quantify displacements or cracks on the surface.

*Table 2. Selected studies applying DIC for detection/quantification of shrinkage-induced cracks*

| Ref. | Description of method | High-contrast surface pattern | Quantification method |
|---|---|---|---|
| Zhao et al. [71,81] | Study on restrained plastic shrinkage in cement paste cast on rough underlay (sand paper) using DIP and 2D-DIC for crack detection and quantification. The influence of environmental conditions, restraint roughness and w/c-ratio was studied. | A pattern was applied using white and black spray paint, which caused a lower evaporation rate in the first 3 h, whereupon it was higher than the unpainted surface. | The cracked area was computed using DIP based on a Matlab script counting cracked pixels on the specimen surface. The 2D-DIC technique was used for making contour plots showing the formation of surface strain. |
| Dzaye et al. [85] | Study on free plastic shrinkage in cement paste from 15 min after casting using 3D-DIC. | A pattern was applied using white and black spray paint, which caused a significant decrease in the evaporation rate to only half of that for the un-painted specimen. | Vertical settlement was quantitatively studied based on 3D-DIC data and compared with traditional LVDT measurements. |
| Dzaye et al. [95,98] | Studies on free plastic shrinkage in cement paste similar to [85]. Different materials were used for the high-contrast surface pattern | A pattern was applied using aluminium oxide for the white base layer. Carbon particles for the black speckles were distributed by sieving. The pattern was reported not to be influenced by the presence of bleed water. No information on the water evaporation rate. | Vertical settlement was quantitatively studied based on 3D-DIC data and compared with traditional LVDT measurements. |
| Ghourchian et al. [79,99] | Studies on free and restrained shrinkage in concrete using 3D-DIC. The ASTM C1579 method was applied for the restrained shrinkage test. Various types of cements were tested. | Small wire meshes were placed on the specimen surface on each side of the central stress riser to track the local displacements. The wire meshes are not hindering the evaporation rate and allows bleed water on the surface. | Crack widths and vertical and horizontal strains were computed based on 3D-DIC data and their formation was illustrated from app. 2-6 h after casting. |
| Messan et al. [82] | Study on free plastic shrinkage using 2D-DIC from 27 min after casting; and on restrained plastic shrinkage using the ring test. The influence of fibres (glass, EVA, cellulose) was investigated. | No information on the application of a pattern, but it was reported that bleeding was not significant enough to modify the optical measurement. | Formation of free shrinkage strain on the specimen surface was measured using virtual strain gauges by 2D-DIC over time (24 h). The standard deviation of the variation in surface strain was also analysed. |
| Némoz-Gaillard et al. [80] | Study on plastic shrinkage cracking using 2D-DIC in concrete used for pavements from 9 min after casting. The influence of fibres (AR-glass and PP), size of aggregates, mix proportions, and w/c-ratio was studied. | No information on the application of a pattern. | Displacement fields were calculated using DIC and the strain fields were derived from these. A section view shows the surface strain and the location of a surface crack. |
| Mauroux et al.; Benboudjema et al. [83,100] | Studies on drying shrinkage (from 1d to 11 d after casting) on the surface and at the periphery on thin free and restrained mortar overlays on concrete substrates | A pattern was applied using spray paint. No information on the paints influence on the water evaporation rate. | Surface strain was derived from the surface displacement obtained by DIC data. Quantification of damaged (cracked) areas was calculated as the sum of surface strain above a defined |

| using 2D-DIC. | | strain threshold limit. Crack widths along the periphery were measured from displacement gaps along sections. |
|---|---|---|

From Table 2 it is seen that the general knowledge gaps in the literature are related to the identification of appropriate methods for creation of the high-contrast speckle pattern without influencing the water evaporation rate from the freshly poured cement-based material. Also, there is a limited use of the DIC data to obtain quantitative measures of the degree of surface cracking on the specimen surface.

# 2   Knowledge gaps

Based on Chapter 1, the knowledge gaps (A-C) to be in focus of this thesis were identified.

A. Fishing nets and trawls used today are often made of PE materials consisting of several monofilament fibres, which can be processed into fibres by mechanical cutting operations. These fibres from discarded fishing nets could be used as fibre reinforcement in construction materials. To be able to evaluate this reuse option there is a need for testing and evaluating the material properties of R-PE fibres from discarded fishing nets and for investigating their performance in different types of construction materials.

B. Various types of fibres with large variations in fibres characteristics have been investigated in the literature for mitigation of plastic shrinkage cracking in fresh cement-based materials. However, there seems not to be an exact agreement on which fibre properties are most important for controlling the formation of plastic shrinkage cracking. There is also a lack of standardised test methods for evaluation and quantification of the degree of surface cracking.

C. The evaluation of plastic shrinkage cracking in cement-based materials is commonly based on basic crack parameters, which do not provide very detailed information on the crack formation and propagation. There is a need for more sophisticated methods for detailed crack quantification, which can be obtained by applying the digital image correlation (DIC) technique. The DIC technique requires a high-contrast surface pattern to track surface displacements, which remains a challenge when studying wet surfaces that should be allowed to evaporate freely. The DIC data used for crack detection has still not been post-processed for automated crack quantification, but has mainly been used for mapping surface strain fields or for localized crack measurements.

In the present PhD study, these knowledge gaps were investigated and filled out. Chapters 3-5 in this first part of the thesis give an overview of the research methodology and the major research findings. Table 3 shows the list of the appended papers constituting the second part of the thesis and their relation to the relevant knowledge gaps.

# 3    Research methodology

The overall research methodology is presented in this chapter and is illustrated in Figure 8. For detailed information on the methodology used in the individual studies, please see the relevant appendices, which are listed in Table 3 with information on the title, the aim and the relation to the respective knowledge gap.
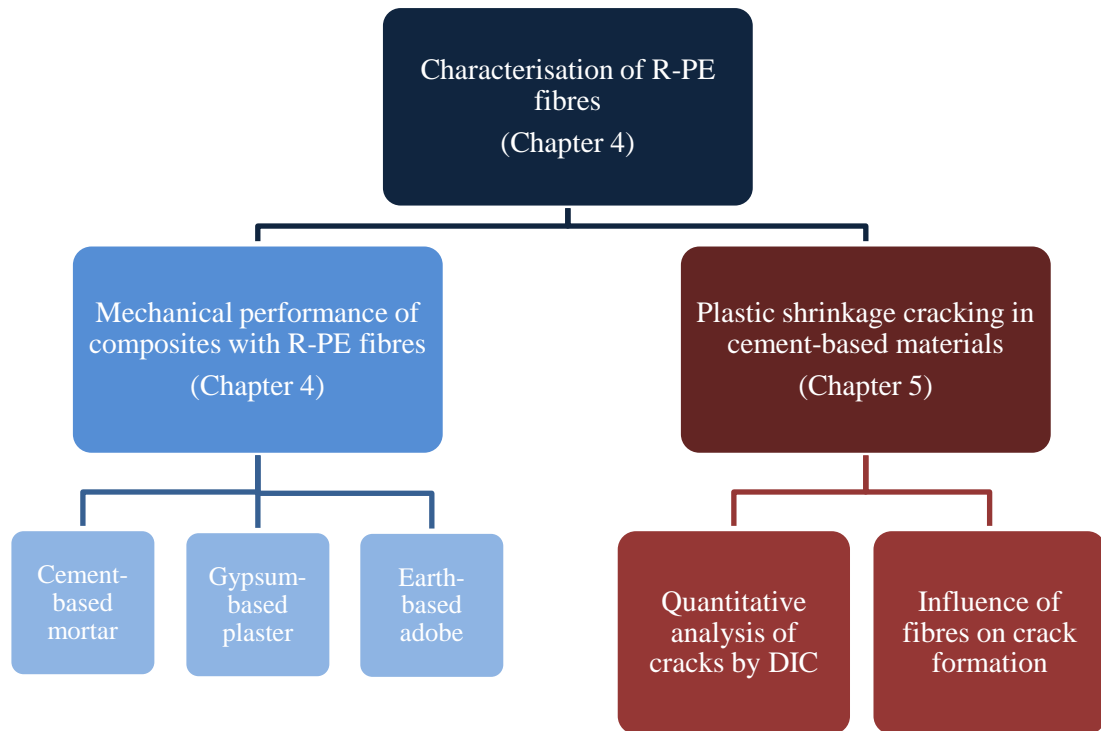


*Figure 8. Illustration of the overall research methodology*

The R-PE fibres from discarded fishing nets are included in most parts of the experimental investigations. The first part of the experimental work was to characterise these fibres and their use as fibre reinforcement in different types of construction materials in order to explore suitable applications for the fibres. This characterisation indicated that the R-PE fibres could be beneficial as a preventative measure in fresh cement-based materials susceptible to plastic shrinkage cracking or for improving the post-crack performance of low-modulus materials.

Broadly, the experimental program on the use of R-PE fibres can be divided into the following branches: 1) R-PE fibre characterisation, 2) for improving the mechanical (post-crack) performance in cement-based, gypsum-based and earth-based materials for a broader screening of possible applications for the fibres, and 3) investigations on the use of R-PE fibres for mitigating plastic shrinkage cracking in fresh cement-based materials and the application of a 2D-DIC system.

*Table 3. List of appendices*

| Appendix | Title | Aim | Knowledge gap |
|---|---|---|---|
| I | Influence of fibre characteristics on plastic shrinkage cracking in cement-based materials: A review | A review study was carried out to investigate the up to date literature on experimental testing of plastic shrinkage cracking in cement-based materials. The tendencies for correlations between fibre characteristics and the performance in mitigating plastic shrinkage cracking were discovered. | B |
| II | Quantification of plastic shrinkage cracking in mortars using digital image correlation | This paper present the results obtained from applying the DIC technique for detection of plastic shrinkage deformation/cracking of free and restrained cement-based mortar overlays. A post-processing procedure was developed for quantifying the degree of cracking. | B, C |
| III | Quantitative analysis of the influence of synthetic fibres on plastic shrinkage cracking using digital image correlation | The influence of R-PE and PP fibres on the formation of plastic shrinkage deformations and cracking in cement-based materials was investigated using the DIC technique described in Appendix II. The results are presented in this paper. | A, B, C |
| IV | Influence of recycled fibre reinforcement on plastic shrinkage cracking of cement-based composites | The influence of R-PE fibres on restrained shrinkage cracking and mechanical performance of cement-based materials was investigated in this conference paper. | A, B, C |
| V | Recycling of waste polyethylene fishing nets as fibre reinforcement in gypsum-based composites | The aim of this paper was to present a characterisation of the R-PE fibres and to test their influence on the mechanical performance of small-scale gypsum-based specimens. | A |
| VI | Adobe bricks of Greenlandic fine-grained rock material | The work investigates the opportunities for producing unfired adobe bricks of Greenlandic fine-grained rock material and gravel. The raw material for the adobes was characterised and R-PE fibres were added as reinforcement to improve the mechanical performance and reducing the drying shrinkage. | A |
| VII | Applications for recycled polyethylene fibres from discarded fishing nets in cement-based materials | This paper presents a characterisation of R-PE fibres when used as fibre reinforcement in cement-based materials. The influence of the addition of R-PE fibres on the mechanical performance of small-scale cement-based mortar specimens was tested. | A |

# 4    R-PE fibres from fishing nets and their influence in construction materials

This chapter presents the characterisation of recycled polyethylene (R-PE) fibres obtained from discarded fishing nets. Subsequently, their use in different types of construction materials was evaluated by mechanical testing.

## 4.1    Characterisation of R-PE fibres

In collaboration with other project partners from the Circular Ocean project, a feasibility study was carried out to map relevant information about the fishing gear being used in the northern periphery and arctic (NPA) region. The study included investigations on the fishing nets with respect to types and materials, the type of fishing operation, waste management of discarded fishing gear and relevant recycling options. Based on this study, it was evident that the most commonly used material for the production of fishing nets was PE of different qualities and mechanical properties.

The R-PE fibres investigated throughout this PhD study were collected by a Danish recycling company, Plastix A/S, at national and international harbours. After being collected, the nets were transported to the recycling plant, sorted into the respective material fractions, pre-washed, mechanically cut into shorter fibres and finally reprocessed to produce new plastic pellets of the recycled material. The R-PE fibres investigated in the present study were obtained prior to the final reprocessing. Hence, they were only pre-washed and processed by mechanical cutting operations. As a result of the variations in the collected net materials, the ways the nets had been used and stored and the mechanical processing, fluctuations in the properties of the R-PE fibres were expected. The fibre characterisation included analysis of the geometrical properties, shape and morphology, mechanical properties, thermal properties and alkali-resistance. These tests were performed on fibres from discarded fishing nets as well as from corresponding new nets to examine the degree of deterioration of the used nets.

Measurements of the fibre diameter, length and morphology were based on the R-PE samples provided by Plastix A/S, which were obtained by a mechanical cutting operation. However, the provided R-PE fibres were not long enough for performing tensile tests. So to get an indication of the variations in the mechanical properties of the R-PE fibres, fibres obtained from selected types of PE fishing nets were tested with respect to tensile strength and stiffness. Three types of fishing nets commonly used in the NPA region were selected for the mechanical testing (Braided Polyethylene, Euroline and Euroline Premium from Euronete). These net types were chosen on the basis of their mechanical properties, which were expected to represent the range of fibres present in the R-PE samples. Mechanical tensile tests were performed on fibres extracted from new nets and discarded nets of the corresponding type. For more details, see Appendices V and VII.

### 4.1.1 Results on the R-PE fibre characterisation

The characterisation of R-PE fibres are presented in this section. The importance of different fibre properties depends on the specific application. Table 4 shows relevant fibre properties for the R-PE fibres obtained by experimental testing.

*Table 4. Properties of R-PE fibres. Density, length and diameter were measured on fibres in the R-PE samples, whereas the tensile strength and stiffness were measured on three types of selected fishing nets commonly used in the NPA region (Braided Polyethylene, Euroline and Euroline Premium from Euronete).*

|  | Density | Length | Diameter | Tensile strength | Stiffness |
|---|---|---|---|---|---|
|  | $\rho$ [g/cm$^3$] | L [mm] | d [µm] | $\sigma_t$ [MPa] | E [GPa] |
| R-PE | ~0.95 | 15 ± 9 (1-65) | 280 ± 30 | 380-450 | 1.0-2.0 |

Despite the R-PE fibres being reprocessed from different types of PE fishing nets, the diameter (280 ± 30 µm) was found to be very consistent. As a result of the mechanical cutting operation, the fibre length varied significantly and was found to be 15 ± 9 mm. From the SEM images (example shown in Figure 9), it was observed that all fibres had an approximate circular cross section, a relatively smooth surface and a straight shape. However, as a result of being used and later stored for an unknown period of time under different environmental conditions, the surface of the recycled fibres was less smooth and more damaged than that of a new fibre. The alkali-resistance of the PE fibres was evaluated to simulate the fibres' deterioration in a highly alkaline environment such as cement-based materials. This was based on SEM images and direct tensile tests of fibres immersed in a highly alkaline solution of 1M NaOH at 50 °C for up to 28 days. See Figure 9.



| (a) New - Unconditioned | (b) Recycled - Unconditioned | (c) Recycled – 7 days in 1M NaOH | (d) Recycled – 28 days in 1M NaOH |
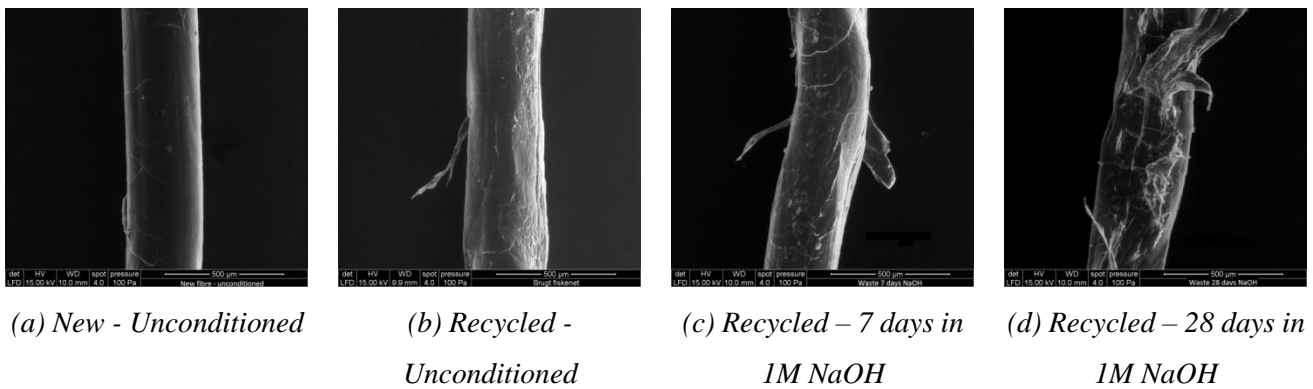
*Figure 9. SEM images (300x) of unconditioned new (a) and recycled (b) fibres from fishing nets of the type "Braided Polyethylene" immersed in a 1M NaOH solution at 50 °C for 7 (c) and 28 days (d), respectively. FOV = 1.27 mm. Figures adapted from Appendix VII*

From the SEM images, it is observed that the recycled fibres were influenced by the alkaline solution by having loose parts on the fibre surface. However, no reduction in cross section area was seen during the 28 days of exposure. The alkali-resistance of fibres is important for the overall durability of the material when added to cement-based materials. If the fibres deteriorate and leave empty channels inside the material, it can be detrimental for the durability, since the channels may enhance the ingress of aggressive agents leading to corrosion of the steel reinforcement.

Regarding the mechanical performance of the fibres, it was found for all the tested fibre types, that fibres extracted from new (N) fishing nets had a higher tensile strength and stiffness than fibres from corresponding recycled (R) fishing nets. Examples of the stress-strain behaviour of N-PE and R-PE fibres are illustrated in Figure 10 and show an almost linear behaviour until failure is observed. All fibres followed approximately the same trend. It was also found that the exposure of the fibres to a highly alkaline environment did not have any significant influence on the tensile behaviour. This is in agreement with Zheng & Feldman and Yin et al. who both reported a good alkali-resistance of polyethylene fibres [31,101].
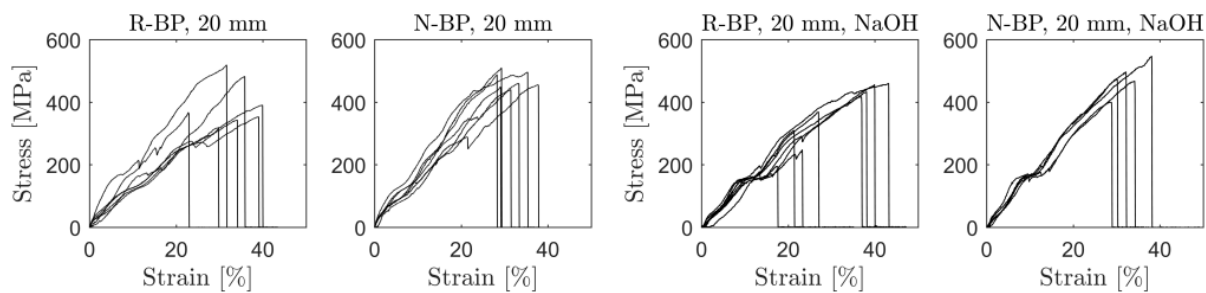


*Figure 10. Tensile stress-strain behaviour of unconditioned and alkali-cured PE fibres from recycled (R) and new (N) fishing nets of the type "Braided Polyethylene" (BP) from Euronete. Gauge lengths of 20 mm. Figure from Appendix VII.*

The mechanical properties are in the same range as other low-modulus fibre types used in construction materials, e.g. PP fibres. PP fibres are reported to typically have a poor adhesive bond to the matrix and a tensile strength and stiffness around 150-800 MPa and 0.5-10 GPa, respectively [29,32,101]. PE fibres have been observed to cover a significantly wider range of mechanical properties, because they can be produced with very different molecular weights and crystallinity. This has resulted in tensile strengths and stiffness's ranging from 200-2585 MPa and 2-117 GPa, respectively [28,29,101] for fibres used in construction materials. The results on the mechanical performance of the R-PE fibres indicate that they are in the lower range of PE fibres used in cement-based materials or other types of construction materials and that the their mechanical properties are very similar to that of PP fibres.

## 4.2 Fibre influence on the mechanical performance of construction materials

The use of R-PE fibres was investigated with the aim of obtaining a broad overview of the fibre influence of different types of construction materials with very different intrinsic mechanical properties. The addition of randomly distributed fibres to quasi-brittle materials is known to improve the post-crack performance and the strain capacity. The tested construction materials were cement-based mortars, gypsum-based plaster and earth-based adobes. Adobe specimens are unfired clay bricks made of a mixture of clay- and gravel-type soils [102]. A test program including small-scale prisms of the three mentioned types of construction materials was employed in accordance with the standard UNI/EN 196-1 on compressive and flexural testing of small-scale prisms [103]. For more details on the test program and the results, see Appendix V, VI and VII. The basic steps in the casting and testing procedure are shown in Figure 11 for the gypsum-based specimens including mixing, casting, and the specimens before and during the three-point bending testing.



(a)         (b)         (c)         (d)
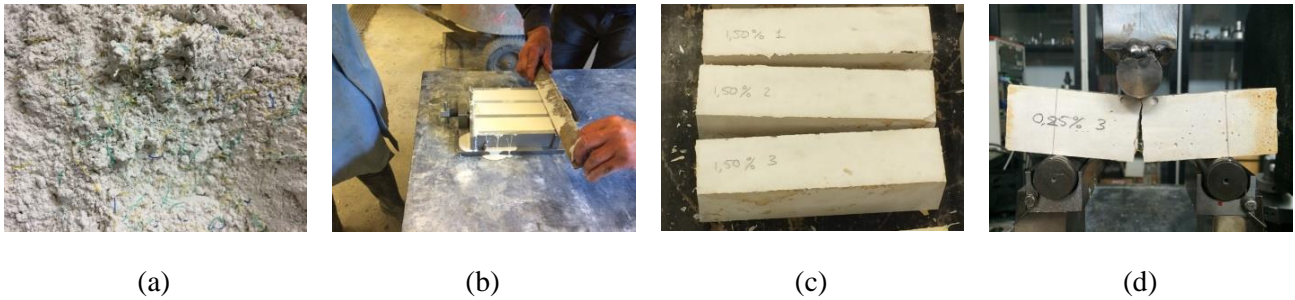
*Figure 11. Example of the preparation and test procedures for the three-point bending tests shown for gypsum-based specimens. a) Mixing raw materials and R-PE fibres; b) casting specimens in steel moulds; c) specimens after curing; d) and three-point bending testing*

*Table 5. Overview of materials, mixture proportions, curing conditions and fibre content for small-scale prisms. The maximum fibre content possible to mix into the respective mix proportions is written in bold.*

| Material | Proportions | Curing | Fibre content [weight%] | Fibre content [volume%] |
|---|---|---|---|---|
| Cement-based mortar | [cement : water : sand] [1.0 : 0.5 : 3.0] | 1 d of dry-curing inside moulds + 27 d of wet-curing at ~21 °C | 0.17, 0.33, 0.50, 0.67, 0.83, 1.00, 1.17, **1.33** | 0.38, 0.77, 1.15, 1.54, 1.92, 2.31, 2.69, **3.07** |
| Gypsum-based plaster | [gypsum : water] [1.0 : 0.44] | 1 d of dry-curing inside moulds + 2 d of air-curing at ~21 °C | 0.25, 0.50, 0.75, 1.00, 1.25, 1.50, 1.75, **2.00** | 0.44. 0.87, 1.31, 1.74, 2.18, 2.62, 3.05, **3.50** |
| Earthe-based adobe | ["clay" : water : gravel] [1.0 : 0.5 : 1.0] | 48 h of dry-curing inside moulds at 30 °C | 0.25, 0.50, 0.75, 1.00, 1.25, 1.50, 1.75, 2.00, 3.00, **4.00** | 0.58, 1.16, 1.73, 2.31, 2.89, 3.41, 3.98, 4.55, 6.83, **9.24** |

All specimens had similar dimension (40 x 40 x 160 mm$^3$) and test procedures were kept constant for all three types of materials, whereas the mixture proportions, curing time and curing method varied. This can be seen in Table 5. The three-point bending tests were all performed in the same hydraulic displacement controlled testing machine with a displacement rate of 1 mm/min. The R-PE fibres were added in weight% of the raw materials, but are for comparative reasons converted to volume% in Table 5.
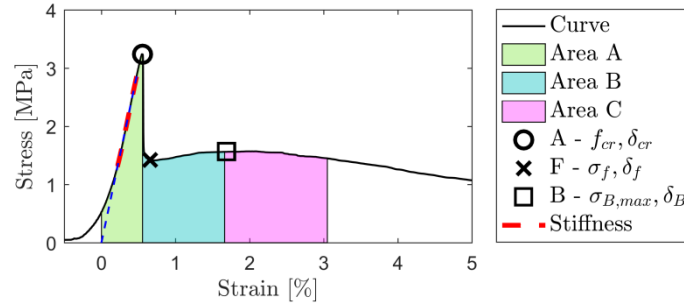


*Figure 12. Theoretical working curve for fibre reinforced prism tested under three-point loading.*

The theoretical working curve for a specimen exposed to three-point loading is shown in Figure 12. The marked points, lines and areas, which were used to evaluate the fibre performance, are described below. The first crack strength $f_{cr}$ (and in all the tested cases, also the largest flexural strength of the composite) and mid-span strain was calculated in accordance with UNI/EN 196-1 [103]. The stiffness of the uncracked material $E$ was calculated as the slope of the linear part on the stress strain curve from 0.4 $f_{cr}$ to 0.9 $f_{cr}$ (marked with the red dotted line in Figure 12). The addition of fibres commonly results in improved post-crack performance and a more ductile failure of the composite. The fibre efficiency factor (FEF) was calculated as the ratio between the stress in point A and F. The flexural toughness $T_{\delta cr}$, $T_{3\delta cr}$ and $T_{5.5\delta cr}$ were calculated as the area under the load-deflection curve from where the linear slope of the uncracked material intersects with the x-axis and to Area A, B, C, respectively. The toughness index is a measure of the load-carrying capacity of the fibres within the material matrix after first crack appears [32]. The methods for calculating the toughness and toughness indices are as described in the ASTM standard C1018 [104]. The equations are shown in Appendix VII. The fibre influence on the flexural performance of the small-scale prisms was represented by the above-mentioned numbers and the three types of tested construction materials are compared.

### 4.2.1    Results on the influence of R-PE fibres in construction materials

The results on the mechanical performance of small-scale prisms of different types of construction materials (cement-based mortar, gypsum-based plaster and earth-based adobe) with very different intrinsic strength and properties are briefly described in this section. The test program consists of three-point bending tests as measure of the fibre performance exposed to tensile stresses. Selected results for the stress-strain behaviour are presented Figure 13 for the respective reference specimens and specimens with an R-PE fibre addition of

approximately 3.0vol%. The red dotted line shows the slope of the uncracked material, i.e. the calculated stiffness.
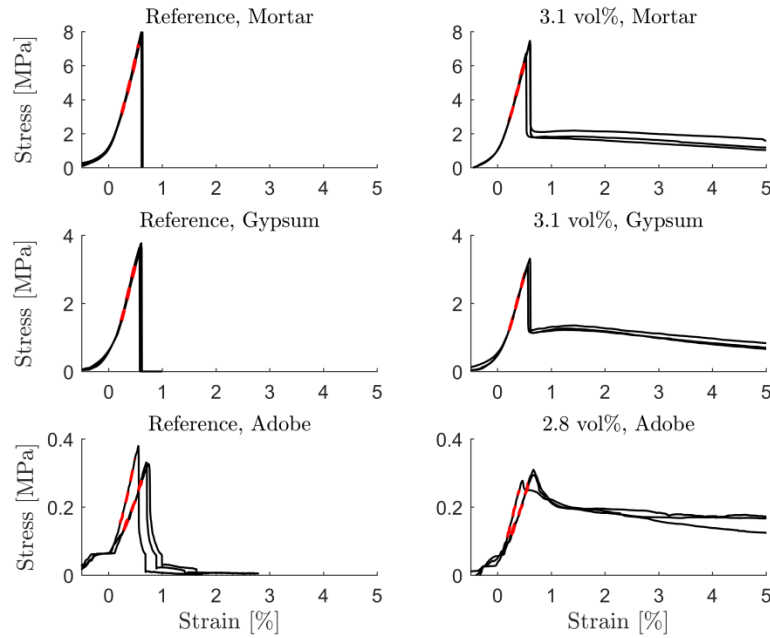


*Figure 13. Stress strain behaviour of prisms with no fibres (Reference) or with R-PE fibre addition of approx. 3.0 vol%. Please note the different scales on the y-axis. Figures adapted from Appendix V, VI and VII*

In Figure 13, it is firstly observed that the flexural strength of the three materials varies significantly. The mortar specimens exhibit the highest flexural strength of ~8 MPa, followed by the gypsum specimens of ~3.5 MPa and finally the adobe specimens, which gained very low flexural strength of ~0.35 MPa. Secondly, the fibres improve the post-crack performance and strain capacity of all three materials, although it is poor for both the cement-based and gypsum-based specimens. A large drop in stress is seen for the mortar and gypsum specimens, whereas almost no drop occurs for the adobe. The fibre influence on different measures such as the first crack strength, the maximum post-crack strength, the stiffness of the uncracked material, the toughness indices and the fibre efficiency factor (FEF) is illustrated in Figure 14 to Figure 16. Please note the different scales on the *y*-axis for some of the figures.
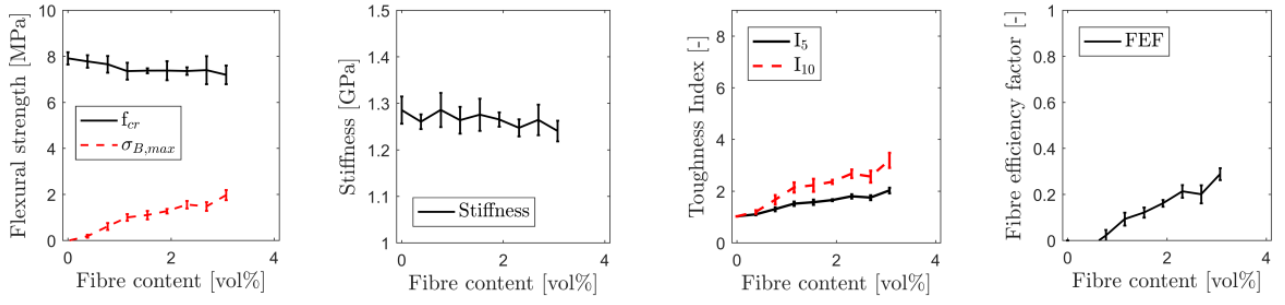
*Figure 14. Influence of R-PE fibres on the mechanical properties of cement-based mortar specimens*
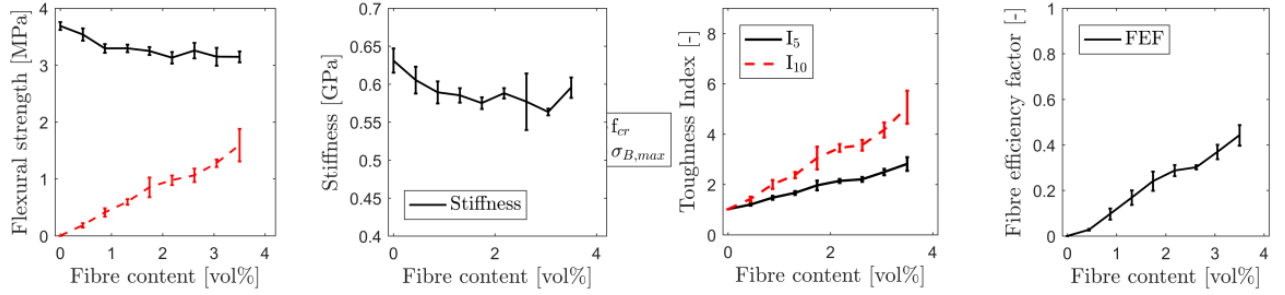


*Figure 15. Influence of R-PE fibres on the mechanical properties of gypsum-based plaster specimens*
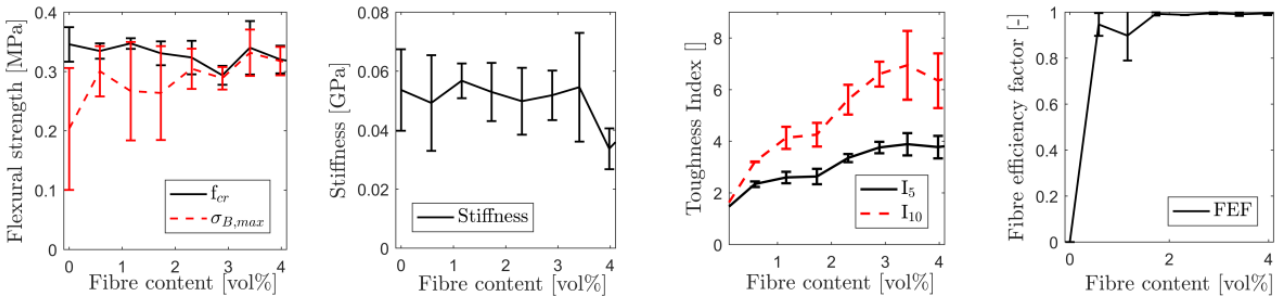


*Figure 16. Influence of R-PE fibres on the mechanical properties of earth-based adobe specimens*

From the figures above, the following tendencies are observed:

- The first-crack strength and the stiffness of the uncracked material decreases slightly with increasing fibre content for all three materials.

- Maximum post-crack strength of ~2 MPa and ~1.5 MPa were obtained for the mortar and gypsum-based specimens, respectively. For the adobe specimens, there was no actual drop in stress after the first crack appeared at fibre contents > 3vol%.

- The toughness index, which is a measure of the relative post-crack performance, increases for all materials as the fibre content increases. The best results are obtained for the adobe specimens followed by the gypsum specimens and the mortar specimens. Still, the toughness values (*T*) obtained for the different materials were highest for the mortar specimens.

- The fibre efficiency factor (FEF) is a measure of the drop in stress right after the first crack appears. As observed in the stress strain curves, this drop was largest for the mortar specimens, since a much

higher first crack strength was obtained compared to the two other materials. Almost no drop in stress was observed for the adobe specimens. Hence a FEF of 1.0 was obtained.

When adding fibres to a quasi-brittle matrix for improving the post-crack performance some of the most important fibre properties are the fibre-to-matrix bonding, stiffness, shape and tensile strength. The stiffness of the matrix itself is also of importance; since stiffer matrixes requires stiffer fibres in order to improve the post-crack performance. From the above results it was observed that the best results in terms of post-crack performance and FEF was obtained with the low-modulus adobe specimens, where almost no drop in strength occurred after the first crack strength was reached. However, these results are relative, because the adobe specimens had gained very low strength and stiffness, and their post-crack performance was likewise very small. For comparisons with other studies, please refer to the relevant appendices.

The bond between the binder and the R-PE fibre is found to be poor for all three types of materials. This is considered to be due to the straight shape and the smooth fibre surface. Other studies confirmed this poor bonding and suggested the use of deformed fibre shapes to improve the mechanical fibre-to-matrix bonding [7,105]. The fibre dimensions are approximately in the same range as many other waste fibres, which have shown good results for improving toughness and post-crack performance [7,8,10,43].

### 4.2.2   *Directions for future studies*

The obtained results point to a number of interesting topics that would be interesting for further investigations.

- It was observed that the fibres have a relatively low adhesion to the matrix. It would therefore be relevant to look into different types of modifications of the fibre surface (chemical or mechanical) for improving the fibre-to-matrix bonding.
- Longer fibre lengths could result in improved performance since the surface area between the matrix and the fibre would be larger. Hence a modification to the mechanical cutting operation would be needed.

# 5 Plastic shrinkage cracking in cement-based materials

The investigations on plastic shrinkage cracking in cement-based materials were initiated with a comprehensive literature review presented in Appendix I covering existing experimental test setups, crack measuring techniques, fibre types and matrix materials previously dealt with in the literature. In addition, an analysis of the influence of different fibre characteristics on the formation of plastic shrinkage cracking was carried out and the results are presented in the review study. Based on the literature review, it became clear that various types of fibres can be beneficial in controlling plastic shrinkage cracking and that there is a lack of more sophisticated techniques for automated quantification of crack patterns in fresh cement-based materials. By using image-based techniques such as DIC, it is possible to obtain much more detailed information on the plastic shrinkage behaviour. Therefore, this method could enable an objective comparison of the influence of e.g. different fibre types and other relevant parameters. Therefore, the possibilities and challenges for applying a 2D-DIC technique for monitoring surface deformations in fresh cement-based materials were identified (Appendix II). Finally, a test program on the influence of R-PE fibres and commercially available PP fibres on the cracking formation in restrained mortar overlays was done (Appendix III and IV).

## 5.1 Development of an experimental program for studying plastic shrinkage cracking using 2D-DIC

The overall methodology for performing the shrinkage tests is shown in Figure 17. It consists of casting cement-based mortar overlays, applying a high-contrast surface pattern, transferring the specimens into a climate-controlled chamber and turning on wind fans to ensure sufficient water evaporation rate from the surface. Thereupon, the DIC monitoring of the shrinkage specimens using optical cameras (starting at 1 h after adding mixing water to the dry materials) was initiated. The DIC monitoring continued for 24 h (until 25 h). Finally, the images were processed using the DIC software, GOM Correlate 2016.
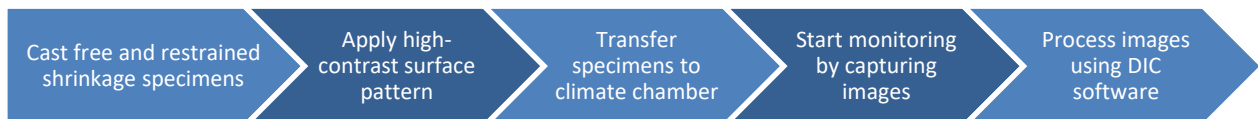


*Figure 17. Diagram showing the steps related to carrying out the plastic shrinkage tests*
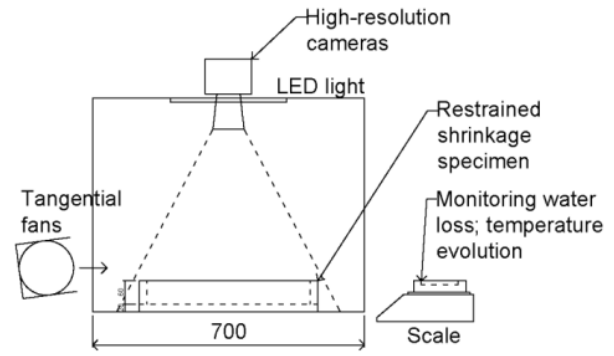
*Figure 18. a) Specimens used for plastic shrinkage testing; b) Test setup using DIC for monitoring in-plane deformations Figures adapted from Appendix II, III, and IV*

A 2D-DIC technique was applied for continuous monitoring of the specimen surfaces. Prior to implementing the test program, some challenges were identified and resolved to ensure a successful application of the DIC technique:

- A high-contrast surface pattern that enables the DIC software to track surface displacements should be applied without hindering the evaporation of mixing water from the specimen surface. There is no standardized method for the application of a high-contrast surface pattern, especially not for wet materials, and few attempts for applying the pattern on a wet cement-based surface have been presented in the literature [71,79,85,98].

- The presence of bleeding water on the surface could limit the options for creating a high-contrast surface pattern using spray paints, because the speckles might get absorbed or move during the test [79,98]. Since the use of spray paint was considered to be most appropriate, a mixture design for the fresh mortar overlay needed to be chosen in order to have limited bleeding water on the surface, while ensuring that it would foster plastic shrinkage when exposed to a harsh environment.

- In order to demonstrate the ability of the DIC technique to detect and quantify scattered crack patterns without knowing the crack locations beforehand, specimens with an expectedly scattered crack pattern were designed specifically for the restrained shrinkage tests.

- The input parameters for the DIC software (virtual mesh, subset size and overlap) should be chosen to ensure a reasonable relation between the subset dimensions and the black speckles in the high-contrast surface pattern [90].

After several iterations, the above-mentioned challenges were overcome and the resulting procedure is presented in this section. Figure 18b illustrates the test setup used for continuous DIC monitoring of in-plane surface deformations. The proposed specimen design (Figure 18a) was inspired by several studies on

restrained shrinkage cracking cast on top of an underlying rough substrate [28,63,67,70,83,106,107]. A mixture design and a low thickness of the specimens of 10 mm were chosen for several reasons: 1) to reduce the amount of bleed water on the surface, 2) for promoting scattered crack patterns induced by plastic shrinkage, and 3) to limit the analysis to in-plane deformations by neglecting the very limited formation of plastic settlement. This design allowed the application of a high-contrast surface pattern, which comprised of white and black chalk-based spray paint. A pattern of evenly distributed black speckles was considered most appropriate because of the scattered nature of the crack pattern. The influence of chalk- and acrylic-based paint types for creating the pattern was evaluated by the evaporation rate from fresh mortar specimens from 1h to 25 hours after casting. Figure 19 shows that the acrylic-based paint caused a significant decrease in the evaporation rate by creating a sealing layer on the surface. Because of the diffusion-open nature of the chalk-based paint, the specimens were allowed to evaporate without any sealing layer on the surface. Thus the chalk-based paint type was chosen.
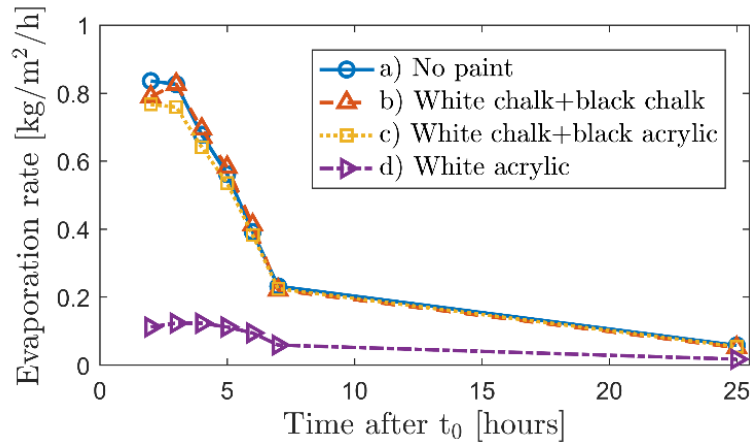


*Figure 19. Water evaporation rate from fresh mortar specimens prepared with different types of surface paintings; a) Reference with no paint; b) base of white acrylic-based paint; c) base of white chalk-based with speckles of black chalk-based paint; d) base of white chalk-based with speckles of black acrylic-based paint. Figure adapted from Appendix II.*

For the DIC analysis, a virtual mesh was defined for each specimen surface consisting of overlapping subsets creating a fine mesh. The size and overlap of the subsets were chosen in accordance with the recommendations by Sutton et al. [90] for the fineness of the black speckles of chalk paint and the required fineness of the DIC computation. The finer the speckle pattern, the more precise the DIC computation. The DIC software recognizes the grey intensity level in an undeformed subset and compares it to that of a deformed subset [96]. Figure 20 is an example of the fineness of the speckle pattern and the selected subset dimensions of 20 x 20 pixels = 1.6 x 1.6 mm and a subset overlap of 15 pixels = to 1.2 mm for an undeformed subset. With these subset dimensions, the desired precision of the DIC analysis was achieved.
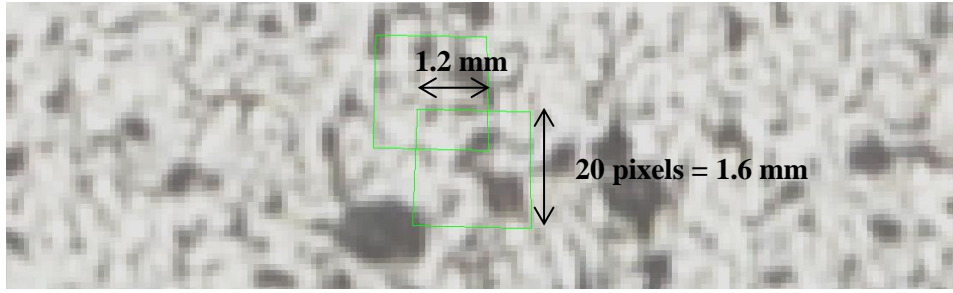
*Figure 20. Magnification of high-contrast surface pattern comprising of a white base and black speckles of chalk paint. The green squares represent subsets (dimension: 20 pixels = 1.6 mm; overlap: 15 pixels = 1.2 mm) defined in the DIC software. FOV = 12.9 x 3.85 mm*

### 5.1.1 Using R-PE fibres for mitigation of plastic shrinkage cracking

Based on the R-PE fibre characterization (main results shown in Chapter 4), the R-PE fibres were considered to be most applicable for controlling plastic shrinkage cracking. A test program was carried out to investigate the influence of two types of fibre reinforcement on the crack formation and free shrinkage behaviour. The performance of the R-PE (d = 280 ± 30 µm, L = 15 ± 9 mm) fibres added in volume fractions of 0.2%-2.0% was compared to that of commercially available PP fibres (d = 19.5 µm, L = 12 mm) added in volume fractions of 0.1%-0.2%.

## 5.2 Post-processing of DIC data for evaluation of plastic shrinkage cracking

This section gives an overview of an approach for numerical post-processing developed for crack quantification in restrained cement-based mortar overlays. The details can be found Appendix II, III and IV.

### 5.2.1 Using DIC for studying the formation of plastic shrinkage cracking

Traditionally, the degree of surface cracking is measured by basic crack parameters such as the total crack area (TCA), the mean/maximum crack width or crack length (MCW/MCL). These numbers provide good information on the degree of surface cracking, but they do not provide any quantitative number on the amount of wide/long cracks, i.e. the distribution of crack widths/lengths over the total surface area. This is of importance, since wider and longer surface cracks can be more detrimental for the durability of the concrete structure, than finer and shorter cracks [108,109]. Previous studies on the topic have shown that it is possible to measure the crack widths on a specimen surface to a high precision based on the displacement data obtained by DIC [83,100,110]. However, a method for automated crack detection and measurements over the entire specimen surface based on DIC data would be highly relevant and advantageous for a quantitative measure of the degree of surface cracking. For enabling a more detailed and objective method for crack

quantification, an iterative procedure was developed for numerical post-processing of the DIC data. The details of the procedure are described in Appendix II and III, while the basic principles are presented in this section and in the diagram below (Figure 21).



*Figure 21. Diagram for the post-processing approach for using DIC data to quantify plastic shrinkage cracking*

In-plane displacement and strain data on a specimen surface can be obtained from the DIC technique. The strain data is a numerical approximation to partial derivatives of the displacement (Eq. 2), which means that abrupt changes in surface displacement, i.e. very large derivatives, appear as local extrema in strain as shown in Figure 22(b-d). These gaps in displacement and peaks in strain reveal surface cracking [111]. From small-deformation theory, the strain tensor is given component-wise by:

$$\varepsilon_{ij} = \frac{1}{2}\left(\frac{\partial u_i}{\partial x_j} + \frac{\partial u_j}{\partial x_i}\right)$$

(Eq. 2)

where *u* is the displacement and *x* is the position vector. Only the crack openings occurring in the *x*-direction (the direction parallel to the long side of the specimen) were considered for simplifying the computation of the crack widths. The physical cracks mostly appeared in this direction as a result of the specimen geometry and the wind direction. This was considered to be a good approximation of the actual crack widths, and effectively reduced the analysis to a one-dimensional problem for each linear segment parallel to the *x*-axis.
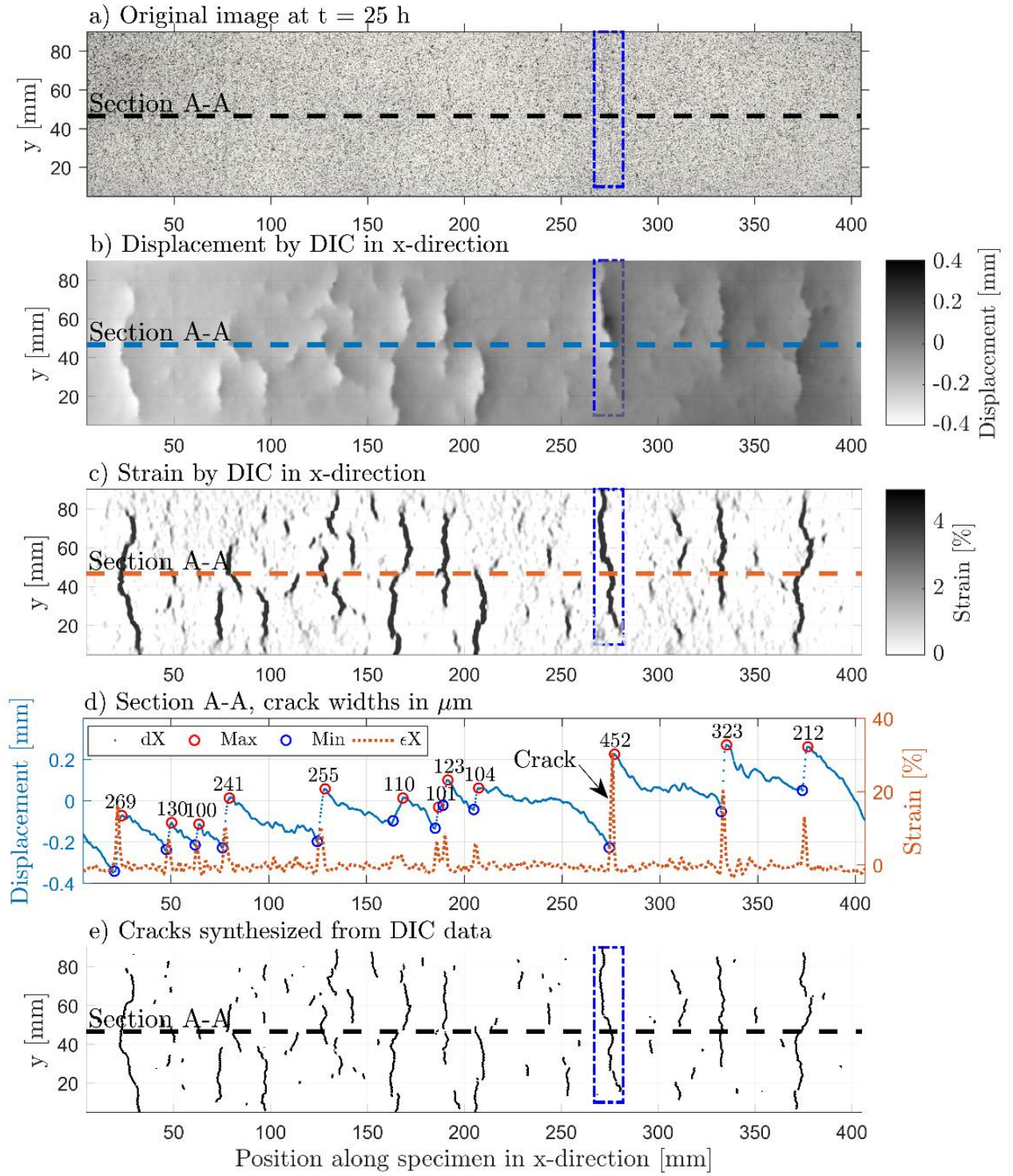
*Figure 22. Surface of restrained mortar overlay at t = 25 h. a) Original image; b,c) In-plane surface displacement and strain in x-direction by DIC data; d) In-plane displacement and strain by DIC data along Section A-A showing detected cracks; e) Crack pattern synthesized from data by the post-processing approach. Figure adapted from Appendix II*

The numerical values of the crack widths occurring in the *x*-direction (parallel to the long side of the specimens) were measured from the "vertical" abrupt changes in surface displacement, i.e. displacement gaps. These are shown in Figure 22d (crack widths given in µm) on a single section along the specimens surface (Section A-A). It is observed that with each displacement gap, a peak in the surface strain appears. Hence, a strain threshold limit $K_0$ for when a displacement gap should be considered as an actual crack was defined to $K_0 = 0.02$ m/m. Repeating this procedure for all section of a defined surface grid with very fine mesh sizes enabled a section-wise analysis of the surface cracks over the entire specimen surface. As a result, a digital reproduction of the crack pattern could be synthesized solely based on the DIC data, see Figure 22e. Similarly, the surface strain and displacements can be illustrated in a 3D plot as done in Figure 23 with the strain and displacements shown on the *z*-axis. The displacement plot reveals how the crack widths were calculated as the sudden drops in displacement (illustrated as the vertical difference between blue and red line shown on the displacement plot). From the strain plot, it is observed that the uncracked area on the specimen surface (dark blue area on strain plot) was also slightly modified during the shrinkage test, although actual surface cracks were not identified.
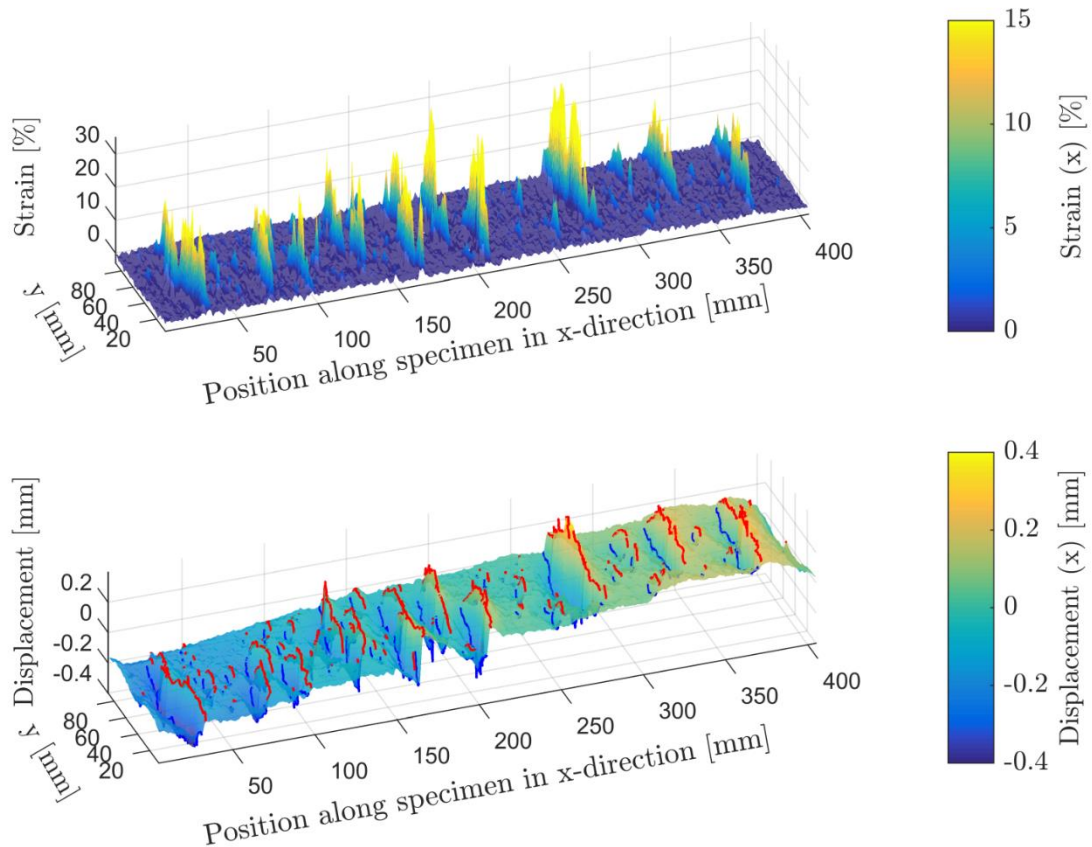


*Figure 23. In-plane surface strain and displacement in x-direction at t = 25 h (end of test). Red lines = maximum values, blue lines = minimum values on each side of the crack.*

A similar approach for identifying cracked areas based on DIC data was suggested by Lagier et al. and Mauroux et al. [83,110]. However, these approaches did not include automated crack measurements. Logically, low strain threshold values would result in the detection of significantly more fine cracks with very low crack widths compared to higher thresholds, where some identified "cracks" could be due to the presence of local fluctuations or noise resulting in interpolation errors. Because of the nature of the tested material, where large deformations occur over a short period of time (few hours), we observed that, for low strain threshold values (e.g. $K_0 = 0.002$ m/m), several very fine and short cracks were identified on the surface, which in some cases could be considered as noise. In addition, when a crack occurs on the specimen surface, the texture of the representative subsets is modified, which can lead to local interpolation errors in the displacement field in the vicinity of a crack. This can result in an overestimation of the crack width [83].

A quantitative measure of the degree of surface cracking can be illustrated as the crack width distribution (CWD) over the entire specimen surface. Figure 24 illustrates the CWD for a reference specimen (no fibres added) at time stages of t = 1.5 h, t = 2.0 h and t = 25 h. Crack width intervals are shown on the *x*-axis. On the *y*-axis, the number of cracks per bin width is converted to the total crack length and total crack area within each bin width.



(a)                                                                              (b)
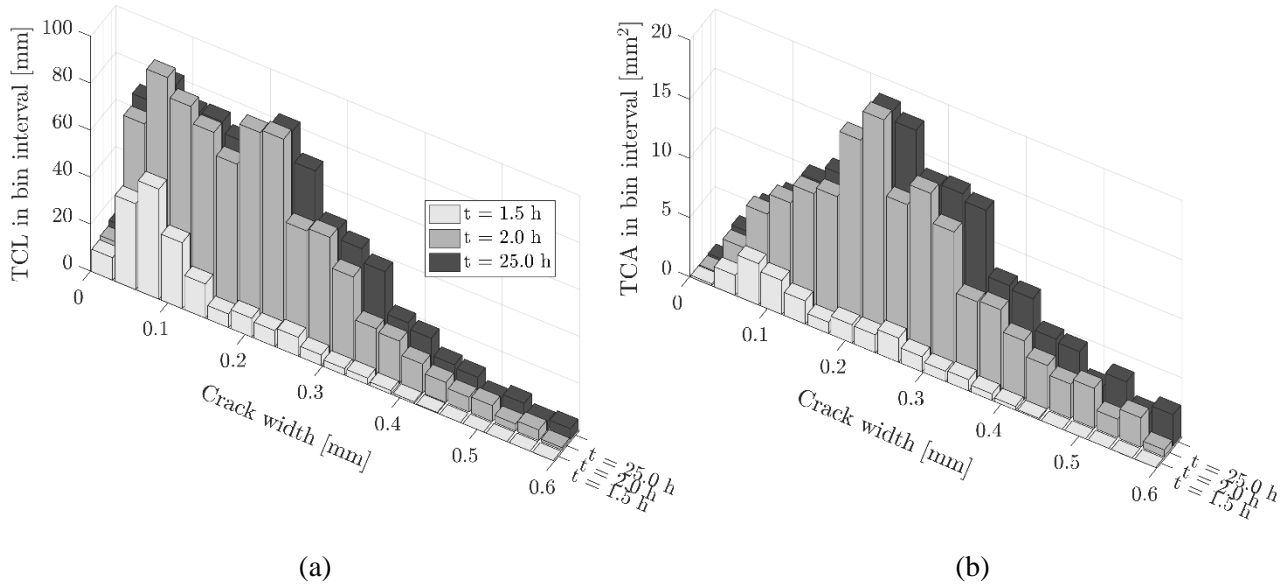
*Figure 24. Histograms of the relation between the crack width distribution (CWD) over the entire specimen surface and a) the total crack length (TCL) [mm] and b) the total crack area (TCA) [mm²] in each bin interval, at selected time intervals of t=1.5 h, 2.0 h, and 25 h.. Figure adapted from Appendix II.*

### 5.2.2    Directions for further improvements of the DIC post-processing approach

Compared to previous studies listed in Table 2, the crack quantification approach suggested in the present project is a major improvement. Still, the method could be further improved and a number of interesting topics for future studies can be pointed out:

- The high-contrast surface pattern should be designed to allow the presence of bleed water on the surface. With inspiration from recent studies by Dzaye et al. [95,98], it would be interesting to investigate the use of different particle-shaped materials for the creation of the speckle pattern. However, the reflection on the images because of the bleed water would probably still be a problem for the DIC analysis.

- The post-processing approach developed for crack measurements should not be limited to a 1D version of the problem, but should be able to compute crack widths in all directions on a specimen surface, thus directly solving the 2D problem.

## 5.3 Influence of R-PE fibres on plastic shrinkage cracking

The addition of randomly distributed fibres to the fresh cement-based matrix is known to have a positive influence on the formation of plastic shrinkage cracking. The influence of different fibre properties is analysed in Appendix I and it was found that the most important properties were the diameter, aspect ratio and fibre-to-matrix bonding (e.g. shape and adhesion of cement to fibre surface) [27,28]. No clear dependency on the fibre length and fibre stiffness was found. The influence of the R-PE fibres were studied on restrained mortar overlays with fibre additions of 0.2-2.0vol%, and compared to the results obtained with commercially available PP fibres. The degree of surface cracking was quantitatively analysed using the DIC technique and the post-processing procedure described in the previous section. The surface strain appearing in the $x$-direction for one of each specimen types is shown in Figure 25a. The CWD (given as the total crack area per bin width) is shown in Figure 25b. The figures clearly demonstrate that the addition of fibres results in reduced surface cracking. It can also be seen, that the obtained CWD corresponds well to the density of cracks that can be visually inspected on the strain plot.

The commercial PP fibres were observed to have a superior performance, which was expected since the fibre diameter was much finer. Hence, the number of fibres per volume unit being much higher than for the coarser R-PE fibres would allow more fibres to bridge a potential plastic shrinkage crack. The smooth surface, relatively coarse diameter and straight shape of the R-PE fibre are considered to be the main factors leading to the reduced performance compared to the PP fibres. Still, good results were obtained with R-PE fibres when added in volume fractions of 2.0%. This volume fraction is rather high compared with industrial levels of fibre additions, but as seen in Table 1, macro fibres with fibre dimensions relatively similar to the R-PE fibres, were found to be beneficial when added in volume fractions up to 1.5-2.0% [8,40,66].
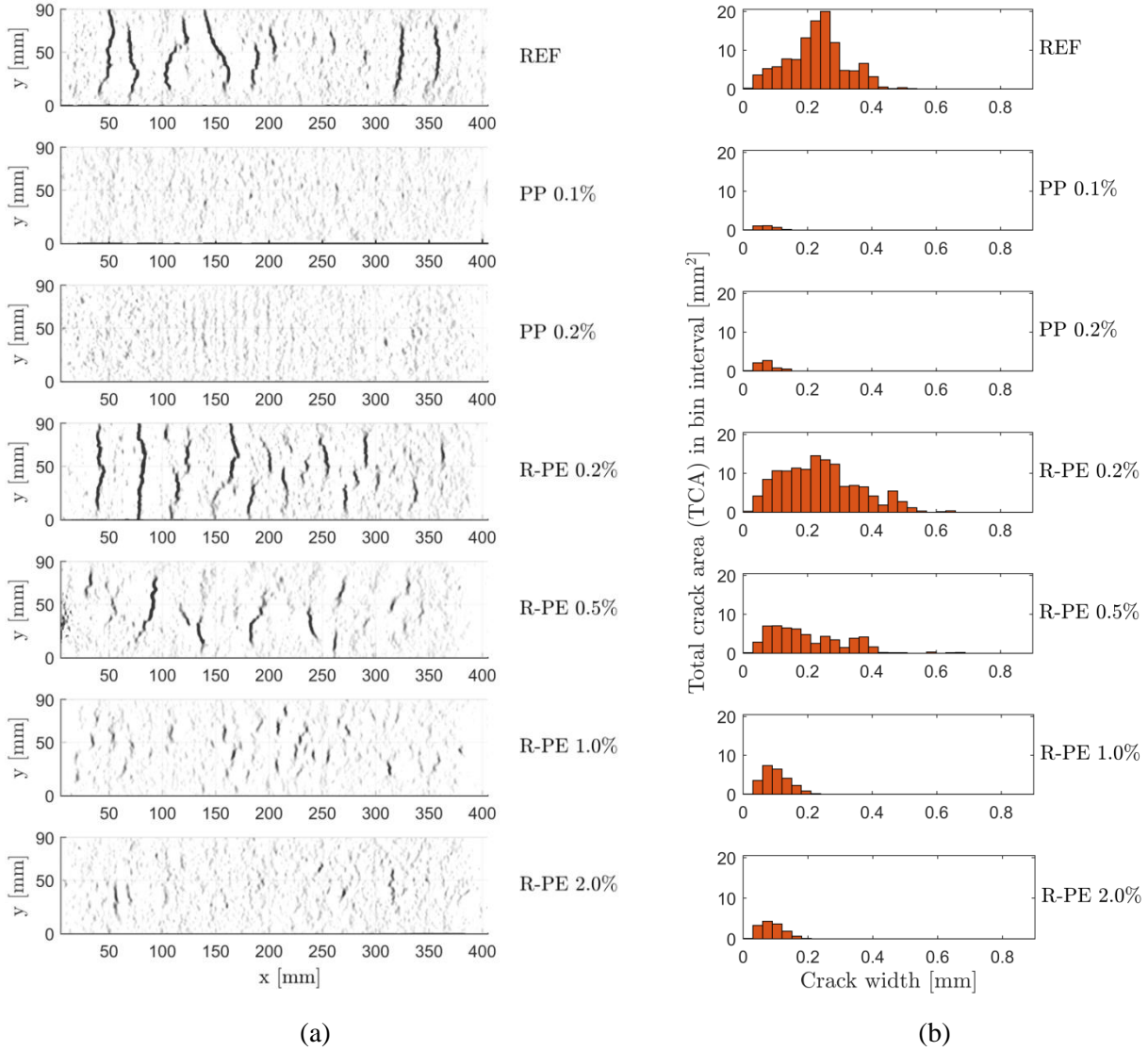
*Figure 25. a) Strain fields parallel to the x-directions on the specimen surfaces by DIC data at t = 25 h. Cracks are illustrated by dark colours in the strain data. Colour scale: White, $e_x = 0\%$; Black, $e_x = 5\%$. b) Histograms of the total crack area (TCA) [mm²] in each bin interval and the crack width distribution (CWD) on the entire specimen surface. Figure adapted from Appendix III.*

### 5.3.1 Performance of R-PE fibres compared to other macro fibres

It was necessary to add a relatively high volume fraction of 2.0% of R-PE fibres to the restrained mortar overlay to achieve a satisfactory reduction in plastic shrinkage induced surface cracking. A crack reduction ratio (CRR) of 85% (with respect to the total crack area) calculated in accordance with the ASTM C1579 standard [64] was obtained for the overlays with an R-PE fibre addition of 2.0%.

An overview of other studies investigating the performance of various types of macro fibres of virgin or waste materials is given in Table 1. These fibres are compared to the R-PE fibres in Figure 26. The figure

shows the crack reduction ratio (CRR) for the total crack area (TCA) on the specimen surface as a function of the specific fibre surface $S_f$. The specific fibre surface is a combined measure of the fibre diameter and the added volume fraction and serves as a geometrical parameter for the representation of the fibres. It is given by

$$S_f = \frac{4\,V_f}{d} \qquad \text{(Eq. 3)}$$

where $V_f$ is the fibre volume fraction [-] and $d$ [mm] the fibre diameter [28,36,67]. Note that different test methods and crack measuring techniques were employed in the different studies. The TCA was computed from the DIC data in the present study as described in the previous sections.
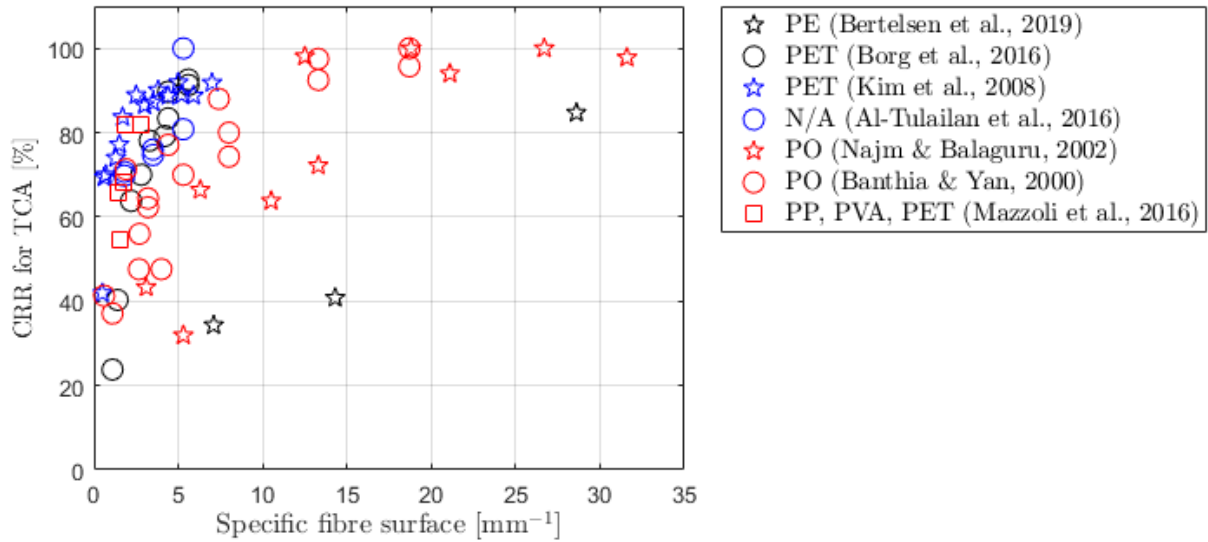


*Figure 26. Crack reduction ratio (CRR) for the total crack area (TCA) as a function of the specific fibre surface. Results from Appendix III (Bertelsen et al, 2019) and the studies presented in Table 1 are displayed. Black markers are recycled fibres obtained by mechanical processing [8,86]. Blue markers are recycled fibres obtained by thermal reprocessing [6,40]. Red markers are virgin fibres [66–68].*

From Figure 26 it is observed that, as anticipated, an increase in the specific fibre surface results in a better control of the surface cracking (increased CRR for TCA). Moreover, it is seen that the R-PE fibres do not perform as well as other synthetic fibre types of both virgin materials [66–68] and recycled materials [6,8,40]. This could be due to the different test methods and that some of the fibres had deformed shapes to improve the fibre-to-matrix bonding [6,8,68]. The improved fibre-to-matrix bonding resulted in a good fibre performance when added in volume fractions of 0.3% [68], 0.5% [6] and 1.5% [8]. Studies using thermal reprocessing can produce fibres with the desired shape [6,7]. Apart from the R-PE fibres, the only fibres obtained solely by mechanical processing were those studied by Borg et al. [8].

The most similar fibres to the R-PE fibres in terms of performance and dimensions were the virgin PO fibres studied by Najm & Balaguru [66]. These are shown alongside with the R-PE fibres in Figure 27 as a function of the CRR for the TCA. From the figure, it is found that using fibres with the finest diameter (d = 0.15 mm, L = 25 mm) results in the best performance. The R-PE fibres are most similar to the PO fibres measuring d = 0.38 mm, L = 25 mm. Both fibre types had a good performance (CRR > 85%) when added in volume fractions of 2%.
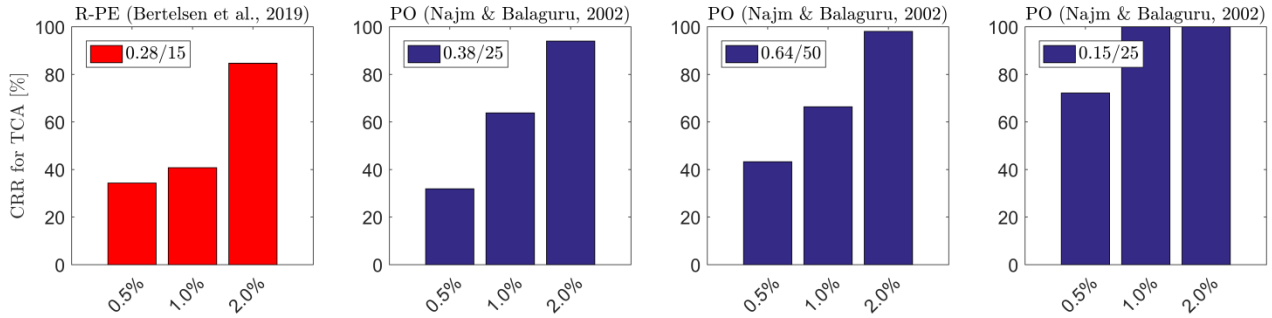


*Figure 27. CRR for TCA for R-PE fibres and PO fibres studied by Najm and Balaguru [66]. The labels give the diameter and the length in mm. E.g. 0.28/15: d = 0.28 mm, L = 15 mm.*

Longer fibres would be beneficial in the case where there is a relatively poor bond to the cement matrix [27]. In that case, the stress transferred across a crack has a larger fibre surface area to be transferred over. The macro fibres presented in other studies in Table 1 are in most cases longer than the R-PE fibres used in this study,  i.e. 23-54 mm versus to 15 ± 9 mm for the R-PE fibres [6–8,40,66,67]. Some studies found that longer fibre lengths resulted in improved performance [8,67], whereas other studies did not find the fibre length to have a significant influence [40]. Note that the fibre length is not included in the specific fibre surface. In order to improve the performance of the R-PE fibres for controlling plastic shrinkage cracking without thermally reprocessing the fibres, it would be relevant to look into alternative cutting operations allowing fibres to be longer and with more uniformly distributed lengths. It would also be worthwhile to investigate the influence of different fibre surface modifications for improving the fibre-to-matrix bonding.

# 6 Overall conclusions

Recycled polyethylene (R-PE) fibres obtained from discarded fishing nets were characterised and the potentials of using the fibre as reinforcing material in construction materials were investigated in this PhD project. Based on the tested fibre characteristics, it was found that the R-PE fibres could be beneficial for controlling the formation of plastic shrinkage cracking in cement-based materials or for improving the post-crack performance of low-modulus types of construction materials. The overall conclusions of the study are related to 1) the R-PE fibres in construction materials and 2) the numerical post-processing of data obtained by the digital image correlation (DIC) technique for monitoring plastic shrinkage cracking.

The following main conclusions related to the R-PE fibres are:

- Fibres of different types of polyethylene fishing nets obtained by mechanical cutting, had a homogenous fibre diameter, but large variations in length due to the processing method. The fibres showed good alkali-resistance. The tensile strength and stiffness were in the same range as other synthetic fibres, i.e. PP fibres, which are also used as fibre reinforcement in construction materials.

- A test program was carried out to investigate the influence of R-PE fibres on the mechanical performance of different types of construction materials with very different mechanical properties: Cement-based mortars, gypsum-based plaster and earth-based adobe. Three-point bending tests showed that the fibres improved the post-crack performance and strain capacity of all materials. The effect was most evident for the adobe specimens, which is a low-modulus material with poor mechanical performance. The post-crack performance of hardened cement-based mortar specimens was not affected noticeably by the R-PE fibres given the flexural strength of the matrix.

- Commercially available PP fibres of virgin materials were superior in controlling the degree of plastic shrinkage cracking. However, when adding a higher volume fraction of R-PE fibres a similar result could be achieved. The need for a higher volume percentage of R-PE fibres was likely due to the coarser nature of the R-E fibres and the poor fibre-to-matrix bonding. An addition of 2.0% of R-PE fibres was beneficial in controlling the formation of plastic shrinkage cracking.

A 2D-DIC technique was applied for monitoring the formation of plastic shrinkage cracking in restrained cement-based mortar overlays. A numerical post-processing approach was developed for enabling an objective and quantitative analysis of the degree of cracking. The main contributions in this part of the project are:

- Chalk-based spray paints were used for creating a high-contrast surface pattern on the fresh cement-based surface, which is essential for the DIC analysis. This was to overcome the challenge of applying a pattern without influencing the evaporation rate of mixing water from the specimen. It

was found that the diffusion-open chalk-based paint successfully allowed the same evaporation rate as in a reference specimen with no paint.

- A numerical post-processing approach was developed for further analysis of the DIC data, which enabled an objective quantification of the degree of surface cracking. It was possible to automatically compute the one-directional crack widths for all cracks over the entire specimen surface, which facilitated the crack pattern to be synthesized. This is a major advancement compared to the sole visualisation of the surface displacement and strain fields obtained directly from the raw DIC data.

- The degree of surface cracking is traditionally presented by basic crack parameters such as the crack area, width and length, but no information about the number of finer and wider cracks are provided by these measures. Post-processing the DIC data enabled quantification of the degree of surface cracking in terms of crack width distributions. This is a major improvement compared to the basic crack parameters.

# References

[1]     R. Siddique, J. Khatib, I. Kaur, Use of recycled plastic in concrete: A review, Waste Manag. 28.10 (2008) 1835–1852. doi:10.1016/j.wasman.2007.09.011.

[2]     European_Commission, A European Strategy for Plastics in a Circular Economy, 2018.

[3]     Miljø-og-Fødevareministeriet, Erhvervsministeriet, Strategi for cirkulær økonomi, 2018. https://mfvm.dk/fileadmin/user_upload/MFVM/Miljoe/Cirkulaer_oekonomi/Strategi_for_cirkulaer_oekonomi.pdf.

[4]     R. Sharma, P.P. Bansal, Use of different forms of waste plastic in concrete - A review, J. Clean. Prod. 112(1) (2016) 473–482. doi:10.1016/j.jclepro.2015.08.042.

[5]     L. Gu, T. Ozbakkaloglu, Use of recycled plastics in concrete: A critical review, Waste Manag. 51 (2016) 19–42. doi:10.1016/j.wasman.2016.03.005.

[6]     J.H.J. Kim, C.G. Park, S.W. Lee, S.W. Lee, J.P. Won, Effects of the geometry of recycled PET fiber reinforcement on shrinkage cracking of cement-based composites, Compos. Part B Eng. 39.3 (2008) 442–450. doi:10.1016/j.compositesb.2007.05.001.

[7]     N. Pešić, S. Živanović, R. Garcia, P. Papastergiou, Mechanical properties of concrete reinforced with recycled HDPE plastic fibres, Constr. Build. Mater. 115 (2016) 362–370. doi:10.1016/j.conbuildmat.2016.04.050.

[8]     R.P. Borg, O. Baldacchino, L. Ferrara, Early age performance and mechanical characteristics of recycled PET fibre reinforced concrete, Constr. Build. Mater. 108 (2016) 29–47. doi:10.1016/j.conbuildmat.2016.01.029.

[9]     D. Foti, Use of recycled waste pet bottles fibers for the reinforcement of concrete, Compos. Struct. 96 (2013) 396–404. doi:10.1016/j.compstruct.2012.09.019.

[10]    S. Spadea, I. Farina, A. Carrafiello, F. Fraternali, Recycled nylon fibers as cement mortar reinforcement, Constr. Build. Mater. 80 (2015) 200–209. doi:10.1016/j.conbuildmat.2015.01.075.

[11]    N. Saikia, J. De Brito, Use of plastic waste as aggregate in cement mortar and concrete preparation: A review, Constr. Build. Mater. 34 (2012) 385–401. doi:10.1016/j.conbuildmat.2012.02.066.

[12]    M. Frigione, Recycling of PET bottles as fine aggregate in concrete, Waste Manag. 30 (2010) 1101–1106. doi:10.1016/j.wasman.2010.01.030.

[13]    M. Kunieda, N. Ueda, H. Nakamura, Ability of recycling on fiber reinforced concrete, Constr. Build. Mater. 67 (2014) 315–320. doi:10.1016/j.conbuildmat.2014.01.060.

[14]    J.R. Jambeck, R. Geyer, C. Wilcox, T.R. Siegler, M. Perryman, A. Andrady, R. Narayan, K.L. Law, Plastic waste inputs from land into the ocean, Science (80-. ). 347 (2015) 768–771.

[15]    M. Stelfox, J. Hudgins, M. Sweet, A review of ghost gear entanglement amongst marine mammals, reptiles and elasmobranchs, Mar. Pollut. Bull. 111 (2016) 6–17. doi:10.1016/j.marpolbul.2016.06.034.

[16]    U. Oxvig, U.J. Hansen, Fishing gears, Fiskericirklen, 2007.

[17]    J. Brown, G. Macfadyen, Ghost fishing in European waters: Impacts and management responses, Mar. Policy. 31 (2007) 488–504. doi:10.1016/j.marpol.2006.10.007.

[18]    H. Al-Oufi, E. McLean, A.S. Kumar, M. Claereboudt, M. Al-Habsi, The effects of solar radiation upon breaking strength and elongation of fishing nets, Fish. Res. 66 (2004) 115–119. doi:10.1016/S0165-7836(03)00103-6.

[19]    S.N. Thomas, C. Hridayanathan, The effect of natural sunlight on the strength of polyamide 6 multifilament and monofilament fishing net materials, Fish. Res. 81 (2006) 326–330. doi:10.1016/j.fishres.2006.06.012.

[20]    A.L. Andrady, Microplastics in the marine environment, Mar. Pollut. Bull. 62 (2011) 1596–1605. doi:10.1016/j.marpolbul.2011.05.030.

[21]    B. Meenakumari, K. Ravindran, Tensile Strength Properties of Polyethylene Netting Twines Under Exposure to Out-door

and Artificial UV radiation, Cent. Inst. Fish. Technol. 22 (1985) 83–86.

[22]     Vónin, Vónin Fishing Catalogue, (2014).

[23]     M. Charter, Knowledge Base Report Booklet on knowledge base related, 2018.

[24]     M. Charter, R. Carruthers, Products from Waste Fishing Nets Home Ware , Recreation, 2018.

[25]     P.N. Balaguru, S.P. Shah, Fiber Reinforced Cement Composites, McGraw-Hill, 1992.

[26]     A. Bentur, S. Mindess, Fibre-Reinforced Cementitious Composites, 2nd Editio, Taylor & Francis, 2006.

[27]     N. Banthia, R. Gupta, Influence of polypropylene fiber geometry on plastic shrinkage cracking in concrete, Cem. Concr. Res. 36.7 (2006) 1263–1267. doi:10.1016/j.cemconres.2006.01.010.

[28]     A.E. Naaman, T. Wongtanakitcharoen, G. Hauser, Influence of different fibers on plastic shrinkage cracking of concrete, ACI Mater. J. 102.1 (2005) 49–58.

[29]     N. Banthia, V. Bindiganavile, J. Jones, J. Novak, Fiber-reinforced concrete in precast concrete applications: Research leads to innovative products, PCI J. Summer 201 (2012) 33–46.

[30]     Y.S. Heo, J.G. Sanjayan, C.G. Han, M.C. Han, Synergistic effect of combined fibers for spalling protection of concrete in fire, Cem. Concr. Res. 40 (2010) 1547–1554. doi:10.1016/j.cemconres.2010.06.011.

[31]     S. Yin, R. Tuladhar, F. Shi, M. Combe, T. Collister, N. Sivakugan, Use of macro plastic fibres in concrete: A review, Constr. Build. Mater. 93 (2015) 180–188. doi:10.1016/j.conbuildmat.2015.05.105.

[32]     J.I. Daniel et al., State-of-the-Art Report on Fiber Reinforced Concrete Reported by ACI Committee 544, ACI J. 96 (2002).

[33]     S. Yin, Development of Recycled Polypropylene Plastic Fibres to Reinforce Concrete, College of Science, Technology & Engineering James Cook University, 2017. doi:10.1007/978-981-10-3719-1.

[34]     Y. Wang, H.C. Wu, V.C. Li, Concrete Reinforcement with Recycled Fibers: A Review, J. Mater. Civ. Eng. (2000) 314–319. doi:10.1061/(ASCE)0899-1561(2000)12.

[35]     P. Pujadas, A. Blanco, S. Cavalaro, A. Aguado, Plastic fibres as the only reinforcement for flat suspended slabs: Experimental investigation and numerical simulation, Constr. Build. Mater. J. 57 (2014) 92–104. doi:10.1016/j.conbuildmat.2014.01.082.

[36]     R.F. Zollo, Fiber-reinforced concrete: an overview after 30 years of development, Cem. Concr. Compos. 19 (1997) 107–122. doi:10.1016/S0958-9465(96)00046-7.

[37]     S. Eve, M. Gomina, A. Gmouh, A. Samdi, R. Moussa, G. Orange, Microstructural and mechanical behaviour of polyamide fibre-reinforced plaster composites, J. Eur. Ceram. Soc. 22 (2002) 2269–2275. doi:10.1016/S0955-2219(02)00014-6.

[38]     S.M. Abtahi, M. Sheikhzadeh, S.M. Hejazi, Fiber-reinforced asphalt-concrete - A review, Constr. Build. Mater. 24 (2010) 871–877. doi:10.1016/j.conbuildmat.2009.11.009.

[39]     H. Binici, O. Aksogan, T. Shah, Investigation of fibre reinforced mud brick as a building material, Constr. Build. Mater. 19 (2005) 313–318. doi:10.1016/j.conbuildmat.2004.07.013.

[40]     B.S. Al-Tulaian, M.J. Al-Shannag, A.R. Al-Hozaimy, Recycled plastic waste fibers for reinforcing Portland cement mortar, Constr. Build. Mater. 127 (2016) 102–110. doi:10.1016/j.conbuildmat.2016.09.131.

[41]     M. Serdar, A. Baričević, M. Jelčić Rukavina, M. Pezer, D. Bjegović, N. Štirmer, Shrinkage Behaviour of Fibre Reinforced Concrete with Recycled Tyre Polymer Fibres, Int. J. Polym. Sci. 2015.3 (2015) 1–9. doi:10.1155/2015/145918.

[42]     F.L. Auchey, The Use of Recycled Polymer Fibers as Secondary Reinforcement in Concrete Structures, J. Constr. Educ. 3.2 (1998) 131–140.

[43]     S. Orasutthikul, D. Unno, H. Yokota, Effectiveness of recycled nylon fiber from waste fishing net with respect to fiber reinforced mortar, Constr. Build. Mater. 146 (2017) 594–602. doi:10.1016/j.conbuildmat.2017.04.134.

[44]     F. Fraternali, I. Farina, C. Polzone, E. Pagliuca, L. Feo, On the use of R-PET strips for the reinforcement of cement mortars, Compos. Part B Eng. 46 (2013) 207–210. doi:10.1016/j.compositesb.2012.09.070.

[45]     L.A. Pereira De Oliveira, J.P. Castro-Gomes, Physical and mechanical behaviour of recycled PET fibre reinforced mortar,

Constr. Build. Mater. 25 (2011) 1712–1717. doi:10.1016/j.conbuildmat.2010.11.044.

[46]    F. Parres, J.E. Crespo-Amorós, A. Nadal-Gisbert, Mechanical properties analysis of plaster reinforced with fiber and microfiber obtained from shredded tires, Constr. Build. Mater. 23 (2009) 3182–3188. doi:10.1016/j.conbuildmat.2009.06.040.

[47]    G. Vasconcelos, P.B. Lourenço, A. Camões, A. Martins, S. Cunha, Evaluation of the performance of recycled textile fibres in the mechanical behaviour of a gypsum and cork composite material, Cem. Concr. Compos. 58 (2015) 29–39. doi:10.1016/j.cemconcomp.2015.01.001.

[48]    F. Pelisser, A.B.D.S.S. Neto, H.L. La Rovere, R.C.D.A. Pinto, Effect of the addition of synthetic fibers to concrete thin slabs on plastic shrinkage cracking, Constr. Build. Mater. 24 (2010) 2171–2176. doi:10.1016/j.conbuildmat.2010.04.041.

[49]    K.S. Rebeiz, Time-temperature properties of polymer concrete using recycled PET, Cem. Concr. Compos. 17 (1995) 119–124. doi:10.1016/0958-9465(94)00004-I.

[50]    A. Baričević, M. Jelčić Rukavina, M. Pezer, N. Štirmer, Influence of recycled tire polymer fibers on concrete properties, Cem. Concr. Compos. 91 (2018) 29–41. doi:10.1016/j.cemconcomp.2018.04.009.

[51]    F. Sayahi, Plastic shrinkage cracking in concrete. Mitigation and Modelling, Luleå University of Technology, 2019.

[52]    O.B. Ozger, F. Girardi, G.M. Giannuzzi, V.A. Salomoni, C.E. Majorana, L. Fambri, N. Baldassino, R. Di Maggio, Effect of nylon fibres on mechanical and thermal properties of hardened concrete for energy storage systems, Mater. Des. 51 (2013) 989–997. doi:10.1016/j.matdes.2013.04.085.

[53]    Y. Wang, Utilization of recycled carpet waste fibers for reinforcement of concrete and soil, Polym. Plast. Technol. Eng. 38 (1999) 533–546. doi:10.1080/03602559909351598.

[54]    A.R. Khaloo, A. Esrafili, M. Kalani, M.H. Mobini, Use of polymer fibres recovered from waste car timing belts in high performance concrete, Constr. Build. Mater. 80 (2015) 31–37. doi:10.1016/j.conbuildmat.2015.01.011.

[55]    T.R. Naik, S.S. Singh, C.O. Huber, B.S. Brodersen, Use of post-consumer waste plastics in cement-based composites, Cem. Concr. Res. 26 (1996) 1489–1492. doi:10.1016/0008-8846(96)00135-4.

[56]    S. Yin, R. Tuladhar, T. Collister, M. Combe, N. Sivakugan, Z. Deng, Post-cracking performance of recycled polypropylene fibre in concrete, Constr. Build. Mater. 101 (2015) 1069–1077. doi:10.1016/j.conbuildmat.2015.10.056.

[57]    V. Slowik, M. Schmidt, R. Fritzsch, Capillary pressure in fresh cement-based materials and identification of the air entry value, Cem. Concr. Compos. 30.7 (2008) 557–565. doi:10.1016/j.cemconcomp.2008.03.002.

[58]    J. Branston, S. Das, S.Y. Kenno, C. Taylor, Influence of basalt fibres on free and restrained plastic shrinkage, Cem. Concr. Compos. 74 (2016) 182–190. doi:10.1016/j.cemconcomp.2016.10.004.

[59]    P. Soroushian, F. Mirza, A. Alhozaimy, Plastic shrinkage cracking of polypropylene fiber-reinforced concrete, ACI Mater. J. 92.5 (1995) 553–560.

[60]    F. Sayahi, Plastic shrinkage cracking in concrete, Luleå University of Technology, 2016. doi:10.3929/ETHZ-B-000249246.

[61]    P.J. Uno, Plastic shrinkage cracking and evaporation formulas, ACI Mater. J. 95.4 (1998) 365–375.

[62]    Z. Bayasi, M. Mclntyre, Application of fibrillated PP fibres for restraint of plastic shrinkage cracking, ACI Mater. J. 99 (2002) 337–343.

[63]    E. Boghossian, L.D. Wegner, Use of flax fibres to reduce plastic shrinkage cracking in concrete, Cem. Concr. Compos. 30.10 (2008) 929–937. doi:10.1016/j.cemconcomp.2008.09.003.

[64]    ASTM C1579-13, Standard Test Method for Evaluating Plastic Shrinkage Cracking of Restrained Fiber Reinforced Concrete (Using a Steel Form Insert), (2013) 1–7. doi:10.1520/C1579-06.2.

[65]    P.P. Kraai, A proposed test to determine the cracking potential due to drying shrinkage of concrete, Concr. Constr. 30.9 (1985) 775–778.

[66]    H. Najm, P. Balaguru, Effect of large-diameter polymeric fibers on shrinkage cracking of cement composites, ACI Mater. J. 99.4 (2002) 345–351.

[67]     N. Banthia, C. Yan, Shrinkage cracking in polyolefin fiber-reinforced concrete, ACI Mater. J. 97.4 (2000) 432–437.

[68]     A. Mazzoli, S. Monosi, E.S. Plescia, Evaluation of the early-age-shrinkage of Fiber Reinforced Concrete (FRC) using image analysis methods, Constr. Build. Mater. 101.1 (2015) 596–601. doi:10.1016/j.conbuildmat.2015.10.090.

[69]     K. Wang, S.P. Shah, P. Phuaksuk, Plastic shrinkage cracking in concrete materials - Influence of fly ash and fibers, ACI Mater. J. 98.6 (2001) 458–464.

[70]     C.A. Juarez, G. Fajardo, S. Monroy, A. Duran-Herrera, P. Valdez, C. Magniont, Comparative study between natural and PVA fibers to reduce plastic shrinkage cracking in cement-based composite, Constr. Build. Mater. 91 (2015) 164–170. doi:10.1016/j.conbuildmat.2015.05.028.

[71]     P. Zhao, A.M. Zsaki, M.R. Nokken, Using digital image correlation to evaluate plastic shrinkage cracking in cement-based materials, Constr. Build. Mater. 182 (2018) 108–117. doi:10.1016/j.conbuildmat.2018.05.239.

[72]     M.R. Jahanshahi, S.F. Masri, C.W. Padgett, G.S. Sukhatme, An innovative methodology for detection and quantification of cracks through incorporation of depth perception, Mach. Vis. Appl. 24 (2013) 227–241. doi:10.1007/s00138-011-0394-0.

[73]     S. Lee, J. Won, Shrinkage characteristics of structural nano-synthetic fibre-reinforced cementitious composites, Compos. Struct. 157 (2016) 236–243. doi:10.1016/j.compstruct.2016.09.001.

[74]     G.M. Sadiqul Islam, S. Das Gupta, Evaluating plastic shrinkage and permeability of polypropylene fiber reinforced concrete, Int. J. Sustain. Built Environ. 5.2 (2016) 345–354. doi:10.1016/j.ijsbe.2016.05.007.

[75]     N. Banthia, R. Gupta, Plastic shrinkage cracking in cementitious repairs and overlays, Mater. Struct. 42.5 (2009) 567–579. doi:10.1617/s11527-008-9403-9.

[76]     C. Qi, J. Weiss, J. Olek, Characterization of plastic shrinkage cracking in fiber reinforced concrete using image analysis and a modified Weibull function, Mater. Struct. 36.6 (2003) 386–395. doi:10.1007/BF02481064.

[77]     C. Liu, C.-S. Tang, B. Shi, W.-B. Suo, Automatic quantification of crack patterns by image processing, Comput. Geosci. 57 (2013) 77–80. doi:10.1016/j.cageo.2013.04.008.

[78]     L. Ruiz-Ripoll, B.E. Barragán, S. Moro, J. Turmo, Digital imaging methodology for measuring early shrinkage cracking in concrete, Strain. 49 (2013) 267–275. doi:10.1111/str.12034.

[79]     S. Ghourchian, M. Wyrzykowski, L. Baquerizo, P. Lura, Susceptibility of Portland cement and blended cement concretes to plastic shrinkage cracking, Cem. Concr. Compos. 85 (2018) 44–55. doi:10.1016/j.cemconcomp.2017.10.002.

[80]     M. Némoz-Gaillard, D. Nectoux, E. Dallies, D. Muller, Influence of AR glass fibers on the cracking of concrete : analysis at the very early age by digital image correlation, in: PRO 23 Int. RILEM Conf. Early Age Crack. Cem. Syst., 2002: pp. 237–244.

[81]     P. Zhao, Master thesis. Digital Image Correlation to Evaluate Plastic Shrinkage Cracking in Cement-Based Materials, Concordia University, Montreal, Canada, 2016.

[82]     A. Messan, P. Ienny, D. Nectoux, Free and restrained early-age shrinkage of mortar: Influence of glass fiber, cellulose ether and EVA (ethylene-vinyl acetate), Cem. Concr. Compos. 33.3 (2011) 402–410. doi:10.1016/j.cemconcomp.2010.10.019.

[83]     T. Mauroux, F. Benboudjema, P. Turcry, A. Aït-Mokhtar, O. Deves, Study of cracking due to drying in coating mortars by digital image correlation, Cem. Concr. Res. 42.7 (2012) 1014–1023. doi:10.1016/j.cemconres.2012.04.002.

[84]     E. Roziere, R. Cortas, A. Loukili, Tensile behaviour of early age concrete: New methods of investigation, Cem. Concr. Compos. 55 (2015) 153–161. doi:10.1016/j.cemconcomp.2014.07.024.

[85]     E.D. Dzaye, E. Tsangouri, K. Spiessens, G. De Schutter, D.G. Aggelis, Digital image correlation (DIC) on fresh cement mortar to quantify settlement and shrinkage, Arch. Civ. Mech. Eng. 19 (2019) 205–214. doi:10.1016/j.acme.2018.10.003.

[86]     I.M.G. Bertelsen, L.M. Ottosen, G. Fischer, Quantitative analysis of the influence of synthetic fibres on plastic shrinkage cracking using digital image correlation, Constr. Build. Mater. 199 (2019) 124–137. doi:10.1001/archinte.168.13.1371.

[87]     I.M.G. Bertelsen, C. Kragh, G. Cardinaud, L.M. Ottosen, G. Fischer, Quantification of plastic shrinkage cracking in mortars using digital image correlation, Cem. Concr. Res. 123 (2019) 105761. doi:10.1016/j.cemconres.2019.05.006.

[88]	C.G. Berrocal, I. Löfgren, K. Lundgren, N. Görander, C. Halldén, Characterisation of bending cracks in R/FRC using image analysis, Cem. Concr. Res. 90 (2016) 104–116. doi:10.1016/j.cemconres.2016.09.016.

[89]	B. Pan, K. Qian, H. Xie, A. Asundi, Two-dimensional digital image correlation for in-plane displacement and strain measurement: a review, Meas. Sci. Technol. 20.6 (2009) 062001. doi:10.1088/0957-0233/20/6/062001.

[90]	M.A. Sutton, J.J. Orteu, H. Schreier, Image correlation for shape, motion and deformation measurements: basic concepts, theory and applications, Springer Science & Business Media, 2009.

[91]	A. Gheitasi, D.K. Harris, M. Hansen, An experimental-computational correlated study for describing the failure characteristics of concrete across two scale levels : Mixture and structural component, Exp. Mech. (2018) 11–32. doi:10.1007/s11340-017-0319-6.

[92]	W.P. Boshoff, F. Altmann, C.J. Adendorff, V. Mechtcherine, A new approach for modelling the ingress of deleterious materials in cracked strain hardening cement-based composites, Mater. Struct. 49.6 (2016) 2285–2295. doi:10.1617/s11527-015-0649-8.

[93]	I. Maruyama, H. Sasano, M. Lin, Impact of aggregate properties on the development of shrinkage-induced cracking in concrete under restraint conditions, Cem. Concr. Res. 85 (2016) 82–101. doi:10.1016/j.cemconres.2016.04.004.

[94]	I. Paegle, F. Minelli, G. Fischer, Cracking and load-deformation behavior of fiber reinforced concrete: Influence of testing method, Cem. Concr. Compos. 73 (2016) 147–163. doi:10.1016/j.cemconcomp.2016.06.012.

[95]	E.D. Dzaye, G. De Schutter, D. Aggelis, Monitoring fresh cementitious material by digital image correlation ( DIC ), in: SynerCrete18, 2018: pp. 267–272.

[96]	D. Lecompte, A. Smits, S. Bossuyt, H. Sol, J. Vantomme, D. Van Hemelrijck, A.M. Habraken, Quality assessment of speckle patterns for digital image correlation, Opt. Lasers Eng. 44.11 (2006) 1132–1145. doi:10.1016/j.optlaseng.2005.10.004.

[97]	Y.L. Dong, B. Pan, A review of speckle pattern fabrication and assessment for digital image correlation, Exp. Mech. 57 (2017) 1161–1181. doi:10.1007/s11340-017-0283-1.

[98]	E.D. Dzaye, G. De Schutter, D. Aggelis, Application of digital image correlation to cement paste, in: Proceedings. Eighteenth Int. Conf. Exp. Mech., 2018. doi:10.3390/ICEM18-05332.

[99]	S. Ghourchian, M. Wyrzykowski, L. Baquerizo, P. Lura, Performance of passive methods in plastic shrinkage cracking mitigation, Cem. Concr. Compos. 91 (2018) 148–155. doi:10.1016/j.cemconcomp.2018.05.008.

[100]	F. Benboudjema, T. Mauroux, P. Turcry, A. Ait-Mokthar, O. Deves, Experimental Analysis of Drying Shrinkage Cracking in Coating Mortars by Digital Image Correlation, in: 2013. doi:10.1061/9780784413111.027.

[101]	Z. Zheng, D. Feldman, Synthetic fibre-reinforced concrete, Prog. Polym. Sci. 20 (1995) 185–210. doi:10.1016/0079-6700(94)00030-6.

[102]	H. Houben, H. Guillaud, Earth Construction: A Comprehensive Guide, Intermediate Technology, 1993.

[103]	UNI/EN-196-1, Methods of testing cement – Part 1 : Determination of strength, (2005).

[104]	ASTM C1018-02, Standard Test Method for Flexural Toughness and First-Crack Strength of Fiber-Reinforced Concrete ( Using Beam With, 04 (1998) 1–8. doi:10.1520/D3762-98.

[105]	K. Kobayashi, R. Cho, Flexural behaviour of polyethylene fibre reinforced concrete, Int. J. Cem. Compos. Light. Concr. 3 (1981) 19–25.

[106]	N. Banthia, R. Gupta, Test method for evaluation of plastic shrinkage cracking in fiber-reinforced cementitious materials, Exp. Tech. 31.6 (2007) 44–48. doi:10.1111/j.1747-1567.2007.00191.x.

[107]	B. Nabil, A. Aissa, B.I. Aguida, Use of a New Approach (Design of Experiments Method) to Study Different Procedures to Avoid Plastic Shrinkage Cracking of Concrete in Hot Climates, J. Adv. Concr. Technol. 9.2 (2011) 149–157. doi:10.3151/jact.9.149.

[108]	L. Bertolini, B. Elsener, P. Pedeferri, E. Redaelli, R.B. Polder, Corrosion of Steel in Concrete: Prevention, Diagnosis,

Repair, 2013. https://books.google.com/books?id=7B9sug5DDHkC&pgis=1.

[109]  C.G. Berrocal, I. Löfgren, K. Lundgren, L. Tang, Corrosion initiation in cracked fibre reinforced concrete: Influence of crack width, fibre type and loading conditions, Corros. Sci. 98 (2015) 128–139. doi:10.1016/j.corsci.2015.05.021.

[110]  F. Lagier, X. Jourdain, C. De Sa, F. Benboudjema, J.B. Colliat, Numerical strategies for prediction of drying cracks in heterogeneous materials: Comparison upon experimental results, Eng. Struct. 33.3 (2011) 920–931. doi:10.1016/j.engstruct.2010.12.013.

[111]  Ł. Skarzynski, J. Kozicki, J. Tejchman, Application of DIC technique to concrete — study on objectivity of measured surface displacements, Exp. Mech. (2013) 1545–1559. doi:10.1007/s11340-013-9781-y.

# Own publications (Appendix I-VII)

Bertelsen, I. M. G., Ottosen, L. M., & Fischer, G. (2020). Influence of fibre characteristics on plastic shrinkage cracking in cement-based materials: A review. *Construction and Building Materials, 230.* https://doi.org/10.1016/j.conbuildmat.2019.116769.

Bertelsen, I. M. G., Kragh, C., Cardinaud, G., Ottosen, L. M., & Fischer, G. (2019). Quantification of plastic shrinkage cracking in mortars using digital image correlation. *Cement and Concrete Research, 123.* doi:10.1016/j.cemconres.2019.05.006.

Bertelsen, I. M. G., Ottosen, L. M., & Fischer, G. (2019). Quantitative analysis of the influence of synthetic fibres on plastic shrinkage cracking using digital image correlation. *Construction and Building Materials*, *199*, 124–137. http://doi.org/10.1001/archinte.168.13.1371

Bertelsen, I. M. G., Ottosen, L. M., & Fischer, G. (2019). Influence of recycled fibre reinforcement on plastic shrinkage cracking of cement-based composites. In *RILEM International Conference on Sustainable Materials, Systems and Structures*.

Bertelsen, I. M. G., & Ottosen, L. M. (n.d.). Recycling of waste polyethylene fishing nets as fibre reinforcement in gypsum-based composites. *Submitted.*

Bertelsen, I. M. G., Belmonte, L. J., & Ottosen, L. M. (2019). Adobe bricks of Greenlandic fine-grained rock material. In *3rd International Conference on Bio-Based Building Materials*.

Bertelsen, I. M. G., & Ottosen, L. M. (n.d.). Applications for recycled polyethylene fibres from discarded fishing nets in cement-based materials.

# Appendix I

**Title:** Influence of fibre characteristics on plastic shrinkage cracking in cement-based materials: A review

# Influence of fibre characteristics on plastic shrinkage cracking in cement-based materials: A review

I.M.G. Bertelsen, L.M. Ottosen[a], G. Fischer[a]

Technical University of Denmark, Department of Civil Engineering

E-mail: imgber@byg.dtu.dk

**Abstract**

Plastic shrinkage cracking in cement-based materials may occur at early age and the formation can negatively impact the long-term durability. A detailed review on existing research related to plastic shrinkage cracking is hereby presented including comparisons of laboratory-scale evaluation methods, crack measuring techniques and the influence of various types of fibres. The use of randomly distributed fibres for controlling plastic shrinkage cracking has shown good results and several fibres of different materials, mechanical properties, geometries, shapes, and volume fractions have been presented in the literature. These fibre characteristics were analysed on data from previous studies by descriptive statistics. From this analysis, many relevant fibre characteristics were discovered to have a positive influence on controlling crack formation. These positive effects were found for fibres with a finer fibre diameter, a higher aspect ratio, an increase in number of fibres per volume unit and specific fibre surface as well as the influence of chemical and mechanical interfacial fibre-to-matrix bonds. Also the increase in fibre volume fraction was found to have a positive effect when added to the mixture at an upper limit. No clear correlation was found between the fibre influence on the degree of surface cracking and the fibre length or the fibre modulus.

**Keywords:** Plastic shrinkage cracking; Fibre characteristics; Experimental techniques; Crack measurements

## 1    Introduction

Severe early-age cracking, which compose of the combined effects of plastic settlement, plastic shrinkage and autogenous shrinkage, is not only aesthetically undesirable, but can also affect the long-term durability of concrete structures [1]. The cracks may propagate further during drying and allow the ingress of aggressive agents such as water and chlorides leading to corrosion of the steel rebars and premature deterioration of the structure [2,3]. The volume

27  changes that occur before the hardening of cement-based materials can be divided into different phases [4,5]. First,

28  bleeding water begins to rise to the surface while the solid particles settle, which results in plastic settlement [6].

29  Secondly, plastic shrinkage deformations begin while the layer of bleeding water gradually evaporates, whereupon water

30  menisci form between the solid particles and the capillary pressure starts to build-up. The capillary pressure results in the

31  contraction of the plastic materials and if a critical limit is reached, cracks may start to form. It is generally considered

32  that precautions regarding plastic shrinkage cracking should be taken when the loss of mixing water from the fresh

33  material exceeds the bleeding water. The loss of mixing water is mainly due to water evaporation from the surface but

34  can also be a result of moisture absorption at the interface with underlying materials [7]. Hence, the formation of plastic

35  shrinkage cracks is highly dependent on parameters such as the environmental conditions during the first few hours after

36  casting, the material composition, the geometry of the structure and the on-site building practices [8]. Specific

37  environmental conditions such as low relative humidity, elevated temperatures, solar radiation and exposure to high wind

38  flows are enhancing a high rate of evaporation and are known to make the cement-based material more susceptible to

39  plastic shrinkage cracking [9]. When the cement-based material is plastic, the tensile strength is very low, but while the

40  material hydrates it gains strength the risk of cracking is continuously reduced [2]. Some of the early-age volume

41  changes are also related to autogenous shrinkage (shrinkage due to chemical reactions and cement hydration) [10,11].

42  However, these deformations are, depending on the material composition and mixture proportions, generally considered

43  to have a small influence on the total degree of shrinkage at this early age for mixtures with a high w/c-ratio exposed to a

44  high evaporation rate [4,5].

45  Plastic shrinkage cracking is mostly a concern for concrete structures with large surface area to volume ratios such as

46  bridge decks, parking slabs, industrial floors, tunnel linings and thin concrete surface repairs. Unrestrained plastic

47  shrinkage is normally not leading to any crack formation, because the material is allowed to deform freely. However,

48  concrete structures are almost always restrained either internally or externally, with the restraints arising from steel

49  rebars, large aggregates, underlying surface, support conditions, non-uniform drying or differential shrinkage [1,12,13].

50  **1.1    Precautionary measures**

51  The literature describes several precautionary measures for preventing plastic shrinkage cracking in cement-based

52  materials. The most effective technique for mitigating plastic shrinkage cracking is by preventing the water evaporating

53  from the surface. Thus, preventing the surface from extensive drying [7,12,14]; e.g. by controlling the environmental

54  conditions during casting [14,15], by reducing the evaporation rate from the fresh material by covering the surface or

55  applying curing compound [15], and by applying correct surface finishing operations [12,16,17]. If the moisture loss

56  cannot be reduced to the desired level in the early stages after casting, other mitigation strategies can be applied. The

57  addition of randomly distributed fibres [2,7,13,18] or shrinkage reducing admixtures (SRA) [10] are known to be

58  especially effective. In the present study, the emphasis is on the influence of randomly distributed fibres on cracking

59  caused by plastic shrinkage. Therefore, the influence of other crack mitigating strategies is not within the scope of this

60  paper and will not be discussed further.


61  *1.1.1   Fibre mechanisms in controlling plastic shrinkage cracking*

62  The addition of randomly distributed fibres is a widely accepted technique for controlling plastic shrinkage cracking but

63  the exact role of the fibres and the mechanisms related to controlling the crack formation is still a topic of discussion. The

64  literature describes hypotheses, of which some are related to the fibre influence on the properties of the fresh material

65  matrix:

66  ▪ The role of adding fibres is reported not only to reduce crack formation, but to disperse the cracks so that many micro

67  cracks appear instead of fewer larger ones by improving the strain capacity of the fresh mixture [12].

68  ▪ The fibres are mitigating the micro crack propagation from developing into actual plastic shrinkage cracks by

69  providing bridging forces across the cracks to prevent crack propagation [12,13,17,19].

70  ▪ Some types of fibres have also been shown to increase the early-age tensile strength of the material [20], thus

71  lowering the possibilities for the stresses to reach the strength of the fresh cement-based material [1].

72  ▪ Fibres added to the fresh mixture tend to reduce the segregation of especially coarser aggregates, which therefore tend

73  to remain closer to the surface [12,17]. Extensive segregation could also lead to an uneven fibre distribution [21].

74  Wang et al. [4] observed that fine fibres had a better distribution inside the matrix than coarser fibres with a high

75  density (e.g. steel fibres), which tended to segregate.

76  Since the formation of plastic shrinkage cracking is closely correlated with the water evaporation rate, many studies also

77  investigated the fibre influence on the degree of moisture loss and bleeding. However, there seem to be some

78  contradictions in the literature. Some studies reported that fibres tend to reduce the quantity of bleeding water by

79  reducing segregation, which succeeds in lower water evaporation rates [12,17,22]. On the contrary, other studies reported

80  higher water evaporation rates that were attributed to the development of so-called bleeding channels along the fibres

81  [3,23–26]. These channels are suggested to allow mixing water arising to the surface, which supplies water to replenish

82  the drying surface.

83  It is demonstrated in several studies that fibres with a variety of materials and characteristics can be beneficial on the

84  early-age cracking behaviour. These beneficial effects of adding fibres to control early-age cracking were also observed

85  for autogenous shrinkage [11]. The studied fibre materials mainly include various types of polymeric materials, but also

86  fibres of materials such as steel, carbon, glass, basalt and natural fibres. Despite that most studies concluded that the

87  investigated fibre type was successful in controlling the degree of plastic shrinkage cracking, there is no conclusive

88  finding on which fibre properties are most influential. Hence, the focus of this study is to reveal tendencies on which

89  fibre properties that are influencing the formation of plastic shrinkage cracking.


90  **1.2    Research objective and outline**

91  The aim of this study is to review existing literature on experimental testing of restrained plastic shrinkage cracking in

92  cement-based materials and the influence of fibre additions on controlling the degree of cracking. The literature presents

93  various fibre types and experimental test methods, at which some are evaluated in the present study. The properties of

94  fibres from previous studies are included in a database containing information about the fibre material, fibre volume

95  fraction, geometry (shape, length, width, and aspect ratio), and mechanical properties (tensile strength and modulus). The

96  results on the fibre efficiency are presented as the crack reduction ratio (CRR) for the total crack area (TCA) or the

97  maximum crack width (MCW) on the surface of cement-based specimens. This data is illustrated in various plots in

98  Section 3, and includes an evaluation of the efficiency of various fibre properties in controlling plastic shrinkage cracking

99  carried out by analysing this data by descriptive statistics.


100  **2    Materials and methods**


101  **2.1    Experimental test methods**

102  Test methods intended for studying restrained plastic shrinkage cracking in cement-based materials presents various

103  types of internal or external restraints, which induce cracking by preventing the specimen from deforming freely. Some

104  of the techniques for experimental testing of restrained plastic shrinkage presented in the literature include:

105  ▪ Slab- or prism-like specimens with bottom-restraints made by casting the fresh material on top of an underlying

106      concrete substrate or other types of rough underlay (e.g. as suggested by Banthia & Gupta [7]).

107  ▪ A test method initially proposed by Kraai [27] suggests the use of thin slab-like panels with edge-restraints along the

108      entire periphery of the mould.

109   ▪ The ASTM standard C1579 [28] suggest the use of a larger mould with internal restraints formed as three triangular

110      stress risers providing one-dimensional restraints causing localized stress zones above the central stress riser.

111   ▪ The standards NT Build 433 [29] and ASTM C1581 [30] suggest the use of a ring-shaped steel mould with an inner

112      restraining ring.

113   ▪ Linear specimens with restrained ends have also been proposed in the literature for studying specimens exposed to

114      one-dimensional restraining conditions [31,32].

115   Because these test methods present a broad range of crack patterns due to the very different types of restraining

116   conditions, the different methods can be a subject to different interpretations of the obtained results  [3]. Also, it is still a

117   challenge to produce repeatable crack patterns on relatively small laboratory specimens, and the efficiency of the

118   different methods is repeatedly under discussion.



                  (a)              (b)                (c)                    (d)
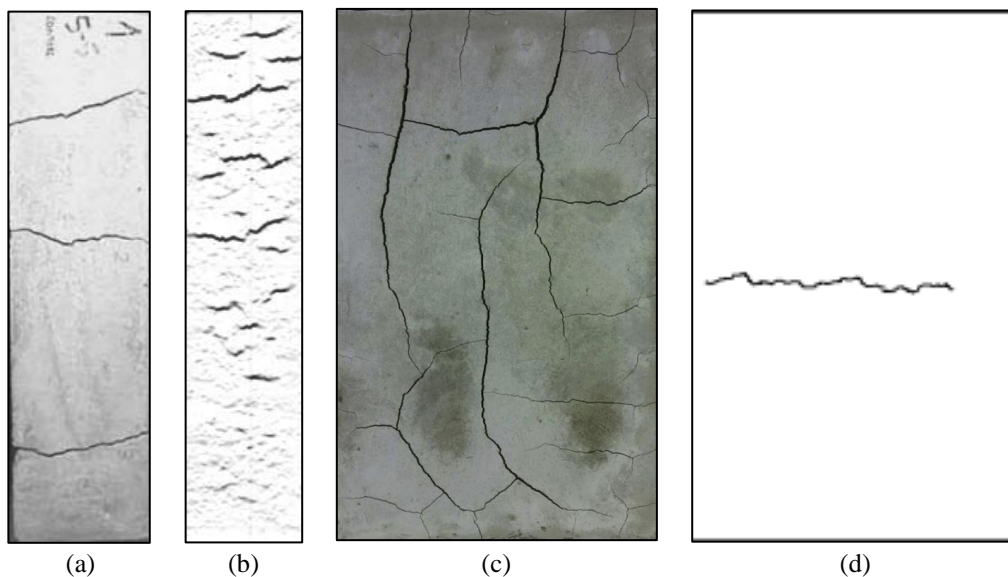
119   *Figure 1. Typical plastic shrinkage crack patterns obtained by laboratory-scale testing using different test methods: a)*
120   *Mortar overlay cast on concrete substrate with spherical protuberances (exposed surface area: 100 x 375 mm$^2$) [33];*
121   *b) Mortar overlay cast on top of concrete substrate with rough surface (95 x 420 mm$^2$) [34]; c) Kraai method (600 x*
122   *900 mm$^2$) [35]; d) ASTM C1579 method (355 x 560 mm$^2$) [36]*
123

124   To enable a comprehensive analysis of results obtained in previous studies for further evaluation of the influence of

125   different fibre types, specific requirements were defined for the selection of studies:

126   ▪ Studies applying restrained shrinkage tests as either the Kraai method [27], the ASTM C1579 method [28] or

127      one of the overlay methods using bottom-restraints were included in this review.

128   ▪ Information about test setup and crack measuring techniques.

129   ▪ Information about fibre characteristics (material, geometry, volume fraction and mechanical properties).

130        ▪   Results on basic crack parameters such as the total crack area (TCA) and/or maximum crack width (MCW)

131            when available.

132   Based on these requirements, 25 studies were selected for a detailed comparison and data analysis. All three selected test

133   methods are useful for studying the efficiency of fibres added to a cement-based material. In the subsequent sections and

134   in Table 1, the concepts of the three test methods and selected studies are described with respect to the geometry,

135   materials, casting methods and environmental conditions. Typical crack patterns obtained by using one of the three types

136   of test methods are illustrated in Figure 1. The figures clearly illustrate the large differences in size and shape of the crack

137   patterns.

138   *2.1.1   Overlay method with bottom-restraints*

139   Several methods have been presented in the literature where a fresh cement-based overlay is cast on top of an underlying

140   substrate or rough surface to provide uniform bottom-restraints. These methods aim at designing the bottom-restraints to

141   simulate realistic restraining conditions, but since there has still not been a standardized method approved for this type of

142   restrained shrinkage test, it results in great variations in both the specimen geometry, type of restraints and the

143   environmental conditions within studies using this type of method. The literature reports geometries for the restraints

144   such as spherical protuberances [1,7,20,33,37,38], quadratic protuberances (notched surface) [2,15], roughened concrete

145   surface [34,39], sheet of sandpaper placed in the bottom of the mould [4,40], and aggregates sticking up from the

146   substrate surface placed during casting [21,41]. Two examples of very different crack patterns obtained with two

147   variations of the overlay methods are shown in Figure 1(a,b).

148   *2.1.2   Kraai method with edge-restraints*

149   The method developed by Kraai [27] proposes a slab-like specimen cast in a mould with built-in edge-restraints provided

150   along the perimeter. The test specimen is rather thin with a large surface area to volume ratio making it vulnerable to

151   plastic shrinkage cracking as intended. This method often results in scattered crack patterns as shown in Figure 1c. The

152   slab dimensions are commonly reported to be approximately 900 x 600 x 19 mm, but modifications of both the thickness,

153   width and length of the slab was encountered in the literature [12,17–19,24,42]. The edge-restraints installed along the

154   entire perimeter of the mould consist of L-shaped hardware cloth/wire mesh [27,43,44], horizontal bolts [45,46] or steel

155   blocks placed on the bottom of the mould with a fixed distance [19,35,42]. One study reported that the perimeter restraint

156   was not successful in eliminating the movement of the slab completely [18]. Because of the small height of the slab, the

157 method is commonly used for testing cement or mortar materials and not concrete, since the coarse aggregates in

158 concrete would possibly introduce internal restraints in the matrix. The influence of the slab dimensions (surface area and

159 thickness) were studied by Balaguru [18] and it was observed that larger slab thickness allowed testing concrete mixtures

160 instead of only mortar mixtures.

161 *2.1.3    ASTM C1579 method with stress risers*

162 The ASTM standard C1579 [28], prescribes the use of a mould with the dimensions 560 x 355 x 100 mm with restraints

163 provided by three triangular steel stress risers placed inward from each end (height of $64 \pm 2$ mm (centre), and $32 \pm 1$ mm

164 (sides)). The stress risers are producing a localized stress zone that induces cracking in a single line above the central

165 stress riser. Deviations from the geometry proposed in the ASTM C1579 standard involves the geometry of the stress

166 risers, mould and additional restraints [23,25,47–49]. Some studies reported the need for additional restraints in the

167 mould, since the stress risers alone were not successful in restraining the specimens to an extent that facilitated plastic

168 shrinkage cracking [47], especially if the environmental conditions were less severe than those prescribed in the standard.

169 These advancements included rebars or bolts mounted in each side of the mould parallel to the stress risers [43,48,50],

170 and bolts with nuts mounted at each end of the mould [23,47,49]. This method is especially effective for studying plastic

171 shrinkage cracking of concrete under laboratory-scale conditions, because of the repeatability in cracking behaviour

172 occurring in the same line above the central stress riser in every experiment [36]. However, the method does not simulate

173 scattered crack patterns and neither provides information about the crack width distribution.

174

175 *Table 1. Details of the experimental test setups in the studies included in this review. T = Temperature, RH = Relative*
176 *humidity, Wind = Wind flow over specimen surface, Evaporation rate from cement-based material or pan of water*

| Ref. | Specimen size (t x b x l) | Environmental conditions | Crack measuring technique |
|---|---|---|---|
| **Studies using one of the overlay methods with bottom-restraints** | | | |
| [7] | Mortar overlay: 60 x 100 x 375 mm Concrete substrate (surface with protuberances): 40 x 95 x 325 mm + two M10 rebars | T = $50 \pm 1$°C RH = 5% Wind = N/A (Heater/fan) Evaporation = 0.80 kg/m$^2$/h | (A) Cracks measured using a high magnification microscope with an accuracy of 0.01 mm. |
| [2] | Concrete overlay: 38.1 x 76.2 x 1016 mm Concrete substrate (notched surface): 38.1 x 76.2 x 1016 mm | T = 35-41 °C RH = $22.5 \pm 2.5$% Wind = N/A (fans) Evaporation = N/A | (A) Crack width and length were measured using a crack comparator and a handheld microscope during the test (until 8 h), and with a microscope after 24 h. |
| [20] | Mortar overlay: 60 x 100 x 375 mm Concrete substrate (surface with protuberances): 40x95x325 mm + two M16 rebars | T = $45 \pm 2$°C RH = < 3% Wind = 1.03 m/s Evaporation = 1.0 kg/m$^2$/h | (A) Cracks measured after 24 h. Crack length measured to the nearest 1 mm using a string. Crack width measured at three locations per crack with a hand-held 0.01 mm precision microscope. |

| | | | |
|---|---|---|---|
| [41] | Mortar overlay:<br>70 x 200 x 1000 mm<br>Substrate (surface with 40 mm aggregates):<br>50x150x1000 mm + grid of steel rebars | T = 40 ± 2°C<br>RH = 32 ± 2 %<br>Wind = 1.39 m/s<br>Evaporation = 1.1 kg/m²/h | (A) Crack width measured using a 0.02 mm precision microscope every 10 min until stabilization was reached. |
| [1] | Mortar overlay: 35 x 100 x 550 mm<br>Substrate (surface with protuberances): 40 x 95 x 500 mm | T = 48 ± 2 °C<br>RH = 15 ± 3%<br>Wind = N/A (heater/fan)<br>Evaporation = 0.75 kg/m²/h | (A) Cracks measured using a 240x magnification digital microscope after 4 h. |
| [21] | Concrete overlay: 60 x 95 x 980 mm<br>Concrete substrate (surface with 25 mm aggregates): 40 x 95 x 980 mm + two M15 rebars | T = 38 °C<br>RH = 5%<br>Wind = 340 cfm = 0.16 m³/s<br>Evaporation = 0.8 kg/m²/h (w)** | (A) Continuous recording of crack width to the nearest 50 µm with 10x microscope. Crack length measured using a string to the nearest 5 mm. |
| [34] | Mortar overlay: 10 x 95 x 420 mm<br>Precast concrete substrate (roughened surface): 50 x 94 x 418 mm | T = 32 ± 1.5 °C<br>RH = 33.5 ± 5%<br>Wind = 3.9-4.5 m/s<br>Evaporation = 0.5 kg/m²/h | (B) DIC: Images captured continuously of specimen surface. Crack dimensions measured using DIC software + post-processing in MATLAB. |
| [4] | Cement overlay: 8 x 100 x 100 mm<br>Restraint provided by fine sandpaper | T = 40 °C<br>RH = 18%<br>Wind = 0.8-1.4 m/s<br>Evaporation = N/A | (B) Image analysis.<br>Mercury-intrusion porosimeter (MIP) was used to analyse the structure of the pastes |

**Studies using the Kraai method [27] with edge-restraints**

| | | | |
|---|---|---|---|
| [44] | 19 x 600 x 900 mm<br>Strip of 12.5x25 mm steel wire mesh along edge | T = 22-23°C<br>RH = 50 %<br>Wind = 5-6 m/s<br>Evaporation = N/A | Crack length and width were measured after 24 h and grouped into categories (3, 2, 1, 0.5 mm). No info about measuring technique. |
| [19] | 150* x 600 x 900 mm<br>Restraints per 100 mm along the edge | T = 28 ± 2°C<br>RH = 40 ± 3 %<br>Wind = 6 m/s<br>Evaporation > 0.5 kg/m²/h | N/A |
| [12] | 38 x 533 x 838 mm<br>No info about restraints | T = 24-27 °C<br>RH = 50 ± 5 %<br>Wind = 3.6 m/s<br>Evaporation=0.5-0.65 kg/m²/h | (A) Crack initiation reported by visual inspection. Cracks were measured using optical lenses after 5 h. |
| [24] | 40 x 540 x 840 mm<br>No info about restraints | T = 24-27 °C<br>RH = 60 ± 5 %<br>Wind = 5 m/s<br>Evaporation = 0.5-0.7 kg/m²/h | (A) Cracks were measured after 5.5 h. Widths with a hand-held microscope and crack lengths with a planimeter. |
| [43] | Kraai: 19 x 610 x 914 mm<br>L-shaped steel wire mesh provided at 12.7 mm intervals, h = 13 mm | T = 22 ± 2 °C<br>RH = 50 ± 2 %<br>Wind = 6 m/s<br>Evaporation = N/A | Crack lengths and average crack widths were measured after 24 h. No information about measuring technique. |
| [17] | 40 x 530 x 840 mm | T = 17-18 °C<br>RH = ~60 %<br>Wind = Fans<br>Evap. concrete = 0.06 kg/m²/h<br>Evap. water = 0.3 kg/m²/h | (A) Cracks were measured by a hand-held microscope after 5 h. |
| [35] | 15 x 600 x 900 mm.<br>13x13x7 mm restraints per 100 mm | T = 28 ± 2 °C<br>RH = 40 ± 5%<br>Wind = 6 m/s<br>Evaporation = N/A | (A) Cracks were measured after 24 h using a microscope with 0.01 mm accuracy |
| [45] | 100 x 800 x 800 mm<br>with lateral bolts along edge and a roughened wood panel at the bottom | T = 45 °C<br>RH = 75%<br>Wind = 1.94 m/s<br>Evaporation = 0.3-0.54 kg/m²/h | (B) DIP as described in [46] |
| [51] | No information about panel dimensions. | T = 25 ± 1 °C | (A) Handheld microscope after 24 ± 2 h + |

| | | | |
|---|---|---|---|
| | Anchors creating two dimensional restraints. | RH = 50 ± 2%<br>Wind = 2.2 m/s<br>Evaporation = | (B) DIP: Crack measurements based on pixels using ImageJ |
| [52] | 100 x 600 x 900 mm.<br>No info about restraints | T = 24 ± 2 °C<br>RH = 42 ± 3%<br>Wind = 4.5 m/s<br>Evaporation = 0.97 kg/m$^2$/h | (A) Crack width measured by microscope and crack length using a string. |
| [18] | 19 x 600 x 900 mm; (19 x 900 x 900 mm)<br>L-shaped steel wire mesh, h = 12.7 mm | T = 22 ± 1 °C<br>RH = 50 ± 3%<br>Wind = 5.3 m/s<br>Evaporation = N/A | (A) Manual crack measurements |

**Studies using the ASTM C1579 method [28] with stress risers**

| | | | |
|---|---|---|---|
| [23] | 75 x 250 x 500 mm<br>Stress risers: h = 55 mm/35 mm + additional lateral bolts mounted at the short side of the mould | T = 35 ± 1 °C<br>RH = 40 ± 1 %<br>Wind = 6 m/s<br>Evaporation = 0.62 kg/m$^2$/h | (B) DIP: Images captured by optimal camera. Crack measurements based on pixels using image analysis software. |
| [25] | 85 x 360 x 560 mm<br>Stress risers: h = 63.5 mm/32 mm | T = 36 °C<br>RH = 25 %<br>Wind = 6 m/s<br>Evaporation = 2 kg/m$^2$/h (w) | (B) DIP: Images of specimen surface after 24 h. Cracks were analysed using a MATLAB algorithm and crack width measured every 10 pixels along the crack. |
| [53] | 100 x 350 x 560 mm<br>Stress risers: dimensions not given | T = 37 °C<br>RH = N/A<br>Wind = N/A<br>Evaporation = N/A | (A) Images of cracks taken after 24 h + 24 h of additional cooling with a 40x magnification optical microscope and cracks were measured. |
| [43] | ASTM: 100 x 355 x 560 mm<br>Stress risers: h = 63.5mm/32 mm + 4 additional M17 bolts at the end of the mould parallel to the stress risers | T = 40°C<br>RH = N/A<br>Wind = Fans<br>Evaporation = 1.0 kg/m$^2$/h (5.5 h) | (A) Cracking was monitored by visual inspection during the first 6 h. (B) DIP: Images of specimen surface were captured after 24 h using an optical zoom camera at 10 intervals along each crack. Cracks were measured using CAD software. |
| [54] | 100 x 365 x 560 mm<br>Stress risers: h = 63.5mm/32 mm | T = 36.6 °C<br>RH = 20%<br>Wind = 9.5 m/s<br>Evaporation = N/A | (A) Cracks were recorded after 3 h. No information about measuring technique. |
| [55] | 100 x 355 x 560 mm<br>Stress risers: h = 63.5mm/32 mm | T = 42 ± 1 °C<br>RH = 35 ± 2%<br>Wind = 4.5 ± 1 m/s<br>Evaporation = N/A | Crack width measured using a 0.025 mm precision microscope per 10 mm per crack. Crack length measured by placing a thin thread along the crack. |
| [48] | 100 x 200 x 600 mm<br>Stress risers: h = 63.5mm/ 32mm | T = 40 °C<br>RH = 20%<br>Wind = 9.2 m/s<br>Evaporation = 1 kg/m$^2$/h | (B) DIP: Images captured continuously of specimen surface and cracks were measured using CAD software. |

177    * Height of slab is written as 150 mm in the articles, but is shown as 15 mm on the figures [19,42]

178    ** Evaporation rate of water [21,25]

179    *2.1.4    Environmental conditions and evaporation rate*

180    Besides the influence of the type of restraints, the crack formation is also correlated with the degree of water evaporation

181    from the fresh cement-based material. The water evaporation rate mainly depends on the environmental conditions, but

182    also on the absorption from underlying materials and the material composition. Commonly, precautions regarding plastic

183    shrinkage cracking should be taken when all water has evaporated from the surface and enough bleeding water can be

184    supplied [5]. There seems to be a general agreement on a critical evaporation rate of 0.50 kg/m$^2$/h from the specimen

185    surface [7,19] or a minimum evaporation rate of 1.0 kg/h/m$^2$ from a pan of water [28,56]. The evaporation rate is not

186    constant, but gradually slows down alongside with the hardening of the material [19]. Different strategies have been used

187    to obtain evaporation rates sufficiently high for developing plastic shrinkage cracking in laboratory conditions. These are

188    shown in Figure 2 for each of the three chosen test methods. For an overview of the environmental conditions for each of

189    the studies included in this review, see Table 1.
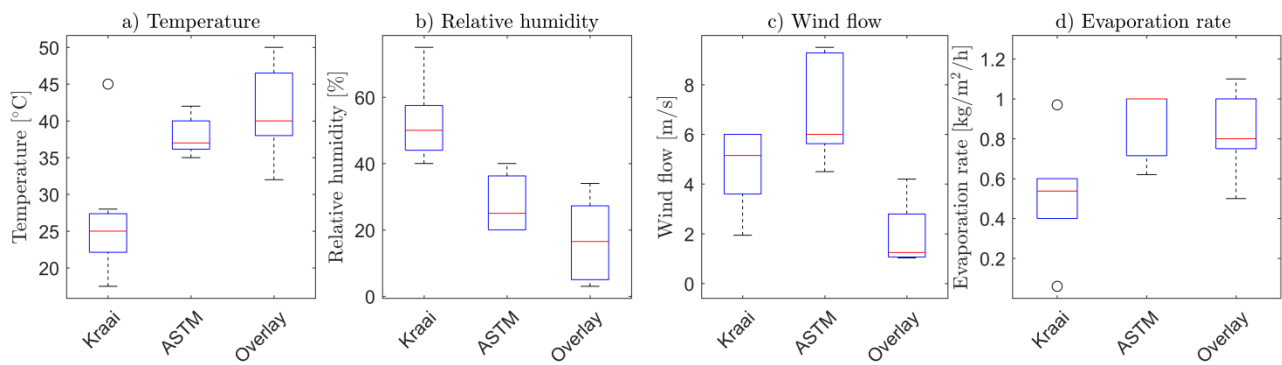


190

191   *Figure 2. Variations in environmental conditions for the three selected test methods a) temperature; b) relative*
192   *humidity; c) wind flow; d) evaporation rate from cement-based material*
193

194    From Figure 2, it is observed that some of the three selected test methods (Overlay with bottom-restraints, Kraai and

195    ASTM C1579) used different strategies to obtain the necessary evaporation rate to promote surface cracking. I.e.

196    elevated temperature (mainly the Overlay methods, but also the ASTM C1579 method), low relative humidity (mainly

197    the Overlay methods, but also the ASTM C1579 method) or high wind flow (both the Kraai method and ASTM C1579

198    method, but in most cases not the Overlay method). The resulting evaporation rates from the specimen surface are shown

199    in Figure 2d. The studies using the Kraai method exposed the specimens to the least harsh environment resulting in the

200    lowest evaporation rates. The highest evaporation rate was found in studies using the ASTM C1579 method. This is in

201    agreement with the fact that the Kraai panels have a large surface area to volume ratio making them more susceptible to

202    plastic shrinkage cracking. The measured rate of water evaporation from the fresh cement-based material in the studies

203    included in this review are ranging from 0.06 kg/m$^2$/h [17] to 1.1 kg/m$^2$/h [41]. An evaporation rate of 0.06 kg/m$^2$/h [17]

204    is significantly lower than the evaporation rates in most other studies, which presumably is a consequence of the low

205    temperatures and high relative humidity used in the experiments. The study still reported that the early-age cracking was

206    due to plastic shrinkage, although some autogenous shrinkage probably also took place. Moreover, elevated temperatures

207    have been reported to may have an influence on the performance of the mechanical fibre properties [18].

208    Newlands [31] investigated the influence of environmental conditions ranging from completely sealed conditions (~20

209    °C temp., >95% RH), to laboratory conditions (~20 °C temp., ~50 % RH) to harsh conditions (~40 °C temp., ~10 % RH).

210    It was concluded that the shrinkage, when exposed to the sealed condition, was mainly attributed to autogenous

211    shrinkage, whereas the two other conditions both were attributed to plastic shrinkage.

212    *2.1.5    Crack measuring techniques*

213    Plastic shrinkage cracking in concrete structures is considered a highly irregular and variable process and, depending on

214    the type of restraint, often results in scattered crack patterns [20,21] as illustrated in Figure 1. The rates at which the

215    cracks occur can vary significantly depending on parameters such as the test setup, material properties, environmental

216    conditions etc. Thus, studying the formation of plastic shrinkage cracking is challenging, since the material properties are

217    time-dependent and change rapidly over time [12]. Banthia & Yan [21] observed that the time from initiation of a crack

218    to the time when the crack had stabilized was as short as 10 min. The crack measuring technique is, therefore, highly

219    relevant for the detection and quantification of the formation of plastic shrinkage cracking. Especially, if the crack

220    propagation over short intervals of time is considered. There is no standardized technique for crack detection and crack

221    measurements; the literature presents both (A) manual measuring techniques using microscopes, handheld lenses etc.;

222    and (B) more advanced image-based techniques such as digital image processing (DIP) and digital image correlation

223    (DIC) [57]. With the more advanced techniques, very fine flaws can theoretically be detected on the surface. Hence, there

224    is also a need for a standardized definition of which fineness of such flaws that should be defined as actual cracks.

225    The manual methods (A) includes the use of various types of optical lenses or microscopes (with precision in the range of

226    0.005 mm to 0.02 mm) [1,2,7,12,20,21,24,37,41,42,53] to measure crack parameters such as the crack width, crack

227    length, spacing etc.. Crack lengths were in some studies measured by placing a string along the entire crack length and

228    measuring its length [20,52,55]. An average value of the crack widths multiplied by the length of the crack is often used

229    for calculating the total crack area, and the accuracy of the results therefore depends on the number of measurements.

230    These manual crack measurements are traditionally carried out at the end of the test period because of the difficulties

231    related to measuring the cracks during the test, although some studies recorded the crack development by actual

232    continuous crack measurements [2,21]. The advantages of using these manual techniques are that they are relatively

233    simple and can be carried out on site. On the contrary, they are criticised for being subjective, time consuming,

234    complicating continuous monitoring, being difficult to apply when studying scattered crack patterns with many fine

235    cracks, and prone to human errors and qualities (experience, expertise etc.) [18,58]. Therefore, more advanced techniques

236    are requested for a more objective quantification of the degree of surface cracking [3,18]. The more advanced image-

237    based techniques (B) include the use of optical cameras for capturing high-resolution images of the specimen surface,

238    which are subsequently processed by different types of software. These techniques allow non-contact optical analysis,

239    continuous monitoring of crack formation over time, and high-precision and objective measuring strategies. The DIP

240    techniques work by processing the images and measuring the crack dimensions based on pixels

241    [3,23,25,37,43,46,48,50,51,59,60]. Other studies on surface cracking of hardened concrete have presented post-

242    processing strategies for analyzing the images and enabling automated crack measurements, which could also be applied

243    for studying plastic shrinkage cracking [58,61]. The DIC technique is considered to be more informative than the DIP,

244    since the technique not only allows automated computation of the crack widths, but also monitoring of surface strain and

245    displacement fields [34,40,56,57,62–67]. However, there are still challenges related to applying the DIC method for

246    studying the plastic shrinkage crack formation, since a high-contrast surface pattern is required for tracking the surface

247    displacements, which is difficult to apply on a wet surface with bleeding water [34,56,67]. Crack widths and other crack

248    parameters can be automatically computed based on the DIC displacement data, allowing quantitative measures of the

249    degree of surface cracking [34,57].


250    *2.1.6    Evaluation of crack measurements*

251    The extent of plastic shrinkage cracking in cement-based specimens is often evaluated based on basic crack parameters

252    such as the total crack area (TCA), the mean or maximum crack width (MCW), and the mean or maximum (MCL) crack

253    length on the specimen surface. The total crack area is commonly calculated as

$$A_{tot,i} = \sum w_{i,avg.} \cdot l_i \qquad \text{(Eq. 1)}$$

254

255    Where $w_{i,avg}$ is the average width of the crack, and $l_i$ the length of the crack. To illustrate the variations in magnitude of

256    some basic crack parameters (TCA, MCW) for the three selected test methods used in the studies included in this review,

257    Figure 3 shows the results obtained for the control specimens without any fibre addition used in each study.
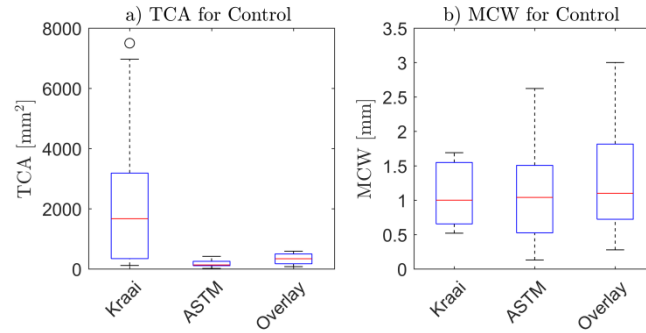
*Figure 3. Variation in total crack area (TCA) and maximum crack width (MCW) for control specimens for the three selected test methods*

Based on Figure 3, it is observed that there are large variations in the results depending on the test method, both with respect to intrinsic variations within each method and among the three test methods. Considering the results for the TCA obtained with the Kraai method, these are significantly larger than the results obtained for the TCA with the two other test methods, the Overlay method and ASTM C1579 method. The design and geometry of the Kraai slab-like specimen makes it highly vulnerable to plastic shrinkage cracking. In some studies, the Kraai method resulted in very large TCA in the range of 3500-7500 mm$^2$ [19,35,43], while other studies applying the Kraai method using relatively similar environmental conditions observed much lower TCA in the range of 100-800 mm$^2$ [12,17,24,44,52]. The variations for the MCW are significantly lower, and the results obtained with the three test methods are all in the same range with very few outliers. It is difficult to compare results obtained in different studies based on such crack parameters (TCA, MCW) because of the large variations in the results. Therefore, to enable a direct comparison of the results obtained in the studies included in this review, the TCA and MCW are converted to a crack reduction ratio (CRR). The CRR is calculated by the following equation in accordance with [28]:

$$CRR\ (TCA) = \left[1 - \frac{A_{tot,fib}}{A_{tot,ctr}}\right] \cdot 100\ \%\ ;$$

$$CRR(MCW) = \left[1 - \frac{W_{max,fib}}{W_{max,ctr}}\right] \cdot 100\ \%$$

(Eq. 2)

Although these basic crack parameters give an indication of the degree of cracking on a specimen surface, they do not provide any information on the crack width distribution (CWD). The CWD enables a more detailed measure of the surface cracking, as it also provides information about the number of cracks within specific crack width intervals. In a previous study conducted by the authors, the degree of surface cracking is presented in such histograms based on numerical post-processing of DIC data [34,57].

279 **2.2    Materials**

280 *2.2.1    Fibres*

281 Various types of fibres with very different properties have been studied with the aim of preventing plastic shrinkage

282 cracking in cement-based materials. The properties of the fibres investigated in the studies included in this review are

283 shown in Table 2. Besides different materials, the studied fibres range over many relevant properties such as fibre shapes

284 (monofilament straight, crimped, embossed, twisted, undulated, hooked-end, fibrillated etc.), geometries (length,

285 diameter, aspect ratio, number of fibres, specific fibre surface), mechanical properties (tensile strength, modulus) and

286 tested volume fraction.

287 As seen in Table 2, it is mainly polymeric fibres that have been studied. These especially include PP

288 [2,4,7,12,15,17,18,20,21,23,25,34,37,42,45,48,50,51,53,55,59,68], but also many other polymeric fibre materials such as

289 polyvinyl acetate (PVA) [2,41,42,51], polyethylene (PE) [2,18,34,53,55], polyethylene terephthalate (PET)

290 [19,43,51,68], polyamid (PA) [18,68], polyester (PES) [23,48], polyacrylonitrile (PAN) [55], and polyolefins (PO)

291 without further specification of the polymer type [21,44]. Polyolefin polymers cover a broader definition of the types of

292 polymers that consist of simple olefin monomer units and cover e.g. PP and PE materials. Fibres reprocessed from

293 different types of polymeric waste materials have also been studied [19,34,43,52,53,69]. Moreover, some studies also

294 tested fibres of natural materials [20,41,54,70], steel [2,21,23–25,42,51], glass [20,23,25,55,68], carbon [2], basalt [1]

295 and hybrid combinations of the above mentioned fibres [23,49].

296

297 *Table 2. Details of the fibres used as reinforcement in the studies included in this review. MF = monofilament*

| Ref. | Material | Shape | Diameter/size (µm) | Length (mm) | Density (kg/m$^3$) | Tensile strength (MPa) | Modulus (GPa) | Fibre content (vol%) |
|---|---|---|---|---|---|---|---|---|
| [7] | PP | MF straight | 20; 30 | 6.35; 12.5 | 900 | N/A | N/A | 0.1-0.3 |
| | PP | Fibrillated | N/A | 12.5 | 900 | N/A | N/A | 0.1-0.3 |
| [2] | PP | MF straight | 68 | 6.35; 12.7; 19.05 | 900 | 821 | 3.5 | 0.05-0.4 |
| | PP | Fibrillated | N/A | 19 | N/A | N/A | N/A | 0.1-0.3 |
| | HDPE | MF straight | 38 | 12.7; 63.5 | 970 | 2585 | 117 | 0.1-0.4 |
| | Carbon | MF straight | 9 | 6.35 | 1900 | 2870 | 24.1 | 0.1-0.4 |
| | Carbon | Cotton-like | 7 | Long | N/A | N/A | N/A | 0.1-0.4 |
| | PVA | MF straight | 14; 40; 100; 197 | 4; 12 | 1300 | 1010-1560 | 20.2; 30; 40 | 0.1-0.4 |
| | Metallic | Rectangular | 175 (eq.) | 15 | 7200 | 1300 | 200 | 0.1-0.4 |
| [20] | PP | Fibrillated | N/A | 19; 38 | 910 | 620-758 | 4-5 | 0.05-0.3 |
| | PP | MF straight | 52 | 19 | 910 | 620-758 | 4-5 | 0.05-0.3 |
| | Flax | MF straight | 10-60 | 10; 19; 38 | 1520 | 840-1500 | 50-100 | 0.05-0.3 |
| | Glass | Rectangular | 200 (eq.) | 18; 40 | 2680 | 1700 | 72 | 0.05-0.3 |
| [41] | Flax | MF straight | 30 | 10; 20; 40 | 1420 | N/A | N/A | 0.1; 0.7 |
| | Lechuguilla | MF straight | 240 | 10; 20; 40 | 1480 | N/A | N/A | 0.1; 0.7 |
| | PVA | MF straight | 10; 40; 100 | 4; 8; 12 | 1300 | N/A | N/A | 0.1; 0.7 |
| [1] | Basalt | Filament | 16 | 12; 25 | N/A | N/A | N/A | 0.05-0.3 |
| | Basalt | Bundle | 16 | 25 | N/A | N/A | N/A | 0.05-0.3 |
| | Basalt | Minibars | 17 | 43 | N/A | N/A | N/A | 0.5; 1.0 |

| Ref | Material | Type | Length | Diameter | Density | Tensile strength | E-modulus | Dosage |
|---|---|---|---|---|---|---|---|---|
| [21] | PO | MF straight | 150; 380, 630 | 19; 25; 50 | 910 | 275 | 2.647 | 0.1-0.7 |
| | PP | Fibrillated | 30 | 55 | N/A | N/A | N/A | 0.1 |
| | Steel | Hooked-end | 500 | 50 | N/A | N/A | N/A | 0.5 |
| [34] | PP | MF straight | 19.5 | 12 | 910 | N/A | N/A | 0.1; 0.2 |
| | R-PE | MF straight | 280 ± 30 | 15 ± 9 | 950 | N/A | N/A | 0.2-2.0 |
| [4] | PVA | MF straight | 14 | 6 | 1300 | 1900 | 41 | 0.1; 0.5 |
| | PP | MF straight | 50 | 13 | 910 | 700 | 5 | 0.1; 0.5 |
| | PP | Fibrillated | - | - | 910 | 700 | 5 | 0.1 |
| | Steel | MF straight | 381 | 12.7 | 7840 | N/A | 210 | 0.1 |
| | Cellulose | MF straight | 15 | 3 | 1500 | 600 | 60 | 0.1 |
| [44] | PO | MF straight | 380; 640; 150 | 25.4; 50.8 | 900 | N/A | N/A | 0.5-3.0 |
| [19] | R-PET | MF straight | 500 x 1000 | 50 | N/A | N/A | N/A | 0.10-1.0 |
| | R-PET | MF Embossed | 200 x 1300 | 50 | N/A | N/A | N/A | 0.10-1.0 |
| | R-PET | MF Crimped | 300 x 1200 | 50 | N/A | N/A | N/A | 0.10-1.0 |
| [12] | PP | Fibrillated | N/A | 13; 19 | 900 | 550-760 | 3.5 | 0.05-0.2 |
| [24] | Steel | MF Hooked-end | L/d=55; 65; 80 | N/A | N/A | N/A | N/A | 0.5-1.5 |
| [17] | PP | Fibrillated | N/A | 6-50 | 910 | N/A | N/A | 0.1; 0.3 |
| [35] | Synthetic | MF Twist/crimp | 600 | 50 | 910 | 579 [71] | N/A | 0.26 |
| | Steel | MF Hooked-end | 750 | 60 | N/A | N/A | N/A | 0.26 |
| [45] | PP macro | MF straight | 75 | 40 | N/A | N/A | N/A | 0.22-0.5 |
| | PP micro | MF straight | 31-35 | 12 | N/A | N/A | N/A | 0.06-0.22 |
| [51] | PP | MF Undulated | 750 | 40 | 910 | 338 | 4.8 | 0.3 |
| | PP | MF embossed | 820 | 54 | 910 | 481 | 5.4 | 0.3 |
| | PP | MF Straight | 430 | 40 | 910 | 620 | 9.5 | 0.3 |
| | PVA | MF smooth | 660 | 50 | 1300 | 800 | 29 | 0.3 |
| | PET | MF embossed | 640 | 52 | 1350 | 238 | 5.5 | 0.3 |
| | Steel | MF Hooked-end | 1050 | 50 | 7800 | 1000 | 210 | 0.3 |
| [52] | Recycled plastic | MF Straight | 500 x 2000 | 20; 50 | 1380 | 310 | 10.2 | 0.5-1.5 |
| [18] | PP | Fibrillated | N/A | 19 | N/A | N/A | 3.4 | 0.07-0.2 |
| | PES | MF straight | N/A | 19 | N/A | N/A | 17.2 | 0.044 |
| | PA | MF straight | N/A | 19 | N/A | N/A | 5.2 | 0.04-0.08 |
| | Steel | MF Hooked-end | 500;800 | 30; 50; 60 | N/A | N/A | N/A | 0.95-1-3 |
| [23] | Steel ** | MF Hooked-end | 500 | 30 | 7800 | 1700 | 200 | 0.5 Hybrid |
| | PP | MF straight | 100 | 20 | 900 | 450 | 5 | 0.5 |
| | Glass | MF straight | 10 | 6 | 2720 | 2280 | 80 | 0.5 |
| | PES | MF straight | 50 | 12 | 1350 | 970 | 15 | 0.5 |
| [25] | Steel | MF Hooked-end | 550 | 35 | 8000 | 1100 | N/A | 0.1 |
| | Glass | MF straight | 12 | 15 | 2740 | 2450 | N/A | 0.1 |
| | PP | MF straight | 22 | 12 | 910 | 300-400 | N/A | 0.1 |
| [53] | R-HDPE | MF straight | 250; 400 | 23; 30 | 940 | 37 *** | 0.5 *** | 0.4-1.25 |
| [43] | R-PET | MF straight | 909 (eq.) | 30; 50 | N/A | 110 | N/A | 0.5-1.5 |
| | R-PET | MF Deformed | 714 (eq.) | 30; 50 | N/A | 110 | N/A | 0.5-1.5 |
| [54] | Cellulose | MF | 15 | 3 | 1500 | 500 | 50 | 0.06 |
| [55] | PAN | MF | 14.4 | 12 | 1170 | 690 | 12 | 0.04 |
| | PP | MF | 20 | 12 | 920 | 550 | 6.8 | 0.1 |
| | Glass | MF | 14 | 12 | 2680 | 1700 | 72 | 0.02 |
| | PE | MF | 20 | 12 | 1340 | 500 | 5.0 | 0.07 |
| [48] | PES | MF | 18 | 12 | 1380 | N/A | N/A | 0.07 |
| | PP | MF | 30-40 | 12 | 910 | N/A | N/A | 0.1 |
| | F-PP* | MF | 30-40 | 12 | 910 | N/A | N/A | 0.1 |

298   * R-fibres = recycled fibres [19,34,43,52,53]. F-fibres = Fluourinated [48]

299   ** Hybrid fibre reinforcement by mixing steel fibres with PP fibres, glass fibres or PES fibres, respectively [23]

300   *** Tensile strengths given in the reference seem unrealistically low compared to other fibres of PE and PP [53]

301   *2.2.2   Material composition*

302   Besides the harshness of the environmental and restraining conditions, the material composition and matrix is highly

303   relevant for the susceptibility of the material to cracking due to plastic shrinkage deformations. Since plastic shrinkage

304   occurs in the paste (cement or other binder types), a high content of paste in the material matrix will most likely promote

305   larger plastic shrinkage deformations than a similar material with lower cement content [18]. The introduction of

306  aggregates to the material matrix (mortar or concrete) would commonly result in smaller shrinkage deformations [17],

307  although larger aggregates could act as internal restraints [60,72]. The addition of other binder types, e.g. fly ash, silica

308  fume, GGBS etc., for cement replacement has also been shown to have an influence of the plastic shrinkage behaviour

309  [17,55,73]. The influence of different binder types and the mix proportions of the material matrix on the plastic shrinkage

310  behaviour will not be evaluated further in this review.

311  The material composition used in the studies included in this review are given in Table 3. The table provides information

312  about the binder type, matrix proportions and additives. For the studies using one of the Overlay methods, the

313  composition of both the substrate bases and the fresh overlay are given. A low w/c-ratio, superplasticizer and rebars are

314  in some studies added to the substrate bases to ensure a stiff base for the fresh overlay [7,15,20,41,43].

315

316  *Table 3. Details of material composition used in the studies included in this review*

| Ref. | Type | water : binder : fine : coarse | Binder type | Additives |
|------|------|-------------------------------|-------------|-----------|
| [7] | Mortar overlay | 0.48 : 1.0 : 0.50 : 0 | Cement | |
| | Concrete substrate | 0.28 : 1.0 : 1.36 : 1.36 | Cement + SF | SP |
| [2] | Concrete overlay | 0.53 : 1.0 : 1.0 : 1.0 | ASTM C150 Type III PC | |
| | Concrete substrate | 0.37 : 1.0 : 1.5 : 2.54 | | WRA |
| [20] | Mortar overlay | 0.46 : 1.0 : 0.95 : 0 | PC Type I, SF | |
| | Concrete substrate | 0.28 : 1.0 : 1.36 : 1.36 | PC Type I, SF | SP |
| [41] | Mortar overlay | 0.75 : 1.0 : 12.69 : 0 | PC Blend CPC30R | |
| | Concrete substrate | 0.47 : 1.0 : 1.67 : 1.71 | PC Blend CPC30R | SP |
| [1] | Mortar Overlay | 0.5:1.0:2.0:0 (M1) | GUL CEM | |
| | Concrete substrate | N/A | | |
| [21] | Concrete overlay | 0.48:1.05:1.0:1.0 | ASTM type I + SF | |
| | Concrete substrate | 0.28:1.0:1.36:1.36 | ASTM type I + SF | SP |
| [34] | Mortar overlay | 0.5:1.0:1.47:0 | CEM I | |
| | Concrete substrate | N/A | | |
| [4] | Cement | (0.25)-0.55:1.0:0:0 | CEM I, Fly ash Class F and C | |
| [44] | Mortar | 0.5 : 1.0 : 1.5 : | PC Type I | |
| [19] | Mortar | 0.55 : 1.0 : 2.0 : 0 | N/A | |
| [12] | Concrete | 0.47 : 1.0 : 2.0 : 2.5 | PC Type I | |
| [24] | Concrete (A) | 0.54 : 1.0 : 1.68 : 2.05 | Ordinary PC | SP |
| | Concrete (B) | 0.43 : 1.0 : 1.26 : 1.55 | Ordinary PC | SP |
| [17] | Concrete | 0.45 : 1.0 : 2.0 : 2.0 | PC type II + SF | WRA |
| [43] | Mortar (Kraai) | 0.55 : 1.0 : 2.20 : 0 | CEM II/A LL | SP |
| [35] | Mortar | 0.55 : 1.0 : 1.2 : 0 | PC Type I | |
| [45] | Concrete | 0.57 : 1.0 : 2.6 : 2.8 | CEM II/B LL | SP, SRA |
| [51] | Concrete | 0.55 : 1.0 : 2.7 : 2.8 | CEM II/B LL | SP |
| [52] | Mortar | 0.5 : 1.0 : 2.0 : 0 | PC Type I | |
| [18] | Mortar | 0.4-0.7 : 1.0 : 1.0-3.0 | PC I | Acc. Admixtures in some mixes |
| | Concrete (no cracks) | 0.6 : 1.0 : 2.0-2.3 : 1.5-3.5 | PC I or PC III | |
| [23] | Concrete | 0.40 : 1.0 : 1.88 : 2.85 | Ordinary PC + SF | SP |
| [25] | Concrete | 0.47 : 1.0: 2.73 : 2.24 | PC type II | |
| [53] | Concrete | 0.62 : 1.0 : 2.05 : 2.26 | CEM II/A-L | |
| [43] | Concrete (ASTM) | 0.55 : 1.0 : 2.20 : 1.8 | CEM II/A LL | SP |
| [54] | Concrete | 0.56 : 1.0 : 2.0 : 2.0 | PC Type I | |

| | HPC | 0.42 : 1.0 : 1.2 : 2.1 | | |
| [55] | Concrete | 0.55:1.0:2.3:3.2 | GGBS + OPC + (FA) | (SRA) |
| [48] | Concrete | Mix 1: 0.7:1.0:3.7:3.5 | CEM I | Plastizicer, Accelerater, Retarder |
| | | Mix 2: 0.4:1.0:1.0:1.8 | | (Mix 1: No cracks with fibres) |

## 3  Influence of fibre properties on plastic shrinkage cracking

In the following sections, the influence of selected fibre properties is illustrated as a function of the crack reduction ratio (CRR) for the total crack area (TCA) and/or the maximum crack width (MCW) based on the results from the 25 studies included in this review. Relevant data was added to a database containing information about the available fibre properties and the influence on the degree of cracking presented as the CRR. Table 4 presents the types of studied fibre materials, the variations in fibre characteristics and the number of data points collected from the selected studies. The studied fibres have been grouped into four material categories covering: **polymeric fibres, natural fibres, metallic fibres and other non-metallic high-modulus fibres (glass, carbon, basalt)**. The largest number of data points covers polymeric fibres, compared to the other material categories.

*Table 4. Overview of database of selected fibre properties from studies included in this review. Minimum and maximum values are given.*

| Material group | Polymeric fibres | Natural fibres | Metallic fibres | Other high-modulus fibres |
|---|---|---|---|---|
| Materials | PP, PVA, PE, PET, PO, PAN, PES, N/A | Flax, Lechuguilla, Cellulose | Steel, metal | Glass, carbon, basalt |
| Data points | 198 | 25 | 34 | 28 |
| Eq. fibre diameter ($\mu$m) | 10-1130 | 15-240 | 175-1050 | 7-200 |
| Fibre length (mm) | 4-63.5 | 3-40 | 15-60 | 6-43 |
| E-modulus (GPa) | 0.5-117 | 50-75 | 200-210 | 24.1-80 |
| Tensile strength (MPa) | 37-2585 | 1170-1500 | 1000-1700 | 1700-2870 |
| Volume fraction (%) | 0.04-3.0 | 0.05-0.7 | 0.1-1.5 | 0.02-1.0 |

Figure 4 provides an overview of the range of relevant fibre characteristics presented in histograms. From the figure it is observed that most studied fibres were added at volume fractions of $\leq 0.2\%$; with a fine diameter of $\leq 0.1$ mm; with a low modulus of E$\leq 7$ GP. Regarding the fibre length, there were larger variations.
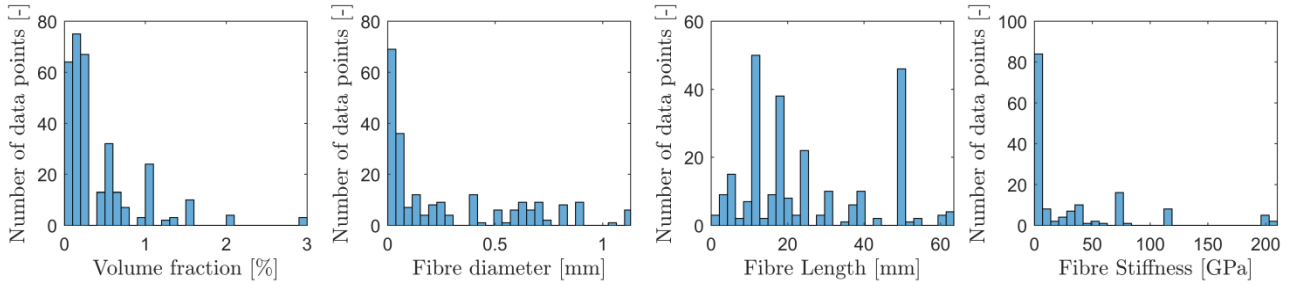
*Figure 4. Fibre characteristics as a function of the number of data points included to the database*

The large variations in the experimental test setups, exposure conditions, material compositions, fibre properties and crack measuring techniques, limited the elaboration of clear conclusions and further analysis. Therefore, most of the data is presented in boxplots to display the trends for selected fibre properties: fibre material; fibre modulus; fibre-to-matrix bonding; fibre shape (fibrillated, monofilament straight or monofilament deformed); fibre volume fraction; or geometry (length, diameter, aspect ratio, number of fibres per volume unit, specific fibre surface).

Fibres of finer diameter (d ≤ 0.1 mm) are commonly added at lower volume fractions, while fibres of larger diameter (d > 0.1 mm) are commonly added at higher volume fractions to obtain similar results as with finer fibres [2]. For this reason, the influence of fibre properties were in the following boxplots shown for different intervals of fibre diameter and volume fractions to make the tendencies clearer. I.e. micro fibres (d ≤ 0.1 mm) or macro fibres (d > 0.1 mm) added at low-volume fractions (vol ≤ 0.2%) or high-volume fractions (vol > 0.2%).

**3.1    Influence of fibre material and mechanical properties**

The influence of fibres on the CRR for the TCA for four categories of fibre materials; polymeric fibres, natural fibres, metallic fibres and other high-modulus fibres (e.g. glass, carbon, basalt) are evaluated in the boxplots in Figure 5. The fibre materials are highly related to the mechanical properties. In these figures, there is a distinction between micro fibres (d ≤ 0.1 mm), macro fibres (d > 0.1 mm) added at low-volume fractions (vol ≤ 0.2%) or high-volume fractions (vol > 0.2%) as explained in the previous section. Please note that no metallic micro fibres (d ≤ 0.1 mm) were investigated in the included studies, while no glass/carbon/basalt macro fibres (d > 0.1 mm) were investigated.
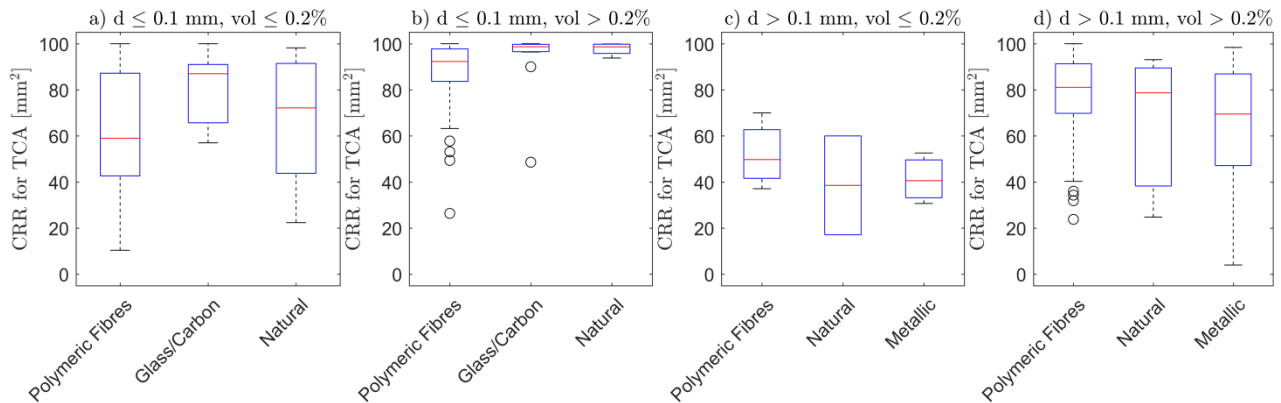
*Figure 5. Influence of fibres of different materials on CRR for TCA: a) Fibres with diameter ≤ 0.1 mm added at volume fraction of ≤ 0.2%; b) d ≤ 0.1 mm, vol > 0.2%; c) d > 0.1 mm, vol ≤ 0.2%; d) d > 0.1 mm, vol > 0.2%*

From the boxplots in Figure 5 it is found difficult to draw any clear conclusions on which fibre material gives the best performance. However, this result was expected due to the large variations in fibre characteristics within each material group. When the fibres were added in larger volume fractions, the micro fibres show good results for all material categories. Some studies compared the performance of different fibre materials at similar volume fractions, but with different diameter, length and geometry [2,20,23,25,41,42,51]. This complicates objective comparisons solely based on the fibre material. Thus, it can be concluded that fibre properties other than the fibre material must play a considerable role in reducing plastic shrinkage cracking.

### 3.1.1 Polymeric fibres

Most studies on plastic shrinkage cracking have focused on the performance of polymeric fibres due to the good performance in controlling plastic shrinkage cracking, often low price and wide range of fibre properties. The large variations in intrinsic fibre properties especially concern the fibre strength, stiffness and the fibre surface. The latter plays a significant role with respect to the fibre-to-matrix bond. The fibre dimensions and geometry can typically be controlled in the production process. However, some studies investigated recycled fibres processed from different types of polymeric waste fractions with the aim of producing more eco-friendly and sustainable materials [19,34,43,52,53,69,74]. The recycled fibres were either reprocessed by thermal reprocessing or by simple mechanical cutting or shredding operations. The latter is considered more energy efficient since it does not require any melting of the polymers. On the contrary, the inherent dimensions and geometries of the waste could not easily be modified or controlled [34,43,69].

### 3.1.2 Natural fibres

376     Some studies have investigated different types of natural fibres. These include natural fibres of cellulose [4,18,38,54],

377     lechuguilla, flax [20,41], sisal, coconut [75,76]. Animal fibres were also studied [77]. One of the reasons for the

378     relatively low number of studies including natural fibres could be related to challenges with the degradation and poor

379     durability of the fibres inside the highly alkaline cement-based matrix [78]. The fibre diameter and modulus is often

380     dependent on the inherent nature of the natural material, while the fibres can be cut into the desired length. The modulus

381     of the investigated natural fibres is generally found to be in the high range, i.e. $\geq 50$ GPa, but depends on factors such as

382     the processing method, the content of cellulose and the microstructure of the fibre [78]. Natural fibres are generally

383     hydrophilic and have a high degree of water absorption compared to most other fibre materials [79]. Boghossian &

384     Wegner [20] found that low volume fractions ($\leq 0.3\%$) of flax fibres (d = 0.035 mm, L = 10-38 mm) were excellent in

385     controlling plastic shrinkage cracking. This positive effect was attributed to the hydrophilic nature of the fibre, which

386     was considered to improve the fibre-to-matrix bonding. However, other studies reported the need for higher volume

387     fractions to achieve such positive results [41,77].


388     *3.1.3    Glass, carbon, and basalt fibres*

389     Other types of high-modulus fibres of non-metallic materials cover glass, carbon and basalt fibres. Carbon fibres used as

390     reinforcing material in concrete are generally valued for their high strength and modulus, good alkali-resistance and fine

391     diameter of <15 µm. However, the main limitation is reported to be the high cost [79,80]. It was found that carbon fibres

392     were superior in controlling plastic shrinkage cracking when added at only 0.1% (CRR for TCA of >90%) [2]; however,

393     similar results were found in the same study for the addition of monofilament PP fibres.

394     The modulus of glass fibres used for controlling plastic shrinkage cracking is in the range of 70-80 GPa and the fibre

395     diameter around 10-40 µm [20,23,25,55]. Studies by Rahmani et al. [25] and Sirajuddin & Gettu [55] found that low-

396     modulus polymeric fibres performed better than glass fibres. On the contrary, Boghossian & Wegner [20] found that AR-

397     glass fibres performed superior to all other tested fibres (PP fibrillated, PP monofilament and flax fibres). This was

398     explained by the ability of the glass fibres to reduce the free shrinkage strain, which was not observed for any of the other

399     fibre types included in the study. Similar to some types of glass fibres, untreated basalt fibres without any coating are

400     reported to have poor alkali-resistance [1,81]. The mechanical properties are reported to be in the same range as glass

401     fibres [82]. Branston et al. [1] studied the influence of basalt fibres in forms as filaments, bundles and minibars (d = ~16

402     µm, L = 12-43 mm). Fibres in filament forms showed the best performance and were able to eliminate the surface

403     cracking when added at fractions of 0.1%.

404 *3.1.4    Metallic fibres*

405 Metallic fibres are most commonly produced as macro fibres with hooked ends or other deformed shapes to improve the

406 fibre-to-matrix bonding [22–25,35]. Naaman et al. [2] found that relatively fine metallic fibres (d = 0.175 mm, L = 15

407 mm) could almost completely reduce the total crack area when added at volume fractions of 0.4%. Balaguru [18] also

408 achieved good results with coarser steel fibres (d = 0.5 mm, L = 30-60 mm), but much higher volume fractions (0.95-

409 1.3%) were required to obtain a decent crack reduction. Eren & Marar [24] studied steel fibres with aspect ratios of 55-80

410 added at volume fractions of 0.5-1.5% and concluded that the added volume fraction was much more influential than the

411 fibre aspect ratio. Most studies that compared the effect of steel fibres and polymeric fibres concluded that the latter type

412 is significantly better at controlling plastic shrinkage cracking than steel fibres [2,23,42]. However, this could also be a

413 result of the coarser fibre diameter for metallic fibres. The influence of hybrid fibre additions including both steel, glass

414 and polymeric fibres were also studied [23,49]. It was found that these composites with hybrid fibre additions performed

415 well in controlling the crack formation, while other beneficial mechanical properties were obtained with the addition of

416 steel fibres. Steel fibres extracted from recycled tyres were studied by Sayahi [22] who found that the recycled steel

417 fibres performed almost as good as commercially available steel fibres with hooked ends.


418 *3.1.5    Influence of fibre modulus*

419 The mechanical performance of the fibres, such as the tensile strength, modulus and fibre-to-matrix bonding is directly

420 related to the specific fibre material. Different types of polymeric fibres have a wide range of elastic moduli: PP (~4

421 GPa), PA (~5 GPa), PET (~5 GPa), PO (2-10 GPa), PAN (~12 GPa), PES (~15 GPa), PVA (~30 GPa), (LD/HD)PE (0.5-

422 117 GPa). However, as seen in Figure 4, mainly low-modulus fibres have been investigated in the literature for

423 controlling plastic shrinkage cracking. Other fibres of non-polymeric materials have the following modulus: steel (210

424 MPa), carbon (~25 GPa), glass and basalt (~80 GPa), and fibres of natural materials (50-75 GPa).

425 The influence of the fibre modulus on the CRR for TCA is illustrated in Figure 6 for fibres added at low-volume

426 fractions (vol ≤ 0.2%) or high-volume fractions (vol > 0.2%), respectively. The boxplot does not show any clear trend

427 regarding the influence of the fibre modulus, besides those fibres with modulus ≤ 3 GPa show the poorest performance.
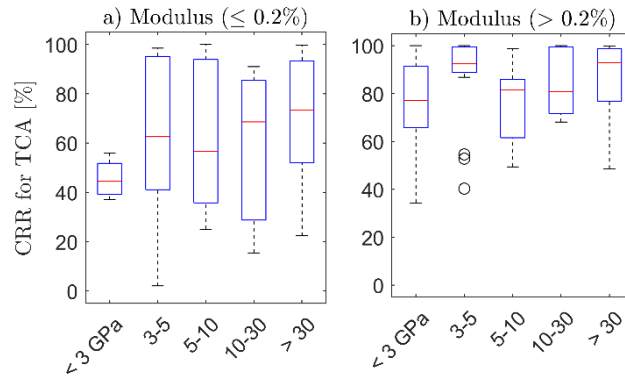
428

*Figure 6. Influence of fibre modulus on: a) CRR for TCA for fibres added in volume fraction of ≤ 0.2%; b) CRR for*
*TCA, vol > 0.2%*

432    In order for the fibres to possibly have a positive influence on the crack formation, the modulus of the fibres should be

433    higher than that of the matrix material. Considering the stiffness of the fresh cement-based material, it is very low during

434    the first few hours after casting until the material begins to harden and gains strength [83]. Thus the low-modulus fibres

435    are still stiffer in this period. This explains why low-modulus fibres such as PP fibres perform so well for restricting

436    plastic shrinkage cracking. According to Naaman et al. [2], the fibre stiffness does not have a significant influence on

437    plastic shrinkage cracking as long as the fibre modulus is higher than the modulus of the matrix. It was also reported that

438    fibres with higher modulus required a better fibre-to-matrix bonding capacity and that their higher modulus initiated

439    cracking earlier resulting in wider cracks [1].


440    *3.1.6    Influence of fibre-to-matrix bonding*

441    The interfacial bond between the fibre and the fresh cement-based matrix has been reported to be an influencing

442    parameter, since it is a measure of the stresses that can be transferred from the matrix to the fibres. The fibre-to-matrix

443    bonding can both be mechanical and chemical. Thus, the ability of a fibre to transfer stress across a crack depends on the

444    fibre shape as well as the chemical structure of the material. The latter is commonly defined by the hydrophilic nature of

445    the fibre and the ability of the fibre to create a chemical reaction with the paste [84,85]. Some studies investigated the

446    influence of deformed shapes of macro fibres on improving the bonding strength [19,43,51]. Also fibrillated fibre

447    networks are considered to improve the bond to the matrix [17]. The influence of different fibre shapes will be discussed

448    in Section 3.2. The hydrophilic nature of the fibres is essential for the development of a good bond with the cement

449    matrix. While hydrophobic fibres such as PP and PE have a relatively poor bonding, hydrophilic fibres such as PVA are

450    reported to have a better bond to the cement matrix [2,85]. The fibre-to-matrix bond for PVA fibres is reported to

451    develop rapidly, which is a result of the chemical hydrogen bond created between fibre the cement paste [2,41,80]. This

452    correlates with the fact that PVA fibres are reported to be excellent in controlling plastic shrinkage cracking [2,41,42].


453    **3.2    Fibre shape**

454    Various fibre shapes and fibrillations have been investigated with the aim of improving the fibre-to-matrix bonding

455    compared to fibres with straight shapes. Fibrillated fibres compose of micro fibres that have been connected in a network

456    [17]. During mixing, this network breaks down to fibrillated fibres providing an effective mechanical anchorage and

457    improving the bonding   [7,17]. The performance of fibrillated PP fibres have in some studies been compared to

458    monofilament PP fibres with similar fibre length [2,3,7,20]. Banthia & Gupta [7] studied the effect of both monofilament

459    PP fibres and fibrillated PP fibres with similar fibre length of 12.5 mm. It was found that the monofilament fibres with

460    finer diameter (d = 3 denier, ~22 µm) performed best followed by the fibrillated fibres and finally the monofilament

461    fibres with the coarser diameter (d = 6 denier, ~31 µm). The results obtained by Boghossian & Wegner [20] showed

462    almost identical performance of fibrillated and monofilament PP fibres with similar length, whereas Naaman et al. [2]

463    observed significantly better performance of monofilament PP fibres (d = 68 µm, L = 6-19 mm) for all fibre lengths

464    (fibrillated: L = 19 mm). On the contrary, Qi et al. [3] reported that higher amounts of monofilament PP fibres were

465    necessary to achieve a similar reduction in total crack width as achieved with fibrillated PP fibres. Other studies that

466    investigated the effect of fibrillated PP fibres without comparing with other fibre types reported excellent performance

467    for addition of volume fractions down to 0.1 % [12,17]. Based on these observations, it is not possible to draw any clear

468    conclusions on whether fibrillated or monofilament PP fibres perform better in reducing plastic shrinkage cracking, since

469    the performance is found to be highly influenced by the fibre diameter.

470    Although micro fibres are reported to perform superior to macro fibres, an advantage for macro fibres is that they can

471    easily be produced with deformed shapes leading to improved bonding [86]. Monofilament macro fibres of polymeric

472    materials have been deformed into various shapes such as embossed, twisted, crimped, and undulated, while steel fibres

473    are commonly produced with hooked-ends. Kim et al. [19] and Borg et al. [43] studied macro fibres of reprocessed PET

474    (R-PET) of different shapes; straight monofilament and deformed monofilament fibres. Borg et al. [43] observed a slight

475    improvement for crimped fibres compared to straight fibres. However, none of the fibres in this study succeeded in

476    complete control of the cracking, even at fibre volume fractions up to 1.5 %. The results by Kim et al. [19] revealed an

477    improvement for deformed R-PET fibres (crimped or embossed) compared to straight R-PET fibres at low fibre volume

478    fraction (0.1 %). This became less significant at higher fibre volume fractions (0.5-1.0 %). These R-PET fibers all had a

479 significant ability to control plastic shrinkage cracking, when added at a minimum volume fraction of 0.5%. Lee & Won

480 [35,71] investigated the use of structural polymeric nanoclay synthetic fibre with twisted + crimped deformations and

481 compared the performance to that of hooked-end steel fibres. Both fibre types were added at volume fractions of 0.26%.

482 It was found that the synthetic fibres performed better than the steel fibres, but they were not able to achieve significant

483 reductions in the total crack area (CRR of 36%) when added at this volume fraction. Mazzoli et al. [51] studied various

484 types of macro fibres of different shapes and materials added at volume fractions of 0.3% and concluded that the use of

485 deformed macro fibres were more effective in reducing the width and length of the surface cracks compared to straight

486 fibres. However, since the remaining fibre properties were not kept constant, it hindered any clear conclusions regarding

487 the influence of the fibre shape.

488 **3.3 Influence of fibre dimensions and volume fraction**

489 The influence of the fibre dimensions is evaluated based on parameters such as the fibre diameter, length, aspect ratio,

490 numbers of fibres per volume unit ($N_V$) and specific fibre surface ($S_F$). The three latter parameters are somehow

491 combining the influence of the fibre diameter, length and added volume fraction.

492 *3.3.1 Fibre volume fraction*

493 The influence of the fibre volume fraction is presented as the CRR for the total crack area (TCA) or maximum crack

494 width (MCW), see Figure 7. Again, there is a distinction between micro fibres (d ≤ 0.1 mm) and macro fibres (d > 0.1

495 mm).



496
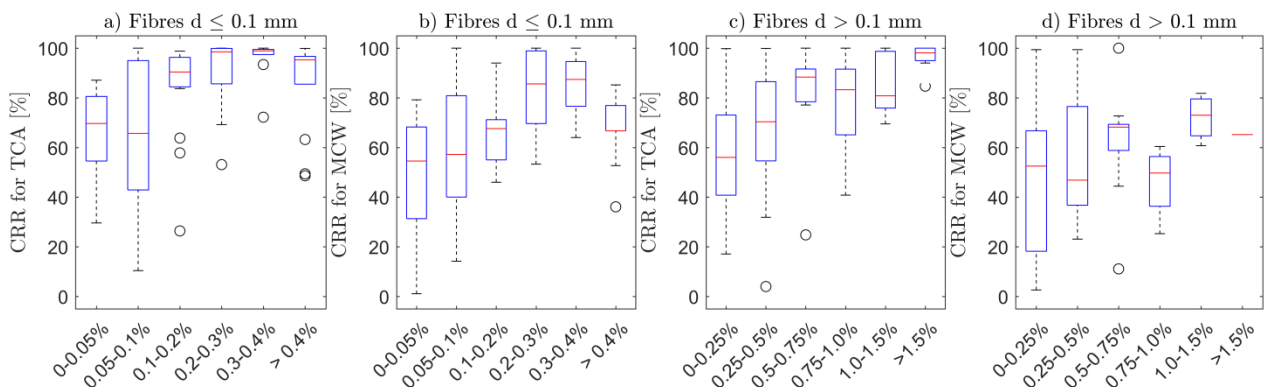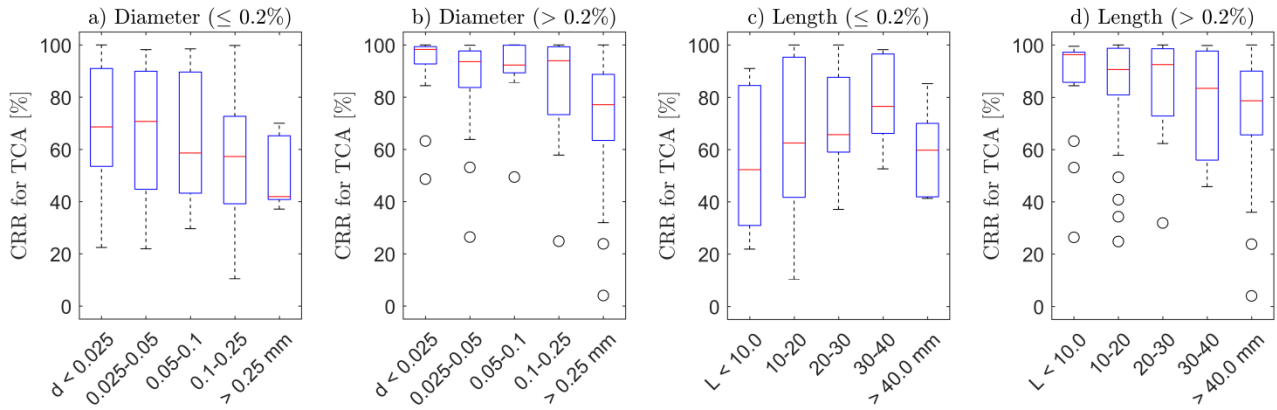
497 *Figure 7. Influence of fibre volume fractions on: a) CRR for TCA for fibres with d ≤ 0.1 mm; b) CRR for MCW, d ≤ 0.1*
498 *mm; c) CRR for TCA, d > 0.1 mm; b) CRR for MCW, d > 0.1 mm*

499

First, it is observed that there is a clear tendency showing that an increase in fibre volume fraction results in an increased reduction in surface cracking. This is both with respect to the CRR for TCA and MCW, although the effect of increased fibre content is more evident for the TCA than for the MCW. A noticeable reduction in the CRR for TCA was observed for micro fibres (d ≤ 0.1 mm) at additions of only > 0.1 vol%, and for macro fibres (d > 0.1 mm) at additions of > 0.5 vol%. As anticipated, much higher volume fractions were required for macro fibres, i.e. > 0.5%, to obtain similar reduction in the CRR for the TCA as for micro fibres. Regarding the CRR for the MCW for both the micro and macro fibres, the results did not show the same superior reduction. Even at the higher volume fractions of e.g. > 0.3% for micro fibres and > 1.0% for macro fibres, the results for the CRR for MCW were in the range of 60-80 % and 50-75%, respectively.  This reveals that the fibres have the overall ability to control the crack area on the specimen surface, whereas some larger cracks would still be present on the specimen surface despite very high fibre additions. These observations are in general in accordance with the literature that agrees on the fibre volume fraction being one of the most important factors influencing the degree of plastic shrinkage cracking [2,7,18,20]. According to Naaman et al. [2], the fibre volume fraction is the most influencing parameter together with the fibre diameter. However, there is an upper limit for the volume fraction depending on the specific fibre type. An excessive addition of fibres may result in poor fibre distribution leading to impaired properties of the cement-based material. Kim et al. [19] reported that a great improvement in reducing the TCA was obtained when adding 0.25% of PET fibres to the mixture, whereas no significant additional improvements were achieved with further increasing fibre volume fractions. Similar tendencies were observed by Boghossian [20], where no further improvements were observed for fibre additions > 0.1%.

*3.3.2    Fibre diameter and length*

The influence of the fibre diameter and length on the CRR for TCA is shown in Figure 8. Regarding the fibre diameter, a trend is found in the boxplot showing that fibres with finer diameter generally perform better than coarser fibres. Studies investigating the influence of the fibre diameter for fibres with all other properties kept constant, concluded that the decrease in fibre diameter had a positive influence on controlling the crack formation  [2,7]. According to Naaman [2], despite the type of material, any fibre with a diameter ≤ 40 µm added at volume fractions of 0.2-0.4% should be able to eliminate the formation of plastic shrinkage cracking. Yet, several studies also found that coarser fibres were able to significantly reduce surface cracking [19,21,34,43,44,51]. Although, coarser fibres had to be added at larger volume fractions of approximately 0.5-2.0% to obtain a CRR for the TCA in the same range as with the addition of micro fibres. These positive effects of using macro fibres were even more significant for macro fibres with deformed shapes [19,43].

528 Note that results for fibrillated fibres are not shown in the plot, since the diameter of these fibres is not given in the

529 studies.



531 *Figure 8. Influence of fibre diameter [mm] and fibre length [mm] on: a) Diameter: CRR for TCA for fibres added at*
532 *volume fraction of ≤ 0.2%; b) Diameter: CRR for TCA, vol > 0.2%; c) Length: CRR for TCA, vol ≤ 0.2%; d) Length:*
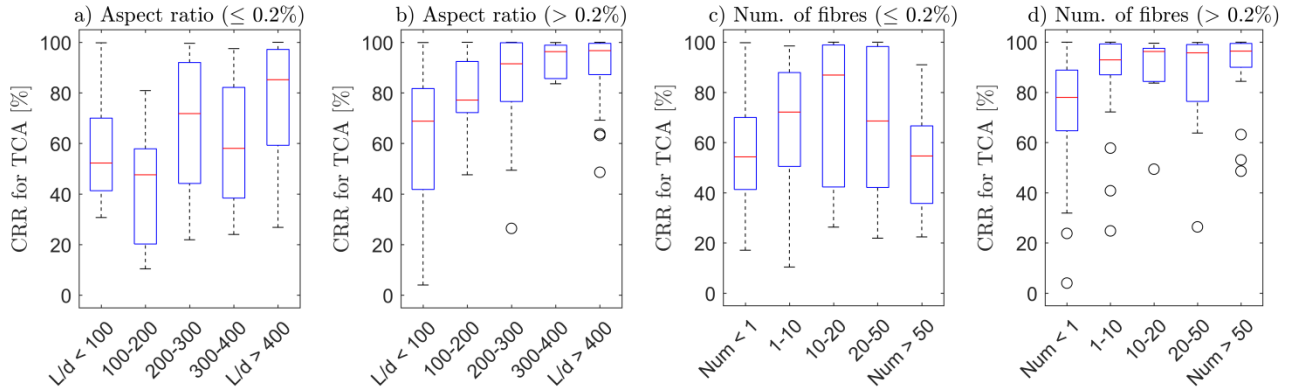533 *CRR for TCA, vol > 0.2%*
534

535 As for the fibre length, no clear correlation between the fibre length and the CRR for the TCA was observed in the

536 boxplot. This could indicate that the influence of the fibre diameter was more evident than the influence of the fibre

537 length. There are also disagreements in the literature about the influence of the fibre length. Some studies stated that

538 longer fibres resulted in improved performance with respect to the TCA [7,12,43,52,87], whereas other studies found that

539 the influence of longer fibre length was very weak or insignificant [2,20,21,41]. Moreover, the optimum fibre length can

540 vary significantly depending on specific fibre type and mixture proportions [18,20]. Balaguru [18] found that short fibres

541 (pulp) of PP or PE were more effective in richer cement mortars, whereas longer fibres (19 mm) performed better in lean

542 mortars or concretes, which might be attributed to the fact that mixtures containing larger aggregates need longer fibres

543 to bridge the cracks. It was also reported that fibres with a poor bond to the cement matrix (e.g. PP fibres) required a

544 longer fibre length to obtain sufficient stress transfer across the cracks [7].


545 *3.3.3    Fibre aspect ratio*

546 The fibre aspect ratio is a measure of the slenderness of monofilament fibres and is calculated as the length over the

547 equivalent diameter, *L/d,* [84]. The CRR for the TCA is plotted against intervals of the aspect ratio for fibres added at

548 low-volume fractions of ≤ 0.2% and high-volume fractions of > 0.2%, respectively. See Figure 9 that indicates that an

549 increase in aspect ratio often reduces the crack formation. This is more evident for fibres added at volume fractions >

550 0.2%. In studies where fibres of similar materials but different aspect ratios were investigated, it was commonly observed

551 that fibres of higher aspect ratios performed better [7,18,24,44]. Balaguru [18] even claimed that the aspect ratio seems to

552 be one of the primary parameters contributing to crack reduction. Mazzoli et al. [51] also found that fibres with higher

553 aspect ratio resulted in the best performance. On the contrary, Naaman et al. [2] reported no beneficial effect of higher

554 aspect ratios.



556 *Figure 9. Influence of aspect ratio and number of fibres per mm³ on: a) Aspect ratio: CRR for TCA for fibres added at*
557 *volume fraction of ≤ 0.2%; b) Aspect ratio: CRR for TCA, vol > 0.2%; c) Number of fibres: CRR for TCA, vol of ≤*
558 *0.2%; d) Number of fibres: CRR for TCA, vol > 0.2%*

559 *3.3.4    Number of fibres*

560 Based on the observation that the finer fibres are considered to perform better than coarser fibres at similar volume

561 fractions, it is relevant to consider the effect of numbers of fibres added to the matrix (fibres per mm³), $N_V$. This describes

562 the combined influence of fibre volume fraction, diameter and length [2,84]:

$$N_V = \frac{4\,V_f}{\pi\,d^2\,l} \qquad \text{(Eq. 3)}$$

563

564 where $V_f$ is the fibre volume fraction, $d$ the equivalent fibre diameter, and $l$ the fibre length. The influence of the number

565 of fibres on the CCR for TCA is plotted in Figure 9 for fibres at low-volume fractions of ≤ 0.2% and high-volume

566 fractions of > 0.2%, respectively. Although the trend is not as clear as for the aspect ratio, it seems that an increase in

567 number of fibres lead to a reduction in the total crack area for vol > 0.2%. When fibres are added at larger quantities

568 there should theoretically be an increase in the number of fibres bridging a potential crack. In the literature, there are

569 indications on increasing numbers of fibres per volume leading to lower CRR for TCA in [2,44], and less evident in [7].

570 *3.3.5    Specific fibre surface*

571   The specific fibre surface, $S_f$, is a the combined effect of the fibre diameter and the added volume fraction [2,21,84] and

572   is calculated as

$$S_f = \frac{4\,V_f}{d}$$

(Eq. 4)

573   where $V_f$ is the fibre volume fraction, and $d$ the equivalent fibre diameter. Figure 10 shows the specific fibre surface for

574   all fibre materials investigated in the studies included in this review. In the plot, there is a distinction between fibres with

575   diameters of $\geq 0.1$ mm and $< 0.1$ mm, respectively. Results for fibrillated fibres are not shown in the plot.
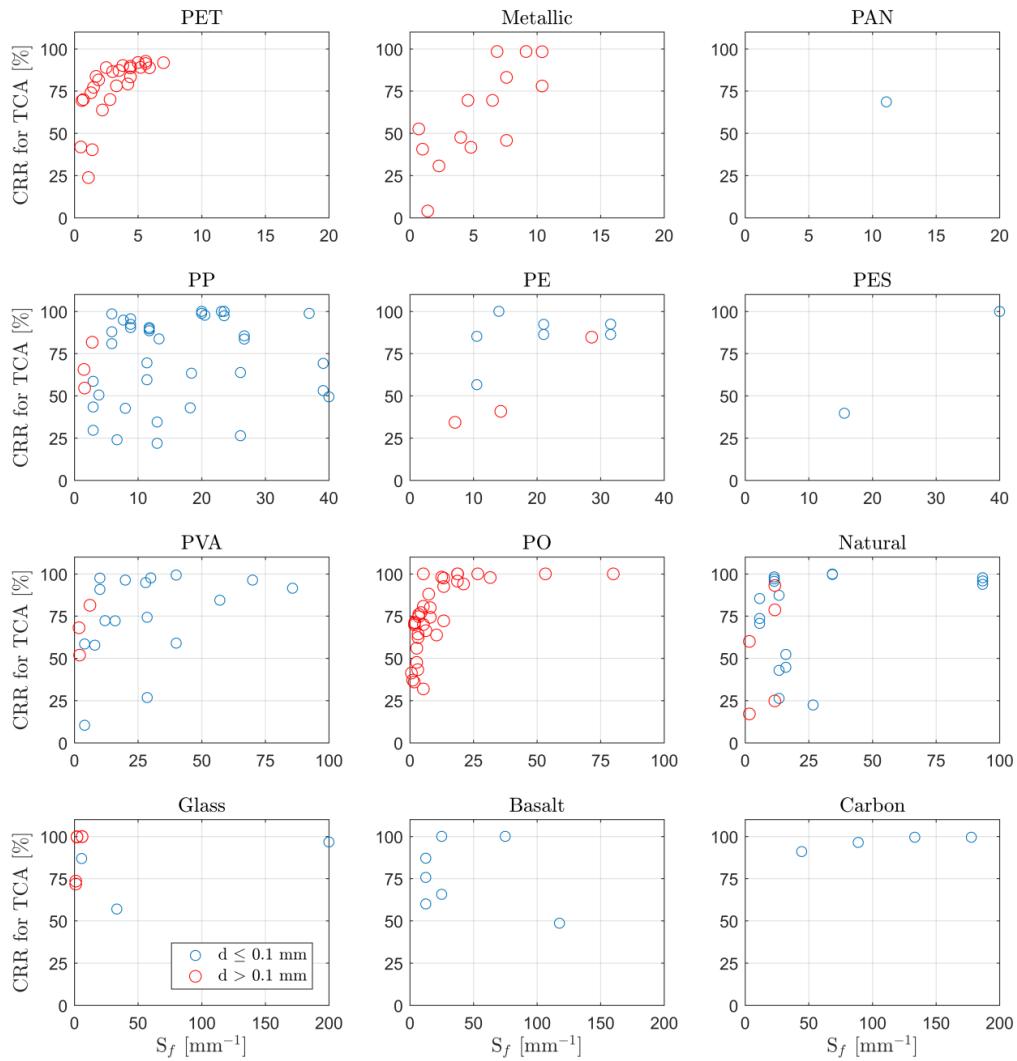
576



577   *Figure 10. Influence of specific fibre surface on CRR for TCA for all evaluated fibre types included in this review. Note*
578   *the different values on the x-axis.*
579

580      Theoretically, an increased specific fibre surface should be beneficial for controlling crack formation since it leads to

581      greater frictional restraints [1,7]. However, Naaman et al. [2] found that fibres with higher specific surface not

582      necessarily resulted in the largest reduction in the total crack area.

583      Considering the monofilament PP fibres, which are the most studied fibre type for controlling plastic shrinkage cracking,

584      very scattered results with no correlation between the CRR for TCA and the specific fibre surface are observed in the

585      figure. Still, most studies concluded that the PP fibres had good performance in controlling the plastic shrinkage cracking

586      when added at volume fractions of > 0.1% [2,7,20,34,55]. The PVA fibres were observed to perform well for almost any

587      specific fibre surface. Only few results deviate from this: Juarez et al. [41] found that the addition of 0.1% PVA fibres (d

588      = 0.1 mm, L = 12 mm) resulted in a very low reduction of the total crack area (CRR for TCA of 10%). However, when

589      the same fibre type was added at 0.7%, a significant reduction of surface cracking was achieved. Wang et al. [4] likewise

590      found that the addition of 0.1% PVA fibres (d = 0.014 mm, L = 6 mm) was not sufficient (CRR for TCA of 26%).

591      A larger scatter was seen in the results for PE fibres, which is considered to be a result of the very different properties

592      and qualities of PE materials. Naaman et al. [2] studied HDPE fibres with high modulus and fine diameter, which were

593      added at low volume fractions, while Bertelsen et al. [34] and Pešić et al. [53] investigated recycled PE fibres with a

594      coarser diameter and lower modulus found that much higher volume fraction were necessary to achieve good results. The

595      investigated PET fibres were macro fibres with straight or deformed shapes [19,43,51]. From the figure it is observed

596      that these fibres in most cases show good performance at very low values for the specific fibre surface, which is mainly

597      attributed to the deformed fibre shapes. In studies investigating PO fibres, no exact definition of the polymer was given,

598      i.e. the fibres were probably made of PP or PE. Only PO macro fibres were studied and it was observed that good results

599      could be achieved at low specific fibre surfaces. As a result of the low number of data points for PES and PAN fibres, no

600      definitive trends can be observed in the plots. Naaman found good performance of metallic macro fibres added at volume

601      fractions ≥ 0.3%, while coarser steel fibres showed inferior performance despite the deformed shapes [4,21].

602      It was observed that fibres of different types of natural materials had large fluctuations both in the intrinsic properties and

603      the performance in controlling plastic shrinkage cracking. While Boghossian & Wegner [20] found that flax fibres were

604      efficient in reducing the crack formations even at low volume fractions of 0.1%, other studies on cellulose or lechuguilla

605      fibres showed poor performance when added at such low volume fractions [4,41,54]. Regarding fibres of glass, the

606      performance was observed to vary significantly and those fibres with finer fibre diameter showed better performance.

607      Also the basalt fibres were found to be more influenced by the fibre shape and form (filament, bundles or minibars) than

608    by the specific fibre surface. Finally, the carbon fibres studied by Naaman et al. [2] show a clear trend and it would be

609    interesting to investigate the addition of even lower fibre additions, since the addition of 0.1% was resulting in an almost

610    complete reduction in the total crack area.

## 611    4    Summary and conclusions

612    A review covering existing research on plastic shrinkage cracking in cement-based materials was carried out to analyse

613    the influence of the addition of different types of fibres. The addition of randomly distributed fibres is a well-known

614    technique for mitigating plastic shrinkage cracking. Several fibres of different materials, geometries, shapes and

615    mechanical properties have been investigated. Yet, there are still no conclusive findings on which fibre properties that are

616    most influential in terms of controlling this type of cracking. Therefore, an analysis of the fibre influence was carried out.

617    Data from previous studies were collected in a database for analysing the results by descriptive statistics. The literature

618    presents several test methods for studying restrained plastic shrinkage cracking at laboratory scale, which results in very

619    different types and magnitudes of crack patterns. The main differences concern the type of geometry, type and stiffness

620    of the restraints, the exposure conditions and the crack measuring techniques. The evaluation of the degree of plastic

621    shrinkage cracking is often presented as basic crack parameters such as the total crack area (TCA), and mean or

622    maximum crack width (MCW) or length (MCL). These basic crack parameters are often presented as the crack reduction

623    ratio (CRR) compared to a reference specimen. The effect of fibres were evaluated by including the results for TCA and

624    MCW in a database together with information on the fibre volume fraction, material, geometry, dimensions, and

625    mechanical properties. Various fibre properties were illustrated in boxplots to discover any trends in the performance of

626    the fibres for controlling plastic shrinkage cracking. The following trends were observed:

627    ▪    By plotting all data included in the database in histograms against relevant fibre properties it was observed that the

628        most studied fibre types were polymeric fibres with a fine diameter (d ≤ 0.1 mm) and low modulus (E ≤ 7 GPa),

629        added at lower volume fractions (vol ≤ 0.2 %). The fibre length studied in the literature was found to vary more.

630    ▪    The studied fibre materials cover polymeric fibres, natural fibres, metallic fibres and other non-metallic high-modulus

631        fibres. These materials have a wide range of elastic properties as well as fibre-to-matrix bonding. No clear trends

632        were found for the fibre modulus in reducing the degree of cracking, but it was generally found that a good bonding

633        provides better results.

- The increase in fibre volume fraction added to the cement-based material was observed to play a major role in controlling plastic shrinkage cracking. However, there is an upper limit for the addition of fibres. Generally, good results were found for micro fibres added at volume fractions > 0.1% and for macro fibres at > 0.5%. Regarding the coarser macro fibres it was found necessary to add these at higher volume fractions compared to micro fibres.

- Similar clear trends were established for the fibre diameter, showing that fibres with finer diameter perform superior to coarser fibres. It was found that most micro fibres (d ≤ 0.1 mm) added at volume fractions of > 0.2% were able to achieve an almost crack free surface independent of the material. Regarding the fibre length, no obvious correlation was demonstrated in the boxplots.

- The increase in fibre aspect ratio as well as in number of fibres per volume unit was found to reduce the crack formation. The specific fibre surface is the combined measure of fibre diameter and added volume fraction and was plotted for all studied fibre materials. Generally, the plots illustrate that an increase in specific fibre surface leads to improved results, however, the trends were not equally clear for all studied materials.

## 5    Acknowledgement

## 6    References

[1]    J. Branston, S. Das, S.Y. Kenno, C. Taylor, Influence of basalt fibres on free and restrained plastic shrinkage, Cem. Concr. Compos. 74 (2016) 182–190. doi:10.1016/j.cemconcomp.2016.10.004.

[2]    A.E. Naaman, T. Wongtanakitcharoen, G. Hauser, Influence of different fibers on plastic shrinkage cracking of concrete, ACI Mater. J. 102.1 (2005) 49–58.

[3]    C. Qi, J. Weiss, J. Olek, Characterization of plastic shrinkage cracking in fiber reinforced concrete using image analysis and a modified Weibull function, Mater. Struct. 36.6 (2003) 386–395. doi:10.1007/BF02481064.

[4]    K. Wang, S.P. Shah, P. Phuaksuk, Plastic shrinkage cracking in concrete materials - Influence of fly ash and fibers, ACI Mater. J. 98.6 (2001) 458–464.

[5]    V. Slowik, M. Schmidt, R. Fritzsch, Capillary pressure in fresh cement-based materials and identification of the air entry value, Cem. Concr. Compos. 30.7 (2008) 557–565. doi:10.1016/j.cemconcomp.2008.03.002.

[6]    P.K. Mehta, P.J.M. Monteiro, Concrete: microstructure, properties, and materials, 2006. doi:10.1036/0071462899.

[7]    N. Banthia, R. Gupta, Influence of polypropylene fiber geometry on plastic shrinkage cracking in concrete, Cem. Concr. Res. 36.7 (2006) 1263–1267. doi:10.1016/j.cemconres.2006.01.010.

[8]    F. Sayahi, Plastic shrinkage cracking in concrete, Luleå University of Technology, 2016. doi:10.3929/ETHZ-B-000249246.

[9]    P.J. Uno, Plastic shrinkage cracking and evaporation formulas, ACI Mater. J. 95.4 (1998) 365–375.

[10]    P. Lura, W.J. Weiss, Influence of Shrinkage-Reducing Admixtures on Development of Plastic Shrinkage Cracks, ACI Mater. J. 104 (2007). doi:10.14359/18582.

[11]    D. Shen, X. Liu, Q. Li, L. Sun, W. Wang, Early-age behavior and cracking resistance of high-strength concrete reinforced with Dramix 3D

668      steel fiber, Constr. Build. Mater. 196 (2019) 307–316. doi:10.1016/j.conbuildmat.2018.10.125.

669 [12] P. Soroushian, F. Mirza, A. Alhozaimy, Plastic shrinkage cracking of polypropylene fiber-reinforced concrete, ACI Mater. J. 92.5 (1995)
670      553–560.

671 [13] P.N. Balaguru, S.P. Shah, Fiber Reinforced Cement Composites, McGraw-Hill, 1992.

672 [14] W.P. Boshoff, R. Combrinck, Modelling the severity of plastic shrinkage cracking in concrete, Cem. Concr. Res. 48 (2013) 34–39.
673      doi:10.1016/j.cemconres.2013.02.003.

674 [15] B. Nabil, A. Aissa, B.I. Aguida, Use of a New Approach (Design of Experiments Method) to Study Different Procedures to Avoid Plastic
675      Shrinkage Cracking of Concrete in Hot Climates, J. Adv. Concr. Technol. 9.2 (2011) 149–157. doi:10.3151/jact.9.149.

676 [16] C.A. Shaeles, K.C. Hover, Influence of mix proportions and construction operations on plastic shrinkage cracking in thin slabs, ACI Mater. J.
677      85.6 (1998) 495–504.

678 [17] Z. Bayasi, M. Mclntyre, Application of fibrillated PP fibres for restraint of plastic shrinkage cracking, ACI Mater. J. 99 (2002) 337–343.

679 [18] P. Balaguru, Contribution of fibers to crack reduction of cement composites during the initial and final setting period, ACI Mater. J. 91.3
680      (1994) 280–288.

681 [19] J.H.J. Kim, C.G. Park, S.W. Lee, S.W. Lee, J.P. Won, Effects of the geometry of recycled PET fiber reinforcement on shrinkage cracking of
682      cement-based composites, Compos. Part B Eng. 39.3 (2008) 442–450. doi:10.1016/j.compositesb.2007.05.001.

683 [20] E. Boghossian, L.D. Wegner, Use of flax fibres to reduce plastic shrinkage cracking in concrete, Cem. Concr. Compos. 30.10 (2008) 929–
684      937. doi:10.1016/j.cemconcomp.2008.09.003.

685 [21] N. Banthia, C. Yan, Shrinkage cracking in polyolefin fiber-reinforced concrete, ACI Mater. J. 97.4 (2000) 432–437.

686 [22] F. Sayahi, Plastic shrinkage cracking in concrete. Mitigation and Modelling, Luleå University of Technology, 2019.

687 [23] A. Sivakumar, M. Santhanam, A quantitative study on the plastic shrinkage cracking in high strength hybrid fibre reinforced concrete, Cem.
688      Concr. Compos. 29.7 (2007) 575–581. doi:10.1016/j.cemconcomp.2007.03.005.

689 [24] Ö. Eren, K. Marar, Effect of steel fibers on plastic shrinkage cracking of normal and high strength concretes, Mater. Res. 13 (2010) 135–141.
690      doi:10.1590/S1516-14392010000200004.

691 [25] T. Rahmani, B. Kiani, M. Bakhshi, M. Shekarchizadeh, Application of different fibers to reduce plastic shrinkage cracking of concrete,
692      RILEM Bookseries. 4 (2012) 635–642.

693 [26] T. Wongtanakitcharoen, A.E. Naaman, Unrestrained early age shrinkage of concrete with polypropylene, PVA, and carbon fibers, Mater.
694      Struct. 40 (2007) 289–300. doi:10.1617/s11527-006-9106-z.

695 [27] P.P. Kraai, A proposed test to determine the cracking potential due to drying shrinkage of concrete, Concr. Constr. 30.9 (1985) 775–778.

696 [28] ASTM C1579-13, Standard Test Method for Evaluating Plastic Shrinkage Cracking of Restrained Fiber Reinforced Concrete (Using a Steel
697      Form Insert), (2013) 1–7. doi:10.1520/C1579-06.2.

698 [29] Nordtest, Concrete : Cracking Tendency - Exposure To Drying During the First 24 Hours, (1995) 1–5.

699 [30] ASTM C1581, Standard Test Method for Determining Age at Cracking and Induced Tensile Stress Characteristics of Mortar and Concrete
700      under Restrained Shrinkage, 2009. doi:10.1520/C1581.

701 [31] M.D. Newlands, K.A. Paine, N.A. Vemuri, R.K. Dhir, A linear test method for determining early-age shrinkage of concrete, Mag. Concr.
702      Res. 60 (2008) 747–757. doi:10.1680/macr.2008.00004.

703 [32] N. Banthia, M. Azzabi, M. Pigeon, Restrained shrinkage cracking in fibre-reinforced cementitious composites, Mater. Struct. 26 (1993) 405–
704      413.

705 [33] N. Banthia, R. Gupta, Test method for evaluation of plastic shrinkage cracking in fiber-reinforced cementitious materials, Exp. Tech. 31.6
706      (2007) 44–48. doi:10.1111/j.1747-1567.2007.00191.x.

707 [34] I.M.G. Bertelsen, L.M. Ottosen, G. Fischer, Quantitative analysis of the influence of synthetic fibres on plastic shrinkage cracking using
708      digital image correlation, Constr. Build. Mater. 199 (2019) 124–137. doi:10.1001/archinte.168.13.1371.

709 [35] S. Lee, J. Won, Shrinkage characteristics of structural nano-synthetic fibre-reinforced cementitious composites, Compos. Struct. 157 (2016)
710      236–243. doi:10.1016/j.compstruct.2016.09.001.

711 [36] P. Fontana, S. Pirskawetz, P. Lura, Plastic Shrinkage Cracking Risk of Concrete -- Evaluation of Test Methods, (2012) 591–600.

712 [37] R. Gupta, Development, application and early-age monitoring of fiber-reinforced 'crack-free' cement-based, The University of British
713      Colombia, 2008.

714 [38] E. Booya, K. Gorospe, H. Ghaednia, S. Das, Free and restrained plastic shrinkage of cementitious materials made of engineered kraft pulp
715      fibres, Constr. Build. Mater. 212 (2019) 236–246. doi:10.1016/j.conbuildmat.2019.03.296.

716 [39] T. Mauroux, F. Benboudjema, P. Turcry, A. Aït-Mokhtar, O. Deves, Study of cracking due to drying in coating mortars by digital image
717      correlation, Cem. Concr. Res. 42.7 (2012) 1014–1023. doi:10.1016/j.cemconres.2012.04.002.

718 [40] P. Zhao, A.M. Zsaki, M.R. Nokken, Using digital image correlation to evaluate plastic shrinkage cracking in cement-based materials, Constr.
719      Build. Mater. 182 (2018) 108–117. doi:10.1016/j.conbuildmat.2018.05.239.

720 [41] C.A. Juarez, G. Fajardo, S. Monroy, A. Duran-Herrera, P. Valdez, C. Magniont, Comparative study between natural and PVA fibers to reduce
721      plastic shrinkage cracking in cement-based composite, Constr. Build. Mater. 91 (2015) 164–170. doi:10.1016/j.conbuildmat.2015.05.028.

722 [42] S.J. Choi, B.T. Hong, S.J. Lee, J.P. Won, Shrinkage and corrosion resistance of amorphous metallic-fiber-reinforced cement composites,
723      Compos. Struct. 107 (2014) 537–543. doi:10.1016/j.compstruct.2013.08.010.

724 [43] R.P. Borg, O. Baldacchino, L. Ferrara, Early age performance and mechanical characteristics of recycled PET fibre reinforced concrete,
725      Constr. Build. Mater. 108 (2016) 29–47. doi:10.1016/j.conbuildmat.2016.01.029.

726 [44] H. Najm, P. Balaguru, Effect of large-diameter polymeric fibers on shrinkage cracking of cement composites, ACI Mater. J. 99.4 (2002) 345–
727      351.

728 [45] L. Ruiz-Ripoll, B.E. Barragán, S. Moro, J. Turmo, Evaluation of the Techniques to Mitigate Early Shrinkage Cracking through an Image
729      Analysis Methodology, Strain. 52 (2016) 492–502. doi:10.1111/str.12191.

730 [46] L. Ruiz-Ripoll, B.E. Barragán, S. Moro, J. Turmo, Digital imaging methodology for measuring early shrinkage cracking in concrete, Strain.
731      49 (2013) 267–275. doi:10.1111/str.12034.

732 [47] F. Sayahi, M. Emborg, H. Hedlund, Plastic shrinkage cracking in concrete – Influence of test methods, 2nd Int. RILEM/COST Conf. Early
733      Age Crackinh Serv. Cem. Mater. Struct. - EAC2. (2017).

734 [48] R. Combrinck, Investigation of plastic shrinkage cracking in conventional and low volume fibre reinforced concrete, Universtity of
735      Stellenbosch, 2012.

736 [49] M. Cao, C. Zhang, H. Lv, Mechanical response and shrinkage performance of cementitious composites with a new fiber hybridization,
737      Constr. Build. Mater. 57 (2014) 45–52. doi:10.1016/j.conbuildmat.2014.01.088.

738 [50] G. Olivier, R. Combrinck, M. Kayondo, W.P. Boshoff, Combined effect of nano-silica, super absorbent polymers, and synthetic fibres on
739      plastic shrinkage cracking in concrete, Constr. Build. Mater. 192 (2018) 85–98. doi:10.1016/j.conbuildmat.2018.10.102.

740 [51] A. Mazzoli, S. Monosi, E.S. Plescia, Evaluation of the early-age-shrinkage of Fiber Reinforced Concrete (FRC) using image analysis
741      methods, Constr. Build. Mater. 101.1 (2015) 596–601. doi:10.1016/j.conbuildmat.2015.10.090.

742 [52] B.S. Al-Tulaian, M.J. Al-Shannag, A.R. Al-Hozaimy, Recycled plastic waste fibers for reinforcing Portland cement mortar, Constr. Build.
743      Mater. 127 (2016) 102–110. doi:10.1016/j.conbuildmat.2016.09.131.

744 [53] N. Pešić, S. Živanović, R. Garcia, P. Papastergiou, Mechanical properties of concrete reinforced with recycled HDPE plastic fibres, Constr.
745      Build. Mater. 115 (2016) 362–370. doi:10.1016/j.conbuildmat.2016.04.050.

746 [54] P. Soroushian, S. Ravanbakhsh, Control of plastic shrinkage cracking with specialty cellulose fibers, Aci Mater. J. (1998).

747 [55] M. Sirajuddin, R. Gettu, Plastic shrinkage cracking of concrete incorporating mineral admixtures and its mitigation, Mater. Struct. Constr. 51
748      (2018) 1–10. doi:10.1617/s11527-018-1173-4.

749 [56] S. Ghourchian, M. Wyrzykowski, L. Baquerizo, P. Lura, Susceptibility of Portland cement and blended cement concretes to plastic shrinkage
750      cracking, Cem. Concr. Compos. 85 (2018) 44–55. doi:10.1016/j.cemconcomp.2017.10.002.

751 [57] I.M.G. Bertelsen, C. Kragh, G. Cardinaud, L.M. Ottosen, G. Fischer, Quantification of plastic shrinkage cracking in mortars using digital
752      image correlation, Cem. Concr. Res. 123 (2019) 105761. doi:10.1016/j.cemconres.2019.05.006.

753 [58] M.R. Jahanshahi, S.F. Masri, C.W. Padgett, G.S. Sukhatme, An innovative methodology for detection and quantification of cracks through
754      incorporation of depth perception, Mach. Vis. Appl. 24 (2013) 227–241. doi:10.1007/s00138-011-0394-0.

755 [59] G.M. Sadiqul Islam, S. Das Gupta, Evaluating plastic shrinkage and permeability of polypropylene fiber reinforced concrete, Int. J. Sustain.
756      Built Environ. 5.2 (2016) 345–354. doi:10.1016/j.ijsbe.2016.05.007.

757 [60] N. Banthia, R. Gupta, Plastic shrinkage cracking in cementitious repairs and overlays, Mater. Struct. 42.5 (2009) 567–579.
758      doi:10.1617/s11527-008-9403-9.

759 [61] C.G. Berrocal, I. Löfgren, K. Lundgren, N. Görander, C. Halldén, Characterisation of bending cracks in R/FRC using image analysis, Cem.
760      Concr. Res. 90 (2016) 104–116. doi:10.1016/j.cemconres.2016.09.016.

761 [62] A. Messan, P. Ienny, D. Nectoux, Free and restrained early-age shrinkage of mortar: Influence of glass fiber, cellulose ether and EVA
762      (ethylene-vinyl acetate), Cem. Concr. Compos. 33.3 (2011) 402–410. doi:10.1016/j.cemconcomp.2010.10.019.

763 [63] P. Zhao, Master thesis. Digital Image Correlation to Evaluate Plastic Shrinkage Cracking in Cement-Based Materials, Concordia University,
764      Montreal, Canada, 2016.

765 [64] M. Némoz-Gaillard, D. Nectoux, E. Dallies, D. Muller, Influence of AR glass fibers on the cracking of concrete : analysis at the very early
766      age by digital image correlation, in: PRO 23 Int. RILEM Conf. Early Age Crack. Cem. Syst., 2002: pp. 237–244.

767 [65] E.D. Dzaye, G. De Schutter, D. Aggelis, Monitoring fresh cementitious material by digital image correlation ( DIC ), in: SynerCrete18, 2018:
768      pp. 267–272.

769 [66] E.D. Dzaye, G. De Schutter, D. Aggelis, Application of digital image correlation to cement paste, in: Proceedings. Eighteenth Int. Conf. Exp.
770      Mech., 2018. doi:10.3390/ICEM18-05332.

771 [67] E.D. Dzaye, E. Tsangouri, K. Spiessens, G. De Schutter, D.G. Aggelis, Digital image correlation (DIC) on fresh cement mortar to quantify
772      settlement and shrinkage, Arch. Civ. Mech. Eng. 19 (2019) 205–214. doi:10.1016/j.acme.2018.10.003.

773 [68] F. Pelisser, A.B.D.S.S. Neto, H.L. La Rovere, R.C.D.A. Pinto, Effect of the addition of synthetic fibers to concrete thin slabs on plastic
774      shrinkage cracking, Constr. Build. Mater. 24 (2010) 2171–2176. doi:10.1016/j.conbuildmat.2010.04.041.

775 [69] M. Serdar, A. Baričević, M. Jelčić Rukavina, M. Pezer, D. Bjegović, N. Štirmer, Shrinkage Behaviour of Fibre Reinforced Concrete with
776      Recycled Tyre Polymer Fibres, Int. J. Polym. Sci. 2015.3 (2015) 1–9. doi:10.1155/2015/145918.

777 [70] R.D.T. Filho, M.A. Sanjuán, Effect of low modulus sisal and polypropylene fibre on the free and restrained shrinkage of mortars at early age,
778      Cem. Concr. Res. 29 (1999) 1597–1604.

779 [71] S. Lee, S. Kim, J. Won, Bond-flexural behaviour of structural nano-synthetic fibre-reinforced cementitious composites, Compos. Struct. 152
780      (2016) 20–33. doi:10.1016/j.compstruct.2016.05.041.

781 [72] D. Hobbs, Influence of aggregate restraint on the shrinkage of concrete.pdf, ACI J. September (1974) 445–450.

782 [73] H. Toutanji, S. McNeil, Z. Bayasi, Chloride permeability and impact resistance of polypropylene-fiber-reinforced silica fume concrete, Cem.
783      Concr. Res. 28 (1998) 961–968. doi:10.1017/CBO9781107415324.004.

784 [74] F.L. Auchey, The Use of Recycled Polymer Fibers as Secondary Reinforcement in Concrete Structures, J. Constr. Educ. 3.2 (1998) 131–140.

785 [75] M.A. Sanjuán, R.D. Tolêdo Filho, Effectiveness of crack control at early age on the corrosion of steel bars in low modulussisal and coconut
786      fibre-reinforced mortars, Cem. Concr. Res. 28 (1998) 555–565. doi:10.1016/S0008-8846(98)00003-9.

787 [76] R.D. Toledo Filho, K. Ghavami, M.A. Sanjuan, G.L. England, Free , restrained and drying shrinkage of cement mortar composites reinforced
788      with vegetable fibres, Cem. Concr. Compos. 27 (2005) 537–546. doi:10.1016/j.cemconcomp.2004.09.005.

789 [77] G. Araya-Letelier, F.C. Antico, M. Carrasco, P. Rojas, C.M. García-Herrera, Effectiveness of new natural fibers on damage-mechanical
790      performance of mortar, Constr. Build. Mater. 152 (2017) 672–682. doi:10.1016/j.conbuildmat.2017.07.072.

791 [78] O. Onuaguluchi, N. Banthia, Plant-based natural fi bre reinforced cement composites : A review, Cem. Concr. Compos. 68 (2016) 96–108.
792      doi:10.1016/j.cemconcomp.2016.02.014.

793 [79] J.I. Daniel et al., State-of-the-Art Report on Fiber Reinforced Concrete Reported by ACI Committee 544, ACI J. 96 (2002).

794 [80] Z. Zheng, D. Feldman, Synthetic fibre-reinforced concrete, Prog. Polym. Sci. 20 (1995) 185–210. doi:10.1016/0079-6700(94)00030-6.

795 [81] J. Sim, C. Park, D.Y. Moon, Characteristics of basalt fiber as a strengthening material for concrete structures, Compos. Part B Eng. 36 (2005)
796      504–512. doi:10.1016/j.compositesb.2005.02.002.

797 [82] T. Deák, T. Czigány, Chemical Composition and Mechanical Properties of Basalt and Glass Fibers : A Comparison, 79 (2009) 645–651.
798      doi:10.1177/0040517508095597.

799 [83] E. Roziere, R. Cortas, A. Loukili, Tensile behaviour of early age concrete: New methods of investigation, Cem. Concr. Compos. 55 (2015)
800      153–161. doi:10.1016/j.cemconcomp.2014.07.024.

801 [84] R.F. Zollo, Fiber-reinforced concrete: an overview after 30 years of development, Cem. Concr. Compos. 19 (1997) 107–122.
802      doi:10.1016/S0958-9465(96)00046-7.

803 [85] A. Peled, E. Zaguri, G. Marom, Bonding characteristics of multifilament polymer yarns and cement matrices, Compos. Part A Appl. Sci.
804      Manuf. 39 (2008) 930–939. doi:10.1016/j.compositesa.2008.03.012.

805 [86] B.H. Oh, J.C. Kim, Y.C. Choi, Fracture behavior of concrete members reinforced with structural synthetic fibers, Eng. Fract. Mech. 74 (2007)
806      243–257. doi:10.1016/j.engfracmech.2006.01.032.

807 [87] A.M. Alhozaimy, P. Soroushian, F. Mirza, Mechanical properties of polypropylene fiber reinforced concrete and the effects of pozzolanic
808      materials, Cem. Concr. Compos. 18 (1996) 85–92. doi:10.1016/0958-9465(95)00003-8.

809

# Appendix II

**Title:** Quantification of plastic shrinkage cracking in mortars using digital image correlation

1 **Quantification of plastic shrinkage cracking in mortars using digital image correlation**

2 I. M. G. Bertelsen[a*], C. Kragh[a], G. Cardinaud[a,b], L. M. Ottosen[a], G. Fischer[a],

3 [a] Department of Civil Engineering, Technical University of Denmark, Brovej 118, 2800 Kgs. Lyngby, Denmark

4 [b] GeM, Ecole Centrale de Nantes, 1 Rue de la Noë, 44300 Nantes, France

5 * Corresponding author. E-mail: imgber@byg.dtu.dk

6

7 **Abstract**

8 This study presents a digital image correlation (DIC) technique for the detection and quantification of plastic shrinkage

9 cracking in thin restrained mortar overlays applied on concrete substrates. The non-contact 2D-DIC technique enables

10 measurements of in-plane surface strain and displacement under continuous monitoring. A post-processing procedure to

11 compute various crack parameters, such as crack location, width, length and area on the specimen surface is presented,

12 which enables the crack patterns to be synthesized and digitally reproduced from DIC data. The formation of surface

13 cracking is illustrated in histograms facilitating a quantitative analysis. The crack width measurements obtained by DIC

14 data were verified using an optical microscope. The temperature evolution, evaporation rate and free shrinkage

15 behaviour of unrestrained mortar specimens were also tested to increase the knowledge of the early-age behaviour. This

16 method is intended for evaluation of various shrinkage mitigation strategies in cement-based mortars and other repair

17 mortars.

18

19 **Key words:** Plastic shrinkage, Image Analysis, Crack detection, Cement-based materials, Digital image correlation

20

21 **1 Introduction**

22 Plastic shrinkage is the volumetric contraction of cement-based materials that occurs in the first few hours after casting

23 when the concrete is still in a plastic stage. In restrained overlays, the material is not allowed to deform freely, so the

24 contraction will generate tensile stresses that may result in surface cracking [1]. The restraint may be due to adhesion to

25 an underlying concrete substrate, steel reinforcement, large aggregates, deviation in overlay geometry, adjacent

26 formwork, or deformation gradients between layers in the material [1–4]. Most plastic shrinkage cracking is caused by

27 the evaporation of mixing water and capillary pressure inside the pores of the cement. The loss of mixing water from

28 the fresh material is mostly a result of surface evaporation or moisture absorption at the interface with underlying

29  substrate materials [5]. Specific environmental conditions, such as low relative humidity, elevated temperatures and

30  exposure to high wind velocities, can enhance the water evaporation rate, and thereby the severity of plastic shrinkage

31  cracking. Large plastic shrinkage deformations can result in severe crack formation on the surface of the material,

32  which will affect its long-term durability, so it is essential to avoid the development of this type of cracking [1]. After

33  setting, the cracks may propagate, allowing the ingress of aggressive agents and leading to the premature deterioration

34  of the steel reinforcement.

35  The literature describes several methods for characterizing early-age shrinkage-induced cracking in cement-based

36  materials. These include the method proposed in ASTM C1579 (2013) [6], where cracking is induced by triangular

37  stress risers; the ring test method proposed in [7,8]; the linear dogbone-shaped specimens with restrained ends [9,10];

38  the plate-shaped specimens with edge-restraints proposed by Kraai [11]. These methods are effective for comparative

39  testing of the cracking behaviour under laboratory conditions, but are not considered appropriate for simulation of

40  realistic stress fields and crack patterns in the material [5]. Methods where a fresh overlay is cast on top of a restraining

41  concrete substrate or rough surface have also been developed for bonded overlays and are considered to provide more

42  realistic stress fields [1,3,12–17]. In these experiments, the fresh overlay may be simulating a repair mortar applied on a

43  damaged concrete surface (substrate) to increase the structural capacity, to replace deteriorated concrete and/or to

44  improve the durability by increasing the thickness of the concrete cover, thus protecting the steel reinforcement against

45  corrosion. The method developed in this study addresses crack formation in these last-mentioned bonded overlay-

46  substrate methods with restraints provided at the interface.

47

48  **1.1  Quantification of crack patterns**

49  Quantification of shrinkage cracking in restrained cement-based overlays can be challenging due to the unknown

50  location of the cracks being formed and the difficulties in instrumenting these cracks to quantify their formation and

51  growth. The evaluation of plastic shrinkage cracking is often based on visual inspection of the cracked surface and

52  subsequent determination of crack parameters such as the mean and maximum crack width and length and the total

53  crack area based on manual measuring techniques. However, parameters such as time of crack formation, crack width

54  development, spacing between cracks, crack depth, crack length and crack width distribution are also of importance for

55  future durability [18], and are difficult to quantify with manual measuring techniques. Actual measuring techniques

56  presented in the literature include manual crack measurements using optical microscopes or hand-held lenses [14,19,20]

57  or more sophisticated image-based techniques. The first mentioned techniques are considered to be time consuming,

58 difficult to apply while the experiment is running, and therefore not optimal for observing crack propagation at early

59 age occurring over short periods of time. The quality of the crack measurements relies upon various operator-dependent

60 factors such as experience and expertise, and is therefore prone to human error [21]. Moreover, these techniques often

61 provide very limited information about the cracked area and it is especially challenging to quantify crack patterns such

62 as those that often occur in evenly restrained materials. More advanced image analysis techniques, such as digital image

63 processing (DIP) [21–27] and digital image correlation (DIC) [13,15,16,28–33], have recently been successfully applied

64 for detection of shrinkage-induced cracking in cement-based structures. These are non-contact techniques and work by

65 capturing high-resolution images of the cracked surface, which makes it possible to track the evolution in crack growth

66 in a series of pictures taken almost directly after casting. These techniques do not rely on operator-dependent factors;

67 their accuracy simply depends on the setup, e.g. the resolution of the images, constant light source, and quality of the

68 investigated surface [34]. In the DIP method, it is possible to analyse crack patterns by modifying the contrast of the

69 images and then analyse whether a pixel is "cracked" or "uncracked". The DIC technique also enables strain and

70 displacement contour maps to be created with sub-pixel accuracy, and DIC is suitable in order to achieve a better

71 understanding of the surface deformations and cracking behaviour [35].

72

73 *1.1.1 2D-DIC principles*

74 The DIC technique is an optical method for tracking displacements in images based on changes in the grey scale

75 intensity of an applied speckle pattern [36]. The method has been widely accepted as an effective tool for surface

76 deformation measurements in the field of experimental solid mechanics [35,37]. A single fixed digital charge coupled

77 device (CCD) camera, a constant light source, and a high-contrast surface pattern for the detection of displacements on

78 the investigated surface are all that is needed for two-dimensional DIC, which is limited to in-plane deformations [38].

79 The technique has also gained attention in concrete-related research, but has mostly been used to evaluate deformations

80 and fractures in already hardened cementitious materials in several types of test e.g. [13,38–41]. Mauroux et al. [13,42]

81 studied the formation of drying shrinkage of coating mortars (both free and restrained specimens) and applied a 2D-DIC

82 system for monitoring of displacements and micro-cracking. The DIC results that were obtained for the free shrinkage

83 specimens showed good correlation with results obtained by traditional LVDT measurements. Micro-cracking was

84 detected on the surface of the restrained specimens by the DIC technique, which was subsequently compared with

85 microscopic measurements. Good correlation between the respective methods was found and it was concluded that the

86 DIC technique is a strong tool for detection of shrinkage-induced surface cracking.

87  Nevertheless, the technique has only been used in a few studies on the early-age behaviour of cement-based materials,

88  because of difficulties related to the creation of a high-contrast surface pattern when the material is still fresh and the

89  presence of  bleeding water on the surface [28,33]. The speckles may move or get absorbed on the wet surface, which

90  can result in a blurred speckle pattern with low contrast between black and white colors. The quality of the high-

91  contrast surface pattern is known to be closely related to the correlation precision of the image and is therefore essential

92  for the quality of the DIC post-processing [36,43]. High-contrast surface patterns at macro- or meso-scale are usually

93  achieved by applying a white-coloured base layer and a black speckle pattern using spray bottles or air brushes  [43].

94  Previous studies have used various strategies to construct such a pattern. Zhao [15,30] used spray paint to create the

95  pattern on a fresh concrete surface, but observed a decrease in evaporation rate in the first 3 h after the start of mixing.

96  Dzaye et al. [33] that studied the free plastic shrinkage behaviour of cement paste by 3D-DIC from 15 min after casting

97  also used spray paint to first create a white base layer before applying black ink dots by spraying from a distance. A

98  significant decrease in water evaporation was observed during the entire test period. The choice of spray paint type is

99  considered to be highly relevant, because plastic shrinkage cracking is associated with rapid surface drying in the first

100  hours after casting [44]. In other studies by Dzaye et al. [45,46] using a similar test setup as in [33] but different

101  materials for creation of the high-contrast surface pattern, the white base layer was applied with a layer of aluminium

102  oxide powder and black speckles with carbon particles distributed through a sieve. This method was reported not to be

103  influenced by the layer of bleeding water due to the density of the materials used for the speckle pattern, but no

104  information on the surface evaporation was given. Another strategy was applied by Ghourchian et al. [28,47] who

105  placed small wire meshes on top of the specimen surface instead of applying surface painting to allow the presence of

106  bleeding water and to avoid the paint slowing the evaporation rate. This technique was adequate due to the type of the

107  mould and restraints causing a localized stress field above the triangular stress riser [6], but would not be suitable for

108  more stochastic crack patterns with unknown locations as the ones obtained in the present study. In the present study,

109  spray-painting the specimen surface was considered to be the most appropriate method for analysing scattered crack

110  patterns, although it resulted in some limitations in the design of the specimen material and the geometry. To analyse

111  the influence on the evaporation rate, different paint types, including acrylic-based and chalk-based paints, were

112  evaluated in this study by monitoring the weight loss from mortar specimens.

113

114

115

*Table 1. Raw materials for mortar overlay mixture*

| Material | Type | Quantity [kg/m$^3$] | Proportions |
|---|---|---|---|
| Cement | CEM I 52.5 N | 700 | 1.0 |
| Fine aggregate | Sand (0–4 mm) | 1032 | 1.47 |
| Water | Tap water | 350 | 0.5 |

117

## 2    Experimental programme

### 2.1  Materials

The main objects of the experimental programme were a mortar overlay and, in the restrained tests, a concrete substrate.

The mortar's basic raw material properties are shown in Table 1. A low sand-to-cement ratio for the mortar overlay was

chosen to foster plastic shrinkage deformations and the mix proportions were chosen in an attempt to produce results

comparable to other studies that have investigated plastic shrinkage cracking [1,20,48,49].

The mixing of the mortar material was carried out in a Hobart-type paddle mixer. The sand and cement were dry-mixed

for 2 min, whereupon water was added (time zero = $t_0$) and wet-mixed for 3 min at low speed and 5 min at high speed.

Specimens used for both free and restrained shrinkage tests and for monitoring the temperature and weight loss were

cast by applying the fresh mortar into the respective moulds and using a vibration table at 60 Hz for up to 1 min. A

smooth steel trowel was used to finish the surface of the fresh mortar under continuous vibration. The total casting

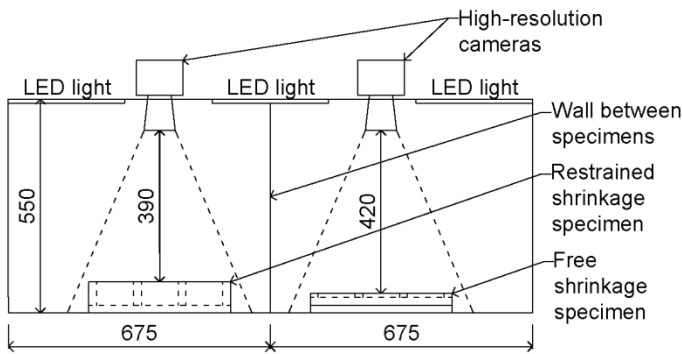process took approx. 15 min from start of wet-mixing (t = 15 min).
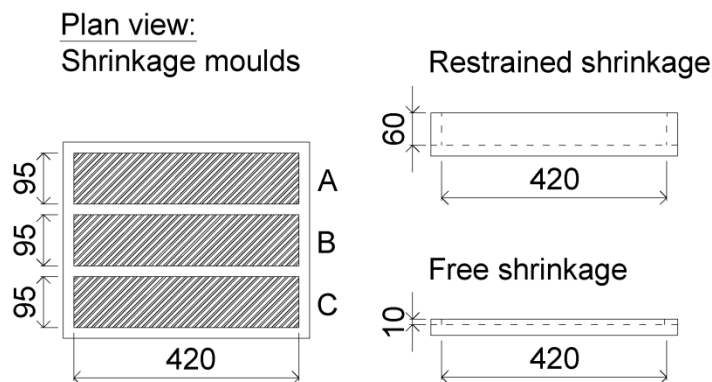


*Fig. 1. Geometry of moulds and specimens for free and restrained shrinkage tests.*

132

133

134

**2.2 Shrinkage tests**

135
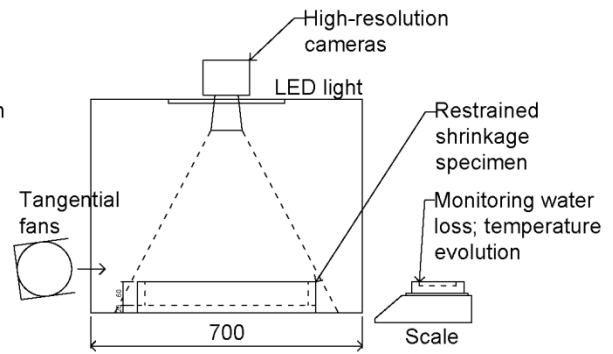
Experiments on the plastic shrinkage behaviour of free and restrained mortar specimens were carried out and a

136

contactless DIC technique was applied. The specimens were monitored continuously in the period of t = 1–25 h,

137

capturing information about the formation of surface displacement and cracking over time. For the restrained shrinkage

138

test, a fresh mortar overlay measuring 420 x 95 x 10 mm was cast on top of a concrete substrate produced in accordance

139

with UNI/EN 1339 (2003) [50] with the desired roughness, see Fig. 1. The developed method was inspired by several

140

studies on shrinkage cracking of cement-based materials restrained by an underlying hardened substrate [3,12–

141

14,16,48,51]. The geometry and mixture design of the restrained mortar overlay was chosen in order to have limited

142

bleeding water so that a high-contrast surface pattern for the DIC monitoring could be applied on the overlay surface

143

shortly after pouring the fresh mortar overlay. Moreover, the geometry of the restrained mortar overlay was designed to

144

promote scattered surface cracking, which would be challenging to measure quantitatively with manual measuring

145

techniques.

146

The concrete substrate surface was roughened using a needle hammer to a depth of about 1 mm to restrain the mortar

147

overlay during the plastic shrinkage period and cause the formation of plastic shrinkage surface cracking. The concrete

148

substrates were cut into beams with a length of $418 \pm 0.3$ mm, a width of $93.5 \pm 0.2$ mm, and a height of $49.6 \pm 0.2$ mm,

149

which fit into plywood moulds with the dimensions 420 x 95 x 60 mm and were then kept in the climate-controlled

150

chamber until they were used. The compressive strength of the substrates was tested in accordance with UNI/EN

151

12390-3 (2012) [52] on cylinders measuring 50 mm x 100 mm cut out of the concrete plates and was found to $35.5 \pm 6$

152

MPa and the dry density to 2.180 kg/m$^3$. Prior to each test series, three concrete substrates were wetted and positioned

153

inside the moulds. After the shrinkage tests, the surface cracking (i.e. crack widths) was analysed using an optical microscope to compare the results obtained by the DIC measurements. Some of the tested overlay-substrate specimens were subsequently impregnated with fluorescence epoxy and cut into longitudinal cross-sections to measure the internal crack width and depth of cracks appearing along these longitudinal sections.

The free shrinkage behaviour was measured on mortar specimens measuring 420 x 95 x 10 mm, a geometry similar to the mortar overlay used in the restrained shrinkage tests. The free shrinkage specimens were placed inside lubricated moulds with a smooth surface avoiding any restraints. Three test series (Series 1–3) were conducted to confirm the reproducibility of results from the proposed setup; each test consisted of three free shrinkage specimens, three restrained shrinkage specimens, and two smaller specimens used to monitor the temperature evolution and evaporation rate.

### 2.2.1 *Temperature and evaporation rate*

The internal temperature and water evaporation rate of the mortars used for the shrinkage test were monitored on small-size unrestrained mortar specimens measuring 95 x 95 x 10 mm using thermocouples and by measuring weight loss over time (t = 1-25 h). These small-size specimens were prepared in the same way as the shrinkage specimens and were placed next to the shrinkage specimens during the tests.

### 2.2.2 *Climate-controlled chamber and plastic shrinkage test setup*

The setup shown in Fig. 2 for the DIC acquisition was placed inside a climate-controlled chamber without any natural light and with a temperature of 32 ± 1.5 °C and a relative humidity of 33.5 ± 5%, which were documented every 15 min by a data logger. The relative humidity was controlled by a dehumidifier, and electric tangential fans were placed in front of the specimens to ensure a constant wind flow over the specimen surfaces of 3.9-4.5 m/s parallel to the *x*-direction. The wind flow was measured right above the specimen surface at different locations (front, middle, back) and was consistent for all three test series. The climatic parameters were set to ensure an adequate rate of water evaporation from the fresh mortar specimens [44] and they were close to the standard parameters suggested in ASTM C1579-13 (2013) [6].

### 2.3 Specimen preparation for DIC monitoring

The main factors influencing the quality of the displacement measurements by DIC are the quality and resolution of the camera, the lighting conditions, the high-contrast surface pattern, and the correlation software [37]. The same camera and light settings were applied for all three test series, so the accuracy of the DIC computation depended mostly on the quality of the high-contrast surface pattern, which was applied manually for each specimen. The plastic shrinkage-induced surface displacements correlate closely with the rate of water evaporation from the specimens, so the effect of the paint on the evaporation rate is crucial. The influence of both an acrylic-based and a chalk-based paint types was investigated to evaluate their effect on the rate of water evaporating from the specimen surface. The weight loss of specimens with four variations of surface preparation was measured; a) no paint; b) base of white chalk-based with dots of black chalk-based paint; c) base of white chalk-based with dots of black acrylic-based paint; d) base of white acrylic-based paint. The specimens were cast in cylindrical plastic containers with a surface area of 100 cm$^2$ and a volume of 0.47 L. Three replicates were tested. It should be noted that the dimensions of the containers used in this test were not the same as those used during the actual shrinkage test series, so the results cannot be directly compared.

The surface preparation for the specimens used for the evaluation of the types of surface paintings and the actual shrinkage specimens were done in the same way: After casting (at t = 15 min), the specimens were left at 20 ± 3 °C for 30 min (t = 15-45 min), after which they were painted with the respective paint types (t =45-55 min) . The specimens were then transferred to the climate-controlled chamber and placed inside the test setup (at t = 55 min) and at exactly t = 1 h the respective monitoring was initiated (weight loss, temperature or image capturing for DIC). The monitoring continued until t = 25 h.

**2.4 Monitoring of plastic shrinkage deformations using DIC**

The test setup shown in Fig. 2 was arranged in the climate-controlled chamber with a coherent light source of LED panels at the top of the chamber to limit optical noise. Two optical cameras with wide-angle lenses were mounted parallel to the surface of the specimens so that 2D displacements in the plane of the specimen surface could be captured. Vertical deformations were not taken into account due to the low thickness of the specimens. The distance between the lenses and the specimen surface ranged between 390 mm and 420 mm, depending on the type of specimen being tested (free or restrained). The digital cameras used have a resolution of 7360 x 4912 pixels and monochrome colour representation. The respective pixel lengths were 0.087 mm for the free shrinkage specimens and 0.080 mm for the restrained specimens (a difference due to the camera lens-to-specimen distance). The cameras recorded a larger area than the size of the specimen surface in order to avoid edge effects, and the focus was on the centre of the three

specimens. The use of two cameras allowed the testing of two moulds containing three specimens each during each test series (restrained and free specimens).

The DIC software GOM Correlate Professional 2016 was used for the DIC analysis. Images of the specimen surface were first consistently modified in ImageJ to improve contrast and brightness prior to being imported to the DIC software. The first image captured at t = 1 h was defined as the undeformed image (reference image), and subsequent images captured every 30 min were compared to the reference image to compute the displacement fields. The DIC software was used to define a region of interest (ROI) for each specimen surface (95 x 420 mm), which was virtually meshed into subset elements with a size of 20 pixels and a point-to-point distance of 15 pixels. A lower subset size and point distance would result in better data acquisition, but the speckle pattern would have to be of a density allowing a minimum of 2–3 dots in each subset [37]. Each specimen surface consisted of approximately 30,000 facets in the restrained shrinkage tests, and approximately 26,000 facets in the free shrinkage tests. The mesh fineness for each ROI is in agreement with the recommendations by Sutton et al. [37] and, moreover, it corresponds to the number of subsets used in the study by Némoz-Gaillard et al. [29] who also studied plastic shrinkage cracking of cement-based materials.
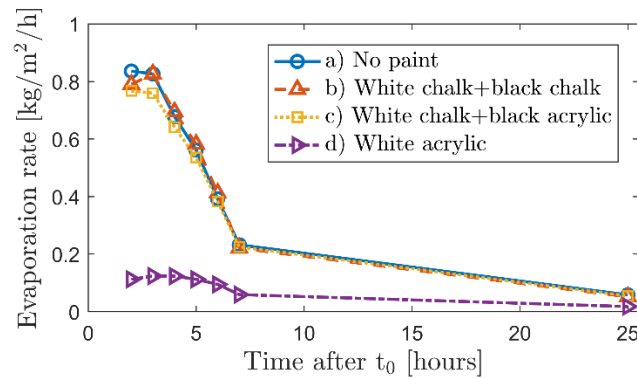


*Fig. 3. Water evaporation rate from mortar specimens prepared with different types of surface paintings; a) Reference with no paint; b) base of white chalk-based with dots of black chalk-based paint; c) base of white chalk-based with dots of black acrylic-based paint; d) base of white acrylic-based paint.*

## 3    Results

### 3.1  Evaluation of evaporation rate for different types of paint used for surface preparation

The weight loss of unrestrained mortar specimens prepared with different types of surface painting used for creation of a high-contrast surface pattern for the DIC analysis was monitored during the test period of t = 1-25 h. The results were used for evaluating the influence of chalk-based and acrylic-based paint types on the evaporation rate and are illustrated

233  in Fig. 3. From the figure it is seen that the application of white acrylic-based paint (type d) clearly causes a significant

234  delay in water evaporation when compared to the reference specimen with no paint (type a), whereas the chalk-based

235  paint (type b), which is diffusion-open, performed similarly to the reference without surface painting. Specimens with a

236  white layer of chalk-based paint and black dots of acrylic-based paint (type c) had a slightly lower evaporation rate.

237  This was probably due to the sealing effect of black acrylic-based paint, and the difference was clear although only a

238  very thin layer of black acrylic-based dots was applied. When examining the specimens during and after the evaporation

239  test, the layer of white acrylic-based painting (type d) detached from the mortar surface by flaking off. It was therefore

240  concluded that acrylic paint is unsuitable as surface paint for plastic shrinkage testing because it seals the mortar surface

241  and significantly delays the water evaporation. Based on these observations, it was found best to use the chalk-based

242  paint for both the white base and the black speckle pattern (type b), although it would not allow testing materials with

243  excessive bleed water. The use of a chalk-based paint, which doesn't influence the evaporation rate is a major

244  achievement for the application of the DIC technique for studying the shrinkage-related behaviour of cement-based

245  materials, since a delay in water evaporation may also delay air penetration and would probably reduce the degree of

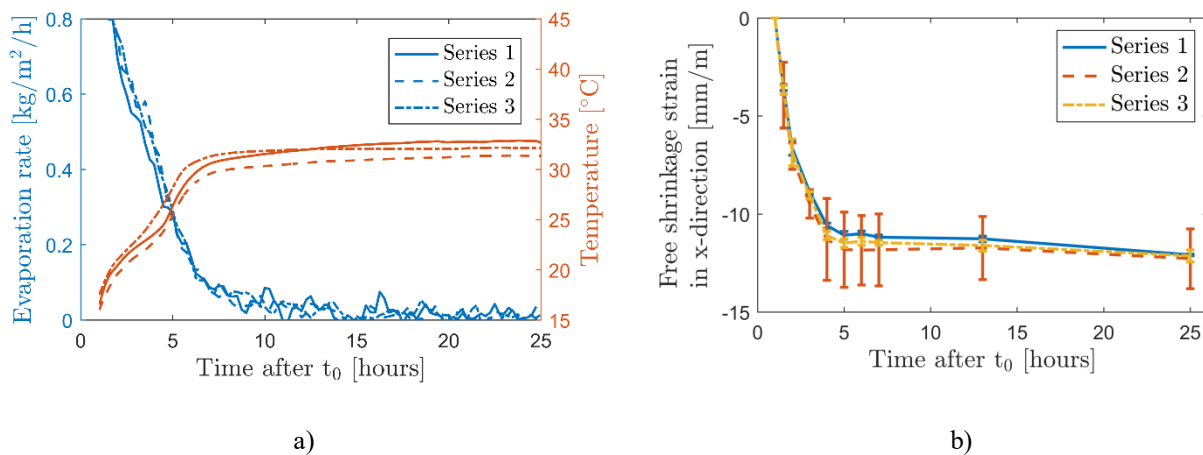246  plastic shrinkage in a concrete specimen [53].



a)

b)

247  *Fig. 4. a) Evaporation rate and temperature evolution for mortar specimens in Series 1-3 (data is smoothened); b) In-plane free*

248  *shrinkage strain in x-direction with mean values of three replicates (A-C).*

249

250  **3.2  Temperature evolution and evaporation rate during shrinkage tests**

251  The temperature evolution and water evaporation rate from unrestrained mortar specimens were monitored parallel to

252  the actual shrinkage test to obtain a better understanding of the material behaviour in the period of t = 1–25 h, see Fig.

253  4a. The evaporation rate was approximately 0.8 kg/m²/h directly after placing the specimens in the harsh environment

254  of the climate-controlled chamber, whereupon it gradually decreased and stabilized at 0 kg/m$^2$/h at approximately t = 9

255  h. Estimations of the evaporation rate based on Menzel's formula and the nomograph in ACI 305R-06 [44,54] were

256  calculated in the range of 0.1–0.5 kg/m$^2$/h depending on the fresh concrete temperature (17–26 C. The cement hydration

257  entered the acceleration period at about t = 4–5 h after $t_0$, which was also the end of the dormant period. The internal

258  temperature evolution of the mortar specimens is also illustrated in Fig. 4. The initial temperature of the fresh mortar

259  was 17 ± 2 C° (at t = 1 h). The temperature and evaporation curves for the specimens monitored during the series of

260  Series 1-3 showed a similar shape for all three test series.

261

262  **3.3  Study of free shrinkage behaviour using DIC**

263  The free shrinkage behaviour of mortar specimens measuring 420 x 95 x 10 mm was monitored from t = 1-25 h. Most

264  significant plastic shrinkage deformations took place in the *x*-direction due to the specimen geometry and wind

265  exposure. Uniform displacement fields were observed and by using the data obtain by the DIC monitoring, the

266  horisontal displacement during the entire test period was quantified. Equivalent displacement and strain data in the

267  centre of each subset were computed as the average value over the subset area (20 x 20 pixels) [28]. With the *x*-

268  direction being parallel to the length of the specimens, the maximum free shrinkage strain (mm/m) in this direction over

269  time was computed using a Matlab routine. This is illustrated in Fig. 4b, where each graph represents the mean value of

270  three specimens tested in each of the respective tests. The free shrinkage strain (contraction) increased rapidly during

271  the first 3–4 hours after $t_0$ and then stabilized. Final contractions of the specimens were in the range of approximately 5

272  mm (relative contraction = -12 mm/m) in the *x*-direction for all specimens tested. Due to the specimen geometry and the

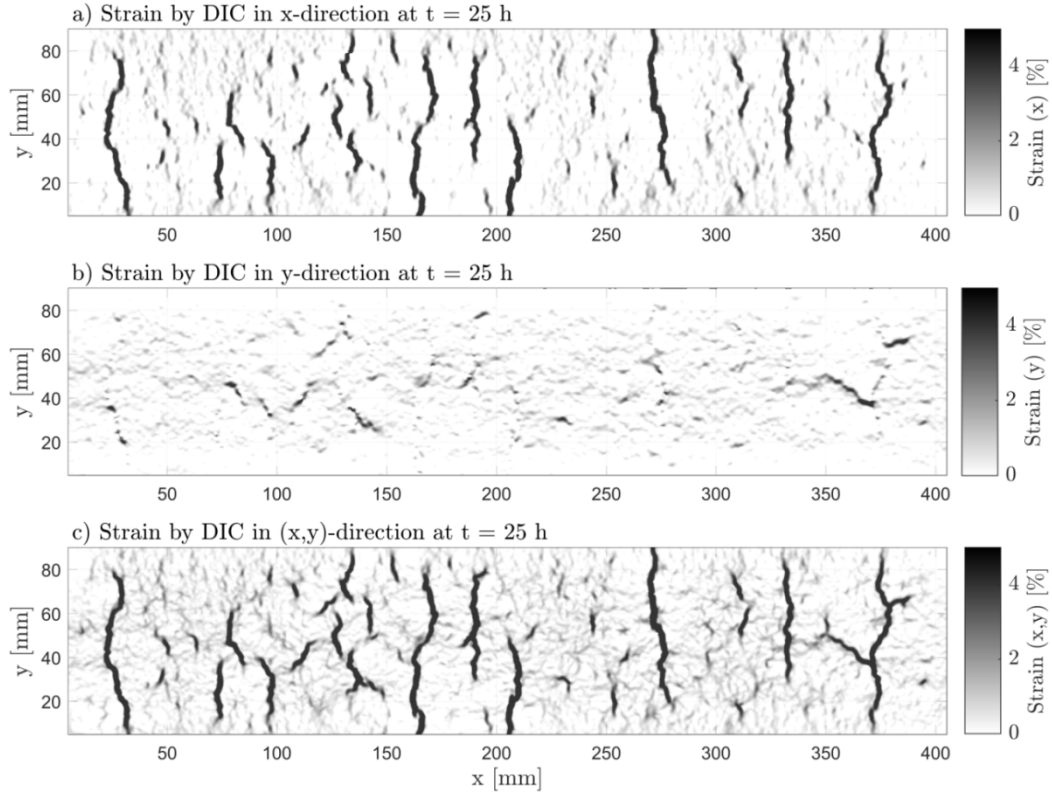273  oriented wind flow, focus was solely on the shrinkage behaviour in the *x*-direction.

a) Strain by DIC in x-direction at t = 25 h

b) Strain by DIC in y-direction at t = 25 h

c) Strain by DIC in (x,y)-direction at t = 25 h

274

275    *Fig. 5. Surface strain fields for Specimen C, Series 2, in: a) x-direction; b) y-direction; c) Major (x,y)-direction*

276

277    **3.4  Study of surface cracking in restrained overlays using DIC**

278    The aim of this section is to quantify the degree of cracking in the restrained mortar overlays in terms of time of

279    cracking, crack location, crack width, crack length, and crack area. During the restrained shrinkage test of the mortar

280    overlays (t = 1-25 h), several visible surface cracks formed. The displacement and strain fields were obtained using the

281    DIC software, and the crack formation was then analysed using a numerical routine for post-processing of the DIC data.

282    Since the strain data is a numerical approximation to partial derivatives of the displacement (Eq. 1), abrupt changes in

283    displacement are simultaneously illustrated as local extrema in strain. These peaks in strain and sudden gaps in

284    displacement reveal surface cracking [55]. From small-deformation theory, the strain tensor is given component-wise

285    by:

$$\varepsilon_{ij} = \frac{1}{2}\left(\frac{\partial u_i}{\partial x_j} + \frac{\partial u_j}{\partial x_i}\right) \tag{1}$$

286    where $u$ is the displacement and $x$ is the position vector.

287     Based on the assumption that most cracking appear in the $x$-direction and for simplicity, the numerical post-processing

288     of the DIC data was restricted to the in-plane displacement and strain in the $x$-direction for the analysis of surface

289     cracking. Considering only the strain in the $x$-direction gives:

$$\varepsilon_{11} = \frac{\partial u_1}{\partial x_1} \tag{2}$$

290     This effectively reduces the analysis to a one-dimensional problem for each linear segment parallel to the $x$-axis. The

291     purpose here is to prove that useful results can be obtained by projecting the data onto just one of the axes when the

292     cracks are evenly oriented. While similar numerical processing would be possible in the full 2D case, one-dimensional

293     analysis was preferable due to its simplicity both in data processing and in the explicability of the method.

294     To describe the post-processing procedure for the computation of the crack data Specimen C, Series 2 is used as an

295     example in the following figures. Fig. 5a–c show the strain data obtained by DIC for the normal strain in the $x$-direction,

296     $y$-direction, and major $(x,y)$-direction. The figure clearly demonstrates the ability of the DIC technique to localize areas

297     with increased strain, i.e. the boundaries of the cracks. In this case, it is clear that the numerically largest normal strain

298     values are parallel to the $x$-direction, which was the case for all 9 specimens tested (Series 1-3, Specimens A-C). This is

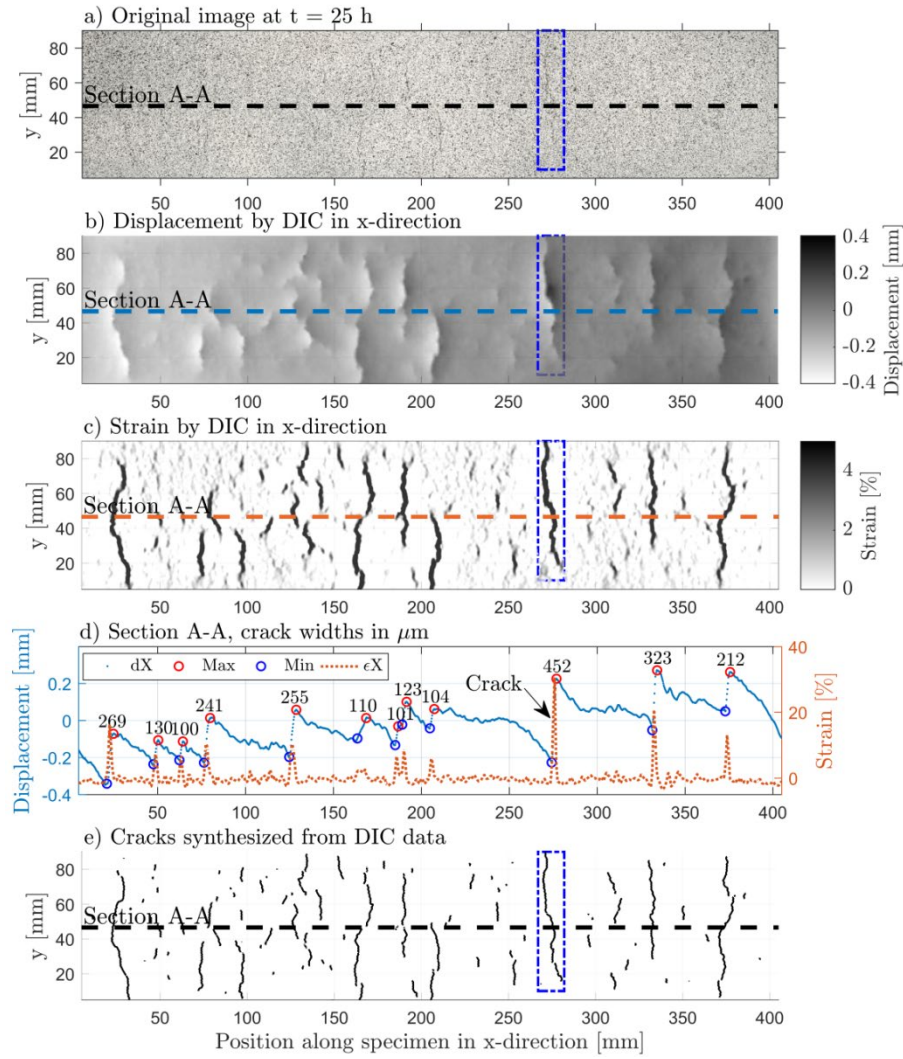299     likely due to the specimen geometry and wind flow orientation.

*Fig. 6. Restrained mortar overlay (Specimen C, Series 2) at t = 25 h. a) Original image; b,c) In-plane surface displacement and strain in x-direction by DIC data; d) In-plane surface displacement and strain by DIC data along Section A-A showing detected cracks; e) Crack pattern synthesized from data by the post-processing approach. A magnification of the rectangular area around a large crack is shown in Fig. 7.*

### 3.4.1 Computation of surface cracking based on DIC data

The first part of the post-processing procedure was to export an array consisting of (*x,y*) coordinates for all subsets in the ROI for each specimen surface and the corresponding displacement and strain data for further analysis in Matlab. The data in each ROI was interpolated onto a rectangular grid with point-to-point distance of 0.25 mm in both *x*- and *y*-directions, which ensures uniformity in the grid, enabling estimation of derivatives and visualizations of the data. In total, there are approximately 380 one-dimensional sections parallel to the *x*-direction per specimen surface. Fig. 6a–c

show an image of the cracked surface of Specimen C, Series 2, at t = 25 h, and surface displacement and strain fields

parallel to the *x*-direction as calculated by DIC. A selected section, Section A-A, along the specimen surface going

through the centre of the specimen is marked with a dashed line is shown in Fig. 6d.

The post-processing procedure used for automated detection of surface cracking can be explained by Fig. 6d, which

shows the surface displacements and strains in the *x*-direction along Section A-A. Damaged areas (surface cracks) are

defined as local gaps in the displacement field and corresponding peaks in surface strain [13,55,56]. To compute these

damaged areas on the specimen surface, i.e. crack widths, the local minimum values (blue circles) and the maximum

values (red circles) neighbouring each displacement gap were identified for each section and corresponds to the
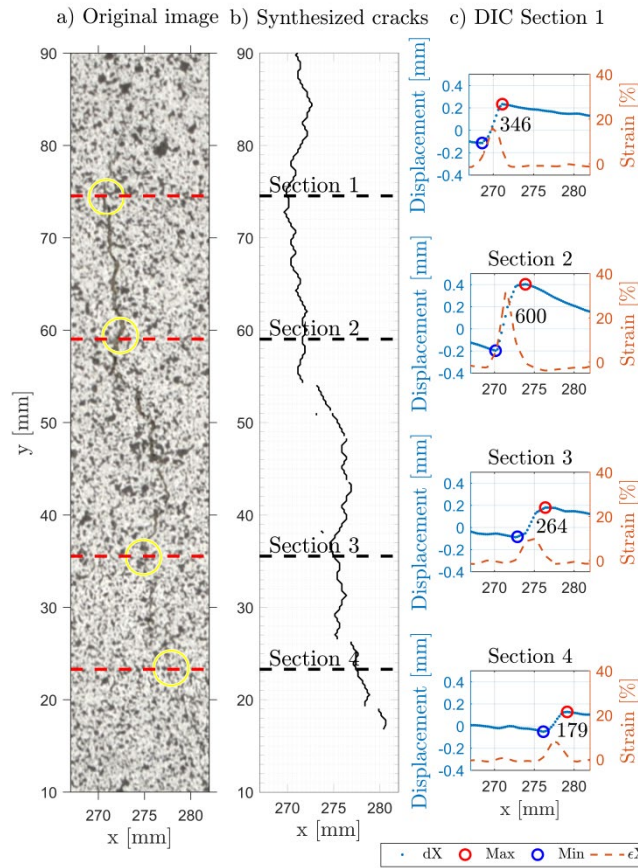
identified crack width ($w_i$).



*Fig. 7. Magnification of the rectangular area shown in Fig. 6 (Specimen C, Series 2, t = 25 h): a) Original image; b) Crack pattern*

*synthesized from DIC data by the post-processing approach; c) In-plane displacement and strain along Section 1–4.*

From the strain data, a strain threshold limit for when a displacement gap is considered as cracked was defined. This

threshold limit is dependent on parameters such as the material properties (the tensile strength and stiffness) under the

specific environmental conditions and the DIC setup (the resolution of the image and subset properties), and should

therefore not be interpreted as a globally applicable number. The strain threshold limit also defines the fineness of the

cracks to be identified. Several strain threshold limits ranging from 0.002 m/m and up to 0.1 m/m were tried in an effort

to find a reasonable level. See also Section 4.1. With very low threshold values, a significant number of short, very fine

cracks were identified, which can be considered as noise. Lagier et al. [57] suggested a strain threshold limit based on

the ratio between tensile strength and Young's modulus in compression (tensile strain capacity) [32]. In the present

study, however, the surface cracking occurred when the overlay material was still fresh and changed rapidly during

hardening and would be difficult to obtain at the exact time of surface cracking. Mauroux et al. [13] studied micro-

cracking of mortars induced by drying shrinkage and defined a maximum strain threshold limit of $5 \cdot 10^{-5}$ m/m. Boshoff

and Adendorff [56] defined a crack as having a displacement gap larger than 15 μm. In this study, the strain threshold

limit is defined in terms of the average strain ($\varepsilon_{i,\text{avg}}$) along the displacement gaps between the local maximum ($x_{i,\text{max}}$,

$u_{i,\text{max}}$) and minimum ($x_{i,\text{min}}$, $u_{i,\text{min}}$) values.

$$\varepsilon_{i,\text{avg.}} = \frac{u_{i,\text{max}} - u_{i,\text{min}}}{x_{i,\text{max}} - x_{i,\text{min}}} \tag{3}$$

Using the average strain makes the strain threshold limit less sensitive to noise than simply requiring an individual

strain value to be above a certain threshold limit. On the basis of microscopy observations and the desired fineness of

crack detection, a strain threshold limit was defined as $K_0 = 0.02$ m/m = 2%, such that a crack is defined as a local

interval where the average tensile strain along the displacement gap is larger than $K_0$, i.e.

$$\varepsilon_{i,\text{avg.}} > K_0 \Longrightarrow \text{Surface crack} \tag{4}$$

Based on the section-wise analysis (sections per 0.25 mm) in accordance with the above procedure, a digital

reproduction of the crack pattern was synthesized including crack location and crack width. See Fig. 6e. Please note that

the crack widths and locations were not derived from pixels, but from computation of DIC data. Also, the line thickness

on the synthesized crack patterns in does not correspond to the real crack width, but is only illustrating the centre line

for all identified cracks using standard line width for plotting.

All displacement gaps with an average tensile strain larger than $K_0$ were identified as cracks and crack widths were

calculated corresponding to these displacement gaps along each separate section. In this way, quantified measures of the

crack width along every section on the specimen surface were obtained. If cracks appeared in adjacent parallel sections,

the cracks were defined as coherent whenever the distance between the cracks was below a crack coherence threshold

defined as three times the distance between adjacent parallel sections. After identifying coherent cracking points (across

parallel sections), the crack length could be defined as the length of a polynomial fit to the points belonging to the same

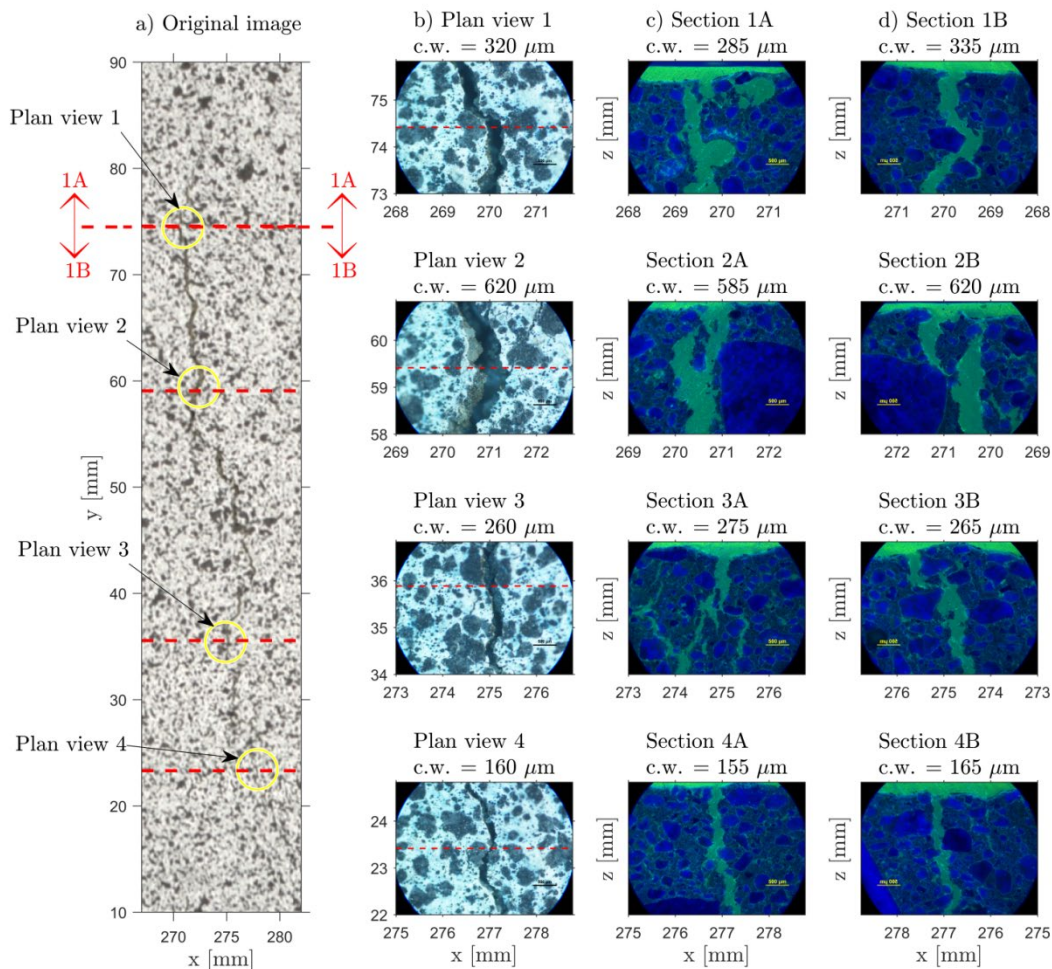crack, making it also robust to more noisy representations of cracks.



*Fig. 8. Measurements by optical microscope of cracks near Section 1-4 as shown in Fig. 7 (Specimen C, series 2, t = 25 h). a)*

*Original image; b) Microscopic plan views; c) Section view A-A "above" section 1-4 for epoxy-impregnated specimens; d) Section*

*view B-B "below" section 1-4. Field of view = 2.83 x 3.77 mm.*

### 3.4.2    Correlation between the DIC results and microscopy measurements

The crack displayed inside the rectangular area shown in Fig. 6, is magnified in Fig. 7 showing a) the original image at t

= 25 h; b) the computed cracks based on the post-processing procedure; c) four selected longitudinal sections crossing

the crack (Section 1-4 parallel to the *x*-axis) illustrating the surface displacement and strain along each of the selected

sections. The post-processing procedure described in Section 3.4.1 was used for the automated computation of the crack

widths from the displacement and strain fields along Section 1-4 on the specimen surface, which in these specific cases

366     are, 346 μm, 600 μm, 264 μm and 179 μm, respectively, as shown in Fig. 7c. To validate the dimension of the crack

367     widths computed based on DIC data, the crack widths along Section 1-4 were measured using an optical microscope.

368     Examples on this is given in Fig. 8 that shows b) Plan view: microscopic images of the specimen surface in the area

369     around the selected Section 1-4, c, d) Section views on each side of the selected section specimens to measure the crack

370     width and depth on epoxy-impregnated samples cut into longitudinal sections as close to Section 1-4 as possible. These

371     manual crack width measurements were done after the shrinkage test series as it would be very challenging to obtain

372     crack measurements with this degree of precision while the shrinkage test was running.

373     First of all, it was observed that the crack width along the length and depth of a crack was highly irregular, which also

374     complicated a manual quantification of the crack width. Cracks in concrete are usually highly irregular and

375     continuously change direction as they propagate [34]. This makes them difficult to quantify with manual measuring

376     techniques, which further demonstrates how important the DIC quantification technique is for evaluating crack patterns.

377     Secondly, the microscopy images showed a good correlation with the crack widths measured from DIC data, both when

378     analysing the crack widths on the specimen surface, b) Plan view; and when analysing the longitudinal sections of the

379     epoxy-impregnated specimen, c,d) Section view.

380     Regarding the detected crack length, some spaces can be seen along the length of the computed crack resulting in

381     discontinuities, although many of the cracks visually appeared to be continuous along the entire length. However, when

382     the cracks were examined using an optical microscope, it was confirmed that the computed discontinuities were actually

383     physically present at the detected locations along the crack. The identification of smaller crack widths is linked to the

384     strain threshold value, so that lower strain threshold values result in the identification of finer cracks. It was also

385     observed that parallel cracks running close to each other or the presence of fine cracks or other irregularities near the

386     measured crack could result in calculation errors. The DIC software is unable to compute the subsets closest to a crack.

387     Thus, the subset texture in the cracked area is being modified by the presence of the crack, which can result in

388     overestimations of the measured crack width [13,16]. Another challenge arises when multiple cracks are present in one

389     subset [58], but in the present study such crack widths were considered to be too small to include because the distance

390     between each subset centre was 1.2 mm (15 pixels). Even though there is a strong correlation between the crack widths

391     measured using DIC and the microscopy measurements, local flaws on the specimen surface could lead to local

392     fluctuations in the correlation computation of the displacement fields [57]. The deformations were monitored while the

393     mortar was still plastic and the following 24 h, and large changes occurred on the surface during the test period. These

394 changes included not only the plastic shrinkage, but also developments in the surface structure due to the material

395 drying and hardening, and the emergence of air bubbles on the surface, which could lead to local flaws.

396 It is acknowledged that this is a simplified method for calculating the crack widths, due to the assumption that all cracks

397 are parallel to a pre-defined axis and that the method can result in local errors in the DIC data and post-processing

398 results. However, the proposed method is a great improvement on more manual measuring techniques and provides

399 excessive information about the materials behaviour.
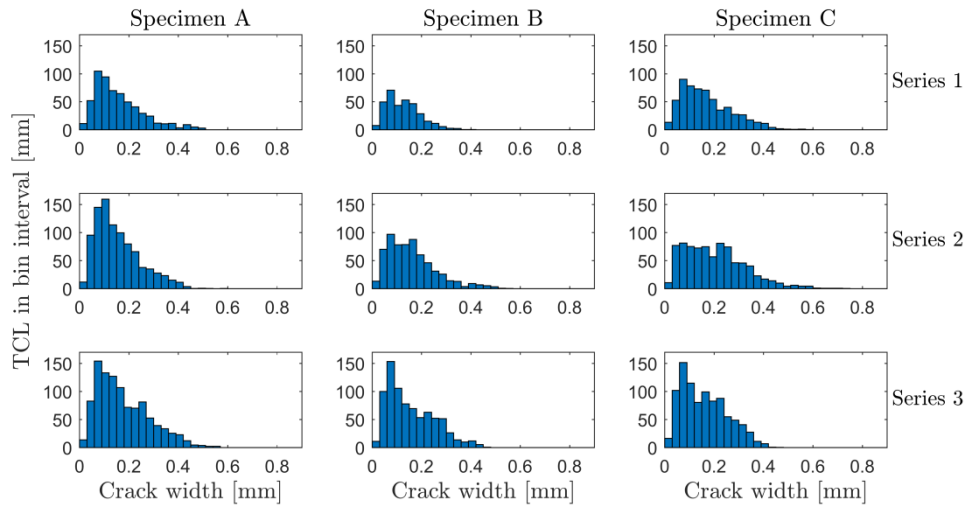
400



401 *Fig. 9. Histograms of the relation between the total crack length (TCL) [mm] in each bin interval and the crack width distribution*

402 *(CWD) over the entire specimen surface for Series 1–3 at t = 25 h.*
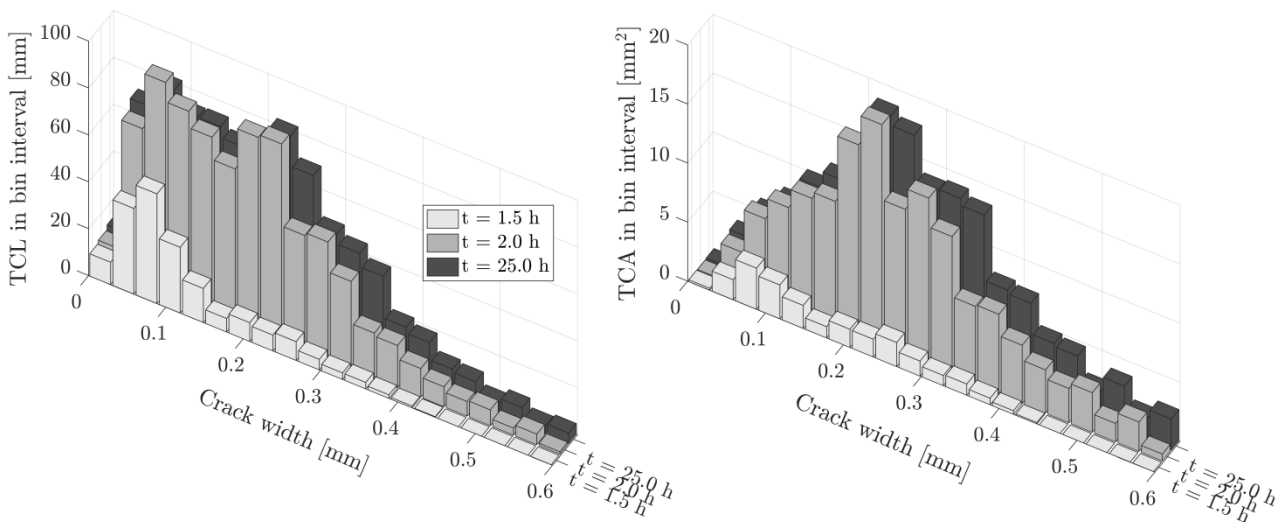
403
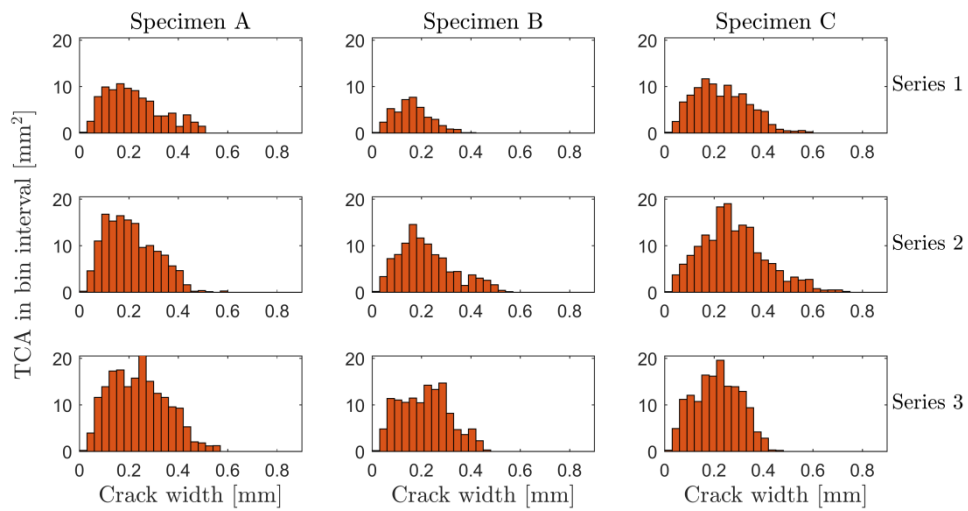
404



405 *Fig. 10. Histograms of the relation between the total crack area (TCA) [mm² ] in each bin interval and the crack width distribution*

406 *(CWD) over the entire specimen surface for Series 1–3 at t = 25 h.*

**3.5 Quantification of surface cracking**

First, all displacement gaps (cracks) with an average strain level above the strain threshold value were detected along the 380 sections parallel to the *x*-direction of the interpolated grid. Computing the crack width ($w_i$) for all these cracks along every section enabled plotting of histograms showing the crack width distribution (CWD). The CWD was plotted so that each bin interval (interval of crack widths) was representing the total length of cracks (TCL) within each bin interval (Fig. 9); and as the total crack area (TCA) within each bin interval (Fig. 10). These plots are shown for all nine specimens (Series 1-3, specimens A-C). Besides the histograms, various crack parameters, such as maximum crack width, mean crack width and total crack area over the entire specimen surface, could easily be calculated using the post-processing procedure. See Table 2. The crack area of each crack ($A_{i,cr}$) and the total crack area ($A_{tot}$) of the entire surface of each specimen was calculated by summing all cracks [12].

The accuracy of these histograms depends on the number of subset properties for each specimen surface and the fineness of the interpolated grid. Since 380 sections parallel to the *x*-direction were analysed for each specimen surface, the fineness of the grid was considered to be sufficient for the purpose of this paper. Similar histograms have been used in other studies to present crack width distributions, e.g. for cracks emerging from tensile loading [56,59] or from shrinkage [60,61]. Traditional crack parameters used for evaluation of the degree of plastic shrinkage cracking such as maximum crack width, crack length, and total crack area are only considered as weak indicators of the degree of surface cracking. Thus, this way of representing the degree of surface cracking is considered to be more informative.

a) Total crack length per bin interval                    b) Total crack area per bin interval

425 *Fig. 11. Histograms of the relation between the crack width distribution (CWD) over the entire specimen surface and a) the total*

426 *crack length [mm] and b) the total crack area [mm$^2$] in each bin interval, at selected time intervals of t = 1.5 h, 2.0 h, h and 25 h.*

427 *Example given for Specimens C, Series 2.*

428

429 *3.7.1 Crack area evolution*

430 Another advantage in using DIC for crack detection and quantification is the opportunity to study the evolution in

431 surface cracking over time. Fig. 11 illustrates the evolution in histograms showing the crack width distribution over the

432 entire surface area with each bin representing the total crack length and total crack area, respectively. The example is

433 again given for Specimen C, Series 2. Initiation of the shrinkage-induced surface cracking had already happened when

434 the first deformed image was captured at t = 1.5 h. This reveals that the images should have been captured more

435 frequently, especially in the beginning of the test, when the largest shrinkage-induced deformations occurred. The crack

436 network had stabilized at the time stage of t = 2.0 h, and only slight propagations in crack widths and number of cracks

437 were observed until the end of the test at t = 25 h (time stages in between are not shown). These observations

438 correspond well with the behaviour of the free shrinkage specimens, which showed most deformation activity during

439 the same time period, although the crack network stabilized faster than the deformation in the free specimens. The

440 initial shape of the crack network remained stable throughout the entire test, though the crack width intensity increased

441 slightly over time.

442 *Table 2. Summary of basic crack parameters for restrained mortar overlays*

| Specimen | Mean crack width | SD | Max crack width | SD | Total crack area | SD |
|---|---|---|---|---|---|---|
| | [μm] | [-] | [μm] | [-] | [mm$^2$] | [-] |
| Series 1 (A-C) | 151.2 | 18.7 | 497.8 | 78.2 | 87.8 | 29.6 |
| Series 2 (A-C) | 173.5 | 22.8 | 631.2 | 80.5 | 151.5 | 30.7 |
| Series 3 (A-C) | 164.9 | 8.9 | 500.0 | 45.5 | 167.5 | 26.4 |

443

444 **3.6 Reproducibility of restrained shrinkage test**

445 Three identical test series (Series 1–3) were carried out on three specimens (Specimen A, B, C) to evaluate the

446 reproducibility of the test method. All the restrained mortar overlays were of the same mix design and exposure

447 conditions. Fig. 9-10 quantitatively illustrate the degree of surface cracking in histograms showing the crack width

448 distribution and Table 2 gives basic crack parameters such as mean and maximum crack width, and total crack area at t

449 = 25 h. Despite some variations in total crack area between the three test series, the mean and maximum crack width are

very much alike. It was difficult to create identical crack patterns from one specimen to another, and the formation of plastic shrinkage cracking is generally known to be a highly irregular and variable process [3,48]. However, the CWD for most of the specimens follows the same trend.

Since the mortar mix design used in this study was the same for all specimens tested, the factors resulting in different surface cracking behaviour mostly stem from the slight variations in environmental conditions, the geometry and surface roughness of the concrete substrate, thus the thickness of the fresh mortar layer. The environmental conditions (temperature and relative humidity) inside the climate-controlled chamber were monitored during the entire test and shown in Fig. 12. Slight variations in the relative humidity are observed with the lowest being for Series 2, however, this still doesn't explain the lower total crack area for Series 1.
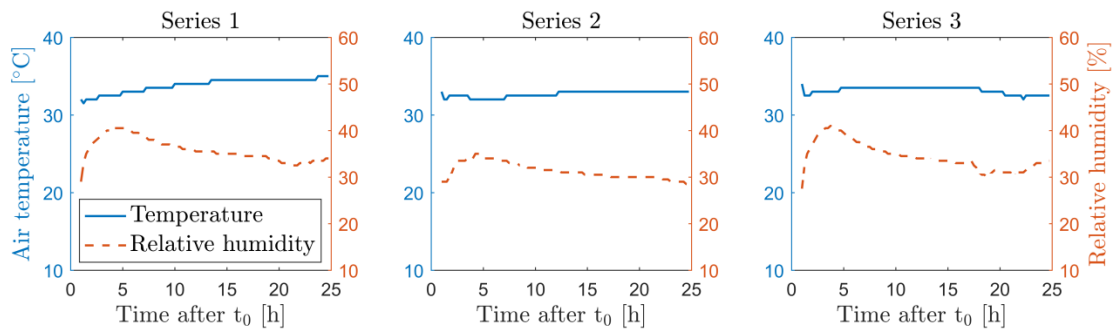


*Fig. 12. Temperature and relative humidity during the shrinkage tests series, Series 1–3.*

## 4   Discussion

### 4.1 Evaluation of defined strain threshold limit

The defined strain threshold limit, $K_0$, determines the fineness of displacement gaps that should be identified as cracks. Low threshold values would result in the detection of significantly more fine cracks with very low crack widths, where some could be due to the presence of local fluctuations or noise resulting in interpolation errors [13]. Since the high-contrast surface pattern was applied when the material was still wet, it could lead to small movements of the paint layer, especially with the presence of bleeding water on the surface. Therefore, other strategies should be used for the application of the high-contrast surface pattern when studying plastic shrinkage cracking in cement-based with excessive bleeding water [28,45,46].

The determination of a crack and its width is still a problem of definition [34], so the strain threshold value was chosen on the basis of visual inspections. Fig. 13a–c illustrate digital reproductions of crack patterns computed for Specimen C, Series 2, using three different strain threshold values: $K_0 = 0.002$; $0.01$; and $0.02$ m/m, respectively. It is clear that a

474  strain threshold value of $K_0 = 0.002$ m/m leads to a large number of fine cracks being identified. The CWD also

475  illustrates how many cracks with a very low crack width are identified with lower threshold values. The identification of

476  wider cracks, i.e. the right side of the CWD, is not influenced by the strain threshold value. A strain threshold value of

477  $K_0 = 0.02$ m/m (Fig. 13c) was chosen for this study because it only shows the widest, most well-defined cracks on the

478  specimen surface with a minimum of identified cracks that could be considered as noise.

479  Fig. 14 shows the total crack area at t = 25 h for each of the specimens (Series 1–3, Specimens A–C) computed for

480  strain threshold values varying from $K_0 = 0.002$ m/m to $K_0 = 0.10$ m/m. It is clear that the total crack area depends

481  entirely on the strain threshold value chosen, and the curves follow the same trend for each specimen.
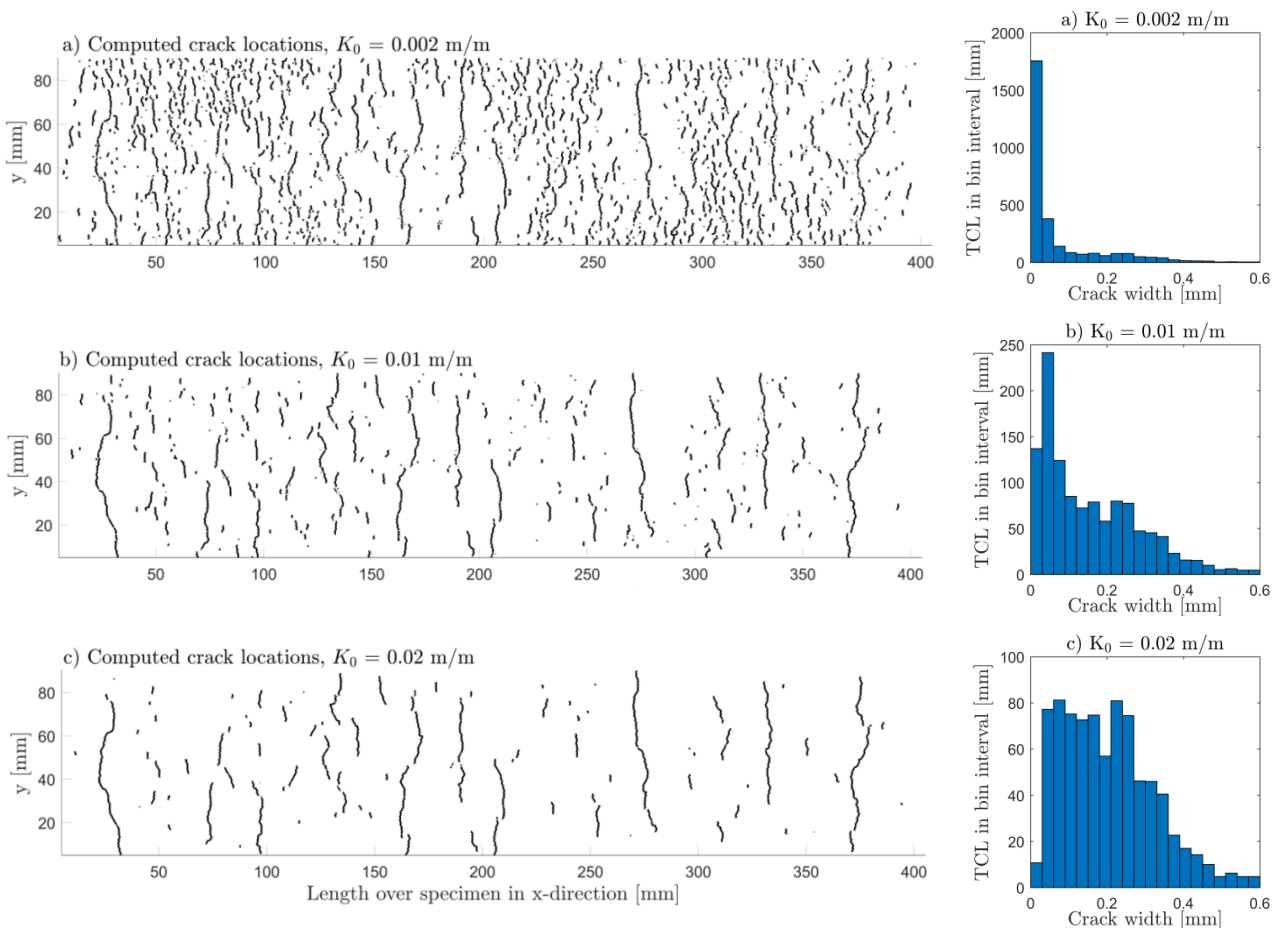


482  *Fig. 13. Examples of crack patterns synthesized from data by the post-processing approach and histograms of the relation between*

483  *the total crack length (TCL) [mm] and CWD using three different strain threshold values, $K_0$: a) 0.002 m/m; b) 0.01 m/m; c) 0.02*

484  *m/m. Examples given for Specimen C, Series 2 at t = 25 h.*

485

486  **4.2 Orientation of cracks**

487   In this study, the focus was on crack openings parallel to the *x*-direction, because most surface cracking occurred in this

488   direction. The post-processing approach is based on a section-wise inspection of parallel sections and computes

489   displacement gaps (cracks) along each of these sections. This enabled an automated computation of crack width

490   distributions and digital reproductions of the crack patterns from surface displacements occurring in a defined direction,

491   which in this study was defined as the *x*-direction. However, there was still some surface displacement occurring

492   perpendicular to the *x*-direction, as shown in Fig. 5b. The "real" crack width should be measured as the crack opening

493   perpendicular to the direction of the crack. Nevertheless, the applied post-processing approach was considered to give a

494   good approximation of the real crack widths for cracks with similar orientation.

495   One limitation of the 2D-DIC technique for crack measurements is that it is only capable of detecting cracks that

496   emerge on the surface and not internal cracking, e.g. cracking due to plastic settlement around rebars [62,63], or

497   cracking in the interface between the overlay and the restraining substrate [39]. In studies by Mauroux et al. [13] and

498   Combrinck et al. [62] it was tried to overcome this limitation by studying internal shrinkage-induced cracks in depth

499   through a transparent plate. However, this can only be done along the periphery of the specimen and is not

500   representative of the whole internal interface. In this study, the restrained shrinkage specimens were epoxy impregnated

501   after the test and cut into longitudinal slices, which enabled an analysis of the crack depth in the z-direction. This was

502   only possible after ended test, so the approach did not enable observations on the crack depth propagation over time.
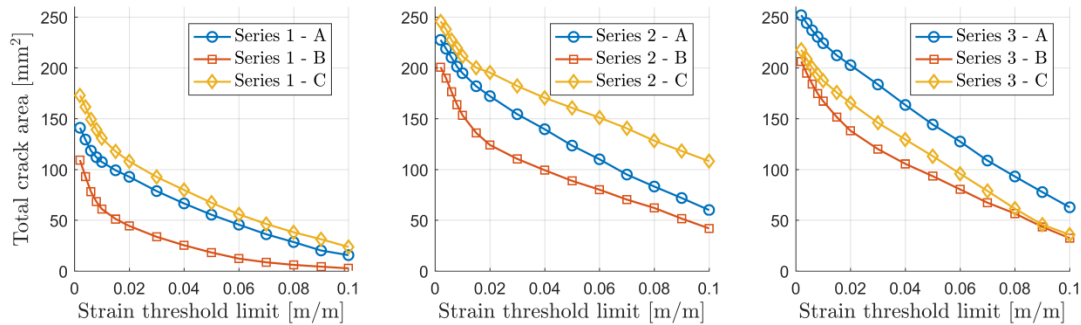


503

504   *Fig. 14. Total crack area at t = 25 h computed for strain threshold values varying from 0.002 to 0.1 m/m for Series 1–3, Specimens*

505   *A–C.*

506

507   **5    Conclusion**

508   The main objective of this study was to present a new test setup for studying the formation of in-plane surface cracking

509   in restrained mortar overlays caused by plastic shrinkage. A digital image correlation (DIC) technique was used for

510   crack detection and quantification. When applying the DIC technique for studying surface displacements, a high-

contrast surface pattern is required, which is often applied using black and white spray paint. Since plastic shrinkage cracking is highly correlated with the rate of water evaporation from the fresh material, it is crucial that this spray paint does not lower the evaporation rate. A chalk-based spray paint was shown to have no influence on the evaporation rate, whereas acrylic-based paints caused a significant decrease in the evaporation rate by sealing the fresh mortar surface.

Quantification of the degree of surface cracking is highly relevant for a deeper understanding of the plastic shrinkage behaviour and this study showed that measurements based on a non-contact 2D-DIC technique allow the monitoring of in-plane strain and displacement fields over time. Based on the DIC data, crack parameters such as crack width, crack length, crack location and crack area could be automatically computed using a Matlab routine. Crack widths parallel to the length of the specimens were computed over a fine interpolated grid covering the entire specimen surface, which enabled a very detailed analysis of the crack width distribution. Moreover, digital reproductions of the surface crack patterns could be synthesized based on the DIC data. To verify the computed crack widths, the results were compared to manual measurements using optical microscope. From the microscope analysis, it was observed that the cracks are highly irregular in terms of crack width along the crack length and along the crack depth. Good correlation for measuring the widths of surface cracks was found between the DIC technique and measurements by optical microscope. Based on these results, it can be concluded that the DIC technique is a very promising method of performing automated measurement of surface displacements and cracking.

## 7  References

[1]    J. Branston, S. Das, S.Y. Kenno, C. Taylor, Influence of basalt fibres on free and restrained plastic shrinkage, Cem. Concr. Compos. 74 (2016) 182–190. doi:10.1016/j.cemconcomp.2016.10.004.

[2]    W.P. Boshoff, R. Combrinck, Modelling the severity of plastic shrinkage cracking in concrete, Cem. Concr. Res. 48 (2013) 34–39. doi:10.1016/j.cemconres.2013.02.003.

[3]    N. Banthia, C. Yan, Shrinkage cracking in polyolefin fiber-reinforced concrete, ACI Mater. J. 97.4 (2000) 432–437.

539     [4]     P. Balaguru, Contribution of fibers to crack reduction of cement composites during the initial and final setting

540             period, ACI Mater. J. 91.3 (1994) 280–288.

541     [5]     N. Banthia, R. Gupta, Influence of polypropylene fiber geometry on plastic shrinkage cracking in concrete,

542             Cem. Concr. Res. 36.7 (2006) 1263–1267. doi:10.1016/j.cemconres.2006.01.010.

543     [6]     ASTM C1579-13, Standard Test Method for Evaluating Plastic Shrinkage Cracking of Restrained Fiber

544             Reinforced Concrete (Using a Steel Form Insert), (2013) 1–7. doi:10.1520/C1579-06.2.

545     [7]     M. Grzybowski, S.P. Shah, Shrinkage cracking of fiber reinforced concrete, ACI Mater. J. 87.2 (1990) 138–

546             148.

547     [8]     ASTM C1581, Standard Test Method for Determining Age at Cracking and Induced Tensile Stress

548             Characteristics of Mortar and Concrete under Restrained Shrinkage, 2009. doi:10.1520/C1581.

549     [9]     R. Bloom, A. Bentur, Free and restrained shrinkage of normal and high-strength concretes, ACI Mater. J. 92.2

550             (1995) 211–217.

551     [10]     N. Banthia, M. Azzabi, M. Pigeon, Restrained shrinkage cracking in fibre-reinforced cementitious composites,

552             Mater. Struct. 26 (1993) 405–413.

553     [11]     P.P. Kraai, A proposed test to determine the cracking potential due to drying shrinkage of concrete, Concr.

554             Constr. 30.9 (1985) 775–778.

555     [12]     N. Banthia, R. Gupta, Test method for evaluation of plastic shrinkage cracking in fiber-reinforced cementitious

556             materials, Exp. Tech. 31.6 (2007) 44–48. doi:10.1111/j.1747-1567.2007.00191.x.

557     [13]     T. Mauroux, F. Benboudjema, P. Turcry, A. Aït-Mokhtar, O. Deves, Study of cracking due to drying in coating

558             mortars by digital image correlation, Cem. Concr. Res. 42.7 (2012) 1014–1023.

559             doi:10.1016/j.cemconres.2012.04.002.

560     [14]     A.E. Naaman, T. Wongtanakitcharoen, G. Hauser, Influence of different fibers on plastic shrinkage cracking of

561             concrete, ACI Mater. J. 102.1 (2005) 49–58.

562     [15]     P. Zhao, A.M. Zsaki, M.R. Nokken, Using digital image correlation to evaluate plastic shrinkage cracking in

563             cement-based materials, Constr. Build. Mater. 182 (2018) 108–117. doi:10.1016/j.conbuildmat.2018.05.239.

564     [16]     I.M.G. Bertelsen, L.M. Ottosen, G. Fischer, Quantitative analysis of the influence of synthetic fibres on plastic

565             shrinkage cracking using digital image correlation, Constr. Build. Mater. 199 (2019) 124–137.

566             doi:10.1001/archinte.168.13.1371.

567 [17] K. Wang, S.P. Shah, P. Phuaksuk, Plastic shrinkage cracking in concrete materials - Influence of fly ash and

568 fibers, ACI Mater. J. 98.6 (2001) 458–464.

569 [18] C. Wagner, B. Villmann, V. Slowik, V. Mechtcherine, Water permeability of cracked strain-hardening cement-

570 based composites, Cem. Concr. Compos. 82 (2017) 234–241. doi:10.1016/j.cemconcomp.2017.06.003.

571 [19] N. Pešić, S. Živanović, R. Garcia, P. Papastergiou, Mechanical properties of concrete reinforced with recycled

572 HDPE plastic fibres, Constr. Build. Mater. 115 (2016) 362–370. doi:10.1016/j.conbuildmat.2016.04.050.

573 [20] P. Soroushian, F. Mirza, A. Alhozaimy, Plastic shrinkage cracking of polypropylene fiber-reinforced concrete,

574 ACI Mater. J. 92.5 (1995) 553–560.

575 [21] M.R. Jahanshahi, S.F. Masri, C.W. Padgett, G.S. Sukhatme, An innovative methodology for detection and

576 quantification of cracks through incorporation of depth perception, Mach. Vis. Appl. 24 (2013) 227–241.

577 doi:10.1007/s00138-011-0394-0.

578 [22] G.M. Sadiqul Islam, S. Das Gupta, Evaluating plastic shrinkage and permeability of polypropylene fiber

579 reinforced concrete, Int. J. Sustain. Built Environ. 5.2 (2016) 345–354. doi:10.1016/j.ijsbe.2016.05.007.

580 [23] N. Banthia, R. Gupta, Plastic shrinkage cracking in cementitious repairs and overlays, Mater. Struct. 42.5

581 (2009) 567–579. doi:10.1617/s11527-008-9403-9.

582 [24] C. Qi, J. Weiss, J. Olek, Characterization of plastic shrinkage cracking in fiber reinforced concrete using image

583 analysis and a modified Weibull function, Mater. Struct. 36.6 (2003) 386–395. doi:10.1007/BF02481064.

584 [25] C. Liu, C.-S. Tang, B. Shi, W.-B. Suo, Automatic quantification of crack patterns by image processing,

585 Comput. Geosci. 57 (2013) 77–80. doi:10.1016/j.cageo.2013.04.008.

586 [26] A. Mazzoli, S. Monosi, E.S. Plescia, Evaluation of the early-age-shrinkage of Fiber Reinforced Concrete (FRC)

587 using image analysis methods, Constr. Build. Mater. 101.1 (2015) 596–601.

588 doi:10.1016/j.conbuildmat.2015.10.090.

589 [27] L. Ruiz-Ripoll, B.E. Barragán, S. Moro, J. Turmo, Digital imaging methodology for measuring early shrinkage

590 cracking in concrete, Strain. 49 (2013) 267–275. doi:10.1111/str.12034.

591 [28] S. Ghourchian, M. Wyrzykowski, L. Baquerizo, P. Lura, Susceptibility of Portland cement and blended cement

592 concretes to plastic shrinkage cracking, Cem. Concr. Compos. 85 (2018) 44–55.

593 doi:10.1016/j.cemconcomp.2017.10.002.

594 [29] M. Némoz-Gaillard, D. Nectoux, E. Dallies, D. Muller, Influence of AR glass fibers on the cracking of

concrete : analysis at the very early age by digital image correlation, in: PRO 23 Int. RILEM Conf. Early Age Crack. Cem. Syst., 2002: pp. 237–244.

[30] P. Zhao, Master thesis. Digital Image Correlation to Evaluate Plastic Shrinkage Cracking in Cement-Based Materials, Concordia University, Montreal, Canada, 2016.

[31] A. Messan, P. Ienny, D. Nectoux, Free and restrained early-age shrinkage of mortar: Influence of glass fiber, cellulose ether and EVA (ethylene-vinyl acetate), Cem. Concr. Compos. 33.3 (2011) 402–410. doi:10.1016/j.cemconcomp.2010.10.019.

[32] E. Roziere, R. Cortas, A. Loukili, Tensile behaviour of early age concrete: New methods of investigation, Cem. Concr. Compos. 55 (2015) 153–161. doi:10.1016/j.cemconcomp.2014.07.024.

[33] E.D. Dzaye, E. Tsangouri, K. Spiessens, G. De Schutter, D.G. Aggelis, Digital image correlation (DIC) on fresh cement mortar to quantify settlement and shrinkage, Arch. Civ. Mech. Eng. 19 (2019) 205–214. doi:10.1016/j.acme.2018.10.003.

[34] C.G. Berrocal, I. Löfgren, K. Lundgren, N. Görander, C. Halldén, Characterisation of bending cracks in R/FRC using image analysis, Cem. Concr. Res. 90 (2016) 104–116. doi:10.1016/j.cemconres.2016.09.016.

[35] B. Pan, K. Qian, H. Xie, A. Asundi, Two-dimensional digital image correlation for in-plane displacement and strain measurement: a review, Meas. Sci. Technol. 20.6 (2009) 062001. doi:10.1088/0957-0233/20/6/062001.

[36] D. Lecompte, A. Smits, S. Bossuyt, H. Sol, J. Vantomme, D. Van Hemelrijck, A.M. Habraken, Quality assessment of speckle patterns for digital image correlation, Opt. Lasers Eng. 44.11 (2006) 1132–1145. doi:10.1016/j.optlaseng.2005.10.004.

[37] M.A. Sutton, J.J. Orteu, H. Schreier, Image correlation for shape, motion and deformation measurements: basic concepts, theory and applications, Springer Science & Business Media, 2009.

[38] A. Gheitasi, D.K. Harris, M. Hansen, An experimental-computational correlated study for describing the failure characteristics of concrete across two scale levels : Mixture and structural component, Exp. Mech. (2018) 11–32. doi:10.1007/s11340-017-0319-6.

[39] W.P. Boshoff, F. Altmann, C.J. Adendorff, V. Mechtcherine, A new approach for modelling the ingress of deleterious materials in cracked strain hardening cement-based composites, Mater. Struct. 49.6 (2016) 2285–2295. doi:10.1617/s11527-015-0649-8.

[40] I. Maruyama, H. Sasano, M. Lin, Impact of aggregate properties on the development of shrinkage-induced

623          cracking in concrete under restraint conditions, Cem. Concr. Res. 85 (2016) 82–101.

624          doi:10.1016/j.cemconres.2016.04.004.

625   [41]    I. Paegle, F. Minelli, G. Fischer, Cracking and load-deformation behavior of fiber reinforced concrete: Influence

626          of testing method, Cem. Concr. Compos. 73 (2016) 147–163. doi:10.1016/j.cemconcomp.2016.06.012.

627   [42]    F. Benboudjema, T. Mauroux, P. Turcry, A. Ait-Mokthar, O. Deves, Experimental Analysis of Drying

628          Shrinkage Cracking in Coating Mortars by Digital Image Correlation, in: 2013.

629          doi:10.1061/9780784413111.027.

630   [43]    Y.L. Dong, B. Pan, A review of speckle pattern fabrication and assessment for digital image correlation, Exp.

631          Mech. 57 (2017) 1161–1181. doi:10.1007/s11340-017-0283-1.

632   [44]    P.J. Uno, Plastic shrinkage cracking and evaporation formulas, ACI Mater. J. 95.4 (1998) 365–375.

633   [45]    E.D. Dzaye, G. De Schutter, D. Aggelis, Monitoring fresh cementitious material by digital image correlation (

634          DIC ), in: SynerCrete18, 2018: pp. 267–272.

635   [46]    E.D. Dzaye, G. De Schutter, D. Aggelis, Application of digital image correlation to cement paste, in:

636          Proceedings. Eighteenth Int. Conf. Exp. Mech., 2018. doi:10.3390/ICEM18-05332.

637   [47]    S. Ghourchian, M. Wyrzykowski, L. Baquerizo, P. Lura, Performance of passive methods in plastic shrinkage

638          cracking mitigation, Cem. Concr. Compos. 91 (2018) 148–155. doi:10.1016/j.cemconcomp.2018.05.008.

639   [48]    E. Boghossian, L.D. Wegner, Use of flax fibres to reduce plastic shrinkage cracking in concrete, Cem. Concr.

640          Compos. 30.10 (2008) 929–937. doi:10.1016/j.cemconcomp.2008.09.003.

641   [49]    J.H.J. Kim, C.G. Park, S.W. Lee, S.W. Lee, J.P. Won, Effects of the geometry of recycled PET fiber

642          reinforcement on shrinkage cracking of cement-based composites, Compos. Part B Eng. 39.3 (2008) 442–450.

643          doi:10.1016/j.compositesb.2007.05.001.

644   [50]    UNI/EN-1339, Concrete Paving Flags - Requirements and Test Methods, (2003).

645   [51]    C.A. Juarez, G. Fajardo, S. Monroy, A. Duran-Herrera, P. Valdez, C. Magniont, Comparative study between

646          natural and PVA fibers to reduce plastic shrinkage cracking in cement-based composite, Constr. Build. Mater.

647          91 (2015) 164–170. doi:10.1016/j.conbuildmat.2015.05.028.

648   [52]    UNI/EN-12390-3, Testing Hardened Concrete – Part 3 : Compressive Strength of Test Specimens, (2012).

649   [53]    V. Slowik, M. Schmidt, R. Fritzsch, Capillary pressure in fresh cement-based materials and identification of the

650          air entry value, Cem. Concr. Compos. 30.7 (2008) 557–565. doi:10.1016/j.cemconcomp.2008.03.002.

651    [54]    ACI Committee 305.1-06, Specification for Hot Weather Concreting, (2007) 305.1–06.

652    [55]    Ł. Skarzynski, J. Kozicki, J. Tejchman, Application of DIC technique to concrete — study on objectivity of
653            measured surface displacements, Exp. Mech. (2013) 1545–1559. doi:10.1007/s11340-013-9781-y.

654    [56]    W.P. Boshoff, C.J. Adendorff, Effect of sustained tensile loading on SHCC crack widths, Cem. Concr. Compos.
655            37 (2013) 119–125. doi:10.1016/j.cemconcomp.2012.11.009.

656    [57]    F. Lagier, X. Jourdain, C. De Sa, F. Benboudjema, J.B. Colliat, Numerical strategies for prediction of drying
657            cracks in heterogeneous materials: Comparison upon experimental results, Eng. Struct. 33.3 (2011) 920–931.
658            doi:10.1016/j.engstruct.2010.12.013.

659    [58]    V. Valle, S. Hedan, P. Cosenza, A.L. Fauchille, M. Berdjane, Digital image correlation development for the
660            study of materials including multiple crossing cracks, Exp. Mech. 55.2 (2015) 379–391. doi:10.1007/s11340-
661            014-9948-1.

662    [59]    R. Ranade, J. Zhang, J.P. Lynch, V.C. Li, Influence of micro-cracking on the composite resistivity of
663            engineered cementitious composites, Cem. Concr. Res. 58 (2014) 1–12. doi:10.1016/j.cemconres.2014.01.002.

664    [60]    N. Yousefieh, A. Joshaghani, E. Hajibandeh, M. Shekarchi, Influence of fibers on drying shrinkage in restrained
665            concrete, Constr. Build. Mater. 148 (2017) 833–845. doi:10.1016/j.conbuildmat.2017.05.093.

666    [61]    L. Ma, Y. Zhao, J. Gong, Restrained early-age shrinkage cracking properties of high-performance concrete
667            containing fly ash and ground granulated blast-furnace slag, Constr. Build. Mater. 191 (2018) 1–12.
668            doi:10.1016/j.conbuildmat.2018.09.154.

669    [62]    R. Combrinck, L. Steyl, W.P. Boshoff, Interaction between settlement and shrinkage cracking in plastic
670            concrete, Constr. Build. Mater. 185 (2018) 1–11. doi:10.1016/j.conbuildmat.2018.07.028.

671    [63]    F. Sayahi, Plastic shrinkage cracking in concrete, Luleå University of Technology, 2016. doi:10.3929/ETHZ-B-
672            000249246.

673

# Appendix III

**Description:** Published in Journal of Construction and Building Materials, 199, 124–137. http://doi.org/10.1001/archinte.168.13.1371

**Title:** Quantitative analysis of the influence of synthetic fibres on plastic shrinkage cracking using digital image correlation

1 **Quantitative analysis of the influence of synthetic fibres on plastic shrinkage cracking using**

2 **digital image correlation**

3

4 I. M. G. Bertelsen[a*], L. M. Ottosen[a], G. Fischer[a]

5 [a] Department of Civil Engineering, Technical University of Denmark, Brovej 118, 2800 Kgs. Lyngby, Denmark

6 * Corresponding author. E-mail: imgber@byg.dtu.dk

7

8 **Abstract**

9 The plastic shrinkage cracking behaviour of restrained mortar overlays on a concrete substrate was studied

10 with the aim of quantifying the influence of commercially available polypropylene (PP) fibres and recycled

11 polyethylene (R-PE) fibres obtained from discarded fishing nets. The use of R-PE fibres was investigated

12 with a view to creating a more eco-friendly construction material. The plastic shrinkage behaviour was

13 evaluated on the basis of a non-contact 2D digital image correlation (DIC) technique that enables the

14 automated detection of surface displacements and strains with high precision. Based on the DIC data, the

15 degree of surface cracking was quantitatively analysed using a MATLAB post-processing procedure and

16 presented in detailed histograms showing the crack width distribution of the entire specimen surface. Using

17 this data, the effect of fibre reinforcement on crack control was objectively quantified and evaluated. The

18 results indicate that while the addition of 2.0% of R-PE is effective in controlling shrinkage cracking in the

19 mortars, the commercial PP fibres perform better even at volume fractions as low as 0.1%. These findings

20 show that the recycled fibres can be used to reduce plastic shrinkage cracking behaviour compared to

21 unreinforced materials, while a waste material is being reused, though, a much larger volume fraction of R-

22 PE fibres than of commercially available PP fibres is necessary to achieve a similar effect.

## 1 Introduction

Deformation of cementitious materials due to plastic shrinkage is one of the reasons for surface cracking occurring in concrete structures, especially when environmental factors create a high rate of water evaporation from the fresh material [1,2]. Concrete structures with internal or underlying restraints and a large surface area-to-volume ratio such as surface repairs, slabs, tunnel linings, etc. are especially vulnerable to plastic shrinkage cracking [3]. Combined with a high degree of mixing water evaporation, such restraints can cause tensile stresses within the cement-based composite that exceed the tensile strength of the plastic material, which causes surface cracking to appear in the composite [4,5]. The plastic shrinkage period of cement-based materials only lasts for a few hours, and depends on parameters such as binder type, geometry and environmental conditions [2].

Several studies have proposed methods for restrained plastic shrinkage testing in which a fresh mortar overlay is cast on top of a bottom-restraining concrete substrate or a rough underlay [6–13]. A test method previously developed by the authors was used in this study for addressing the crack formation in such bonded overlay-substrates by digital image correlation (DIC) [13]. In recent years, various types of image-based techniques have been applied for the detection and analysis of plastic shrinkage-induced surface cracking, which is a great improvement compared to the more manual measuring techniques using optical microscopes to study the crack formation. The image-based techniques are valued for their high-precision, the non-contact optical analysis, which avoids all disturbance of the fresh cementitious material as well as human error [12,14–18]. Among these techniques, DIC is especially effective for monitoring surface strain and displacement fields, which enables automated crack detection and the ability to see the evolution of cracks over time. The application of a high-contrast surface pattern is required for tracking the surface displacements and strains by the DIC technique [19]. Nevertheless, so far very few studies on the shrinkage behaviour of fresh cement-based materials have used the DIC technique [12,20–24]. This could be due to the difficulty of applying a high-contrast surface pattern for the DIC monitoring due to bleeding water present on specimen surfaces [22,24] and the sealing effect of most paint types, which reduces the evaporation rate. In [13] a diffusion open chalk-based paint type was applied for creation of a high-contrast

49  speckle pattern for DIC and it was found not to influence the evaporation rate of mixing water from the

50  fresh mortar surface.

51  The addition of randomly distributed low-modulus fibres of synthetic materials in cementitious composites

52  is often used to control cracking caused by plastic shrinkage deformations [1,2]. These fibres are known to

53  improve the strain capacity of the fresh mixture by providing bridging forces across the cracks so that many

54  very fine cracks appear instead of fewer but larger cracks [1,2,25]. The efficiency of synthetic fibres for

55  controlling plastic shrinkage cracking has been widely studied in the literature and has been shown to

56  depend on several variables, such as the added fibre volume fraction, the fibre material [9,17,26], fibre

57  shape and geometry [3,4,9,17,27–29], and their mechanical properties [9,30]. The literature largely agrees

58  that the best performance in reducing plastic shrinkage cracks results from finer and longer fibres (high

59  aspect ratio) with good fibre-to-matrix bonding properties [3,9]. It has been shown that by adding PP or

60  PVA fibres with a fine diameter in volume fractions as low as 0.1-0.2% to the mixture, it is possible to

61  achieve an apparently crack-free surface [3,9,11,25,27]. However, Najm & Balaguru [31] report that

62  polyolefin macro fibres also perform well when added in volume fractions of 2%. Not only commercially

63  available  virgin fibres have been shown to be effective in controlling plastic shrinkage cracking, but also

64  various types of recycled fibres [4,28,29,32–34]. The use of recycled synthetic fibres has generally gained

65  recognition in the construction industry due to their broad availability, low price and sustainability aspects

66  [35,36]. In this study, recycled fibres obtained from discarded fishing nets were used for controlling plastic

67  shrinkage cracking of restrained mortar overlays. Lost or otherwise discarded fishing nets is a major

68  concern for the vulnerable marine environment and can cause severe damage to fish, sea birds and marine

69  mammals if they continue to drift [37]. Besides being a threat to marine life, the nets are often difficult to

70  transport, dispose of, and occupy high volumes at landfill sites. Fishing nets are nowadays made of

71  synthetic materials such as PE, PP and nylon with fibre-shapes comparable to those of synthetic fibres used

72  in cement-based materials. The performance of recycled nylon fibres from discarded fishing nets as fibre

73  reinforcement in cementitious mortar composites was studied by Spadea et al. and Orasutthikul et al. for

74  improving mechanical properties such as flexural strength and toughness and obtained promising results

75 [38,39]. Likewise, the R-PE fibres investigated in the present study were also expected to positively

76 influence the cracking behaviour induced by plastic shrinkage. Borg et al. [28] studied reprocessed macro

77 fibres from waste PET bottles in volume fractions of 0.5–1.5% to control plastic shrinkage cracking,

78 following the method in ASTM C1579. On the basis of the reduction in the average crack width, they found

79 that deformed and long fibres performed better in controlling plastic shrinkage cracking than short and

80 straight fibres. Kim et al. [4] also investigated reprocessed PET macro fibres of various shapes and

81 geometries (twisted, crimped, embossed) in volume fractions of 0.1–1.0%, and found no significant

82 difference in the performance of the three fibre shapes. All three fibre shapes successfully reduced the

83 total crack area when added in fractions of at least 0.5%. Pešić et al. [29] used straight HDPE macro fibres

84 from mixed post-consumer waste in volume fractions of 0.4–1.25%. They achieved a reduction in crack

85 width of 76-84% with 1.25% fibres added to the concrete mixture.

86

87 **1.1    Research concept and significance**

88 The aim of the present paper is to describe how a 2D-DIC technique recently proposed in [13] has been

89 applied for the evaluation of the plastic shrinkage behaviour of free and restrained mortar overlays with

90 addition of two types of low-modulus synthetic fibres. The DIC technique was used to monitor in-plane

91 surface displacements and strains from t = 1-25 h after casting. This enabled an automated post-processing

92 procedure for the evaluation of the degree of surface cracking, quantified as crack width distribution and

93 evolution in surface cracking, which gives a more detailed understanding of the plastic shrinkage behaviour

94 than traditional approaches. This approach was used to objectively quantify and compare the influence of

95 adding commercially available PP fibres and R-PE obtained from discarded fishing nets for the control of

96 plastic shrinkage cracking in restrained mortar overlays.

97

98 **2    Experimental programme**

99 **2.1    Materials**

100  The elements used in the experimental programme included a fresh mortar overlay and, in the restrained

101  tests, a concrete substrate; see Table 1 for the basic raw material properties of the mortar overlay. When

102  fibres were added to the mixture, they replaced equivalent amounts of sand, which is the reason for the

103  varying proportions of sand in the mixture.

104

105  Table1. Raw materials for mortar mixture

| Material | Type | Quantity [kg/m$^3$] | Proportions [c : s : w] |
|---|---|---|---|
| Cement | Portland Cement (type CEM I 52.5 N) | 700 | 1.0 |
| Fine aggregate | Sea sand (0–4 mm) | 980–1032 | 1.40–1.47 |
| Water | Tap water | 350 | 0.5 |

106

107  *2.1.1  Fibres*

108  Two types of fibres were investigated for the control of shrinkage cracking: PP fibres of the type Fibrin

109  Fiberflex from PP Nordica, a fibre type commonly used to control plastic shrinkage cracking; and R-PE fibres

110  obtained from discarded fishing nets. The R-PE fibres were provided by the Danish recycling company,

111  Plastix A/S, and their properties are shown in Table 2. Variations in length, diameter and mechanical

112  properties were found in the R-PE fibres due to an "uncontrolled" cutting operation and differences in

113  origin. Prior to using the fibres, the fibres were cleaned in tap water to remove impurities such as sand and

114  other residues from the fishing operation. For more information about the recycled fibre properties, see a

115  previous study by the authors [40]. The fibre volume fractions in the mortar overlays investigated were 0.2,

116  0.5, 1.0 and 2.0% for R-PE fibres and 0.1 and 0.2% for PP fibres.

117

118

119     Table 2. Fibre properties and the fibre fractions in mortars investigated

| Material | Image | Fibre type | Density [g/cm$^3$] | Diameter [μm] | Length [mm] | Fibre fractions [vol%] |
|---|---|---|---|---|---|---|
| PP |  | Monofilament | 0.91 | 19.5 | 12 | 0.1, 0.2 |
| R-PE |  | Monofilament | 0.95 | 280 ± 30 | 15 ± 9 mm | 0.2, 0.5, 1.0, 2.0 |

120

121     *2.1.2    Mixing procedure for mortar specimens*

122     The mixing procedure was carried out in a Hobart-type paddle mixer, where sand and cement were first

123     dry-mixed for 2 min before water was gradually added to the mixture. "Time zero" (t = 0 min) was defined

124     as the time when water was added to the dry mixture of sand and cement. Finally, the fibres were added to

125     the mixture under continuous mixing (at t = 3 min) and mixed for another 5 min. Specimens for both free

126     and restrained shrinkage tests were cast by applying the fresh mortar into the respective moulds. The

127     mortar surface was finished using a smooth steel trowel under continuous vibration at 60 Hz for up to 1

128     min on a vibration table. The total casting process took approx. 15 min from the start of wet-mixing

129     (completed at t = 15 min). The fibre contents used did not result in any problems during mixing or casting,

130     and no balling effect was encountered. The workability of the fresh mortar mixtures was determined using

131     the flow table test in accordance with UNI/EN 1015-3 (1999). The fresh mortar was introduced in two layers

132     into a lightly lubricated steel mould with a conical shape measuring 40 x (75–65) mm (h x $d_{i,bottom}$ – $d_{i,top}$). The

133     mean flow diameter was calculated from two measurements perpendicular to each other with each

134     mixture being tested with three replicates.

135

**2.2    Shrinkage tests**

137    Seven test series including free and restrained shrinkage tests of mortar mixtures with the addition of PP

138    fibres, R-PE fibres or no fibres (reference) were carried out and the components are shown in Fig. 1. See

139    also [13]. The restrained shrinkage test was carried out by pouring a fresh mortar overlay with dimensions

140    of 420 x 95 x 10 mm on top of an existing and cured concrete substrate produced in accordance with

141    UNI/EN 1339 (2003) with a desired roughness. The geometry and mixture design of the mortar overlay was

142    designed to have limited bleeding water and promote surface cracking in the restrained reference mortar.

143    The surface of the concrete substrate was roughened using a fine needle hammer to a depth of about 1

144    mm to create an even restraint for the fresh mortar overlay. The substrate dimensions were 418 ± 0.3 mm

145    x 93.5 ± 0.2 mm x 49.6 ± 0.2 mm, so the substrates could fit into plywood moulds measuring 420 x 95 x 60

146    mm. The compressive strength of the substrates was found to 35.5 ± 6 MPa (tested in accordance with

147    UNI/EN 12390-3 (2012) on 50 mm x 100 mm cylinders) and the dry density to 2.180 kg/m$^3$. The concrete

148    substrates were wetted right before the fresh mortar overlay was applied.

149    The free shrinkage behaviour was measured on mortar specimens with the dimensions 420 x 95 x 10 mm.

150    This geometry is the same as the mortar overlay used in the restrained shrinkage tests. Three replicates of

151    both free and restrained specimens were tested in each test series. In the experiment, the x-direction was

152    defined as being parallel to the longer side of the specimens (420 mm) and the y-direction parallel to the

153    shorter side of the specimens (95 mm).
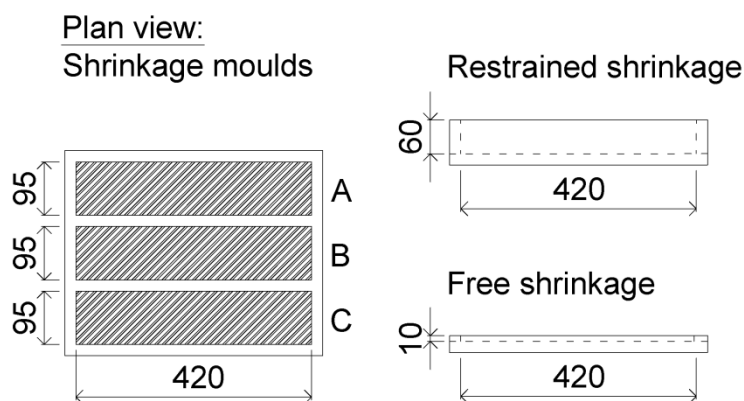
a)                                                                          b)

Fig. 1. a) Geometry of moulds for free and restrained shrinkage tests; b) Restrained mortar overlay on top of concrete substrate after demoulding; concrete substrate; and free shrinkage specimen. Three replicates of each test series were tested and labeled A, B, and C.

After casting (t = 15 min), the specimens were kept in laboratory conditions (20 ± 3 °C), where they were left to rest for 30 min. Limited plastic shrinkage was expected during this period due to the non-aggressive air temperature surrounding the specimens. Chalk-based spray paints were used for the creation of a high-contrast surface pattern in the period of t = 45–55 min, consisting of a base of white chalk-based paint and a speckle pattern of black chalk-based paint, which has been shown not to influence the water evaporation rate from the fresh mortar [13]. The accuracy of the DIC computation mainly depends on the quality of the black speckle pattern, in which a consistent size and distribution of speckles is essential [19]. At t = 55 min, the specimens were transferred to a climate-controlled chamber.

### 2.2.1    Environmental conditions in climate-controlled chamber

The shrinkage tests took place inside a climate-controlled chamber within the period of t = 1-25 h. The test setup constructed for the shrinkage tests is shown in Fig. 2. Inside the chamber, a temperature of 32.0 ± 1.5 °C and a relative humidity of 33.5% ± 5% were maintained during each test series, an environment chosen based on the recommendations in the ASTM standard C1579 (2013). The relative humidity was maintained by a dehumidifier. A wind flow in the range of 3.9–4.5 m/s over the surface of the specimens parallel to the x-direction was applied using electric tangential fans that were placed in front of the specimens to ensure a constant wind flow. The wind speed was within the range as reported in other studies on plastic shrinkage cracking [25,41] and was chosen to ensure that surface cracking appeared on the restrained reference specimens.
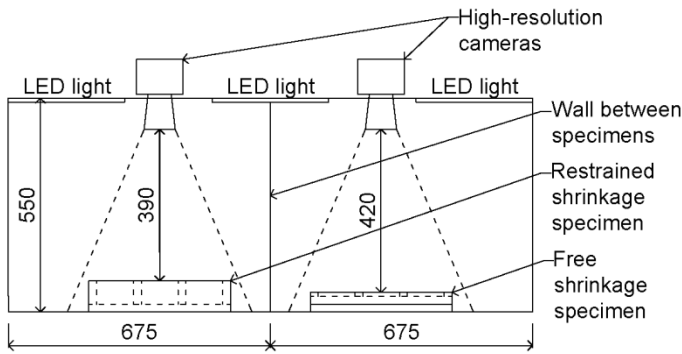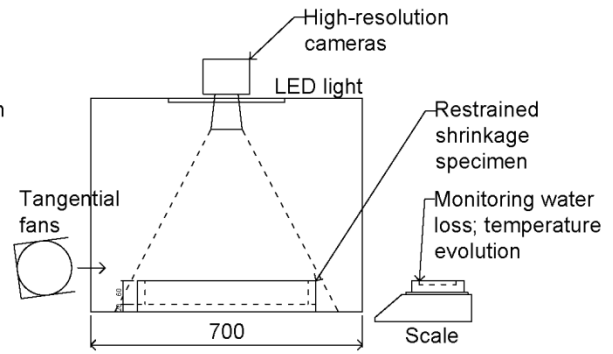
Fig. 2. The plastic shrinkage test setup using a 2D image acquisition system placed inside a climate-controlled chamber.

*2.2.2   Monitoring of the shrinkage deformations by DIC*

The test setup shown in Fig. 2 consisted of two optical cameras with wide-angle lenses and a resolution of 7360 x 4912 pixels. The cameras were fixed parallel to the specimen surfaces capturing in-plane strains and displacements occurring on the specimen surface. The distance from the specimen surface to camera lenses was 390 mm for the restrained shrinkage specimens and 420 mm for the free shrinkage specimens. This difference resulted in slightly different pixel lengths for the two types of specimens (0.087 mm/pixel for the free shrinkage specimens and 0.080 mm/pixel for the restrained shrinkage specimens), but this small difference did not affect the accuracy of the deformation measurements. A constant light source was ensured by placing three LED panels at the top of the test setup.

For the DIC analysis, the software GOM Correlate Professional 2016 was used. The first image captured at t = 1 h was defined as the undeformed image (reference stage), and subsequent images were taken at time intervals of 15 min until t = 25 h. Each series of images was first modified in ImageJ to improve contrast and brightness prior to being imported to the DIC software. A region of interest (ROI) was defined in the DIC software for each specimen and was virtually meshed into a grid with overlapping subset elements with a (facet) size of 20x20 pixels and a centre distance of 15 pixels between each subset. The spacing between two points in the virtual grid is 15 pixels, which is equal to 1.305 mm for the free shrinkage specimens and

197    1.2 mm for the restrained shrinkage specimens. This geometry corresponds well with the applied high-

198    contrast surface pattern and the recommendations suggested by Sutton et al. [19].

199

200    **3    Results**

201    **3.1    Restrained shrinkage behaviour analysed using DIC**

202    The plastic shrinkage behaviour of the restrained mortar overlays with addition of PP or R-PE fibres was

203    tested in the period of t = 1–25 h. At the end of each test series (t = 25 h), visible surface cracking had

204    appeared on some of the specimen types. The displacement and strain fields on the specimen surface were

205    calculated by the DIC software as the average value in each subset element. The strain fields are useful for

206    a visual representation of the surface cracking; see Fig. 3 and Fig. 4 where the in-plane strain fields on the

207    specimen surfaces in the x-direction and y-direction, respectively, are shown for all the specimens tested.

208    The figures clearly demonstrate the ability of the DIC technique to detect areas with increased strain, i.e.

209    position of surface cracks [8,12,42]. When analysing the strain fields by DIC, it was observed that the cracks

210    primarily appeared in the x-direction. This was because of the specimen geometry and wind flow parallel to

211    the x-direction, so the focus was kept on displacements occurring in the x-direction when quantifying the

212    degree of surface cracking (this is more thoroughly discussed in [13]).

213

214

Fig. 3. Strain fields parallel to the x-directions on the specimen surfaces. Plastic shrinkage-induced cracks are visually

represented by peaks in the strain data represented with a black colour. White colour represents $\varepsilon_x$ = 0%; Black colour
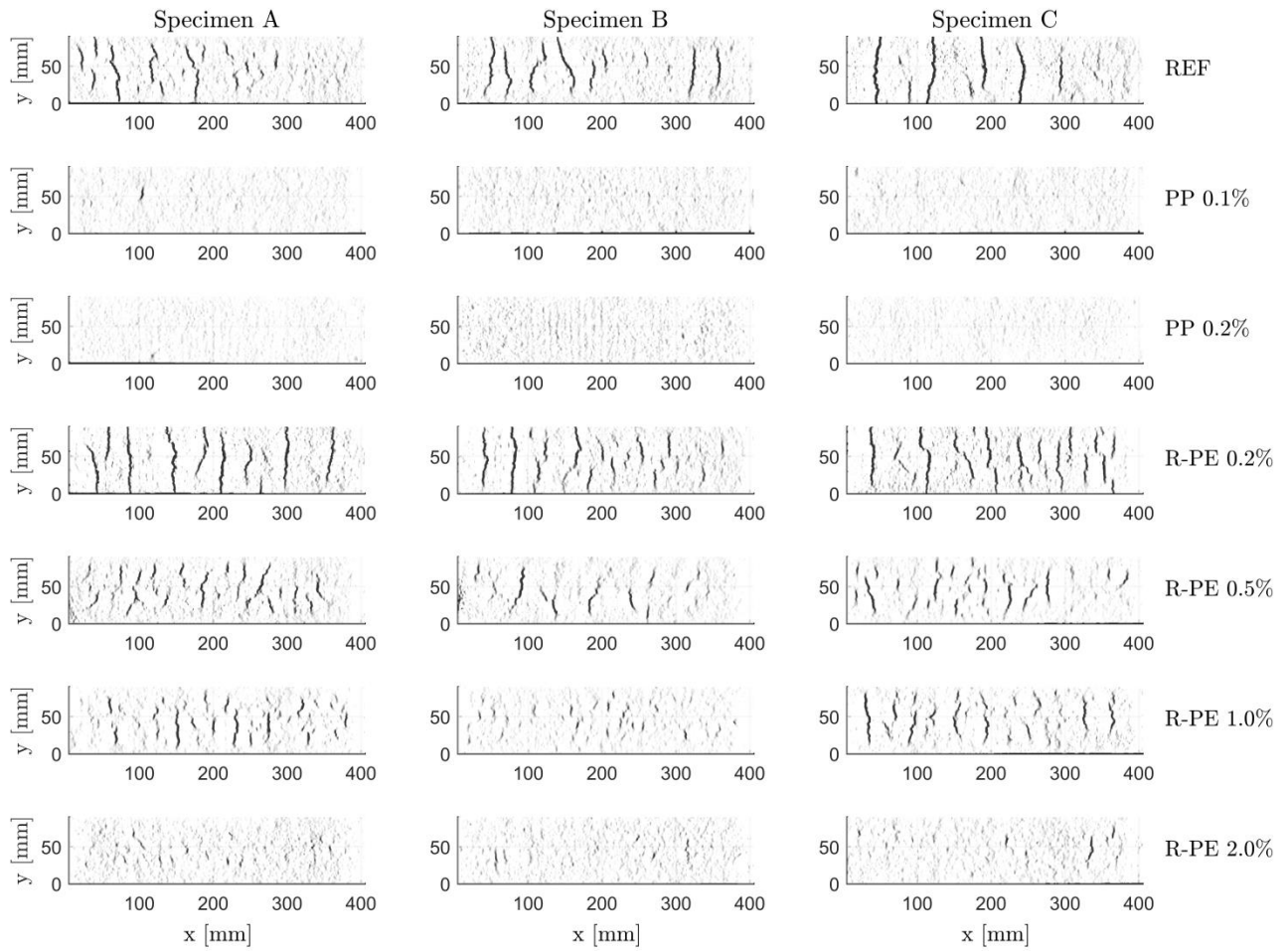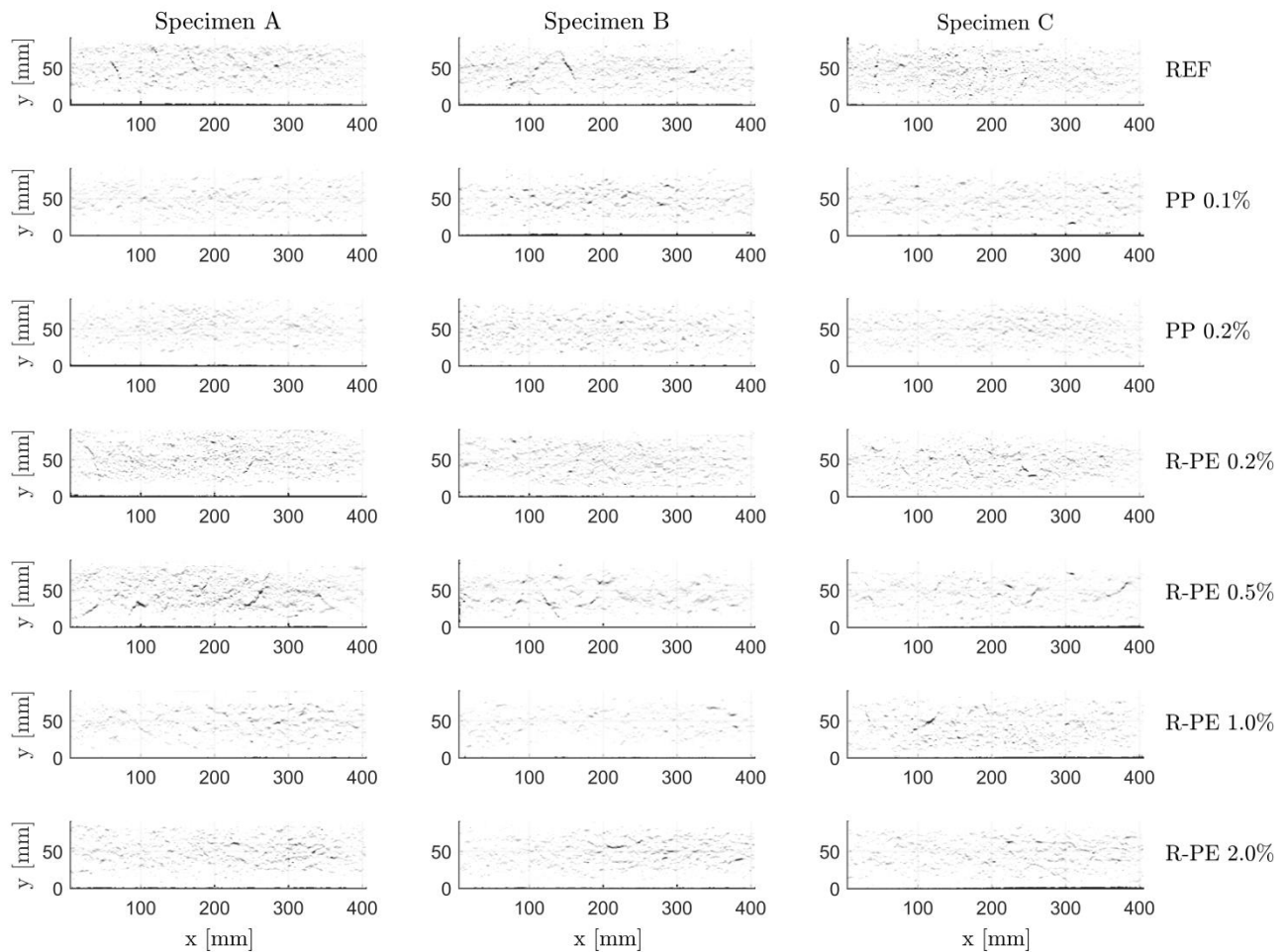
represents $\varepsilon_x$ = 5%.

219



Fig. 4. Strain fields parallel to the y-directions on the specimen surfaces. Plastic shrinkage-induced cracks are visually represented by peaks in the strain data represented with a black colour. White colour represents $\varepsilon_y$ = 0%; Black colour represents $\varepsilon_y$ = 5%.

Even from this simple visual inspection of surface strains, it is clear that the addition of fibres influences the cracking behaviour. As expected, the commercially available PP fibres performed well in controlling the plastic shrinkage cracks. The R-PE fibres were also effective in controlling the surface cracking, though, as anticipated, much larger fibre volume fractions were needed to obtain effects similar to PP fibres. However, Fig. 3 and 4 only give a visual illustration of the surface cracking; the results with respect to the quantitative degree of surface cracking will be given and explained in the following sections.

*3.1.1    Computation of crack parameters*

233    To obtain a quantitative measure of the degree of surface cracking in the restrained mortar overlay, a post-

234    processing procedure developed in MATLAB was used to compute crack parameters such as crack width,

235    crack area, crack location and crack width distribution for the entire surface area based on the DIC data

236    [13]. For each specimen, the DIC data was interpolated onto a rectangular grid with a point-to-point

237    distance of 0.25 mm. This enabled a section-wise analysis of each separate section ($n_{i,sec}$) parallel to the

238    axis. Since the displacement mainly occurred in the x-direction, only the results for this direction are shown,

239    which is considered a good approximation of the actual crack widths. This approach resulted in

240    approximately 380 sections parallel to the x-direction for each specimen, which was considered sufficient

241    for ensuring a high precision and quality of the crack width analysis.

242    The strain data is a numerical approximation to partial derivatives of the displacement, thus displacement

243    gaps are illustrated as local extrema in strain, i.e. surface cracks [8,42]. The crack widths in the x-direction

244    were determined based on sudden gaps in the displacement data along each separate section ($n_{i,sec}$) and

245    were calculated as the increase in displacement between the minimum and maximum coordinate on each

246    side of the displacement gap. This is represented by a blue and a red circle in Fig. 5-8b indicating

247    respectively the displacement and strain along a selected section, A-A and B-B. To distinguish the actual

248    cracks from less abrupt changes in surface displacement, it was relevant to define a criterion for the

249    equivalent strain along a displacement gap. This was defined as a strain threshold value, $K_0$, considered to

250    be the average strain value along a displacement gap, which made it less sensitive to noise rather than

251    simply requiring an individual strain value to be above a threshold. In earlier work [13], the strain threshold

252    limit was defined as $K_0$ = 20.0 mm/m = 2%, chosen in agreement with microscopy observations, such that a

253    crack is a local interval where the average tensile strain along the displacement gap is larger than $K_0$, i.e.

$$\varepsilon_{i,x,avg.} > K_0 \implies \text{"Surface crack"} \tag{1}$$

254    On this basis, it was possible to synthesize a digital reproduction of the crack patterns including crack width,

255    crack length, crack area and crack location. A similar approach for quantification of the cracked surface area

256    based on DIC data and a defined strain threshold value has been used before in studies of drying shrinkage

257    [8,43].

258    Examples on how the DIC data was used to compute these displacement gaps, i.e. surface cracks, are given

259    for different time stages for specimen REF (B) in Fig. 5-7 and for specimen PP 0.2% (B) in Fig. 8. The figures

260    are illustrating: a) the in-plane surface displacement by DIC data, b) a section view going through the

261    centreline of the specimen showing the strain and displacement along the selected sections including crack

262    widths for each displacement gap, and c) the crack pattern synthesized by the post-processing approach.

263    Fig. 5-7 represents the reference specimen with no addition of fibres, REF (B), at different time stages (at t

264    = 2.0 h, t = 2.5 h, and t = 25 h) to illustrate the evolution in surface cracking over time. At t = 2.0 h, there

265    were 5 cracks along Section A-A with crack widths of 44 µm, 75 µm, 29 µm, 156 µm and 314 µm. At t = 2.5

266    h, in addition to the initiation of additional cracks, these 5 cracks had increased in width to 255 µm, 46 µm,

267    291 µm, 259 µm and 394 µm, respectively. But between t = 2.5 h and t = 25 h only small increments in crack

268    widths were observed. Fig. 8 shows the specimen with 0.2% of PP (B) at t = 25 h to illustrate the ability of

269    the synthetic fibres to distribute the displacement, i.e. increase the strain capacity, across the restrained

270    overlay so that very few and fine cracks appear compared to the reference specimen.
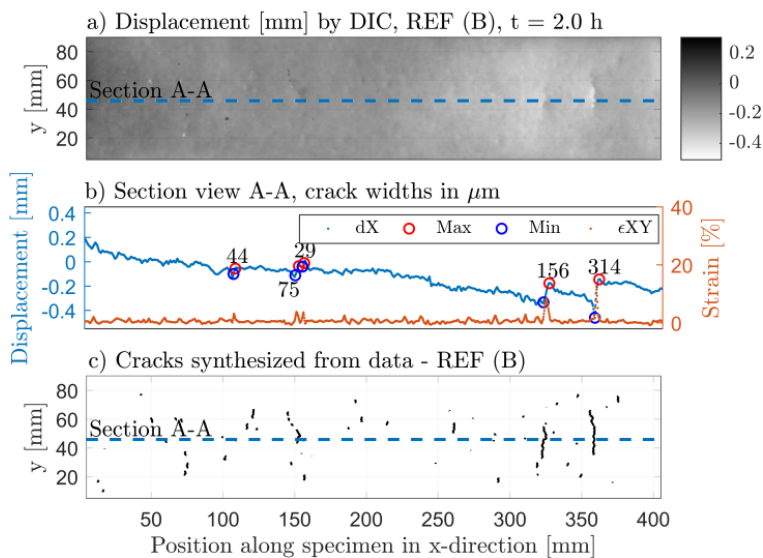


271

272    Fig. 5. Restrained specimen, REF (B), at t = 2.0 h. a) Surface displacement in the x-direction by DIC data; b) Section A-A

273    going through the centerline of the specimen showing the strain and displacement along the section; and c) the crack

274    pattern synthesized from data by the post-processing approach.
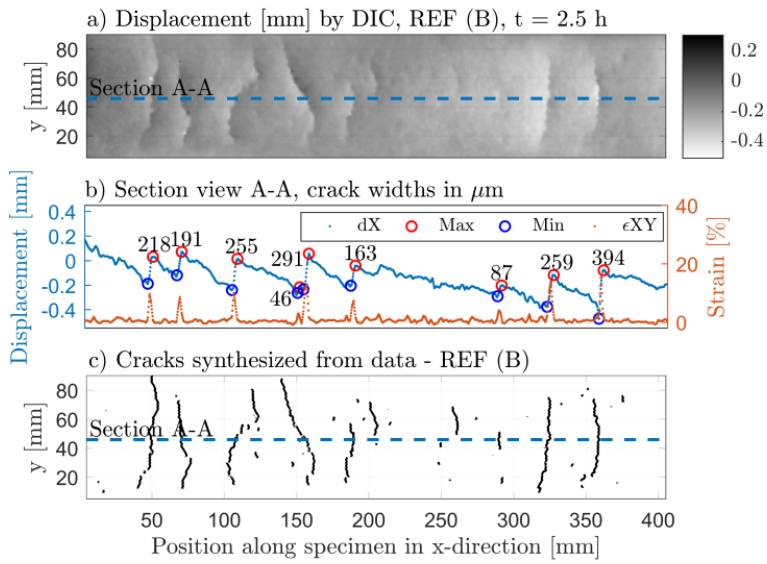
a) Displacement [mm] by DIC, REF (B), t = 2.5 h

b) Section view A-A, crack widths in $\mu$m

c) Cracks synthesized from data - REF (B)

Fig. 6. Restrained specimen, REF (B), at t = 2.5 h.



a) Displacement [mm] by DIC, REF (B), t = 25 h

b) Section view A-A, crack widths in $\mu$m

c) Cracks synthesized from data - REF (B)

Fig. 7. Restrained specimen, REF (B), at t = 25 h.



a) Displacement [mm] by DIC, PP 0.2% (B), t = 25 h

b) Section view B-B, crack widths in $\mu$m

c) Cracks synthesized from data - PP 0.2% (B)
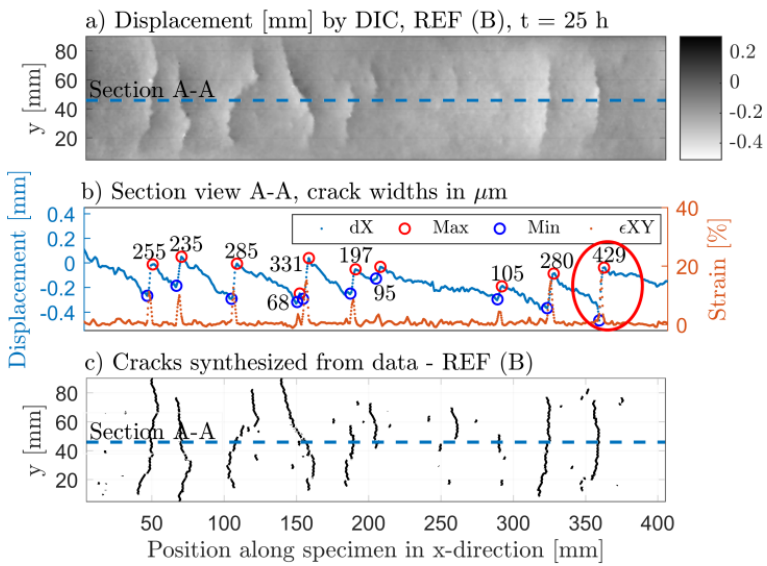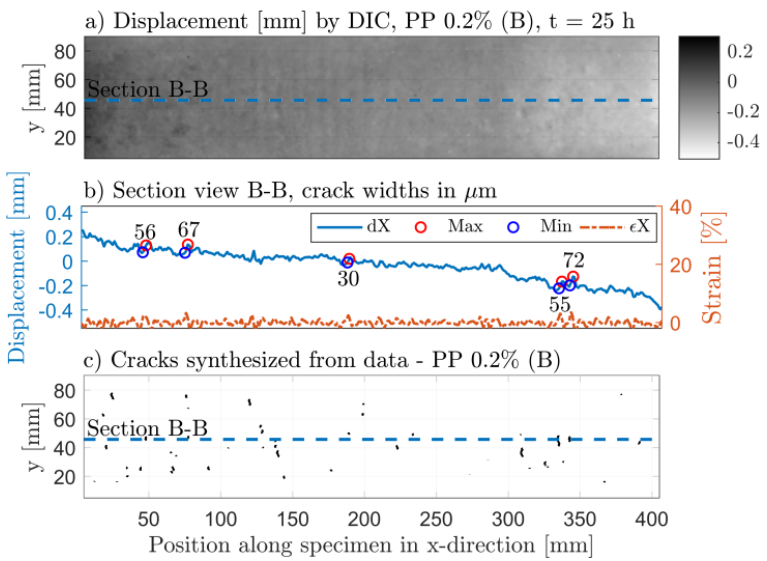
280     Fig. 8. Restrained specimen, PP 0.2% (B), at t = 25 h.

281

282     When a crack occurs on the specimen surface, the texture of the representative subsets is modified, which

283     in some cases can lead to local interpolation errors in the displacement field in close vicinity to a crack

284     resulting in an overestimation of the crack width. These local errors in the DIC data were observed for a few

285     of the identified cracks, but for the majority, a strong correlation between the crack width (vertical

286     displacement gap calculated as the difference between the minimum and maximum value on each side of

287     the crack) and microscopy measurements were observed. In the given example of specimen REF (B) at t =

288     25 h shown in Fig. 7b, such an error is identified for the crack marked inside the red circle (crack width

289     calculated to 429 µm). On the left side of the actual displacement gap (crack), an additional drop in

290     displacement is detected in the digital facet, but when comparing it with microscopy observations this

291     additional drop is not physically present, and, therefore, considered as a local error. Other studies

292     suggested determining the crack widths by interpolating the values of the "uncracked" displacement field

293     along the section in between the cracks [8]. Since the surface deformations in the present study were

294     monitored starting from when the material was still in the fresh, plastic state, and since the overlay was

295     evenly bottom-restrained, the displacement field in between the actual cracks is not completely linear as

296     seen in Fig. 5-8c, thus this method was not considered to give a sufficiently precise estimation of the crack

297     width.  As shown in Section 3.2, the degree of cracking is presented as crack width distributions (CWD) over

298     the entire specimen surface. Despite the very few local errors in the DIC data, which were found to result in

299     an overestimation of the maximum observed crack width, these local anomalies in the digital facets are not

300     significant for the crack width distribution as they involve only a small number of pixels, i.e. crack length

301     and crack area.

302

303     **3.2     Quantification of surface cracking**

304     The degree of surface cracking due to plastic shrinkage has in the literature most commonly been evaluated

305     based on basic crack parameters such as the mean and maximum crack width, mean and maximum crack

length and the total crack area on the specimen surface [4,9]. As the DIC technique enables a precise analysis of the crack widths over the entire specimen surface, it allows an objective quantification, which is essential for the comparison of the restrained plastic shrinkage behaviour of different types of mixture designs. In this study, the crack widths ($w_{i,sec}$) along each of the approximately 380 individual sections ($n_{i,sec}$) of the interpolated grid on each specimen were calculated based on the post-processing procedure described in the previous sections (see also [13]). The total crack area was calculated by summing up all crack widths along each section. Based on the post-processing procedure, basic crack parameters, such as the mean crack width, the maximum crack width, and the total crack area could also be objectively computed and are shown for each specimen (7 types with 3 replicates) in Table 3. The crack reduction ratio (CRR) for the total crack area (TCA) and maximum crack width (MCW), respectively, which were calculated in accordance with the ASTM standard C1579 (2013) are also given in Table 3. From these results it is observed that the addition of fibres in most cases had a positive influence on the degree of surface cracking, however, these discrete values don't provide any information about the distribution of crack widths.

Table 3. Basic crack parameters from restrained shrinkage test series at t = 25 h. Three replicates of each specimen type (A-C). MCW = Maximum crack width; TCA = Total crack area; CRR = Crack reduction ratio

| Fibre | Fraction | Mean crack width | | | Maximum crack width | | | Total crack area | | | CRR for | CRR for |
|-------|----------|------------------|---|---|---------------------|---|---|------------------|---|---|---------|---------|
| | [vol%] | [μm] | | | [μm] | | | [mm$^2$] | | | MCW [-] | TCA [-] |
| | | A | B | C | A | B | C | A | B | C | Mean | Mean |
| REF | 0 | 168 | 176 | 216 | 574 | 521 | 893 | 111 | 122 | 168 | 0.00 | 0.00 |
| PP | 0.1 | 117 | 65 | 54 | 261 | 134 | 97 | 4.4 | 3.1 | 1.9 | 0.75 | 0.98 |
| PP | 0.2 | 74 | 63 | 46 | 132 | 152 | 52 | 0.5 | 6.3 | 0.1 | 0.83 | 0.98 |
| R-PE | 0.2 | 215 | 171 | 189 | 687 | 659 | 593 | 206 | 144 | 207 | 0.02 | -0.39 |
| R-PE | 0.5 | 137 | 137 | 139 | 362 | 682 | 388 | 112 | 63 | 89 | 0.28 | 0.34 |

| R-PE | 1.0 | 140 | 87 | 155 | 405 | 219 | 570 | 94 | 26 | 117 | 0.40 | 0.41 |
| R-PE | 2.0 | 78 | 74 | 92 | 225 | 182 | 286 | 23.1 | 14.4 | 24 | 0.65 | 0.85 |

323

324 Another more comprehensive way of quantifying the surface cracking is based on the crack width

325 distribution (CWD) over the surface area as it was also done in other studies on cracking of cementitious

326 materials [42,44,45]. The CWD appears to give a more quantitative result for the degree of surface

327 cracking, because the basic crack parameters don't give any information about the number of cracks with

328 specific crack widths that are present on the specimen surface. The CWD is relevant since a few wide cracks

329 can be more deteriorative to a steel reinforced concrete structure than a large number of fine cracks due to

330 the penetration of salts and other aggressive agents [46]. In the present study, the CWD was illustrated by

331 the relation between the crack widths and the total crack length or the total crack area within each bin

332 interval, thus revealing the amount of cracks within each specific crack width interval at t = 25 h, see Fig. 9

333 and Fig. 10, respectively. As explained in Section 3.1.1, some of the widest cracks could be a result of local

334 interpolation errors in the DIC data, nevertheless, we have decided to include all identified crack widths in

335 the CWD. First, it is observed that the shape of the CWD showed similar tendency for each type of

336 replicates, thus some variations in the size of the crack widths appear. Secondly, some of the widest cracks

337 are only present in small quantities, i.e. cracks with this crack width are only identified along a few of the

338 sections on the specimen surface and does only reveal when representing the CWD as the total crack area

339 of each bin interval as shown in Fig. 10. Comparing the CWD with the results given in Table 3, it is clear that

340 the CWD provide a much more detailed result of the degree of surface cracking. The specimens with the

341 most severe surface cracking were the specimens with addition of 0.2% R-PE and the REF specimens, where

342 maximum crack widths of approximately 500-900 μm were observed. It was expected that the addition of

343 0.2% R-PE fibres would have had a small influence of the cracking behaviour, but this small amount of R-PE

344 fibres did not improve the performance with regard to the surface cracking. When considering the

345 maximum and mean crack widths, the 0.2% R-PE and REF specimens behaved similarly. Besides the fibre

346 addition of 0.2% R-PE, which was considered too low for this fibre type, the figures illustrate how fewer

347    wide cracks appeared when adding fibres to the mixture. The PP fibres showed a superior ability to control

348    the plastic shrinkage cracks even at volume fractions as low as 0.1%, but these fibres were also produced

349    for controlling plastic shrinkage cracking in cementitious materials, thus this good result was expected. The

350    R-PE fibres, when added in volume fractions of 0.5-2.0% also had an effect on the surface cracking. The

351    addition of 0.5-1.0% R-PE fibres resulted in a significant reduction in cracks with a crack width larger than

352    300 μm, but results indicated that this amount of fibres did not lead to a desirable reduction in surface

353    cracking. Considering the specimens with 2.0% R-PE fibres, a reduction similar to the specimens with PP

354    fibres was almost achieved and no cracks with a crack width larger than 300 μm were found on any of the

355    specimen's surface.
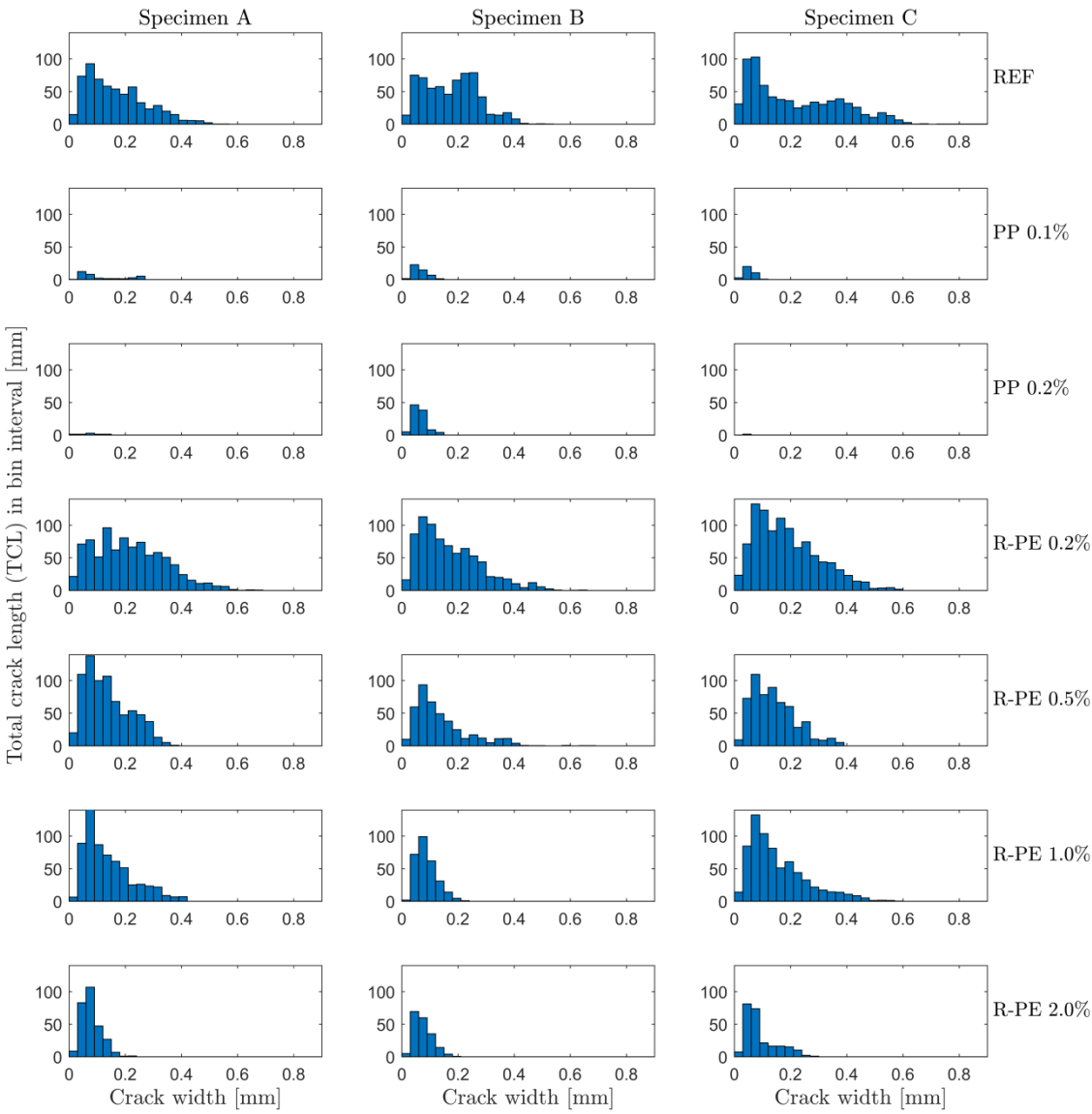


356

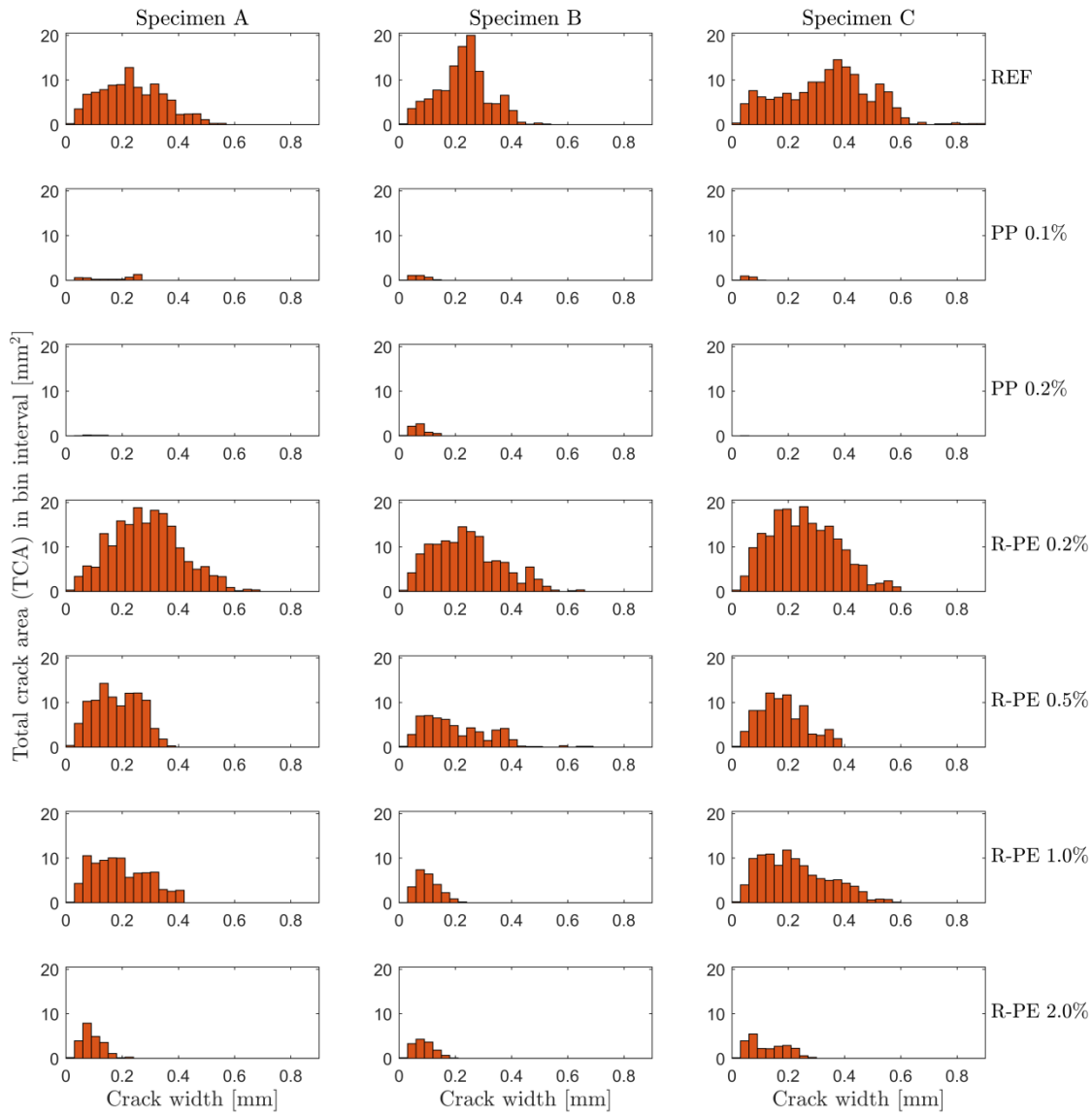357    Fig. 9. Histograms of the relation between the total crack length [mm] in each bin interval and the crack width

358    distribution (CWD) over the entire specimen surface at t = 25 h

359

360

361



362

363    Fig. 10. Histograms of the relation between the total crack area [mm$^2$] in each bin interval and the crack width

364    distribution (CWD) over the entire specimen surface at t = 25 h

365

366  Fig. 9-10 and Table 3 represent different ways of evaluating the degree of surface cracking, with Fig. 9-10

367  being more quantitative than the basic crack parameters in Table 3. However, both evaluation strategies

368  show that the most severe cracking appeared in the 0.2% R-PE specimens and the REF specimens, both

369  with regard to crack widths and total crack area. The R-PE fibres performed well when added in volume

370  fractions of 2.0% and showed varying effect when added in volume fractions below 1.0%. This relatively

371  high volume fraction for R-PE fibres to achieve their best results compared to PP fibres corresponds well

372  with what other studies have found using macro fibres for controlling plastic shrinkage cracking, although

373  the 2.0% of R-PE were in the high end of the range of necessary fractions of macro fibre found by

374  [4,28,29,31]. The R-PE fibres used in this study were straight in shape and had a diameter of 280 ± 30 μm,

375  which is approximately 15 times the diameter of the commercial PP fibres. The R-PE fibres were not

376  reprocessed, but simply cut down to monofilament fibres, which were possible because of the origin of the

377  fibres, as the lines in the fishing nets consisted of several monofilament fibres, which were braided or

378  twisted, thus relatively easy to separate from each other when processing the fibres from the discarded

379  material. Previous studies have found that a deformed fibre shape is beneficial in controlling plastic

380  shrinkage cracking because of the improved fibre-to-matrix bonding [4,28], which could also explain the

381  need for a volume fraction of 2.0% of R-PE fibres. Regarding the performance of the fine PP fibres, similar

382  behaviour has been observed in several other studies on the use of PP fibres for the control of plastic

383  shrinkage cracking [3,9,25,27,30,31].

384

385  *3.2.1    Evolution in surface cracking*

386  The shrinkage specimens were monitored at intervals of 15 min during the entire test period starting at t =

387  1 h (t = 1 h as reference stage, i.e. cracking = 0), so the CWD at different time stages could be computed as

388  a measure of the evolution in surface cracking. The evolution in CWD is of interest as it would reveal if the

389  fibres had any influence on the time of initiation and stabilization of surface cracking. Histograms at

390  selected time stages showing the evolution in CWD in relation to the total crack area (TCA) in each bin

391  interval are given in Fig. 11. Additionally, the evolution in surface cracking is also represented by the
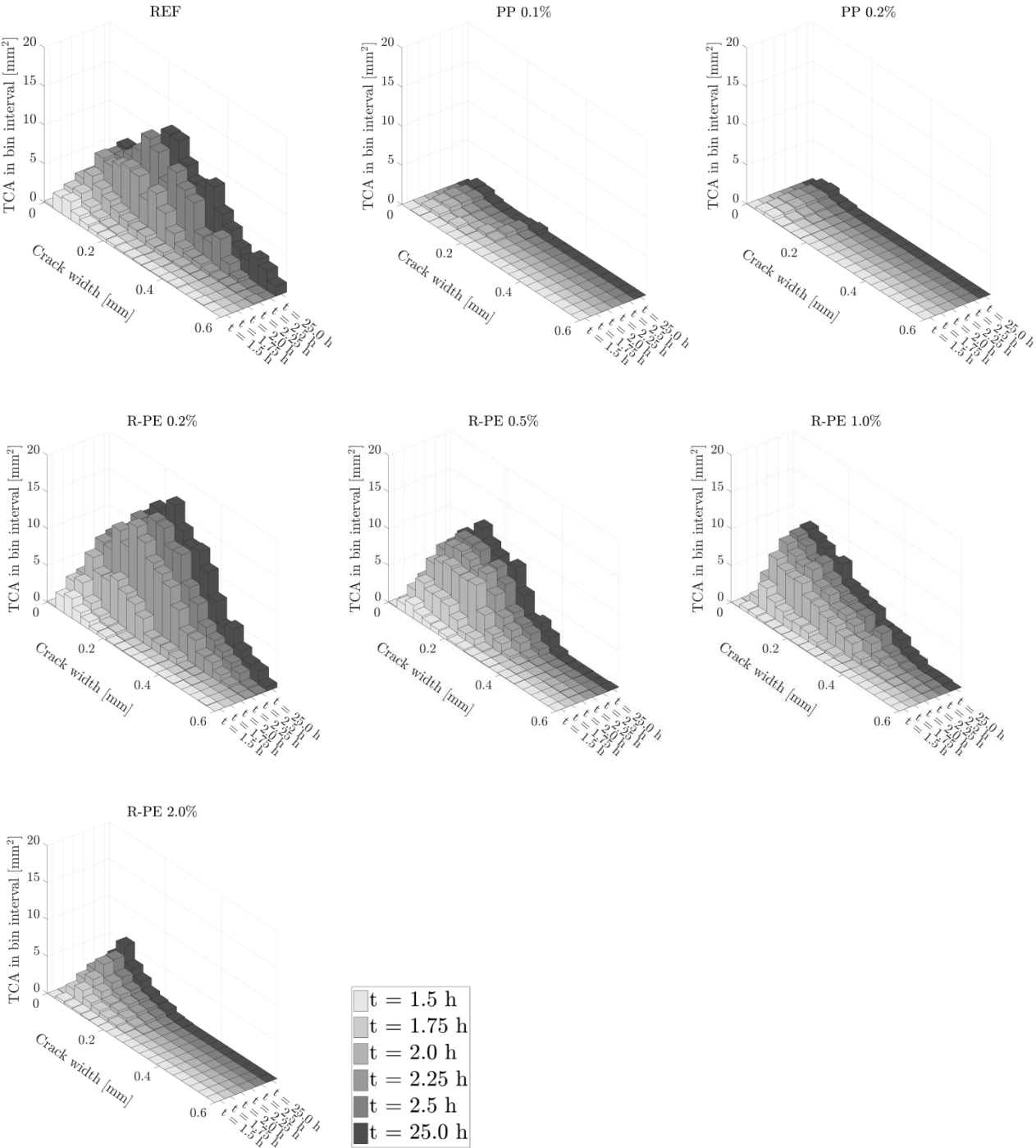
392   increase in total crack area as shown in Fig. 12. Since most plastic shrinkage deformations occur during the

393   first few hours after casting, the evolution in the total crack area is shown for the time period of t = 1-5 h in

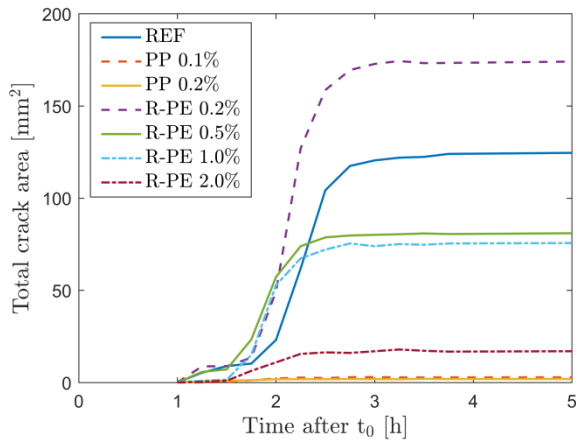394   Fig. 12. Mean values of three replicates (A-C) are given for each specimen type.

395
396



397

398

399

Fig. 11. Histograms of the relation between the total crack area [mm$^2$] in each bin interval and the crack width

401   distribution (CWD) over the entire specimen surface at selected time stages between t = 1.5 h and t = 25 h. Mean

402   values for three replicates (A–C) are given



403

404   Fig. 12. Evolution in total crack area (TCA), mean values for three replicates (A–C) are given.

405

406   According to the CWD shown in Fig. 11, the specimens with the most severe surface cracking, REF and 0.2%

407   R-PE and some very fine cracks had already initiated at t = 1.5 h.  The largest change with respect to

408   initiation of surface cracking (given as total crack area per bin interval of crack widths) for these two

409   specimen types occurred between the time stages t = 2.0 h and t = 2.25 h. At t = 2.25 h, the shape of the

410   crack network as well as the shape of the CWD had formed and the further evolution in surface cracking

411   was mainly because of propagating crack widths during the remaining test period until t = 25 h. Regarding

412   the CWD for the specimens with 0.5% and 1.0% of R-PE fibres, a similar behaviour as for the specimens

413   with 0.2% R-PE fibres was seen until t = 2.0 h, but after that the crack network and shape of CWD stabilized

414   faster and did not increase to the same extent as the REF and 0.2% R-PE specimens, thus the fibres was

415   shown to have an influence on the time and degree of surface cracking. This positive performance of the

416   fibres was even more distinct for the specimens with R-PE fibre fractions of 2.0%. From Fig. 12, it is seen

417   that the final stabilization of the total crack area for the specimens REF and 02.% R-PE happened at

418   approximately t = 3.25 h, while it had stabilized at approximately t = 2.75 h for the specimens with 0.5%

419   and 1.0% of R-PE fibres and at t = 2.25 h for the 2.0% R-PE specimens. The specimens with addition of

420     commercial PP fibres performed best in controlling the surface cracking, and the cracking with respect to

421     the total crack area for the PP 0.2% specimens had stabilized at t = 2.25 h.

422

423     **3.3    Free shrinkage behaviour analysed using DIC**

424     The surface displacement due to the plastic shrinkage of unrestrained mortar specimens that were allowed

425     to deform freely was also monitored using the DIC technique simultaneous to the restrained shrinkage

426     tests to investigate the influence of the fibre reinforcement on the free shrinkage behaviour. The

427     displacement data obtained from the DIC software were used for further calculations in MATLAB, which

428     made it possible to do a section-wise analysis of each individual section ($n_{i,sec}$) parallel to the axis as

429     explained in Section 3.1.1 for the restrained shrinkage study. Most significant plastic shrinkage

430     deformations took place in the x-direction (parallel to the length of the specimen) due to the specimen

431     geometry and the direction of the wind exposure. The change in free shrinkage over time (t = 1–25 h) was

432     calculated as the average of the maximum difference in displacement along each section ($n_{i,sec}$) from one

433     end to the other taking the entire surface area into account. No surface cracking appeared on any of the

434     free shrinkage specimens and it was observed that the sides of the specimens all easily detached from the

435     sides of the moulds. Fig. 13a illustrates the in-plane free shrinkage strain in the x-direction (mm/m). The

436     displacement (contraction) increased rapidly in the plastic phase until approximately t = 2.5 h and then

437     stabilized, thus some irregularities in the displacement data appeared over time. The graph shows that the

438     largest in-plane free shrinkage strains over the length of the specimens were found for the specimens with

439     0.2% R-PE and the REF specimens, closely followed by the specimens with an addition of 0.5–1.0% of R-PE

440     fibres and 0.1% of PP fibres. The specimens with an addition of 2.0% of R-PE fibres and 0.2% of PP fibres

441     experienced the least horizontal shrinkage and performed similarly.
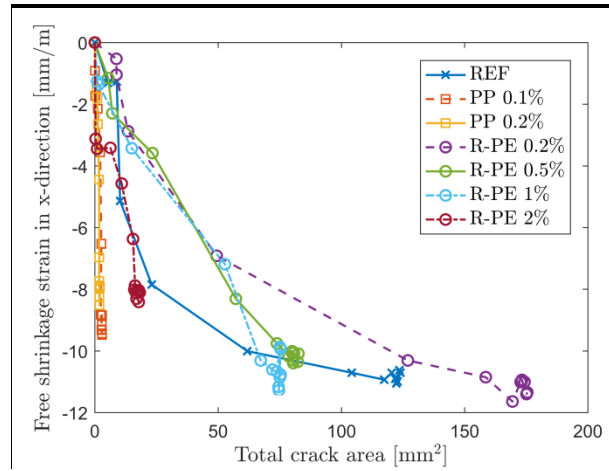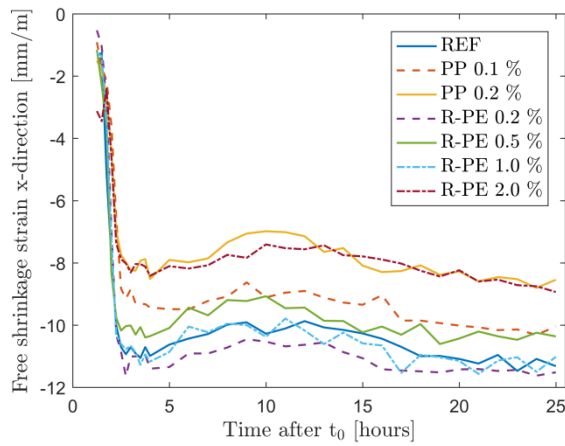
Fig. 13. a) In-plane free shrinkage strain in x-direction; b) In-plane free shrinkage strain in x-direction versus the total crack area of restrained shrinkage specimens. Mean values for three replicates (A–C) are given

### 3.3.1 Comparison of free and restrained shrinkage behaviour

Fig. 13b shows the evolution of the total crack area on the restrained mortar overlays versus the free shrinkage strain of the unrestrained specimens. It is of interest to analyse whether the degree of free shrinkage correlates with the degree of restrained surface cracking. The variations in the free shrinkage behaviour between the different specimens were observed not to be significant compared to the variations in the total crack area of the restrained specimens with addition of varying fibre types and fractions. This is mainly due to the effect of the fibres because they have the ability to distribute the strains in the restrained overlays, which results in a reduced total crack area. A comparison of the specimens with 0.1% PP and 2.0% R-PE showed that even though the 2.0% R-PE fibres had a larger influence on the free shrinkage, the total crack area was smaller for the 0.1% PP fibres. This again shows the superior ability of the commercially available PP fibres to distribute the strains in restrained mortar overlays.

### 3.3.2 Fibre influence on workability of fresh mortar mixtures

The workability of the fresh mortar mixtures with different fibre types and -fractions was evaluated based on the flow diameter and is shown in Fig. 14. The addition of fibres is clearly decreasing the flow diameter of the fresh mortars. As it was observed for the free shrinkage strain, the largest values were found for the

462 REF specimens and the 0.2% R-PE specimens, with these two behaving similarly, followed by the 0.5% and

463 1.0% R-PE specimens. For the PP fibres, an addition of only 0.1 vol% was observed to influence the

464 workability significantly; however, higher fibre fractions of R-PE fibres were necessary to obtain a similar

465 effect. Mortars with an addition of 0.2 vol% PP fibres and 2.0 vol% R-PE fibres had similar workability.
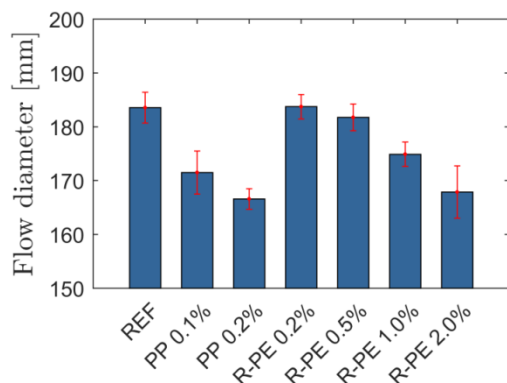
466



467 Fig. 14. Workability of fresh mortar mixtures by flow table test

468

469 **4    Conclusion**

470 A 2D-DIC technique was applied to study the formation of in-plane strains and displacements induced by

471 plastic shrinkage of free and restrained mortar overlays under controlled environmental conditions with

472 the aim of investigating the influence of the addition of two types of synthetic fibres. The two fibre types

473 that were investigated were commercially available polypropylene (PP) fibres and recycled polyethylene (R-

474 PE) fibres obtained by mechanical cutting of discarded fishing nets. The fibre-reinforced mortar overlays

475 were compared with an unreinforced reference mortar. An automated post-processing MATLAB routine

476 enabled computation of basic crack parameters such as total crack area, maximum and mean crack width

477 based on the DIC data. The evolution in total crack area during the test period of 1-25 h after casting was

478 also analysed. The data was then presented in detailed histograms showing the relation between the total

479 crack length/area within each bin interval and the crack width distribution over the entire specimen surface

480 at various time stages.

481 From the results of the free and restrained shrinkage test series, the following conclusions were drawn:

482    At the end of each test series, visible surface cracking appeared in some of the restrained mortar

483    overlays. A more detailed visualization of the surface cracking was enabled by plotting the surface

484    strain based on data obtained by DIC.

485    -    The commercially available PP fibres were added to the fresh mixture in volume fractions of 0.1%

486        and 0.2% and showed the best performance in controlling the restrained plastic shrinkage cracking.

487        A crack reduction ratio (CRR) of 0.98 with respect to the total crack area was obtained for the

488        specimens with PP fibres.

489    -    The R-PE fibres were of a coarser nature than the PP fibres and, therefore, had to be added in

490        higher volume fractions (0.2-2.0%) to obtain results comparable to the PP fibres. The addition of

491        0.2% R-PE fibres did not improve the performance with regard to the total crack area, even though

492        a small improvement was expected. R-PE fibres added in a volume fraction of 2.0% showed a good

493        performance in controlling plastic shrinkage cracking and a CRR of 0.85 with respect to the total

494        crack area was obtained.

495    -    The evolution in surface cracking over time was analysed by the crack width distribution at various

496        time stages. This showed that the surface cracking on the specimens with addition of fibres

497        stabilized faster than the specimens with most surface cracking, the REF specimens and the

498        specimens with 0.2% of R-PE. The evolution in total crack area was also plotted over time, which

499        showed that the plastic shrinkage cracking had stabilized between t = 2.25 h (PP 0.2%) and t = 3.25

500        h (Reference).

501    -    The behaviour of free shrinkage specimens was also monitored and computed from DIC data. The

502        smallest in-plane free shrinkage strain was found for the specimens with addition of 0.2% PP and

503        2.0% R-PE. The largest free shrinkage appeared for the specimens with addition of 0.2% R-PE and

504        for the reference specimen. The free shrinkage in all specimens initially increased rapidly, but

505        stabilized at approximately 2.5 h after the start of mixing.

506    Based on these results it can be concluded that the DIC technique is a suitable tool for objectively studying

507    the shrinkage behaviour of fresh cementitious materials. Furthermore, the R-PE fibres showed a good

508  performance in controlling plastic shrinkage cracks in the retrained overlays when added in volume fraction

509  of 2.0%.

510

511  **5    Acknowledgement**

515

516  **6    References**

517  [1]    A. Bentur, S. Mindess, Fibre-Reinforced Cementitious Composites, 2nd Editio, Taylor & Francis, 2006.

518  [2]    P.N. Balaguru, S.P. Shah, Fiber Reinforced Cement Composites, McGraw-Hill, 1992.

519  [3]    N. Banthia, R. Gupta, Influence of polypropylene fiber geometry on plastic shrinkage cracking in

520        concrete, Cem. Concr. Res. 36.7 (2006) 1263–1267. doi:10.1016/j.cemconres.2006.01.010.

521  [4]    J.H.J. Kim, C.G. Park, S.W. Lee, S.W. Lee, J.P. Won, Effects of the geometry of recycled PET fiber

522        reinforcement on shrinkage cracking of cement-based composites, Compos. Part B Eng. 39.3 (2008)

523        442–450. doi:10.1016/j.compositesb.2007.05.001.

524  [5]    P.J. Uno, Plastic Shrinkage Cracking and Evaporation Formulas, ACI Mater. J. 95.4 (1998) 365–375.

525  [6]    N. Banthia, C. Yan, Shrinkage cracking in polyolefin fiber-reinforced concrete, ACI Mater. J. 97.4

526        (2000) 432–437.

527  [7]    N. Banthia, R. Gupta, Test Method for Evaluation of Plastic Shrinkage Cracking in Fiber-Reinforced

528        Cementitious Materials, Exp. Tech. 31.6 (2007) 44–48. doi:10.1111/j.1747-1567.2007.00191.x.

529  [8]    T. Mauroux, F. Benboudjema, P. Turcry, A. Aït-Mokhtar, O. Deves, Study of cracking due to drying in

530        coating mortars by digital image correlation, Cem. Concr. Res. 42.7 (2012) 1014–1023.

531        doi:10.1016/j.cemconres.2012.04.002.

532    [9]    A.E. Naaman, T. Wongtanakitcharoen, G. Hauser, Influence of different fibers on plastic shrinkage

533           cracking of concrete, ACI Mater. J. 102.1 (2005) 49–58.

534    [10]   J. Branston, S. Das, S.Y. Kenno, C. Taylor, Influence of basalt fibres on free and restrained plastic

535           shrinkage, Cem. Concr. Compos. 74 (2016) 182–190. doi:10.1016/j.cemconcomp.2016.10.004.

536    [11]   C.A. Juarez, G. Fajardo, S. Monroy, A. Duran-Herrera, P. Valdez, C. Magniont, Comparative study

537           between natural and PVA fibers to reduce plastic shrinkage cracking in cement-based composite,

538           Constr. Build. Mater. 91 (2015) 164–170. doi:10.1016/j.conbuildmat.2015.05.028.

539    [12]   P. Zhao, A.M. Zsaki, M.R. Nokken, Using digital image correlation to evaluate plastic shrinkage

540           cracking   in   cement-based   materials,   Constr.   Build.   Mater.   182   (2018)   108–117.

541           doi:10.1016/j.conbuildmat.2018.05.239.

542    [13]   I.M.G. Bertelsen, C. Kragh, G. Cardinaud, L.M. Ottosen, G. Fischer, Quantification of plastic shrinkage

543           cracking in mortars using digital image correlation, Submitt. 2018.04.28. (n.d.).

544    [14]   G.M. Sadiqul Islam, S. Das Gupta, Evaluating plastic shrinkage and permeability of polypropylene

545           fiber   reinforced   concrete,   Int.   J.   Sustain.   Built   Environ.   5.2   (2016)   345–354.

546           doi:10.1016/j.ijsbe.2016.05.007.

547    [15]   N. Banthia, R. Gupta, Plastic shrinkage cracking in cementitious repairs and overlays, Mater. Struct.

548           42.5 (2009) 567–579. doi:10.1617/s11527-008-9403-9.

549    [16]   C. Qi, J. Weiss, J. Olek, Characterization of plastic shrinkage cracking in fiber reinforced concrete

550           using image analysis and a modified Weibull function, Mater. Struct. 36.6 (2003) 386–395.

551           doi:10.1007/BF02481064.

552    [17]   A. Mazzoli, S. Monosi, E.S. Plescia, Evaluation of the early-age-shrinkage of Fiber Reinforced

553           Concrete (FRC) using image analysis methods, Constr. Build. Mater. 101.1 (2015) 596–601.

554           doi:10.1016/j.conbuildmat.2015.10.090.

555    [18]   V. Dey, R. Kachala, A. Bonakdar, N. Neithalath, B. Mobasher, Quantitative 2D Restrained Shrinkage

556           Cracking of Cement Paste with Wollastonite Microfibers, J. Mater. Civ. Eng. 28.9 (2016) 4016082.

557    doi:10.1061/(ASCE)MT.1943-5533.0001592.

[19]    M.A. Sutton, J.J. Orteu, H. Schreier, Image correlation for shape, motion and deformation
559    measurements: basic concepts, theory and applications, Springer Science & Business Media, 2009.

[20]    A. Messan, P. Ienny, D. Nectoux, Free and restrained early-age shrinkage of mortar: Influence of
561    glass fiber, cellulose ether and EVA (ethylene-vinyl acetate), Cem. Concr. Compos. 33.3 (2011) 402–
562    410. doi:10.1016/j.cemconcomp.2010.10.019.

[21]    P. Zhao, Master thesis. Digital Image Correlation to Evaluate Plastic Shrinkage Cracking in Cement-
564    Based Materials, Concordia University, Montreal, Canada, 2016.

[22]    S. Ghourchian, M. Wyrzykowski, L. Baquerizo, P. Lura, Susceptibility of Portland cement and blended
566    cement concretes to plastic shrinkage cracking, Cem. Concr. Compos. 85 (2018) 44–55.
567    doi:10.1016/j.cemconcomp.2017.10.002.

[23]    M. Némoz-Gaillard, D. Nectoux, E. Dallies, D. Muller, Influence of AR glass fibers on the cracking of
569    concrete : analysis at the very early age by digital image correlation, in: PRO 23 Int. RILEM Conf.
570    Early Age Crack. Cem. Syst., 2002: pp. 237–244.

[24]    E.D. Dzaye, G. De Schutter, D. Aggelis, Application of Digital Image Correlation to Cement Paste, in:
572    Proceedings. Eighteenth Int. Conf. Exp. Mech., 2018. doi:10.3390/ICEM18-05332.

[25]    P. Soroushian, F. Mirza, A. Alhozaimy, Plastic Shrinkage cracking of Polypropylene fiber-reinforced
574    concrete, ACI Mater. J. 92.5 (1995) 553–560.

[26]    P. Balaguru, Contribution of fibers to crack reduction of cement composites during the initial and
576    final setting period, ACI Mater. J. 91.3 (1994) 280–288.

[27]    E. Boghossian, L.D. Wegner, Use of flax fibres to reduce plastic shrinkage cracking in concrete, Cem.
578    Concr. Compos. 30.10 (2008) 929–937. doi:10.1016/j.cemconcomp.2008.09.003.

[28]    R.P. Borg, O. Baldacchino, L. Ferrara, Early age performance and mechanical characteristics of
580    recycled    PET    fibre    reinforced    concrete,    Constr.    Build.    Mater.    108    (2016)    29–47.
581    doi:10.1016/j.conbuildmat.2016.01.029.

582    [29]    N. Pešić, S. Živanović, R. Garcia, P. Papastergiou, Mechanical properties of concrete reinforced with

583           recycled HDPE plastic fibres, Constr. Build. Mater. 115 (2016) 362–370.

584           doi:10.1016/j.conbuildmat.2016.04.050.

585    [30]    A. Sivakumar, M. Santhanam, A quantitative study on the plastic shrinkage cracking in high strength

586           hybrid fibre reinforced concrete, Cem. Concr. Compos. 29.7 (2007) 575–581.

587           doi:10.1016/j.cemconcomp.2007.03.005.

588    [31]    H. Najm, P. Balaguru, Effect of large-diameter polymeric fibers on shrinkage cracking of cement

589           composites, ACI Mater. J. 99.4 (2002) 345–351.

590    [32]    B.S. Al-Tulaian, M.J. Al-Shannag, A.R. Al-Hozaimy, Recycled plastic waste fibers for reinforcing

591           Portland cement mortar, Constr. Build. Mater. 127 (2016) 102–110.

592           doi:10.1016/j.conbuildmat.2016.09.131.

593    [33]    M. Serdar, A. Baričević, M. Jelčić Rukavina, M. Pezer, D. Bjegović, N. Štirmer, Shrinkage Behaviour of

594           Fibre Reinforced Concrete with Recycled Tyre Polymer Fibres, Int. J. Polym. Sci. 2015.3 (2015) 1–9.

595           doi:10.1155/2015/145918.

596    [34]    F.L. Auchey, The Use of Recycled Polymer Fibers as Secondary Reinforcement in Concrete

597           Structures, J. Constr. Educ. 3.2 (1998) 131–140.

598    [35]    L. Gu, T. Ozbakkaloglu, Use of recycled plastics in concrete: A critical review, Waste Manag. 51

599           (2016) 19–42. doi:10.1016/j.wasman.2016.03.005.

600    [36]    R. Siddique, J. Khatib, I. Kaur, Use of recycled plastic in concrete: A review, Waste Manag. 28.10

601           (2008) 1835–1852. doi:10.1016/j.wasman.2007.09.011.

602    [37]    C.J. Moore, Synthetic polymers in the marine environment: A rapidly increasing, long-term threat,

603           Environ. Res. 108 (2008) 131–139. doi:10.1016/j.envres.2008.07.025.

604    [38]    S. Spadea, I. Farina, A. Carrafiello, F. Fraternali, Recycled nylon fibers as cement mortar

605           reinforcement, Constr. Build. Mater. 80 (2015) 200–209. doi:10.1016/j.conbuildmat.2015.01.075.

606    [39]    S. Orasutthikul, D. Unno, H. Yokota, Effectiveness of recycled nylon fiber from waste fishing net with

607    respect  to  fiber  reinforced  mortar,  Constr.  Build.  Mater.  146  (2017)  594–602.

608    doi:10.1016/j.conbuildmat.2017.04.134.

609    [40]   I.M.G. Bertelsen, L.M. Ottosen, Recycling of waste PE fishing nets as fibre reinforcement in gypsum-

610    based composites, Submitted. (n.d.).

611    [41]   Ö. Eren, K. Marar, Effect of steel fibers on plastic shrinkage cracking of normal and high strength

612    concretes, Mater. Res. 13 (2010) 135–141. doi:10.1590/S1516-14392010000200004.

613    [42]   W.P. Boshoff, C.J. Adendorff, Effect of sustained tensile loading on SHCC crack widths, Cem. Concr.

614    Compos. 37 (2013) 119–125. doi:10.1016/j.cemconcomp.2012.11.009.

615    [43]   F. Lagier, X. Jourdain, C. De Sa, F. Benboudjema, J.B. Colliat, Numerical strategies for prediction of

616    drying cracks in heterogeneous materials: Comparison upon experimental results, Eng. Struct. 33.3

617    (2011) 920–931. doi:10.1016/j.engstruct.2010.12.013.

618    [44]   R. Ranade, J. Zhang, J.P. Lynch, V.C. Li, Influence of micro-cracking on the composite resistivity of

619    Engineered    Cementitious    Composites,    Cem.    Concr.    Res.    58    (2014)    1–12.

620    doi:10.1016/j.cemconres.2014.01.002.

621    [45]   N. Yousefieh, A. Joshaghani, E. Hajibandeh, M. Shekarchi, Influence of fibers on drying shrinkage in

622    restrained       concrete,       Constr.       Build.       Mater.       148       (2017)       833–845.

623    doi:10.1016/j.conbuildmat.2017.05.093.

624    [46]   T.U. Mohammed, N. Otsuki, M. Hisada, T. Shibata, Effect of Crack Width and Bar Types on Corrosion

625    of  Steel  in  Concrete,  J.  Mater.  Civ.  Eng.  13.3  (2001)  194–201.  doi:10.1061/(ASCE)0899-

626    1561(2001)13:3(194).

627

# Appendix IV

**Description:** Conference paper published in Proceedings of the RILEM International Conference on Sustainable Materials, Systems and Structures 2019

**Title:** Influence of recycled fibre reinforcement on plastic shrinkage cracking of cement-based composites

# INFLUENCE OF RECYCLED FIBRE REINFORCEMENT ON PLASTIC SHRINKAGE CRACKING OF CEMENT-BASED COMPOSITES

**I. M. G. Bertelsen (1), L. M. Ottosen (1) and G. Fischer (1)**

(1) Department of Civil Engineering, Technical University of Denmark, Brovej 118, 2800 Kgs. Lyngby, Denmark

**Abstract**

Recycled polyethylene (R-PE) fibres from discarded waste fishing nets are used as fibre reinforcement in cement-based mortars for control of plastic shrinkage cracking. A thin, fresh mortar overlay is cast directly on top of a restraining concrete substrate and placed under controlled environmental conditions. Mortar overlays with the addition of R-PE fibres up to 2.0 vol% were tested and compared to mortar overlays with a 0.2 vol% addition of commercially available PP fibres. The cracking behaviour is monitored using a digital image correlation (DIC) technique allowing measurements of strain and displacement fields on the overlay surface. The R-PE fibres were successful in controlling the plastic shrinkage cracking of restrained mortar overlays for fibre fractions of 2.0 vol%.

**Keywords:** Plastic shrinkage, crack detection, plastic waste fibres, digital image correlation

## 1.    INTRODUCTION

The amount of marine plastic litter that have been entering the marine environment has accelerated in the last two decades of the 20th century [1]. Among these are lost or otherwise discarded fishing nets one of the most troublesome fractions due to their large volume and their ability to continue to "ghost fish" while floating around [2]. It is, therefore, important to create incentives for reusing these materials. In this study, we show how recycled polyethylene (R-PE) fibres processed by mechanical cutting of discarded fishing nets can be used for controlling plastic shrinkage cracking in cement-based materials. Plastic shrinkage is the volumetric contraction of cementitious materials and occurs within the first few hours after casting, thus it happens when the material is still in a plastic state [3]. Cracking induced by plastic shrinkage deformations may occur if the tensile stresses generated in the material exceed the strength of the fresh material. A laboratory-scale test method comprising of a fresh overlay cast on top of restraining concrete substrates has been used by [4,5] for evaluation of restrained plastic shrinkage cracking of cement-based materials. The addition of low-modulus synthetic fibres to cement-based materials susceptible to plastic shrinkage cracking is a well-known technique for controlling the formation of this type of surface cracking [4]. The fibres

have the ability to improve the strain capacity of the fresh material and to provide bridging forces across the cracks. Also, polymeric fibres from different types of waste fractions have shown positive results in controlling plastic shrinkage cracking [6–10]. The degree of surface cracking induced by plastic shrinkage is most frequently evaluated based on techniques such as manual microscopic measurements, which are commonly resulting in semi-quantitative measures of the degree of surface cracking; or image-based techniques such as digital image correlation (DIC) enabling more quantitative results [11,12]. In this study, a 2D-DIC technique has been used to analyse the degree of surface cracking of restrained mortar overlays and thereby to evaluate the influence of recycled and virgin fibres.

## 2. MATERIALS AND METHODS

The test method used for evaluation of restrained plastic shrinkage behaviour of cement-based mortar overlays using DIC was developed at the Technical University of Denmark as described in [13,14]. Each shrinkage test comprised of a concrete substrate and a fresh, thin mortar overlay with the addition of fibres.

### 2.1 Materials

Substrate bases measuring approximately 50 x 95 x 420 $mm^3$ as shown in Figure 1 were produced in accordance with UNI/EN 1339 [15] and the surface was prepared to a desired roughness using a needle hammer. The compressive strength of the substrate material was tested in accordance with UNI/EN 12390-3 [16] on cylinders and was found to 35.5 ± 6 MPa. At the time of testing, the substrate bases were wetted with tap water and placed inside moulds measuring 60 x 95 x 420 $mm^3$, whereupon a fresh mortar overlay with a thickness of 10 mm was poured on top of the substrate bases directly after mixing. The mixture proportions for the mortar overlay are given in Table 1. The test was carried out with three replicates of each specimen type. Two types of fibres were added to the fresh mortar overlay during the mixing process; 1) commercially available polypropylene (PP) fibres of the type Fiberflex with a diameter of 19.5 µm and a length of 12 mm; and 2) recycled polyethylene (R-PE) fibres obtained from discarded waste fishing nets with a length of 15 ± 9 mm and a diameter of 280 ± 30 µm. The geometrical variations were due to an "uncontrolled" mechanical cutting operation of the waste fishing nets. The recycled R-PE fibres were provided by a Danish recycling company, Plastix A/S that collects, sorts, washes and reprocesses waste fishing nets of difference material fractions. The fishing nets were collected from national and international harbours. The compressive strength and secant modulus of the material used for the mortar overlays was tested on cylinders measuring 60 x 120 mm (three replicates) with the two fibre types at different curing times in accordance with UNI/EN 12390-2 [16] and -13 [17].

Table 1: Mixture proportions for mortar overlay

|  | CEM I | Sand 0-4 mm | Water | Fibres ($V_f$) |
|---|---|---|---|---|
|  | $kg/m^3$ | $kg/m^3$ | $kg/m^3$ |  |
| Mortar overlay | 700 | 980-1032 | 350 | REF: 0%<br>PP: 0.2%<br>R-PE: 0.2-2.0% |

Figure 1: Geometry of substrate bases and mortar overlay; R-PE fibres; and PP fibres

## 2.2    Methods

The shrinkage test was carried out inside a climate-controlled chamber (Figure 2) and the specimens were monitored using DIC. The procedure for the shrinkage tests was as follows:

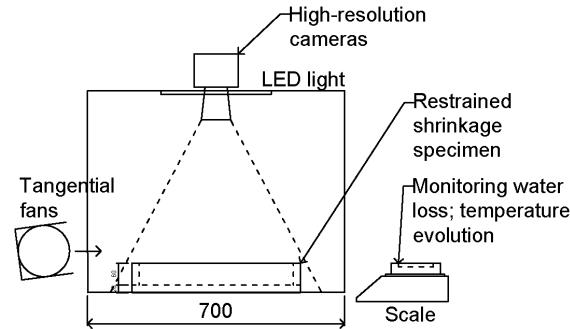| Time | Procedure |
|---|---|
| t = 0 min | Mixing procedure included first dry-mixing of cement and sand, whereupon water was gradually added under continuous mixing. If fibres were added, they were added to the wet mixture. "Time zero" (t = 0 h) was being defined as the time when water was added to the dry mixture. |
| t = 10-15 min | Casting and vibration of the fresh mortar overlay on top of substrate bases. |
| t = 20-45 min | Specimens were left at ambient temperatures of 20 ± 3 °C. |
| t = 45 min | Specimen surfaces were covered with a white layer of chalk-based spray paint and subsequently spray painted with black dots of chalk-based paint for the DIC analysis. The chalk-based paint type was more diffusion open than other paint types such as acrylic paint and was, therefore, not affecting the water evaporation rate [13]. |
| t = 55 min | Specimens were transferred to a climate-controlled chamber with a temperature of 32.0 ± 1.5 °C and a relative humidity of 33.5% ± 5%. Electrical fans were placed in front of the specimens to ensure a wind flow resulting in a maximum water evaporation rate of ~0.5 kg/m$^2$/h. A constant light source was ensured by LED panels and high-resolution optical cameras were fixed parallel to the specimen surfaces as shown in Figure 2. |
| t = 1 h | The DIC monitoring was initiated by capturing the first image of the specimen surface at t = 1 h, and subsequently every 15 min until t = 25 h. The technique enabled continuous monitoring of in-plane strain and displacement fields. |
| t = 25 h | Test finished and images imported to DIC software for processing. |

Figure 2: Plastic shrinkage test setup using DIC

After the test, the high-resolution images of the specimen surfaces were modified in ImageJ to improve the brightness and contrast and subsequently analysed using the DIC software, GOM Correlate Professional 2016. A region of interest (ROI) was defined for each specimen in the DIC software and was virtually meshed into a grid with overlapping subset elements. The subset elements were defined to have a size of 20 x 20 pixels and a point to point distance of 15 pixels with a pixel length corresponding to 0.080 mm/pixel. Finally, the DIC data was exported for further analysis and visualisation in Matlab, see also [13,14].

## 3.     RESULTS AND DISCUSSION

### 3.1     Study of surface cracking using DIC
The DIC software is capable of providing information about the in-plane surface displacement and strain in each subset element, thus the plastic shrinkage behaviour of restrained mortar overlays was evaluated based on this data. The specimens tested included mortar overlays with addition of PP fibres (0.2%), R-PE fibres (0.2-2.0%) or no fibres (REF, 0%). First, we observe one of the reference overlays, REF (A), because this mixture design was expected to be susceptible to plastic shrinkage cracking under the given environmental conditions. The principal strain data in the (x,y)-directions is good for a visual presentation of the surface cracking since peaks in strain (dark colours) represent the crack locations, see Figure 3(a), which illustrates the strain level at the end of the test (t = 25 h). From this figure, it is observed that the crack openings mainly appeared in the x-direction (x-direction defined as being parallel to the longer side of the specimens of 420 mm), which is considered due to the geometry of the specimen and the wind flow in the x-direction. Actual crack widths are calculated based on the displacement data [18], which is only given for the x-direction since the main cracks appeared in this direction, see Figure 3(b). Section A-A is going through the centreline of the specimen surface parallel to the x-direction and shows the surface displacement (dotted blue line) and principal strain (red line) along the section surface; see Figure 3(c). Sudden drops in surface displacement correspond well with the opening of an actual surface crack [18] (marked with red and blue circles). For the reference specimen, REF (A), the crack widths along the selected section A-A at t = 25 h are for example 102, 317, 327, 83, 189, 51, 72 and 31 $\mu$m, which corresponds well with microscopy measurements.
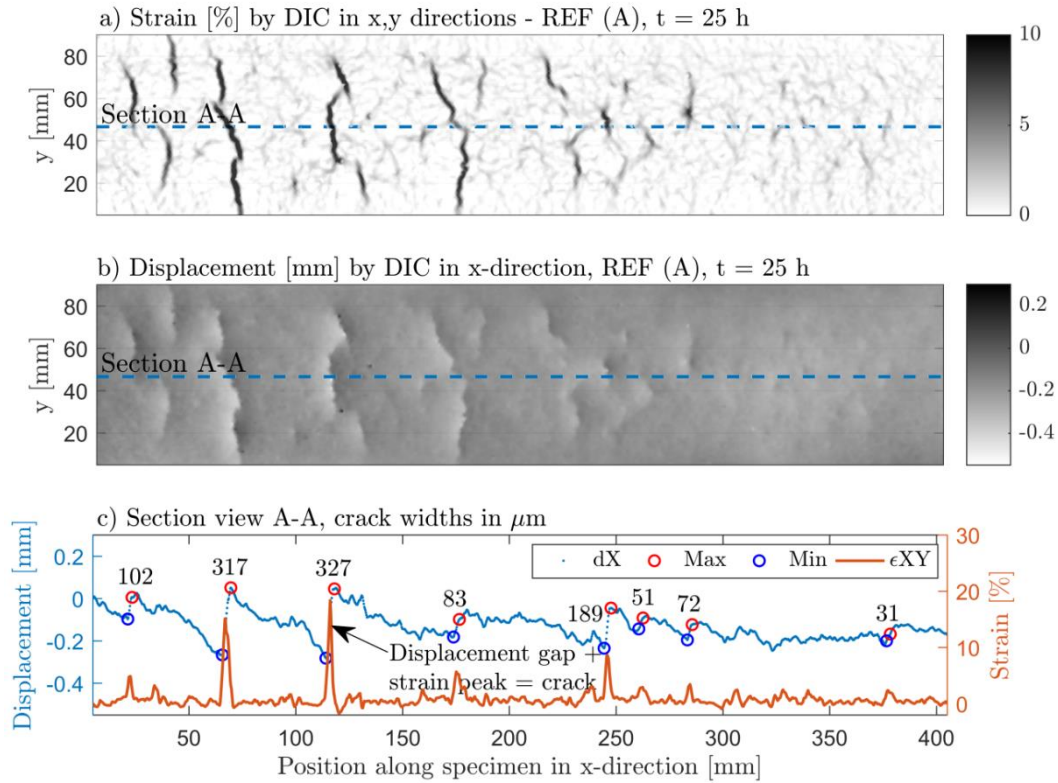
Figure 3: REF (A) specimen at t = 25 h. a) Principal surface strain in the (x,y)-direction by DIC; b) Surface displacement in the x-direction by DIC; c) Section A-A going through specimen showing surface displacement in x-direction and principal strain

## 3.2 Influence of fibres

The surface strains in (x,y)-direction are given for all tested specimens in Figure 4. By visual observations, it is obvious that the addition of fibres had a positive effect on the cracking behaviour of the restrained overlays. As expected, the commercially available PP fibres performed well in controlling the plastic shrinkage surface cracking when added in volume fractions as low as 0.2%. Only very few and fine cracks were visible on the specimen surface and the DIC also revealed areas with increased strain but yet not any visible cracks. Similar results with the use of PP fibres in similar fibre fractions added to restrained cementitious materials were obtained in other studies [4,5]. With respect to the R-PE fibres, which have a diameter that is approximately 15 times coarser than the PP fibres, the influence was not expected to be as good as for the PP fibres. No reduction in surface cracking was observed for the specimens added 0.2% R-PE fibres. For additions of larger fibre fractions such as 0.5% and 1.0% some improvements with respect to the amount and size of cracks were observed, and when 2.0% of R-PE fibres were added to the overlay, only very few visible surface cracks were observed. Despite the fact that 2.0% is a very high volume fraction to add to the material, it was seen that the fibres have a good effect in controlling the plastic shrinkage cracking of the restrained overlays. These results are also in agreement with other studies testing the influence of recycled fibres or fibres with similar coarse diameter, where volume fraction up to 1.5% have been studied [6–8,10,19]. For more elaborated results, please see [14].
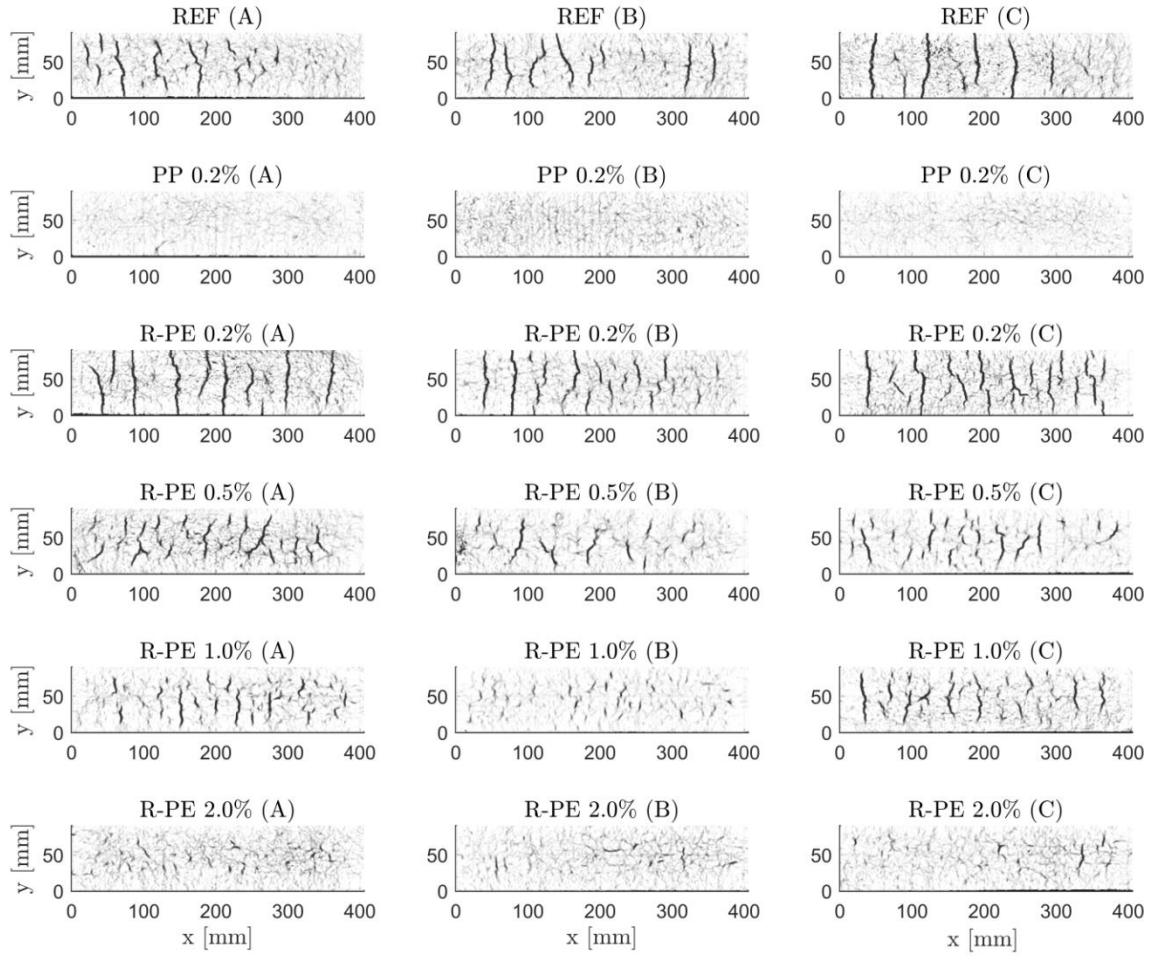
Figure 4: Principal strain for specimens at t = 25 h. White colour represents uncracked area with strain $\varepsilon_{x,y} = 0\%$; Black colour represents surface cracks with strain $\varepsilon_{x,y} = 5\%$.

## 3.3 Mechanical properties of mortar mixtures

As observed in Figure 4, the necessary addition of R-PE fibres for achieving a satisfactory reduction in surface cracking is 2.0% compared to only 0.2% for the commercially available PP fibres. The compressive strength and secant modulus were tested for three different mixture designs similar to the ones used for the fresh mortar overlays; A reference mortar (no fibres); 0.2% PP fibres; and 2.0% R-PE fibres, with the results being illustrated in Figure 5. The REF specimens achieved the highest compressive strength at all curing times, followed by the 0.2% PP specimen and finally by the 2.0% R-PE specimen. The development of compressive strength and secant modulus followed the same curve shape for all specimen types. The 28-days compressive strength was 52.5 MPa for the reference specimens, 49.0 MPa for the 0.2% PP specimens, and 47.1 MPa for the 2.0% R-PE specimens. These results show that the addition of 0.2% PP fibres decreased the compressive strength with 6%, while the much larger amount of 2.0% R-PE fibres decreased the 28-days compressive strength with 10%. Similar tendencies with respect to the influence of fibres were observed for the secant modulus.
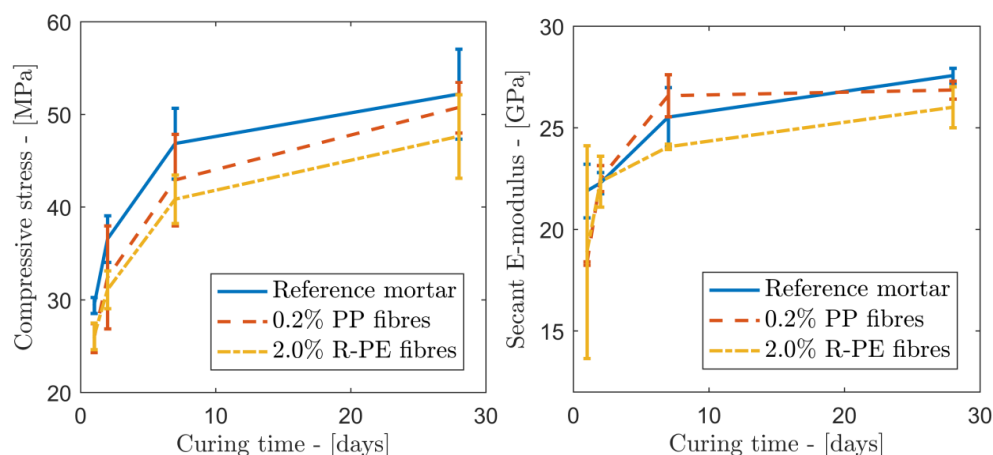
Figure 5: Compressive strength and secant modulus of mixtures used for the mortar overlay in the plastic shrinkage test. Age of wet-curing: 1 day, 2 days, 7 days and 28 days.

## 4.    CONCLUSION

The plastic shrinkage cracking of restrained mortar overlays cast on top of concrete substrates was studied with the aim of evaluating the influence of two fibre types; commercially available PP fibres and recycled polyethylene (R-PE) fibres obtained by mechanical cutting of waste fishing nets. The surface cracking was studied by using a DIC technique enabling the detection of surface strains and displacements. The results showed that the addition of 0.2% PP fibres was successful in controlling the plastic shrinkage surface cracking, while 2.0% of R-PE fibres were necessary to add to the overlay for achieving comparable results.

### REFERENCES

[1]    C.J. Moore, Synthetic polymers in the marine environment: A rapidly increasing, long-term threat, Environ. Res. 108 (2008) 131–139. doi:10.1016/j.envres.2008.07.025.

[2]    J. Brown, G. Macfadyen, Ghost fishing in European waters: Impacts and management responses, Mar. Policy. 31 (2007) 488–504. doi:10.1016/j.marpol.2006.10.007.

[3]    P.N. Balaguru, S.P. Shah, Fiber Reinforced Cement Composites, McGraw-Hill, 1992.

[4]    N. Banthia, R. Gupta, Influence of polypropylene fiber geometry on plastic shrinkage cracking in concrete, Cem. Concr. Res. 36.7 (2006) 1263–1267. doi:10.1016/j.cemconres.2006.01.010.

[5]    A.E. Naaman, T. Wongtanakitcharoen, G. Hauser, Influence of different fibers on plastic shrinkage cracking of concrete, ACI Mater. J. 102.1 (2005) 49–58.

[6]    N. Pešić, S. Živanović, R. Garcia, P. Papastergiou, Mechanical properties of concrete

reinforced with recycled HDPE plastic fibres, Constr. Build. Mater. 115 (2016) 362–370. doi:10.1016/j.conbuildmat.2016.04.050.

[7]   J.H.J. Kim, C.G. Park, S.W. Lee, S.W. Lee, J.P. Won, Effects of the geometry of recycled PET fiber reinforcement on shrinkage cracking of cement-based composites, Compos. Part B Eng. 39.3 (2008) 442–450. doi:10.1016/j.compositesb.2007.05.001.

[8]   R.P. Borg, O. Baldacchino, L. Ferrara, Early age performance and mechanical characteristics of recycled PET fibre reinforced concrete, Constr. Build. Mater. 108 (2016) 29–47. doi:10.1016/j.conbuildmat.2016.01.029.

[9]   M. Serdar, A. Baričević, M. Jelčić Rukavina, M. Pezer, D. Bjegović, N. Štirmer, Shrinkage Behaviour of Fibre Reinforced Concrete with Recycled Tyre Polymer Fibres, Int. J. Polym. Sci. 2015.3 (2015) 1–9. doi:10.1155/2015/145918.

[10]  B.S. Al-Tulaian, M.J. Al-Shannag, A.R. Al-Hozaimy, Recycled plastic waste fibers for reinforcing Portland cement mortar, Constr. Build. Mater. 127 (2016) 102–110. doi:10.1016/j.conbuildmat.2016.09.131.

[11]  S. Ghourchian, M. Wyrzykowski, L. Baquerizo, P. Lura, Susceptibility of Portland cement and blended cement concretes to plastic shrinkage cracking, Cem. Concr. Compos. 85 (2018) 44–55. doi:10.1016/j.cemconcomp.2017.10.002.

[12]  P. Zhao, A.M. Zsaki, M.R. Nokken, Using digital image correlation to evaluate plastic shrinkage cracking in cement-based materials, Constr. Build. Mater. 182 (2018) 108–117. doi:10.1016/j.conbuildmat.2018.05.239.

[13]  I.M.G. Bertelsen, C. Kragh, G. Cardinaud, L.M. Ottosen, G. Fischer, Quantification of plastic shrinkage cracking in mortars using digital image correlation, Submitt. 2018.04.28. (n.d.).

[14]  I.M.G. Bertelsen, L.M. Ottosen, G. Fischer, Quantitative analysis of the influence of synthetic fibres on plastic shrinkage cracking using digital image correlation, Constr. Build. Mater. 199 (2019) 124–137. doi:10.1001/archinte.168.13.1371.

[15]  UNI/EN-1339, Concrete paving flags - Requirements and test methods, (2003).

[16]  UNI/EN-12390-3, Testing hardened concrete – Part 3 : Compressive strength of test specimens, (2012).

[17]  UNI/EN-12390-13, Testing hardened concrete – Part 13: Determination of secant modulus of elasticity in compression, (2013).

[18]  T. Mauroux, F. Benboudjema, P. Turcry, A. Aït-Mokhtar, O. Deves, Study of cracking due to drying in coating mortars by digital image correlation, Cem. Concr. Res. 42.7 (2012) 1014–1023. doi:10.1016/j.cemconres.2012.04.002.

[19]  H. Najm, P. Balaguru, Effect of large-diameter polymeric fibers on shrinkage cracking of cement composites, ACI Mater. J. 99.4 (2002) 345–351.

# Appendix V

**Description:** Submitted

**Title:** Recycling of waste polyethylene fishing nets as fibre reinforcement in gypsum-based composites

1 # Recycling of waste polyethylene fishing nets as fibre reinforcement in gypsum-based composites

2 I. M. G. Bertelsen[a*], L. M. Ottosen[a]

3 [a] Department of civil engineering, Technical University of Denmark, Brovej 118, 2800 Kgs. Lyngby, Denmark

4 * Corresponding author. E-mail: imgber@byg.dtu.dk

5

6 **Abstract**

7 It is important to encounter ways for recycling waste fishing gear to prevent them ending up as marine litter. The aim of

8 this study is to investigate the potential of using recycled polyethylene (R-PE) fibres from waste fishing nets as fibre

9 reinforcement in gypsum-based composites. The PE nets were cut up and washed to create monofilament R-PE fibres and

10 the fibre characterization included tensile tests, geometry, morphology and leaching of anions ($Cl^-$, $NO_3^-$, $SO_4^{2-}$).

11 As the mechanical properties of the fibres were found to be in the same range as the virgin fibres used in gypsum-based

12 composites today, such were cast with the R-PE fibres in fibre fractions varying between 0.25 – 2.00 wt%. Mechanical

13 properties such as compressive strength, flexural strength, post-crack strength, and fibre efficiency factors for fibre-

14 reinforced gypsum-based specimens were determined by laboratory-scale testing. The addition of R-PE fibre resulted in

15 a small reduction in compressive strength and first-crack strength of the gypsum-based composite, but to the positive side,

16 there was a significant increase in post-crack performance. These gypsum-based composites with addition of R-PE fibres

17 have the potential to be used as non-structural elements such as gypsum boards where increased post-crack performance

18 and ductility is required.

19

20 **Graphical abstract**



21 Waste fishing nets | Recycled PE fibres | Fibres in gypsum

22

23 **Keywords:**

24 Gypsum-based composites; Fibres; Waste fishing nets; Plastic recycling; Mechanical properties

**1 Introduction**

Plastic waste is a major concern for the vulnerable marine environment and especially lost or otherwise discarded fishing nets are likely to be the greatest threat to wildlife, since they can lead to entanglements and can cause severe damage to fish, sea birds and marine mammals [1,2]. Approximately 8 million tonnes of plastic enter the ocean each year [3] and of that fishing nets are an important fraction because of their shape and physical size. Historically, fishing gear was made of natural materials such as hemp, cotton, sisal that would decompose relatively quickly and was, as a result, less detrimental to the marine wildlife if lost into the sea [4,5]. However, nowadays nets are typically made of synthetic polymeric fibres of polyethylene (PE), polypropylene (PP), polyester (PES) or polyamide/nylon (PA), which are all non-biodegradable [5]. Furthermore, waste fishing nets are often difficult to dispose of, costly to transport, and take up a lot of space in landfill sites. As a consequence of outdoor- and UV-exposure together with continuous load impacts, the properties of the fishing nets can be impaired during use and can vary significantly [6].

Building materials with gypsum as binder have long been widely used in the construction industry, mostly for plaster elements such as plasterboards and for protective/decorative coating and finishing of walls and ceilings [7,8]. Gypsum-based materials are generally associated with a brittle behaviour when exposed to tension [9], and despite that the material is mainly used for non-structural elements, an adequate mechanical performance is still important. Adding fibre reinforcement to the gypsum matrix is a well-known technique for increasing the post-crack performance and toughness of the composite [9,10]. Fibres of materials with various mechanical and physical properties have been used as reinforcement for gypsum-based composites, including glass [11,12], polymers such as polyamide (PA), polypropylene (PP) and polyvinyl alcohol (PVA) [13–16], and different types of natural fibres [10,17–19]. The incorporation of waste materials as fibre reinforcement is gaining increased attention in the construction industry because it makes it possible to reduce raw materials for the production of virgin fibres. The incorporation of waste materials in both gypsum-based materials [13,20–25] and cement-based materials [26–29] has been studied with the aim of revealing new ways of producing more eco-friendly materials. These recent studies have shown that several types of plastic waste materials can be profitably employed to create low-cost reinforcement techniques of structural and non-structural building materials. It has also previously been demonstrated that fibres from waste fishing nets perform well in cement-based materials [30,31] and other types of composites [32,33]. Spadea et al. [30] found that recycled nylon fibres obtained from waste fishing nets added in fractions of up to 1.5 wt% significantly improved the flexural strength, post-crack performance and toughness of mortar specimens, and that longer fibres resulted in superior performance. Similar tendencies were found by Orasutthikul et al. [31] who also studied recycled nylon fibres from waste fishing nets of different shape (straight fibres

54    or fibres with knots) and fibre length. However, when fibres were added in too large fractions, the effect of the fibres was

55    decreasing, mainly due to balling of the fibres and an uneven fibre distribution. The performance of R-PE fibres similar

56    to the ones used in the present study was tested in restrained cement-based mortar overlays for controlling the formation

57    of plastic shrinkage cracking [34]. Based on the results and a comparison with commercially available PP fibres, it was

58    found that the addition of 2.0vol% of R-PE was successful in reducing plastic shrinkage cracking.

59    Fibres made of recycled plastics can be prepared by either mechanical recycling such as cutting operations, or by thermal

60    reprocessing where the material is heated so that new products can be processed [26]. Although some recycled fibres used

61    as fibre reinforcing materials have been produced by thermal reprocessing [35,36], it is more energy-efficient to produce

62    recycled fibres by mechanical cutting [30,31,37–40]. Fishing lines consist of either twisted or braided fibres, which are

63    easy to separate and cut into smaller fibres applicable as fibre reinforcement in cement-based materials [5,30,31]. Based

64    on the R-PE fibre characteristics, the potential of using these fibres from waste fishing nets as fibre reinforcement in

65    gypsum-based composites was investigated in this study.

66

67    **2 Materials and methods**

68    **2.1 Fibre characterization**

69    The monofilament R-PE fibres obtained from waste fishing nets that in this study were used as fibre reinforcement in

70    gypsum-based specimens were provided by a Danish recycling company Plastix A/S. The recycling company is collecting

71    waste fishing nets and reprocessing them into new plastic pellets. Fishing nets of PE materials comprise an especially

72    large fraction of the waste fishing nets. Prior to the reprocessing, the fishing nets are separated into different polymer

73    material fractions, whereupon they are pre-washed and mechanically cut into short fibres, after which they are melted and

74    reprocessed into new plastic pellets. The R-PE fibres used directly as fibre reinforcement in gypsum-based specimens in

75    the present study were those obtained by the purely mechanical cutting operation.

76    The R-PE fibre samples provided by Plastix A/S contained a small amount of impurities such as sand, salts and residues

77    from the fishing operation. To analyse the influence of an additional cleaning process, the uncleaned fibres were first dry-

78    sieved through a 0.25 mm sieve and subsequently washed in tap water to remove impurities. These were then labelled as

79    "cleaned" R-PE fibres, while the fibres that received no additional cleaning, were labelled "uncleaned" R-PE fibres. Fig.

80    1 shows samples of a) cleaned R-PE fibres, b) uncleaned R-PE fibres and c) the impurities that were dry-sieved from the

81    uncleaned fibre samples. Almost no difference between the cleaned and uncleaned R-PE fibres were observed by a visual

82    examination, but the presence of the impurities on the uncleaned fibres were apparent when touching the fibres. The fibre

83 morphology was evaluated on the basis of Scanning Electron Microscope (SEM) analysis and the geometry (length and

84 diameter) were measured on 500 randomly chosen fibres from the cleaned fibre samples.



| a) | b) | c) |
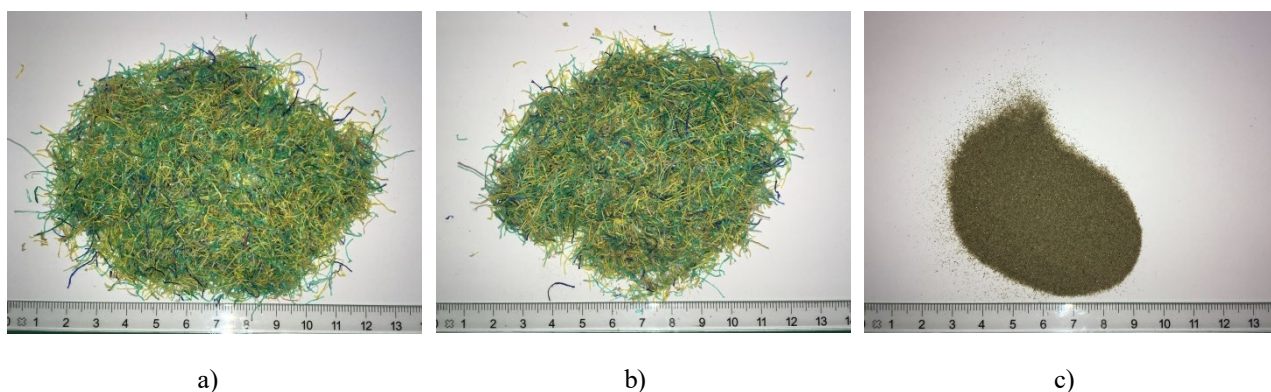
85 *Fig. 1. 20 g of monofilament R-PE fibres after mechanical cutting and the concomitant impurities; a) Cleaned fibres; b) Uncleaned*

86 *fibres; c) Impurities separated from the uncleaned fibres by dry-sieving*

87

88 *2.1.1 Impurities in the uncleaned fibre samples*

89 The uncleaned fibres contained a small amount of dirt from fishing operations. These impurities were separated from the

90 uncleaned fibres by dry-sieving through a 0.25 mm sieve. They were then analysed to determine whether it was necessary

91 to clean the fibres prior to them being mixed into the gypsum-based materials, because some salts, for instance, is known

92 to accelerate the hardening of gypsum-based materials [7]. The characterization of the impurities included Scanning

93 Electron Microscope (SEM) analysis, thermogravimetric analysis (TGA), differential scanning calorimetry (DSC), and

94 X-ray diffraction (XRD). DSC and TGA were carried out on a Netzsch STA 449 Jupiter with a heating rate of 10 °C/min

95 from 25–800 °C.

96

97 *2.1.2 Leaching of fibres and impurities*

98 To simulate the leaching of contaminants from the R-PE fibres (uncleaned, cleaned) and the impurities separated from

99 the uncleaned fibre samples by dry-sieving, a leaching test was conducted. Prior to the leaching test, the material was

100 dried at 50 °C for 24 h. The test was performed following the prescriptions in EN 12457-2 (2002) and included 50 g of

101 material (fibres or impurities) immersed in 500 mL of $CO_2$-saturated water, which was placed into an agitation apparatus

102 for 24 h. The liquid was filtered and the concentrations of anions ($Cl^-$, $NO_3^-$, $SO_4^{2-}$) were measured by ion chromatography

103 (IC).

104

105 *2.1.3 Mechanical properties of fibres*

The R-PE fibres received from Plastix A/S originated from different sources of PE fishing net, so the mechanical properties were expected to vary to some extent. The length of the R-PE fibres received from Plastix A/S were not long enough for performing tensile tests, so to get an indication of the variations in the mechanical properties of the R-PE fibres, fibres extracted from selected PE fishing nets were tested with respect to tensile strength and stiffness. Moreover, to get an indication of the level of deterioration and how impaired the R-PE fibres were with respect to the mechanical properties, fibres from both new and recycled fishing nets of equivalent types were tested, see Fig. 2. Three types of fishing net that are commonly used in Denmark were selected: "Braided Polyethylene" (BP), "Euroline" (EU), and "Euroline Premium" (EP), all from Euronete. These three net types are all made from PE of different mechanical properties (stiffness and tensile strength), with "Braided Polyethylene" being the net with the lowest tensile strength and "Euroline Premium" the net with the highest tensile strength according to data sheets. Thus, these three net types were expected to represent the range of fibres present in the samples. The waste nets were collected at dumpsites or received from Plastix A/S and the new nets were provided by Vonín, Strandbynet A/S. For each type of waste net, the visually most damaged and deteriorated net was chosen to represent the most conservative values for the respective fibre type. Single fibres were extracted from these fishing net lines by loosening the knots and gently separating the single fibres from each other. By testing the tensile strength of these fibres from new and waste nets, knowledge about the built in variations of fibre properties in the industrially produced R-PE fibre samples was gained.



Fig. 2. *Waste and new PE fishing nets from Euronete, used for characterisation of mechanical properties. "Braided Polyethylene" (BP), "Euroline" (EU), and "Euroline Premium" (EP).*

The tensile strength and tensile modulus were tested in accordance with ASTM C1557-14 (2014) on fibres with gauge lengths of 20, 25, and 30 mm. Each fibre was anchored on thick paper with WEICON PP-PE 2-component glue. Tensile load was applied in a displacement controlled Instron 6022 instrument with a constant displacement rate of 20 mm/min to obtain a failure within 30 s. Only failures on the free length of the fibre were counted as successful. Eight tests were

130     carried out for each fibre type and gauge length. To determine the tensile modulus, $E$, the elongation over the force, $\Delta L/F$,

131     was plotted against the initial length over the cross-section area, $l_0/A$. The test setup is shown in Fig. 3.
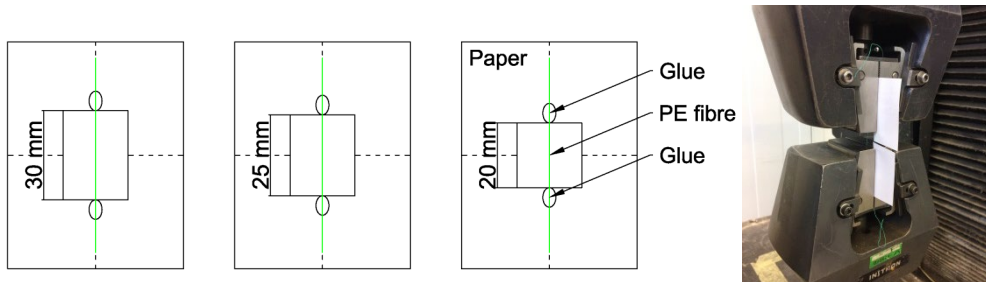


132

133     *Fig. 3. Test setup for tensile testing of monofilament fibres with gauge lengths of 20-30 mm*

134

135     **2.2 Characterization of gypsum-based composites**

136     Gypsum-based composites with various contents of R-PE were cast to study the performance when exposed to

137     compressive and flexural stresses. The matrix material used was a hemihydrate natural gypsum of the type "Miller

138     Modelgips" supplied by C. Flauenskjold. The mineralogical composition was characterised by XRD analysis. The matrix

139     mixture consisted of the following mix design: $700 \pm 1$ g of tap water, $1600 \pm 2$ g of hemihydrate gypsum and a fibre

140     content varying from 0.25 wt% to 2.0 wt% (% by weight with respect to the binder). The addition of 2.0 wt% of fibres

141     was observed to be the maximum fibre content that could successfully be mixed into the gypsum material with the given

142     mixture design and process. Batches reinforced with both cleaned and uncleaned R-PE fibres were prepared.

143     The dry mixture was primarily homogenized to ensure random fibre dispersion. Then the mixture was hydrated by adding

144     all the water under mechanical mixing in a Hobart mixing machine at low speed (corresponding to 140 rotations / min)

145     for 15 s. Two types of specimens were prepared; prismatic specimens measuring 40 x 40 x 160 mm$^3$, and cylinders

146     measuring 60 mm x 120 mm, which were cast in steel/PVC moulds and vibrated on a vibration table at 60 Hz to ensure

147     the complete filling of the moulds and the removal of air bubbles. The moulds were covered with a metal plate on top to

148     prevent non-uniform expansion of the specimen. The specimens were carried out in sets of three replicates with one set

149     unreinforced control batch and sixteen fibre-reinforced batches with different percentages of cleaned or uncleaned R-PE

150     fibres. Finally, the specimens were demoulded after 24 hours and dry-cured for 48 hours at a temperature of $21 \pm 3$ °C

151     until testing.

152

153     **2.3 Mechanical testing of gypsum-based specimens**

Three-point flexural bending tests were carried out on the prismatic specimens in accordance with UNI/EN 196-1 (2005). The tests were performed in an Instron 6022 hydraulic testing machine with a displacement controlled load applied at a rate of 1 mm/min. Fig. 4 shows an example of a working curve for the three-point bending tests. The Young's modulus, E, of the uncracked material was calculated as the slope of the working curve in the linear part from $0.4 \cdot f_{cr}$ until $0.9\, f_{cr}$ is reached (the red dotted line in the stress-strain curve).
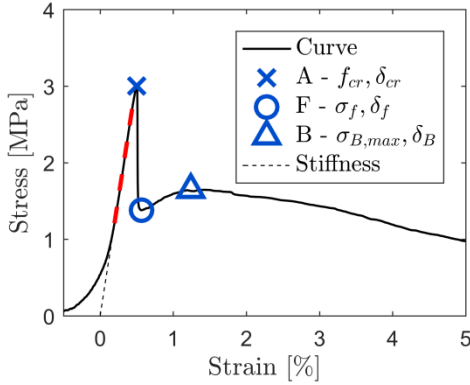


*Fig. 4. Typical stress-strain curve for fibre-reinforced composites (three-point bending test).*

While the unreinforced gypsum-based specimens experience a brittle failure, the fibre-reinforced specimens continue to perform after the $f_{cr}$ is reached, displaying the ability to absorb energy when continuing the deflection [19]. The reinforcing effect of the fibres is achieved by their bridging force across the cracks that lead to a more ductile failure. The performance of the R-PE fibres as reinforcing material in gypsum-based composites was evaluated based on the maximum post-crack strength ($\sigma_{B,\max}$), and a fibre efficiency factor (FEF) calculated as the ratio of the stress where the fibres start working ($\sigma_f$) to the material's flexural strength ($f_{cr}$) [24,41]:

$$\text{FEF} = \frac{\sigma_f}{f_{cr}}$$

After the three-point bending tests, the fracture surfaces of the prisms were analysed using Scanning Electron Microscopy (SEM). The uniaxial compressive strength of cylinders with varying content of cleaned R-PE fibres was determined in accordance with UNI/EN 12390-3 (2012) in a TONI Industries compression machine with a load rate of 0.5 kN/s.

**3  Results**

**3.1 Fibres**

*3.1.1 Physical and morphological characterization of R-PE fibres*

The R-PE fibre samples from Plastix A/S were investigated with respect to the geometry, morphology and leaching behaviour. The length and diameter of the cleaned fibre samples were measured to a mean length of 15 ± 9 mm (varying between 1-65 mm with very few fibres longer than 30 mm), see Fig. 5, and a diameter of 280 ± 30 μm. These large variations in length are due to the industrial mechanical cutting operation, which could potentially be improved to produce fibres with more homogeneous lengths. During the washing process of the uncleaned fibre samples to produce the cleaned fibre samples, it was observed that a few of the shortest fibres (length of 1-2 mm) were washed out with the impurities. Although the R-PE fibres originated from different PE fishing nets, there were only small variations in diameter in the fibre sample.
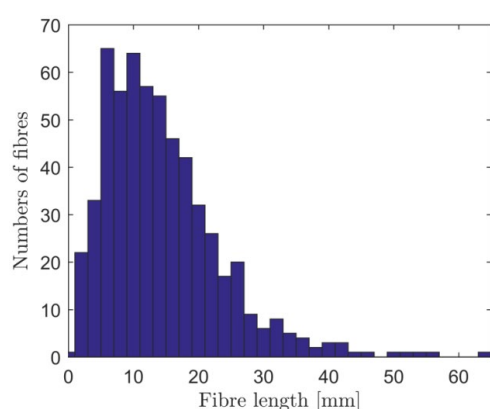


*Fig. 5. Fibre length distribution for cleaned R-PE fibre sample*

Fig. 6a-c shows SEM images of three selected cleaned R-PE fibres. It was observed that there was a difference in degree of surface deterioration of the R-PE fibres, which was to be expected due to factors such as different lifetimes, load history, abrasion with seabed, and exposure to UV-light [6]. All fibres had an approximate circular cross section and a straight shape. The mechanical cutting process may also have damaged the fibres. However, most fibres investigated in SEM appeared with a smooth surface as the one showed in Fig. 6a.



a)          b)          c)
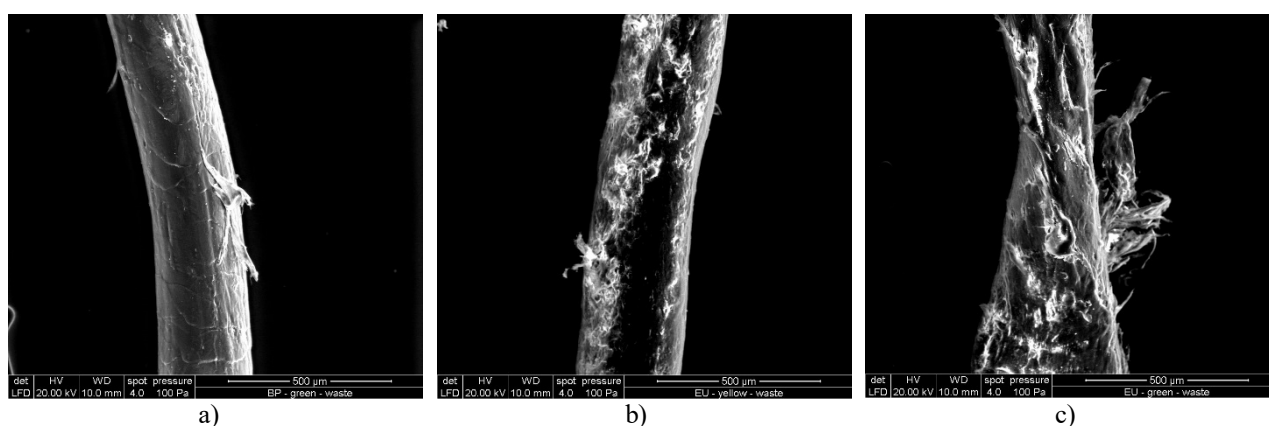
192     *Fig. 6. SEM analysis of three cleaned R-PE fibres with different levels of deterioration. Field of view = 1.27 mm*

193

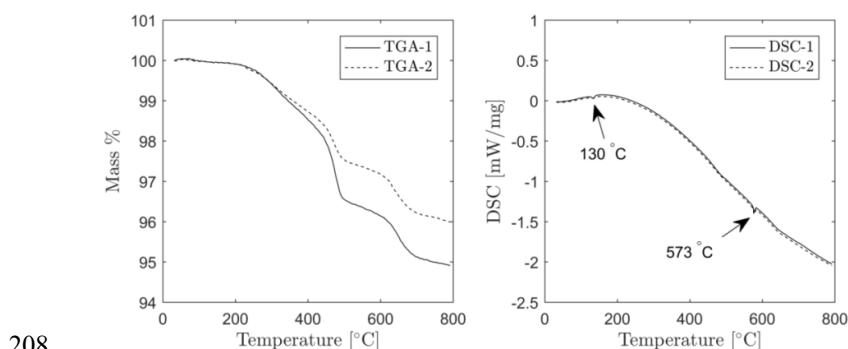194     *3.1.2 Impurities in uncleaned R-PE fibres*

195     The uncleaned R-PE fibres contained a small amount of impurities, which by a visual inspection comprised sand, small

196     particles of plastic and other unidentified types of dirt. These impurities were separated from the uncleaned fibre samples

197     by dry-sieving and are shown in SEM images in Fig. 7. The SEM analysis revealed a mix of sand/silt grains, thin fibres,

198     and small particles of plastic. The XRD results showed a content of quartz ($SiO_2$) together with a small amount of

199     amorphous material, which included small particles of plastic.
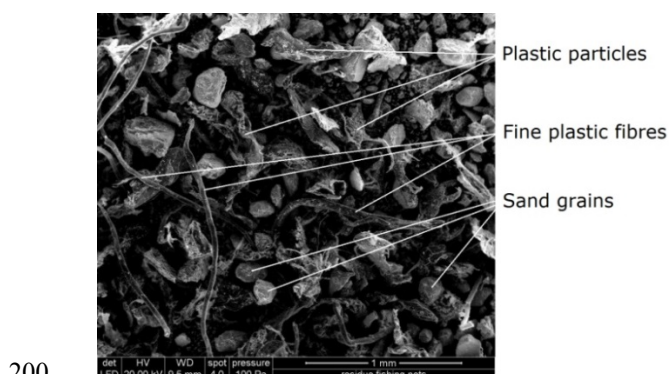


201     *Fig. 7. SEM analysis of impurities separated from the uncleaned R-PE fibres by dry-sieving. Field of view = 2.55 mm*

202

203     The thermal properties of the impurities were determined on two replicates and Fig. 8 shows the TGA and DSC curves.

204     The wt% of the original mass of the material as a function of temperature is shown on the TGA curves and measured to

205     95-96 wt%. The DSC curve shows a small peak at 130 °C, which is the melting point for PE. Another peak can be seen

206     at a temperature of 573 °C, which is the temperature at which quartz undergoes a reversible change in crystal structure

207     from α-quartz to β-quartz.



209     *Fig. 8. TGA and DSC graphs for the impurities in the uncleaned PE fibre samples (DF)*

210

*3.1.3 Leaching*

The leaching of anions (Cl$^-$, NO$_3^-$, SO$_4^{2-}$) from the R-PE fibres (uncleaned, cleaned) and the impurities separated from the uncleaned fibres are shown in Table 1. The concentration of leached anions is highest for the impurities; especially chlorides due to the use of the fishing nets in sea water. It is also observed that a high concentration of anions were leached from the uncleaned R-PE fibres, and that, by simply cleaning the fibres in tap water, it was possible to decrease the content of leachable anions significantly. We compared the concentrations to the values found by Spadea et al. [30] who also studied the leaching behaviour of recycled nylon fibres from waste fishing nets by following the same procedure as in the present study, see Table 1. The fibres studied by [30] were concluded to be safe to use as reinforcing material for cementitious materials. Thus, since the leaching values for the cleaned R-PE fibres are in the same range as the R-nylon fibres found by [30] it was considered necessary to wash the fibres prior to using them as fibre reinforcement in building materials such as gypsum composites. Furthermore, the addition of chlorides to gypsum is known to accelerate the hydration of the matrix [7,42], which is another reason for cleaning the R-PE fibres prior to using them as reinforcing material for gypsum composites.

*Table 1. Leaching of anions from impurities and R-PE fibres (uncleaned, cleaned)*

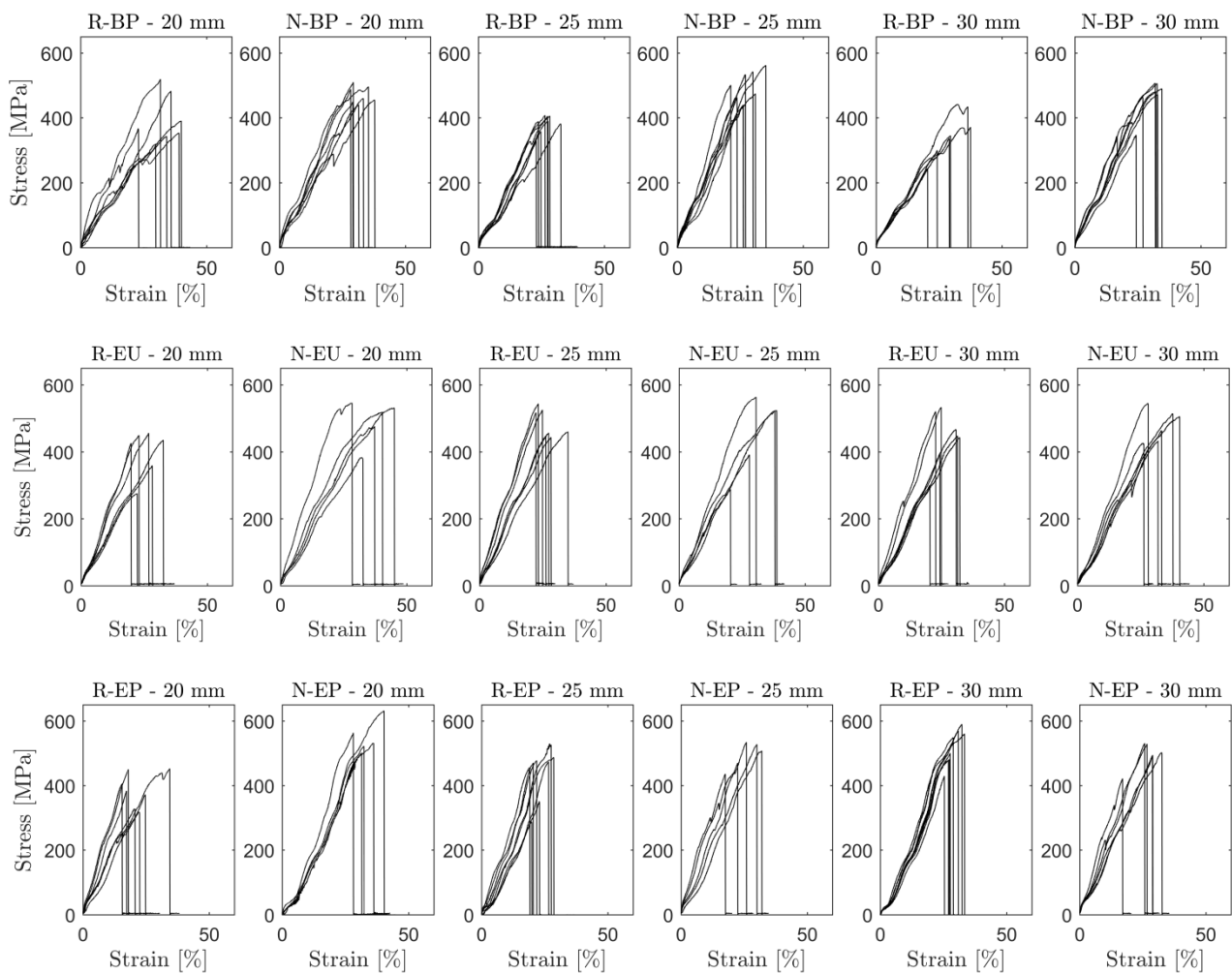| Sample | pH | Cl$^-$ | NO$_3^-$ | SO$_4^{2-}$ |
|---|---|---|---|---|
| | [-] | [mg/L] | [mg/L] | [mg/L] |
| Impurities in uncleaned R-PE fibres | 6.4 | 100.4 | 29.3 | 30.2 |
| Uncleaned R-PE fibres | 6.3 | 61.2 | 20.5 | 22.2 |
| Cleaned R-PE fibres | 5.9 | 3.7 | 1.2 | 3.9 |
| Values found by [30] for R-fibres | 8.2 | 2.2 | 5.9 | 3.6 |

*3.1.4 Characterization of tensile properties of fibres*

The tensile properties were tested on fibres from both recycled and new fishing nets of the types "Braided Polyethylene" (BP), "Euroline" (EU), and "Euroline Premium" (EP). These three selected net types were expected to cover the range of mechanical properties present in the fibre samples from Plastix A/S. Both new (N) and waste/recycled (R) fibres of the three types were tested to get an indication of how impaired the selected R-PE fibres were compared to equivalent new ones. Fig. 9 illustrates the stress-strain behaviour of the fibres exposed to uniaxial tension and Table 2 gives an overview

of their mechanical properties. Roughly, a linear stress-strain behaviour of the fibres was observed until failure. The mean tensile strength for fibres of the type "Braided Polyethylene", R-BP and N-BP, was 376 ± 60 MPa and 480 ± 44 MPa, respectively, for fibres of the type "Euroline", R-EU and N-EU, 445 ± 69 MPa and 477 ± 73 MPa, respectively, and finally, fibres of the type "Euroline Premium", R-EP and N-EP, had a mean tensile strength of 452 ± 81 MPa and 512 ± 47 MPa, respectively. For the BP fibres there was a significant difference in tensile strength between the new and the recycled fibres, whereas it was less noticeable for the two other fibre types. However, the tensile strength was lowest for the recycled fibres in every case. The elongation strain at failure ranged between 22-33 %.



Fig. 9 Tensile stress-strain behaviour of waste/recycled (R) and new (N) fibres from the net types "Braided Polyethylene" (BP), Euroline (EU), and Euroline Premium (EP) with gauge lengths of 20, 25 and 30 mm.

The elastic modulus was derived by using linear regression for the elongation over the force, $\Delta L/F$, between 20% and 50% of the failure load, against the initial length over the cross-section area, $l_0/A$. The results are given in Table 2. Due

248    to a large standard deviation in the fibre strength-strain relationship and thereby a low regression of 0.61-0.87, the results

249    shall be considered as indications of the fibre stiffness.

250

251    *Table 2. Properties of fibres from waste/recycled (R) and new (N) PE fishing nets. Mean values of three gauge lengths (20-30 mm) are*

252    *given for the three types of tested fishing net fibres (BP = Braided polyethylene, EU = Euroline, and EP = Euroline Premium)*

| Net type | Type | Tensile strength $\sigma_t$ [MPa] | Peak strain $\varepsilon_t$ [%] | E-modulus E [GPa] | Regression [-] |
|---|---|---|---|---|---|
| Braided Polyethylene | R-BP | 376 ± 60 | 30 ± 5.5 | 1.03 | 0.65 |
| | N-BP | 480 ± 44 | 30 ± 4.1 | 1.53 | 0.70 |
| Euroline | R-EU | 445 ± 69 | 26 ± 4.2 | 1.96 | 0.63 |
| | N-EU | 477 ± 73 | 33 ± 6.3 | 2.31 | 0.68 |
| Euroline Premium | R-EP | 452 ± 81 | 25 ± 5.2 | 1.41 | 0.87 |
| | N-EP | 512 ± 47 | 28 ± 5.9 | 3.05 | 0.61 |

253

## 3.3 Properties of gypsum-based composites

254

255    The mineralogical composition was revealed by the XRD analysis. The pattern reported in Fig. 10 showed peaks

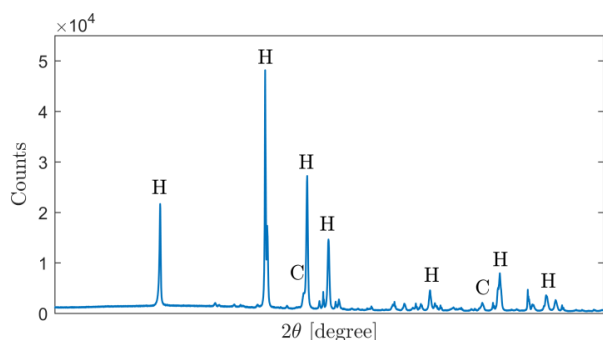256    corresponding to mainly hemihydrate (H) but also calcite (C).



257

258    *Fig. 10. XRD pattern for hemihydrate gypsum (H = CaSO$_4$ 0.5H$_2$O; C = CaCO$_3$).*

259

260    The mechanical properties such as the compressive strength, flexural strength and for fibre reinforced materials also the

261    post-crack performance are important indicators of how well a building material perform, regardless that the composites

262    mainly are intended for non-structural elements. The flexural behaviour of specimens included unreinforced reference

263    specimens and fibre-reinforced specimens with fibre content from 0.25 wt% to 2.0 wt% of cleaned (CF) or uncleaned

264    (UF) R-PE fibres and is illustrated in the stress-strain plots in Fig. 11. As expected, the reference specimen experienced

265    the typical catastrophic failure of a brittle unreinforced gypsum-based material, whereas the presence of fibres affected

266    the post-crack performance of the composite. When the maximum load was reached for the fibre reinforced specimens,

267 the specimens still remained a whole with one crack appearing in the centre of the specimen where the load was applied.

268 The addition of only 0.25 wt% of R-PE fibres resulted in a ductile failure with fibres bridging the crack, although the

269 post-crack performance was very limited. The flexural strength, $f_{cr}$, at which the first crack occurred, decreased with

270 increasing fibre content. The control specimen cracked at a stress of 3.7 MPa, whereas the specimens with 2.0 wt% of

271 cleaned R-PE fibres cracked at 3.2 MPa. The specimens reinforced with cleaned fibres generally experienced a larger

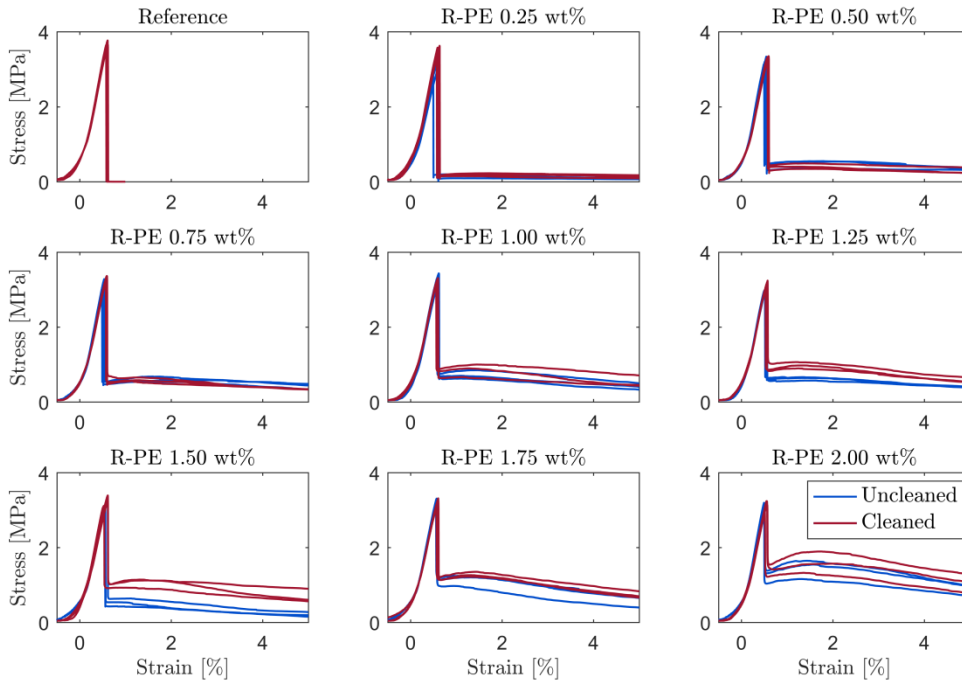272 post-crack performance than those reinforced with uncleaned fibres.



273

*Fig. 11. Stress-strain curves from the three-point bending tests. Fibre contents from 0-2.0 wt%. Results shown for uncleaned and cleaned R-PE fibres*

276

277 Fig. 12 shows the flexural strength, the maximum post-crack strength, the fibre efficiency factor (FEF), the stiffness of

278 the uncracked composite and the compressive strength of specimens with various levels of R-PE fibres. As expected, the

279 graph clearly shows that the addition of fibres significantly increased the post-crack strength, but also reduced the flexural

280 strength. After the first crack appears at point A, $f_{cr}$, (see Fig. 4), the brittle gypsum-based material matrix loses its tensile

281 strength and the curve drops noticeably until the fibres take effect. The sudden drop in stress gives an indication of the

282 fibre-to-matrix bonding. The maximum post-crack strength, $\sigma_{B,\max}$ for cleaned and uncleaned R-PE fibres, respectively,

283 increases from 0.18 MPa/0.15 MPa for a fibre content of 0.25 wt% up to 1.60 MPa/1.45 MPa for a fibre content of 2.00

284 wt%. The fibre efficiency factor (FEF) also increases, which is related to the fibre-to-matrix bonding and shows when the

fibres take effect. The stiffness of the uncracked composite is calculated as the linear part of the curve (illustrated as the red dotted line in Fig. 4) before the first crack appears. There is no clear indication as to whether the addition of fibres reduces the stiffness or not. The cleaned fibres performed slightly superior to the uncleaned fibres in most cases.
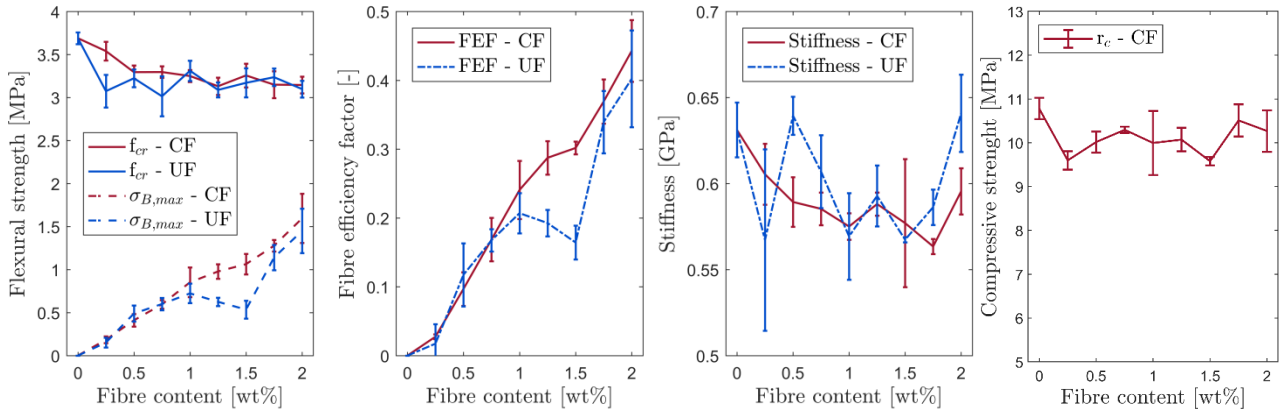


*Fig. 12. Flexural strength, maximum post-crack strength, fibre efficiency factor (FEF); stiffness; and compressive strength of the composites as a function of fibre content (wt%). CF = cleaned fibres; UF = Uncleaned fibres*

Fig. 12 also shows the compressive strength, $r_c$, of cylinders reinforced with cleaned R-PE fibre fractions and Fig. 13 shows four selected specimens reinforced with fractions of 0, 0.25, 1.75 and 2.0 wt% after the compression test. While the unreinforced specimen had a fragile failure, the failure in the fibre-reinforced specimens was ductile even for specimens with the lowest fibre content of 0.25 wt%. The unreinforced control cylinders achieved the highest compressive strength, but there is no clear correlation between the compressive strength and the fibre content for specimens reinforced with R-PE fibres.



*Fig. 13. Compressive failure of selected cylinders with addition of 0 wt% (control), 0.25 wt%, 1.75 wt% and 2.0 wt% of cleaned R-PE fibres*

302 *3.3.1 Fracture surface analysis and microstructure*

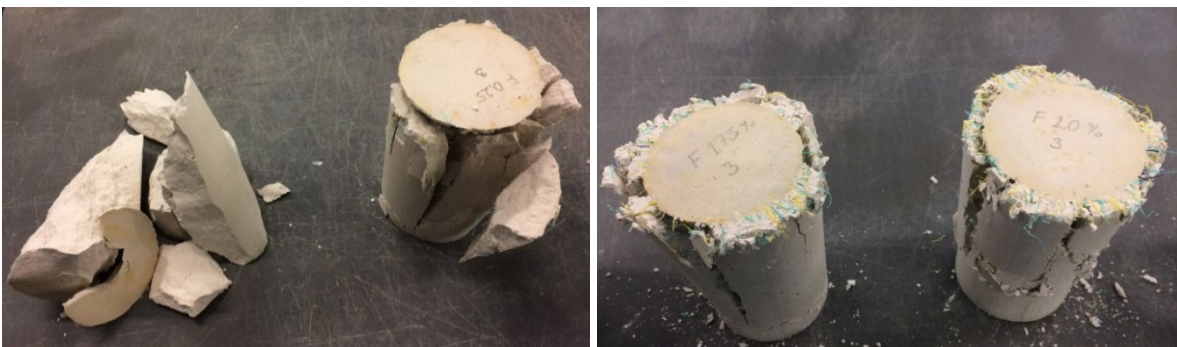303 The mechanisms involved in the improved post-crack performance and toughness of the prisms used for the three-point

304 bending test relate to the fibre-to-matrix bonding, i.e. the pull-out of fibres for brittle materials and the fibre fracture [10].

305 Only fibre pull-outs and no fibre fractures were observed when examining the fracture surfaces of the prisms after the

306 three-point bending test, see Fig. 14. A large number of small holes could also be observed on the fracture surface together

307 with fibres sticking out indicating that fibres were pulled out of the gypsum matrix during the three-point bending test.
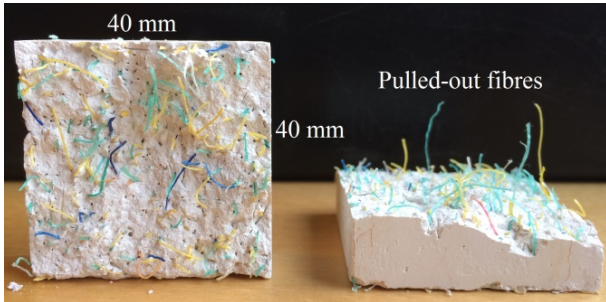


308

309 *Fig. 14. The fracture surface of a prism with 2.0 wt% of cleaned R-PE fibres after the flexural bending test.*

310

311 The SEM images in Fig. 15 show the microstructure of the fractured surface of a composite after the three-point bending

312 test at two magnifications. During the hydration process of the gypsum matrix, randomly orientated small needle-shaped

313 crystals were formed, which can be seen in the SEM images. The interfaces between the R-PE fibres and the material

314 matrix appeared porous with the hydrated needle-shaped crystals of plaster closely gathered around the fibres where a

315 small gap of debonding can be seen. The fibres that were pulled out of the matrix have small particles of plaster on the

316 fibre surface and appeared without any signs of degradation.
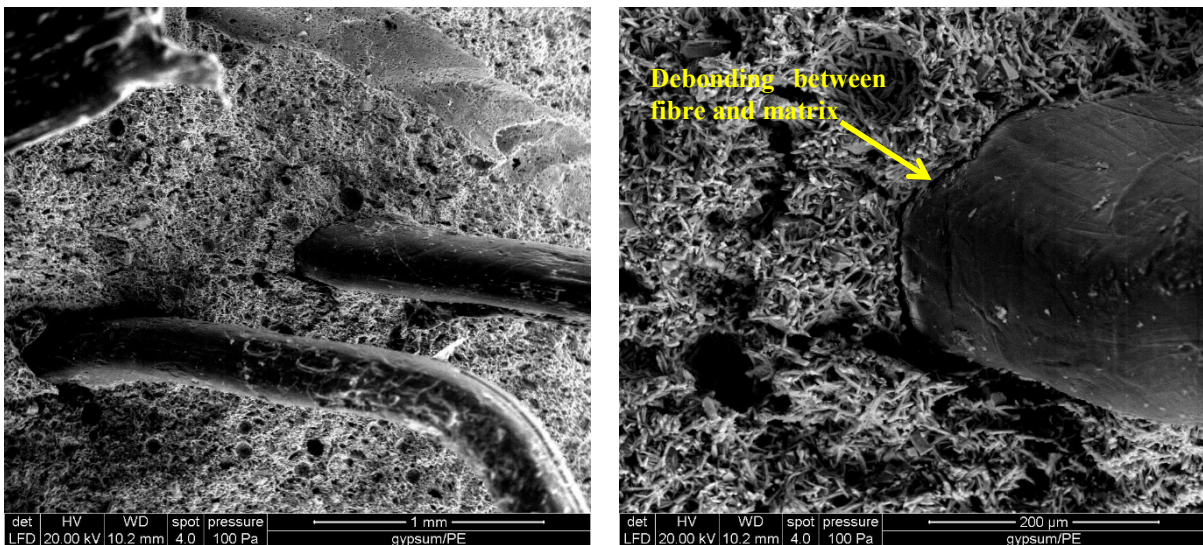


317 *Fig. 15. SEM images of the fracture surface of prism with addition of 2.0 wt% of cleaned R-PE fibres, a) (x50); b) (x250).*

318

**4 Discussion**

The benefits of using fibres from plastic waste materials as fibre reinforcement in brittle building materials include the fact that a waste material is being recycled, while some mechanical properties of the material to which it is added is being improved. The characteristics of the R-PE fibres from waste fishing nets were found to be in the same range as many other low-modulus fibres used as fibre reinforcement in gypsum-based materials. Because of the history of the R-PE fibres that had previously been used for fishing operations, the uncleaned R-PE fibres contained some impurities and residues from the fishing operations. Since these impurities present in the uncleaned fibres had a high concentration of leachable ions, it was considered necessary to clean the fibres in tap water prior to using them as fibre reinforcement in the gypsum-based composites.

**4.1 Influence of fibres on the mechanical performance of gypsum-based composites**

The major benefit of adding fibres to a brittle matrix is to avoid a catastrophic failure of the material by improving the post-crack performance and ductility. These positive effects of adding fibres from waste fishing nets of nylon to other types of brittle matrices such as cement-based specimens were previously studied by [30,31]. The influence of the fibres on the composite post-crack performance depends on their performance in providing bridging forces across the cracks [41], which is a result of the fibre-to-matrix bonding, the fibre pull-out force, and fibre properties such as the geometry, shape, surface, strength and stiffness. One of the challenges when using waste- or natural fibre materials instead of virgin materials relates to the variations in properties [17–19,21,24]. The R-PE fibres extracted from waste fishing nets had variations in fibre length as a result of the industrial, mechanical cutting operation, but the mean fibre length of $15 \pm 9$ mm corresponds well with other fibres studied in the literature with the aim of improving the post-crack performance of gypsum-based composites [11,13,14,18,43,44]. The fibre length is an important parameter with respect to the mechanical performance of the composites, and in particular the post-crack performance and fracture energy [21]. It is generally assumed that fibres of longer length are the main attributers to the gain in fracture energy [41], but longer fibres and too high fibre fractions can also lead to poor mixing and fibre bundling resulting in impaired properties of the composite material [31]. The fibre diameter of the R-PE fibres of $280 \pm 30$ μm is coarser than most other polymeric fibres used as fibre reinforcement in gypsum- or cement-based composites reported in the literature. However, also gypsum-based specimens with addition of fibres with coarser diameter in the range of 0.15-0.6 mm [10,15,17,18,45] have been studied with results showing significant improvements in post-crack performance. The fibre aspect ratio is also a relevant property

347   for the performance of the fibres. As a result of the varying fibre length and diameter, the aspect ratio is as well not similar

348   for all fibres. The mean value is around $L/d = 50$, which is in the low range of other tested fibre types in gypsum-based

349   specimens [24,41]. Vasconcelos et al. [21] studied gypsum-based composites with the addition of granulated cork and

350   PA6 fibre reinforcement obtained from recycled tyres. The study reported variations in fibre geometry, which covered

351   fibre lengths of 0.1-12.5 mm and diameters of 7.2-34.1 μm, and, despite these variations, it was still found that the fibres

352   were successful in improving the fracture energy of the composite. Li et al. [45] used cotton stalk fibres with large

353   variations in geometry (length of 5-20 mm and diameter of 0.5-3.0 mm). Both untreated fibres and fibres treated with

354   styrene acrylic emulsion were used as reinforcement in gypsum-based composites, and it was found that styrene acrylic-

355   treated fibres achieved better fibre-to-matrix bonding.

356   The tensile strength of the R-PE fibres of $420 \pm 50$ MPa was determined by testing fibres from three types of known PE

357   nets, which were assumed to cover the range of mechanical and geometrical properties present in the R-PE fibre samples.

358   The variations were considered to be both because the fibres originally had different mechanical properties and since the

359   fibres had differences in level of deterioration due to mechanical loading and abrasion during fishing operations, exposure

360   to UV-light etc. Furthermore, some nets were stored at dumpsites, harbors or at the recycling plant for an unknown period

361   of time before they were processed. Some of these variables could be improved in consequence of upgraded waste

362   management of the waste fishing gear. The tensile strength of the R-PE fibres from waste fishing nets corresponds well

363   with the strength of other polymeric fibres (especially low-modulus fibres of PP or PA) used as reinforcing materials in

364   gypsum-based composites, where strengths in the range of 300-600 MPa have been reported in the literature

365   [15,16,41,44,46]. Eve et al. [41] studied the influence of virgin PA fibres of different geometries as fibre reinforcement

366   in gypsum-based composites in fibre fractions up to 5 wt%. The PA fibres had tensile properties comparable to those of

367   the R-PE fibres used in this study, although their diameter was finer (15-40 μm compared to $280 \pm 30$ μm). The first crack

368   strength of the gypsum-based composite was also in the same range as the composites used in the present study and it

369   was, therefore, possible to compare the influence of these fibres. Fibre efficiency factors (FEF) of approximately 0.2-0.6

370   were found for the studied PA fibres when added in fractions of 2 wt% [41], which is in the same range as the R-PE fibres

371   (FEF = 0.44 for 2.0 wt%). Zhu et al. [16] studied the influence of PVA and PP fibres on the mechanical properties of

372   gypsum-based composites. The tensile properties of the PP fibres (tensile strength of 570 MPa and modulus of 3.5 GPa)

373   were slightly larger, but still comparable to the R-PE fibres used in the present study (tensile strength of $420 \pm 50$ MPa

374   and modulus of ~1.6 GPa), whereas the tensile properties of the PVA fibres were significantly larger (tensile strength of

375   1580 MPa and modulus of 36 GPa). It was found that the PVA fibers performed superior with respect to improving the

376 toughness of gypsum-based composites, compared to PP fibers, which was ascribed to the higher mechanical properties

377 of the fibres and the good adhesion between PVA fibers and gypsum matrix [16]. These comparisons with other studies

378 indicate that the R-PE fibres are able of achieving results with respect to improved post-crack performance and ductility

379 in the similar range as fibres of virgin PP/PA materials of similar tensile properties.

380 The effect of adding polymeric fibres to brittle materials such as gypsum-based or cement-based composites with respect

381 to the compressive strength has been a topic of much discussion in the literature, with some studies reporting increases in

382 compressive strength [46–49], others reporting decreases in strength [13,30,41,50,51], and yet others reporting either

383 unclear effects or no effect at all [21,52]. In this study, the addition of R-PE fibres of up to 2% did result in a reduction

384 of 5% in compressive strength and there was not observed a clear tendency with increasing fibre addition.

385

386 **5 Conclusion**

387 The aim of this study was to explore new ways of using fibres obtained from waste fishing nets as fibre reinforcement in

388 gypsum-based building materials. First, the fibres obtained from waste fishing nets of recycled polyethylene (R-PE) were

389 characterized. Secondly, fibres obtained from equivalent new and recycled fishing nets were tested with respect to the

390 tensile properties. The outcome of the experimental study of the R-PE fibres indicated that:

391 ▪ R-PE fibres obtained by a mechanical cutting operation of waste fishing nets of different types of PE resulted in

392 fibres with variations in length ($15 \pm 9$ mm), diameter ($280 \pm 30$ mm) and tensile strength ($420 \pm 50$ MPa).

393 ▪ The characterization of R-PE fibres showed that the tensile strength and geometry of the fibres were in the range

394 as other low-modulus fibres used as fibre reinforcement in gypsum-based materials such as PP and PA.

395 ▪ The R-PE fibres contained a small amount of impurities from the fishing operation, which should be extracted

396 from the fibres due to their high concentration of leachable anions. It was found sufficient to wash the fibres in

397 tap water.

398 Since the R-PE fibre characteristics were found to be similar to other low-modulus virgin fibres used in gypsum-based

399 materials today, they were added to a gypsum-based binder to produce fibre reinforced composites. The compressive and

400 flexural behaviour were determined by laboratory-scale testing of gypsum-based composites prepared with addition of

401 fibres varying from 0.25 wt% and up to 2.0 wt%.

402 ▪ The flexural performance of gypsum-based composites with addition of cleaned R-PE fibres showed a significant

403 increase in post-crack performance and fibre efficiency factor (FEF), but also a decrease in first-crack flexural

strength. The unreinforced gypsum-based specimens experienced a brittle failure, whereas the ductility of the composite could significantly benefit from the addition of R-PE fibres.

- Fracture surfaces from the three-point bending test were analysed using Scanning Electron Microscopy (SEM) and revealed that most fibres got pulled out of the matrix. The fibres showed no sign of degradation from having been inside the gypsum composites for 50 days.

- The R-PE fibres were not having any consistent influence on the compressive strength. A reduction in compressive strength of 5% was achieved when adding cleaned R-PE fibres in fractions of 2.0 wt%.

These results support that there is a great potential in using R-PE fibres obtained from waste fishing nets as fibre reinforcement in gypsum-based composites to create a more eco-friendly material as the R-PE fibres performed similarly to other low-modulus polymeric fibres of virgin materials.

## 6 Acknowledgement

## 7 References

[1]  C. Wilcox, N.J. Mallos, G.H. Leonard, A. Rodriguez, B.D. Hardesty, Using expert elicitation to estimate the impacts of plastic pollution on marine wildlife, Mar. Policy. 65 (2016) 107–114. doi:10.1016/j.marpol.2015.10.014.

[2]  C.J. Moore, Synthetic polymers in the marine environment: A rapidly increasing, long-term threat, Environ. Res. 108 (2008) 131–139. doi:10.1016/j.envres.2008.07.025.

[3]  J.R. Jambeck, R. Geyer, C. Wilcox, T.R. Siegler, M. Perryman, A. Andrady, R. Narayan, K.L. Law, Plastic waste inputs from land into the ocean, Science (80-. ). 347 (2015) 768–771.

[4]  M. Stelfox, J. Hudgins, M. Sweet, A review of ghost gear entanglement amongst marine mammals, reptiles and elasmobranchs, Mar. Pollut. Bull. 111 (2016) 6–17. doi:10.1016/j.marpolbul.2016.06.034.

[5]  U. Oxvig, U.J. Hansen, Fishing gears, Fiskericirklen, 2007.

[6]  B. Meenakumari, K. Ravindran, Tensile Strength Properties of Polyethylene Netting Twines Under Exposure to Out-door and Artificial UV radiation, Cent. Inst. Fish. Technol. 22 (1985) 83–86.

[7]  E. Hagemann, Gips, 3rd editio, Polyteknisk Forlag, 1977.

[8]  M. Arikan, K. Sobolev, The optimization of a gypsum-based composite material, 32 (2002) 1725–1728.

[9]  M.A. Ali, F.J. Grimer, Mechanical properties of glass fibre-reinforced gypsum, J. Mater. Sci. 4 (1969) 389–395.

437          doi:10.1007/BF00549703.

438   [10]   F. Hernández-Olivares, I. Oteiza, L. de Villanueva, Experimental analysis of toughness and modulus of rupture
439          increase of sisal short fiber reinforced hemihydrated gypsum, Compos. Struct. 22 (1992) 123–137.
440          doi:10.1016/0263-8223(92)90001-S.

441   [11]   C. Martias, Y. Joliff, C. Favotto, Effects of the addition of glass fibers, mica and vermiculite on the mechanical
442          properties of a gypsum-based composite at room temperature and during a fire test, Compos. Part B Eng. 62
443          (2014) 37–53. doi:10.1016/j.compositesb.2014.02.019.

444   [12]   A.J. Majumdar, Glass fibre reinforced cement and gypsum products, Proc. R. Soc. London. Ser. A, Math. Phys.
445          Sci. 319(1536). (1970) 69–78. doi:http://www.jstor.org/stable/77779.

446   [13]   N.F. Medina, M.M. Barbero-Barrera, Mechanical and physical enhancement of gypsum composites through a
447          synergic work of polypropylene fiber and recycled isostatic graphite filler, Constr. Build. Mater. 131 (2017) 165–
448          177. doi:10.1016/j.conbuildmat.2016.11.073.

449   [14]   O. Gencel, J.J. Del Coz Diaz, M. Sutcu, F. Koksal, F.P. Álvarez Rabanal, G. Martónez-Barrera, W. Brostow,
450          Properties of gypsum composites containing vermiculite and polypropylene fibers: Numerical and experimental
451          results, Energy Build. 70 (2014) 135–144. doi:10.1016/j.enbuild.2013.11.047.

452   [15]   Y.H. Deng, T. Furuno, Properties of gypsum particleboard reinforced with polypropylene fibers, J. Wood Sci. 47
453          (2001) 445–450. doi:10.1007/BF00767896.

454   [16]   C. Zhu, J. Zhang, J. Peng, W. Cao, J. Liu, Physical and mechanical properties of gypsum-based composites
455          reinforced with PVA and PP fibers, Constr. Build. Mater. 163 (2018) 695–705.
456          doi:10.1016/j.conbuildmat.2017.12.168.

457   [17]   F. Iucolano, D. Caputo, F. Leboffe, B. Liguori, Mechanical behavior of plaster reinforced with abaca fibers,
458          Constr. Build. Mater. 99 (2015) 184–191. doi:10.1016/j.conbuildmat.2015.09.020.

459   [18]   F. Iucolano, B. Liguori, P. Aprea, D. Caputo, Evaluation of bio-degummed hemp fi bers as reinforcement in
460          gypsum plaster, Compos. Part B. 138 (2018) 149–156. doi:10.1016/j.compositesb.2017.11.037.

461   [19]   P. Dalmay, A. Smith, T. Chotard, P. Sahay-Turner, V. Gloaguen, P. Krausz, Properties of cellulosic fibre
462          reinforced plaster: Influence of hemp or flax fibres on the properties of set gypsum, J. Mater. Sci. 45 (2010) 793–
463          803. doi:10.1007/s10853-009-4002-x.

464   [20]   M.A. Carvalho, C. Calil, H. Savastano, Microstructure and Mechanical Properties of Gypsum Composites
465          Reinforced with Recycled Cellulose Pulp, Mater. Res. 11 (2008) 391–397. doi:http://doi.org/10.1590/S1516-
466          14392008000400002.

467   [21]   G. Vasconcelos, P.B. Lourenço, A. Camões, A. Martins, S. Cunha, Evaluation of the performance of recycled
468          textile fibres in the mechanical behaviour of a gypsum and cork composite material, Cem. Concr. Compos. 58
469          (2015) 29–39. doi:10.1016/j.cemconcomp.2015.01.001.

470   [22]   Á. Serna, M. del Río, J.G. Palomo, M. González, Improvement of gypsum plaster strain capacity by the addition
471          of rubber particles from recycled tyres, Constr. Build. Mater. 35 (2012) 633–641.
472          doi:10.1016/j.conbuildmat.2012.04.093.

473   [23]   F.J.H.T.V. Ramos, L.C. Mendes, Recycled high-density polyethylene/gypsum composites: evaluation of the
474          microscopic, thermal, flammability, and mechanical properties, Green Chem. Lett. Rev. 7 (2014) 199–208.
475          doi:10.1080/17518253.2014.924591.

476   [24]   F. Parres, J.E. Crespo-Amorós, A. Nadal-Gisbert, Mechanical properties analysis of plaster reinforced with fiber
477          and microfiber obtained from shredded tires, Constr. Build. Mater. 23 (2009) 3182–3188.
478          doi:10.1016/j.conbuildmat.2009.06.040.

479   [25]   Y. Liu, Y. Zhang, Y. Guo, P.K. Chu, S. Tu, Porous Materials Composed of Flue Gas Desulfurization Gypsum
480          and Textile Fiber Wastes, Waste and Biomass Valorization. 8 (2017) 203–207. doi:10.1007/s12649-016-9617-y.

481 [26]  R. Siddique, J. Khatib, I. Kaur, Use of recycled plastic in concrete: A review, Waste Manag. 28.10 (2008) 1835–
482      1852. doi:10.1016/j.wasman.2007.09.011.

483 [27]  L. Gu, T. Ozbakkaloglu, Use of recycled plastics in concrete: A critical review, Waste Manag. 51 (2016) 19–42.
484      doi:10.1016/j.wasman.2016.03.005.

485 [28]  R. Sharma, P.P. Bansal, Use of different forms of waste plastic in concrete - A review, J. Clean. Prod. 112(1)
486      (2016) 473–482. doi:10.1016/j.jclepro.2015.08.042.

487 [29]  F. Pacheco-Torgal, Y. Ding, S. Jalali, Properties and durability of concrete containing polymeric wastes (tyre
488      rubber and polyethylene terephthalate bottles): An overview, Constr. Build. Mater. 30 (2012) 714–724.
489      doi:10.1016/j.conbuildmat.2011.11.047.

490 [30]  S. Spadea, I. Farina, A. Carrafiello, F. Fraternali, Recycled nylon fibers as cement mortar reinforcement, Constr.
491      Build. Mater. 80 (2015) 200–209. doi:10.1016/j.conbuildmat.2015.01.075.

492 [31]  S. Orasutthikul, D. Unno, H. Yokota, Effectiveness of recycled nylon fiber from waste fishing net with respect to
493      fiber reinforced mortar, Constr. Build. Mater. 146 (2017) 594–602. doi:10.1016/j.conbuildmat.2017.04.134.

494 [32]  A. Singh, F. Raj, P. Franco, J. Binoj, Evaluation of mechanical behavior of multifilament discarded fishnet/glass
495      fiber and polyester composites for marine applications, Mar. Struct. 58 (2018) 361–366.
496      doi:10.1016/j.marstruc.2017.11.013.

497 [33]  F.M. Raj, V.A. Nagarajan, S.S. Elsi, Mechanical, physical and dynamical properties of glass fiber and waste
498      fishnet hybrid composites, Polym. Bull. 74 (2017) 1441–1460. doi:10.1007/s00289-016-1783-3.

499 [34]  I.M.G. Bertelsen, L.M. Ottosen, G. Fischer, Quantitative analysis of the influence of synthetic fibres on plastic
500      shrinkage cracking using digital image correlation, Constr. Build. Mater. 199 (2019) 124–137.
501      doi:10.1001/archinte.168.13.1371.

502 [35]  B.S. Al-Tulaian, M.J. Al-Shannag, A.R. Al-Hozaimy, Recycled plastic waste fibers for reinforcing Portland
503      cement mortar, Constr. Build. Mater. 127 (2016) 102–110. doi:10.1016/j.conbuildmat.2016.09.131.

504 [36]  J.H.J. Kim, C.G. Park, S.W. Lee, S.W. Lee, J.P. Won, Effects of the geometry of recycled PET fiber reinforcement
505      on shrinkage cracking of cement-based composites, Compos. Part B Eng. 39.3 (2008) 442–450.
506      doi:10.1016/j.compositesb.2007.05.001.

507 [37]  F. Fraternali, I. Farina, C. Polzone, E. Pagliuca, L. Feo, On the use of R-PET strips for the reinforcement of
508      cement mortars, Compos. Part B Eng. 46 (2013) 207–210. doi:10.1016/j.compositesb.2012.09.070.

509 [38]  R.P. Borg, O. Baldacchino, L. Ferrara, Early age performance and mechanical characteristics of recycled PET
510      fibre reinforced concrete, Constr. Build. Mater. 108 (2016) 29–47. doi:10.1016/j.conbuildmat.2016.01.029.

511 [39]  L.A. Pereira De Oliveira, J.P. Castro-Gomes, Physical and mechanical behaviour of recycled PET fibre reinforced
512      mortar, Constr. Build. Mater. 25 (2011) 1712–1717. doi:10.1016/j.conbuildmat.2010.11.044.

513 [40]  D. Foti, Use of recycled waste pet bottles fibers for the reinforcement of concrete, Compos. Struct. 96 (2013)
514      396–404. doi:10.1016/j.compstruct.2012.09.019.

515 [41]  S. Eve, M. Gomina, A. Gmouh, A. Samdi, R. Moussa, G. Orange, Microstructural and mechanical behaviour of
516      polyamide fibre-reinforced plaster composites, J. Eur. Ceram. Soc. 22 (2002) 2269–2275. doi:10.1016/S0955-
517      2219(02)00014-6.

518 [42]  A.J. Lewry, J. Williamson, The setting of gypsum plaster - Part III The effect of additives and impurities, J. Mater.
519      Sci. 29 (1994) 6085–6090. doi:10.1007/BF00354546.

520 [43]  S. Eve, M. Gomina, J.P. Jernot, J.C. Ozouf, G. Orange, Microstructure characterization of polyamide fibre/latex-
521      filled plaster composites, J. Eur. Ceram. Soc. 27 (2007) 3517–3525. doi:10.1016/j.jeurceramsoc.2005.04.026.

522 [44]  L. Alameda, V. Calderón, C. Junco, A. Rodríguez, J. Gadea, S. Gutiérrez-González, Characterization of gypsum

523    plasterboard with polyurethane foam waste reinforced with polypropylene fibers, Mater. Constr. 66 (2016).
524    doi:10.3989/mc.2016.06015.

525    [45]    G. Li, Y. Yu, Z. Zhao, J. Li, C. Li, Properties study of cotton stalk fiber / gypsum composite, 33 (2003) 43–46.

526    [46]    O. Gencel, J.J. Del Coz Diaz, M. Sutcu, F. Koksal, F.P. Álvarez Rabanal, G. Martínez-Barrera, A novel
527              lightweight gypsum composite with diatomite and polypropylene fibers, Constr. Build. Mater. 113 (2016) 732–
528              740. doi:10.1016/j.conbuildmat.2016.03.125.

529    [47]    P.S. Song, S. Hwang, B.C. Sheu, Strength properties of nylon- and polypropylene-fiber-reinforced concretes,
530              Cem. Concr. Res. 35 (2005) 1546–1550. doi:10.1016/j.cemconres.2004.06.033.

531    [48]    M. Nili, V. Afroughsabet, The effects of silica fume and polypropylene fibers on the impact resistance and
532              mechanical    properties    of    concrete,    Constr.    Build.    Mater.    24    (2010)    927–933.
533              doi:10.1016/j.conbuildmat.2009.11.025.

534    [49]    F. Fraternali, V. Ciancia, R. Chechile, G. Rizzano, L. Feo, L. Incarnato, Experimental study of the thermo-
535              mechanical properties of recycled PET fiber-reinforced concrete, Compos. Struct. 93 (2011) 2368–2374.
536              doi:10.1016/j.compstruct.2011.03.025.

537    [50]    O. Karahan, C.D. Atiş, The durability properties of polypropylene fiber reinforced fly ash concrete, Mater. Des.
538              32 (2011) 1044–1049. doi:10.1016/j.matdes.2010.07.011.

539    [51]    S.B. Kim, N.H. Yi, H.Y. Kim, J.H.J. Kim, Y.C. Song, Material and structural performance evaluation of recycled
540              PET    fiber    reinforced    concrete,    Cem.    Concr.    Compos.    32    (2010)    232–240.
541              doi:10.1016/j.cemconcomp.2009.11.002.

542    [52]    D.A. Silva, A.M. Betioli, P.J.P. Gleize, H.R. Roman, L.A. Gómez, J.L.D. Ribeiro, Degradation of recycled PET
543              fibers    in    Portland    cement-based    materials,    Cem.    Concr.    Res.    35    (2005)    1741–1746.
544              doi:10.1016/j.cemconres.2004.10.040.

545

# Appendix VI

**Description:** Conference paper published in the Proceedings of the RILEM International Conference on Bio-Based Building Materials 2019

**Title:** Adobe bricks of Greenlandic fine-grained rock material

# ADOBE SPECIMENS OF GREENLANDIC FINE-GRAINED ROCK MATERIAL

I.M.G. Bertelsen[1]*, L.J. Belmonte[1], L.M. Ottosen[1]

[1] Department of Civil Engineering, Technical University of Denmark, Brovej 118, 2800 Kgs. Lyngby, Denmark

*Corresponding author; e-mail: imgber@byg.dtu.dk

## Abstract

Every year, glacial rivers in Greenland transport and deposit vast quantities of fine-grained rock material (GP). In the present study we characterise this raw material (GP) and evaluate whether it is possible to produce adobe bricks for a local production in an Arctic region such as Greenland. The raw material characterization included determination of the grain size distribution and the plastic properties. For enabling the production of adobe bricks, it was, based on these tested parameters, found necessary to add a fraction of a coarser gravel-size material (KG) in addition to the fine-grained rock material (GP). Small-scale prisms and cylinders for determination of the drying shrinkage behaviour and the mechanical performance of the composite material were produced containing 50/50 of GP and KG, respectively. Adobe bricks are often reinforced with fibres of natural or synthetic materials to improve the ductility of the composites, such as for example straw, however, in Arctic regions such materials are often a scares resource due to the existing type of vegetation. Therefore, we instead added fibres from discarded polyethylene fishing nets, which is a local waste material often present in coastal towns in Greenland. The addition of fibres from waste fishing nets to the adobe specimens resulted in enhanced drying shrinkage behaviour, post-crack performance and toughness for prisms when exposed to flexural loads.

## Keywords:

Adobe bricks, fine-grained rock material, waste fishing nets, fibre reinforcement, local resources

## 1 INTRODUCTION

Earth-based materials such as adobe bricks are one of the oldest building materials and have been used for construction purposes since antiquity [Houben 1993]. The production of adobe bricks is relatively simple and environmental friendly, since it consists of filling moulds with moist earth-based materials, often with addition of a fibrous material, which are then left to dry [Pacheco-Torgal 2012]. As a result of the simple production method, adobe bricks are relatively cheap and, despite their expected low strength, can advantageously be used as interior building materials.

Previous studies have shown that these fine-grain rock materials, which are accessible in the entire Arctic region, can be successfully used as main raw material in the production of fired clay bricks [Bertelsen 2015; Belmonte 2016; Belmonte 2015]. Belmonte [Belmonte 2015] found that the characteristics of this raw material collected in Greenland is very similar to other marine clays found in North America and North Scandinavia. However, because of the low population density in Greenland, the construction of an actual brick work for a larger scale production of fired bricks is questionable. Therefore, the production of adobe bricks could prove to be a simple and cheap alternative in Greenlandic buildings and replace some of the imported construction

materials. In this experimentally-based research program, we investigate the performance of Greenlandic fine-grain rock materials as the main raw material in adobe specimens.



*Fig. 1: Fine-grained rock material (GP) from glacial rivers in Greenland*

Fibrous materials are added to adobe bricks mainly for improving the mechanical post-crack performance and for controlling the crack formation induced by drying

shrinkage deformations [Binici 2005; Quagliarini 2010; Pacheco-Torgal 2012].

Another locally available material is discarded fishing nets, which can be found in large piles at dumpsites in many coastal towns, see Fig 2. The fishing nets used in Greenland are typically made of polyethylene (PE) and there are currently no large-scale reuse/recycling options for the waste nets, which causes accumulation of the material at the dumpsites. The fibres used for adobe bricks are traditionally straw or other types of vegetable materials, which in this case could be replaced by PE fibres. With the addition of a non-biodegradable synthetic fibrous material such as PE, it would require improved waste management for the demolished adobe bricks, but on the positive side, a local waste fraction can be reused and the fibres don't have the risk of rotting inside the adobe material, which can be the case for some vegetable fibres [Pacheco-Torgal 2012].



*Fig. 2: Discarded fishing nets piled up at the dumpsite in Sisimiut, Greenland*

Besides being a waste management challenge, marine plastic litter, of which fishing gear is a considerable fraction, is a growing global challenge. The vulnerable Arctic environment is also increasingly affected due to climate changes, more regular access to the Arctic Sea route and sea currents from the North Atlantic, which carries a continuous supply of marine waste to the region [Bergmann 2015].

The focus in this research project is on the performance of adobe specimens made from locally available fine-grained rock materials (GP) near Nuuk, Greenland, and gravel (KG) with the addition of recycled fibres of polyethylene (R-PE) obtained from discarded fishing nets.

## 2 MATERIALS AND METHODS

### 2.1 Characterization of raw materials

The raw materials used for the adobe brick production were fine-grained rock material (GP collected near Nuuk, Greenland), as main matrix; gravel (KG) as

stabilizer; R-PE fibres as fibrous materials and water as lubricant. Based on initial investigations of the raw material, it was observed that a coarse, stabilizing fraction should be added to the GP to obtain a satisfactory grain size distribution for the production of adobe bricks [Houben 1993]. Therefore, gravel 0-8 mm (KG) from Kallerup, Denmark, was collected and used in the production of adobe bricks. For practical reasons, the gravel was collected from a gravel pit in Denmark; however, gravel resources are common in Greenland, and a similar gravel fraction could likely by found locally. The grain size distribution for GP and KG was done in accordance with [CEN-ISO/TS-17892-4 2004] on bulk samples of the sand fraction by the sieve analysis and on the silt and clay fraction by the hydrometer analysis. The grain density for GP was determined by following the procedures in [CEN-ISO/TS-17892-3 2004]. For the test, a sample of 10 g dried at 105 °C was used. Organic matter was only present in very small amounts and was therefore not removed from the GP samples. The determination of the liquid- and plastic limit for GP was carried out in accordance with [CEN-ISO/TS-17892-6 2004; CEN-ISO/TS-17892-12 2004], respectively, on a non-dried remoulded GP sample. For the fall cone penetration test, a 60 g/60° fall cone was used.

### 2.2 Fibres from discarded fishing nets

The fishing nets used in Greenland are typically made of PE materials. In this study, monofilament R-PE fibres obtained by mechanical cutting of discarded fishing nets of similar types as the ones used in Greenland, were provided by the Danish recycling company, Plastix A/S. See Fig. 3.



*Fig. 3: R-PE fibres from discarded fishing nets after being cleaned in tap water*

The fibres have a length of 15 ± 9 mm and a diameter of 280± 30 μm. More details on the fibre characteristics are given in [Bertelsen 2019; Bertelsen n.d.]. Since the provided fibres contained some impurities from the fishing operation etc., we investigated the influence of these impurities by both using uncleaned R-PE fibres and R-PE fibres which were cleaned in tap water in the adobe production.

## 2.3 Production and testing of adobe bricks

Prior to the laboratory-scale production of the adobe bricks, several iterations regarding the mixture design and drying procedure were carried out to identify a good result.

Examples on specimens with 100% GP; and 50% GP and 50% KG, respectively, are shown in Fig. 4. As a result of the fine grain sizes of GP and the drying process (30 °C for 48 h), the specimens with 100% GP were shrinking to an extent that resulted in severe drying shrinkage cracks, see Fig. 4a. Regarding the specimens with the addition of 50% GP and 50% KG, only few and very fine drying cracks appeared on the surface as seen in Fig. 4b.



(a)



(b)

*Fig. 4: Influence of mixture proportions on drying shrinkage: a) 100% GP; b) 50% GP and 50% KG*

Not only was the content of fines playing a significant role with respect to the shrinkage behaviour, but also the drying temperature. The specimens were exposed to an accelerated drying process, so that the core of the specimens could be dry after a few days of drying. The drying was primarily done at different temperatures (20, 30 and 50 °C) for at least 48 h to examine the drying efficiency and the drying shrinkage behaviour. The best results were obtained when drying the specimens at 30 °C for 48 h inside steel moulds.

The production of the adobe specimens included the following steps: the raw materials (GP, KG and R-PE fibres) were primarily hand-mixed to ensure an even fibre distribution, whereupon the water was added under continuous mixing for 2 min in a Hobart-type paddle mixer. The mixture proportions were 1.0 : 1.0 : 0.5 for GP, KG and water, respectively. The water content was slightly increased with the addition of fibres to keep a constant workability of the mixture. The fibre content was added in weight fractions of up to 4.0wt% corresponding to approximately 9.2vol%.

Prism-like specimens measuring 40 x 40 x 160 $mm^3$ for a three-point bending test were produced in three replicated per mixture design. The specimens were cast in lubricated steel moulds and tested in accordance with [UNI/EN-196-1 2005]. The drying shrinkage and the dry bulk density were measured on the prisms after 48 h at 30 °C. Cylinders measuring 60 mm x 120 mm with no fibre addition and 1.0wt% of R-PE fibres were prepared for the uniaxial compression test, also in three replicated. The three-point bending test and the compression test were carried out in an Instron 6022 hydraulic testing machine with a displacement controlled load applied at a rate of 1 mm/min.

## 3 RESULTS AND DISCUSSION

### 3.1 Raw material characterization

Table 1 shows the plastic properties and the grain density of GP.

*Table 1: Characteristics of fine-grained rock material (GP)*

| Natural water cont. | Plastic limit | Liquid limit | Plasticity index | Grain density |
|---|---|---|---|---|
| $w_{nat}$ [%] | PL [%] | LL [%] | PI [%] | [g/cm$^3$] |
| 15.4 | 17.1 | 30.9 | 13.8 | 2.74 |

The plasticity index, PI, calculated in accordance with [CEN-ISO/TS-17892-12 2004] as the difference between the liquid limit (*LL*) and plastic limit (*PL*):

$$PI(\%) = LL - PL$$

The plasticity index (PI) is plotted against the liquid limit (LL) in Fig. 5. It is observed that the plastic properties of GP lays within the recommended range for materials used for compressed earth blocks (CEB) [Houben 1993; CRTerre_EAG 1998], but that it is just outside the recommended range for adobe bricks [Houben 1993]. However, the plastic properties of GP are very similar to those of the matrix materials used in other studies on adobe bricks, e.g. Vega et al. [Vega 2011] and Araya-Letelier et al. [Araya-Letelier 2018] that used main

matrix materials with the following plastic properties: PI of 14%, 12% and a LL of 17%, 17%, respectively.
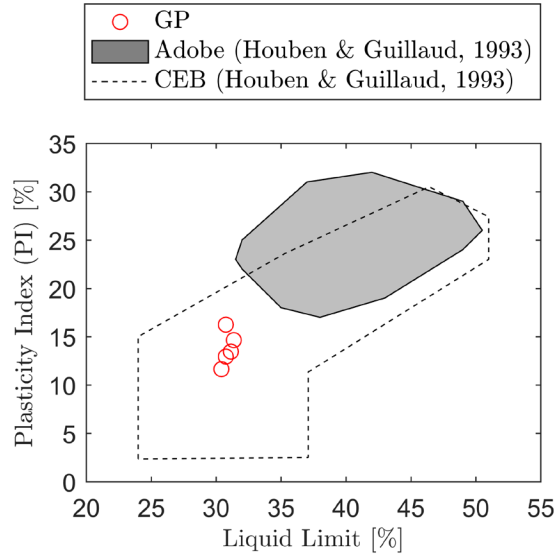


Fig. 5: The plasticity index plotted against the liquid limit for GP. Recommend range for adobe and CEB in accordance with [Houben 1993]
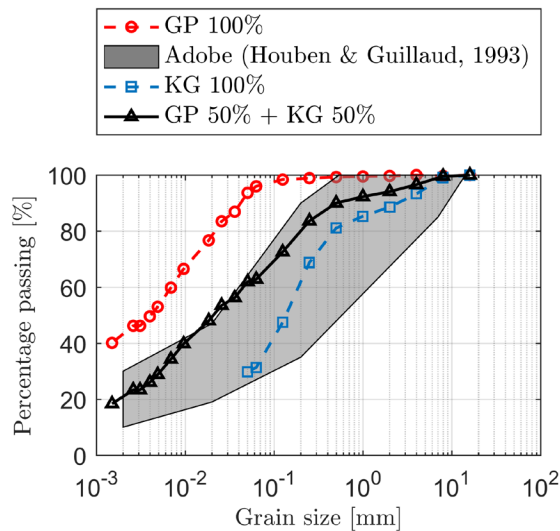


Fig. 6: Grain size distribution for GP, KG and mix of 50% GP and 50% KG. Recommend range in accordance with [Houben 1993]

### Grain size distribution for GP and KG

The grain size distribution for GP, KG and a mix of 50% GP and KG, respectively, are shown in Fig. 6. The recommended range for adobe bricks is shown with the grey area [Houben 1993]. The figure shows that the grain size of the pure GP material is too fine grained, whereas the mix of GP and KG lies within the acceptable range.

## 3.2 Adobe bricks

The performance of the adobe bricks with addition of R-PE fibres were evaluated based on the drying shrinkage behaviour, the three-point bending test and compression tests. All tests were carried out on three replicates.

### Drying shrinkage of adobe specimens

The drying shrinkage was measured as the difference between the width and length of wet adobe specimens cast inside the moulds (W = 40 mm, L = 160 mm) and the specimens dried at 30 °C for 48 h. The dry bulk density was calculated in accordance with [CEN-ISO/TS-17892-2 2004] as

$$\rho = \frac{m}{V}$$

, with $m$ being the mass and $V$ the volume of the dried specimens.

Fig. 7 shows the influence of the addition of R-PE fibres (cleaned in tap water or uncleaned).
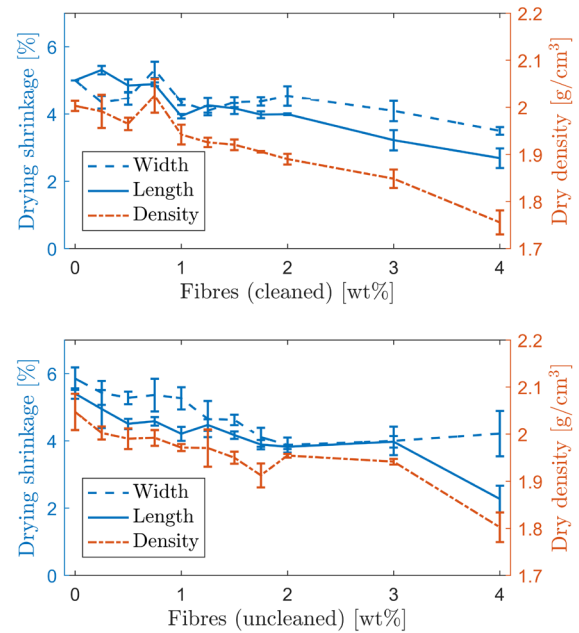


Fig. 7: Drying shrinkage and dry density of adobe prisms with addition of R-PE fibres (cleaned or uncleaned)

First, it is seen that the unreinforced specimens experience/exhibit a large drying shrinkage of 5-6% of the freshly cast specimens. Secondly, it is clearly observed that the addition of R-PE fibres cause a significant decrease in drying shrinkage no matter if the fibres were cleaned in tap water prior to being used or not. This positive influence of fibres on the drying shrinkage in adobe bricks were also observed by [Vega 2011]. Araya-Letelier et al. [Araya-Letelier 2018] studied the influence of pig hair fibres on the formation of restrained drying shrinkage and found that the fibres

were significantly reducing the shrinkage cracks when added in 2.0 wt%.

*Mechanical performance of adobe specimens*

The flexural response of prism-shaped adobe specimens with the addition of cleaned and uncleaned R-PE fibres added in weight fractions of 0.25-4.0wt% are shown in Fig. 8. The first crack strength of ~0.35 MPa was relatively stable for all fibre contents.
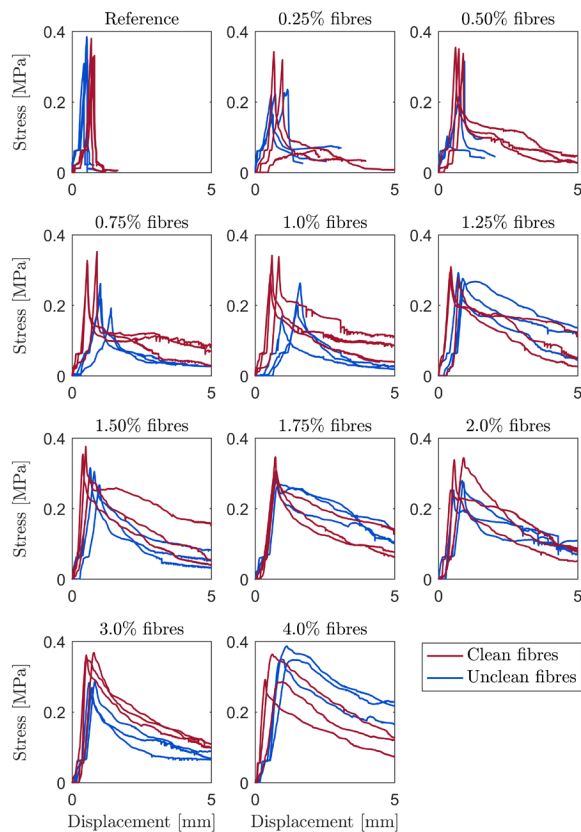


*Fig. 8: Stress deflection curves for fibre-reinforced adobe bricks with addition of uncleaned or cleaned R-PE fibres. Fibre additions in wt%*

The post-crack performance is significantly improved with the increasing fibre content and there is not observed any major difference in the performance of cleaned and uncleaned fibres. No actual drop in load occurs after the first crack appears, for specimens with fibre contents >2.0wt%. However, even at a fibre content of 4.0wt%, no strain hardening was observed, which was attributed to a relatively poor fibre-to-matrix bonding. PE is a hydrophobic material, which can be one of the reasons for the poor bonding. For future studies it is, therefore, suggested to study possible surface modifications for the R-PE fibres for improving bonding and the stress transfer across the cracks.

The compressive strength was determined on adobe cylinders with no fibres and with a fibre addition of 1.0wt% of cleaned R-PE fibres. The unreinforced specimens obtained a compressive strength of 0.8 MPa, while it was app. 1.0 MPa for the specimens added 1.0wt% of R-PE fibres. Besides the slightly higher compressive strength, the fibre reinforced cylinders showed a much more ductile failure mode, see example in Fig. 9. The results are in the same range as e.g. 0.5-1.2 MPa for those found for adobe bricks collected from existing houses in Portugal [Silveira 2012], but are lower than some other studies on "new" adobe bricks (1.75-3.50 MPa) [Quagliarini 2010]. Please note that other dimensions were used in the mentioned studies, which hinders a direct comparison. However, the material characteristics when exposed compressive stresses should be investigated further on more specimens to evaluate the influence on the addition of fibres.
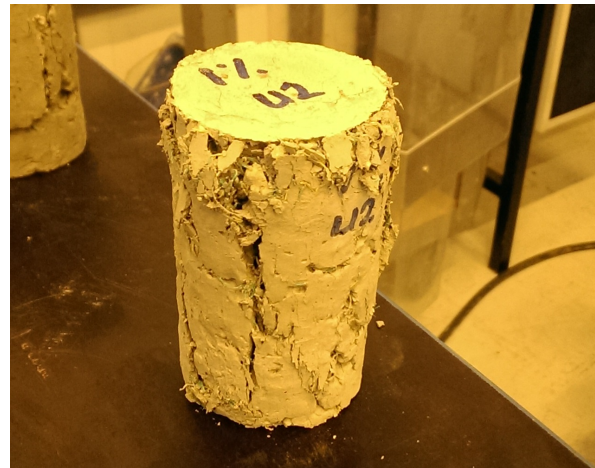


*Fig. 9: Adobe cylinder with addition of 1.0wt% R-PE after compression test*

## 4  RECOMMENDED FUTURE STUDIES

For future studies on the use of GP as main matrix in construction materials, it would be relevant to study other production methods, such as producing CEB instead of adobe bricks. Also, based on the recommendations for the plastic properties by [Houben 1993], the material would be more suitable for CEB than for adobe bricks. By compressing the earth bricks (CEB), it would probably also result in lower drying shrinkage and higher strengths.

Regarding the addition of R-PE fibres obtained from discarded fishing nets, it was observed that the fibre-to-matrix is relatively poor, which could be due to the hydrophobic nature of the PE. For future studies it is therefore recommended to study different types of fibre modifications for improving the bonding. The content of clay minerals in GP could also be a factor related to the poor bonding between the matrix and the R-PE fibres. A high content of clay minerals would probably lead to a better bonding to other materials, because of the high surface area of the clay minerals, thus the content of clay minerals would be relevant to investigate further.

## 5  CONCLUSION

Adobe specimens were produced from fine-grain rock material (GP) from Greenland, gravel 0-8 mm (KG), water and recycled polyethylene (R-PE) fibres obtained from discarded fishing nets. Prior to the actual production of adobe specimens, the raw materials (GP and KG) were characterized:

- The plastic properties of GP correspond well with those found in other studies on adobe bricks and are within the recommended range for CEB, but slightly outside the range for adobe in accordance with [Houben 1993].
- The grain size distribution of 100% GP was too fine compared to the recommendation for adobe bricks, while the addition of 50% KG was sufficient for getting inside the recommended range of grain sizes.

With respect to the production process of adobe specimens (prisms and cylinders), several iterations were done to obtain a successful process. The following observations were made during these iterations:

- The content of materials with fine grain sizes, such as GP, was significantly influencing the drying shrinkage behaviour (dried at 30 °C for 48 h). Specimens with 100% GP experienced severe cracking induced by drying shrinkage, whereas specimens consisting of 50% GP and 50% KG appeared with only few and fine surface cracks after the accelerated drying process.
- High drying temperatures were also enhancing drying shrinkage, and too low temperatures did not result in sufficient drying of the material within 48 h. The best results were gained by drying the specimens at a temperature of 30 °C for 48 h.
- Fibres were pre-mixed with the dry raw materials to ensure an even fibre distribution.

The drying shrinkage behaviour and the mechanical performance of the adobe bricks showed the following tendencies:

- The drying shrinkage was reduced significantly with increasing fibre content.
- The flexural strength of ~0.4 MPa of the adobe composites was more or less unaffected by the fibre addition.
- The post-crack performance was significantly improved by the addition of fibres. However, the fibres showed a relatively poor fibre-to-matrix bonding. Modification of the fibre surface could be relevant for future studies.
- The compressive strength of cylinders was tested, and the performance of reference specimens (no fibres) (~0.8 MPa) was compared to specimens with 1.0wt% of R-PE fibres (~1.0 MPa). A slightly higher strength and a more ductile failure mode were obtained for the fibre reinforced cylinder.

## 6  ACKNOWLEDGEMENT

## 7  REFERENCES

[Araya-Letelier 2018] Araya-Letelier, G. et al., 2018. Influence of natural fiber dosage and length on adobe mixes damage-mechanical behavior. *Construction and Building Materials*, 174(April), pp.645–655.

[Belmonte 2015] Belmonte, L.J., 2015. *Use of Greenlandic resources for the production of bricks*. Technical University of Denmark.

[Belmonte 2016] Belmonte, L.J. & Bertelsen, I.M.G., 2016. Evaluation of the potential for using greenlandic marine sediments for brick production. In *International RILEM Conference on Materials, Systems and Structures in Civil Engineering*.

[Bergmann 2015] Bergmann, M. et al., 2015. Observations of floating anthropogenic litter in the Barents Sea and Fram Strait, Arctic. *Polar Biology*.

[Bertelsen 2015] Bertelsen, I.M.G. et al., 2015. Properties of bricks produced from Greenlandic marine sediments. In *Proceedings of the International Conference on Port and Ocean Engineering under Arctic Conditions*.

[Bertelsen n.d.] Bertelsen, I.M.G. & Ottosen, L.M., Recycling of waste PE fishing nets as fibre reinforcement in gypsum-based composites. *Submitted*.

[Bertelsen 2019] Bertelsen, I.M.G., Ottosen, L.M. & Fischer, G., 2019. Quantitative analysis of the influence of synthetic fibres on plastic shrinkage cracking using digital image correlation. *Construction and Building Materials*, 199, pp.124–137. Available at: https://doi.org/10.1016/j.conbuildmat.2018.11.268.

[Binici 2005] Binici, H., Aksogan, O. & Shah, T., 2005. Investigation of fibre reinforced mud brick as a building material. *Construction and Building Materials*, 19(4), pp.313–318.

[CEN-ISO/TS-17892-12 2004] CEN-ISO/TS-17892-12, 2004. *Geotechnical investigation and testing –*

*Laboratory testing of soil – Part 12: Determination of Atterberg limits*,

[CEN-ISO/TS-17892-2 2004] CEN-ISO/TS-17892-2, 2004. *Geotechnical investigation and testing – Laboratory testing of soil – Part 2: Determination of density of fine- grained soil*,

[CEN-ISO/TS-17892-3 2004] CEN-ISO/TS-17892-3, 2004. *Geotechnical investigation and testing – Laboratory testing of soil – Part 3: Determination of particle density*,

[CEN-ISO/TS-17892-4 2004] CEN-ISO/TS-17892-4, 2004. *Geotechnical investigation and testing – Laboratory testing of soil – Part 4: Determination of particle size distribution*,

[CEN-ISO/TS-17892-6 2004] CEN-ISO/TS-17892-6, 2004. *Geotechnical investigation and testing – Laboratory testing of soil – Part 6: Fall cone test*,

[CRTerre_EAG 1998] CRTerre_EAG, 1998. *Compressed Earth Blocks*,

[Houben 1993] Houben, H. & Guillaud, H., 1993. *Earth Construction: A Comprehensive Guide*, Intermediate Technology.

[Pacheco-Torgal 2012] Pacheco-Torgal, F. & Jalali, S., 2012. Earth construction: Lessons from the past for future eco-efficient construction. *Construction and Building Materials*, 29, pp.512–519. Available at: http://dx.doi.org/10.1016/j.conbuildmat.2011.10.0 54.

[Quagliarini 2010] Quagliarini, E. & Lenci, S., 2010. The influence of natural stabilizers and natural fibres on the mechanical properties of ancient Roman adobe bricks. *Journal of Cultural Heritage*, 11(3), pp.309–314. Available at: http://dx.doi.org/10.1016/j.culher.2009.11.012.

[Silveira 2012] Silveira, D. et al., 2012. Mechanical properties of adobe bricks in ancient constructions. *Construction and Building Materials*, 28(1), pp.36–44. Available at: http://dx.doi.org/10.1016/j.conbuildmat.2011.08.0 46.

[UNI/EN-196-1 2005] UNI/EN-196-1, 2005. Methods of testing cement – Part 1: Determination of strength.

[Vega 2011] Vega, P. et al., 2011. Mechanical characterisation of traditional adobes from the north of Spain. *Construction and Building Materials*, 25(7), pp.3020–3023. Available at: http://dx.doi.org/10.1016/j.conbuildmat.2011.02.0 03.

# Appendix VII

**Description:** Unpublished

**Title:** Applications for recycled polyethylene fibres from discarded fishing nets in cement-based materials

1 # Applications for recycled polyethylene fibres from discarded

2 # fishing nets in cement-based materials

3 **Ida Maria Gieysztor Bertelsen\*, Lisbeth M. Ottosen**

4 Technical University of Denmark, Department of Civil Engineering, DK-2800 Kgs. Lyngby, Denmark
5 \*Corresponding author: imgber@byg.dtu.dk

6
7

8 **Abstract**

9 In this study, the potential of using fibres of recycled polyethylene (R-PE) obtained by mechanical cutting

10 of discarded fishing nets as fibre reinforcement in cement-based mortars was investigated. Mechanical

11 properties such as three-point bending strength, post-crack performance and toughness of fibre reinforced

12 mortar prisms were determined by laboratory-scale testing. The performance was compared to similar

13 prisms with addition of commercially available PP fibres. The alkali-resistance of the R-PE fibres were

14 evaluated based on SEM analysis and direct tensile tests on unconditioned fibres and fibres immersed in a

15 highly alkaline solution.

16 The R-PE fibres showed good alkali-resistance and no reduction in tensile strength was observed for

17 alkali-conditioned fibres. The addition of the fibres to mortar prisms resulted in all cases in improved

18 post-crack performance, but also a small decrease in first-crack strength and stiffness. Compared to the

19 specimens with addition of PP fibres, the R-PE fibres did not perform as well, which was considered due

20 to the straight shape and poor bonding to the matrix.

21

22 **Keywords:** Fibre reinforcement, fiber characterisation, plastic recycling, waste fishing nets.

23

24 **1 Introduction**

25 When lost or otherwise discarded fishing nets of non-biodegradable synthetic materials end up in the

26 ocean, they can become harmful to the marine environment by causing "ghost fishing" and entanglements

27 of marine organisms [1]. To prevent this, it is considered essential to find new applications for discarded

28 fishing nets. Research on the use of plastic waste as fibre reinforcement in cement-based materials has

29  already attracted significant attention by showing promising results for replacing virgin fibres [2,3].

30  Waste plastic fibres have both been tested for improving mechanical properties such as post-crack

31  performance, crack propagation and impact resistance [4–7] and as preventative measures for the

32  formation of plastic shrinkage cracking [8–13].

33  In this study, the potential for utilizing recycled polyethylene (R-PE) fibres obtained from discarded

34  fishing nets in cement-based mortars have been studied with the aim of improving the post-crack

35  performance and toughness of cement-based mortars.

36

37  **2   Materials and methods**

38  **2.1   Fibres**

39  Fibres of recycled polyethylene (R-PE) used as fibre reinforcement in cement-based materials were

40  provided by Plastix A/S, which is a company collecting and reprocessing discarded fishing gear. Prior to

41  the reprocessing, the fishing nets and trawls are separated into different materials fractions: e.g. nylon,

42  PE, PP and PET, with PE materials being the largest fraction of discarded fishing nets. After the

43  separation, the nets are mechanically being cut into smaller fibres, whereupon they are melted and

44  reprocessed into new plastic pellets. To avoid the energy consuming process of re-pelletizing the plastic,

45  the mechanically cut fibres were used directly as fibre reinforcement. A common type of discarded PE

46  fishing nets, Braided Polyethylene from Euronete, is the one shown in Fig. 1(a). The monofilament R-PE

47  fibres provided by Plastix A/S, which are used for fibre reinforcement in the present study, are shown in

48  Fig. 1 and consist of fibres from a mix of different PE nets.

49  The R-PE fibres were originating from different fishing nets, why differences in diameter, density, tensile

50  strength and -stiffness are present among the fibres, see Tab. 1. The mean fibre diameter is 280±30 µm

51  and the mean fibre length is 15±9 mm (varying between 1-65 mm). The large standard deviation for the

52  fibre length is due to the "uncontrolled" cutting operation. The R-PE fibres were being cleaned in tap

53  water to remove impurities from the fishing operations. For a detailed fibre characterization, please see

54  another study by the authors [14]. Two types of commercially available PP fibres were included in this

55  study for enabling a comparison with the R-PE fibres. The PP fibres, which were provided by PP

56  Nordica, are shown in Fig. 1(c-d) and their properties in Tab. 1.

57

*(a) Discarded PE fishing net*

*(b) R-PE fibres*

*(c) PP micro fibres*

*(d) PP macro fibres*

Fig. 1. a) Discarded fishing nets of the type Braided Polyethylene from Euronete; b) R-PE fibres processed by
mechanical cutting operations by Plastix A/S; c) PP Micro fibres; d) PP macro fibres

Tab. 1. Properties of cleaned, unconditioned R-PE fibres and PP micro and macro fibres

|  | Density | Length | Diameter | Tensile strength | Stiffness |
|---|---|---|---|---|---|
|  | $\rho$ [g/cm$^3$] | L [mm] | d [μm] | $\sigma_t$ [MPa] | E [GPa] |
| R-PE | ~0.95 | 15±9 (1-65) | 280±30 | 380-450 | 1.0-2.0 |
| PP Micro | 0.91 | 12 | 19.5 | N/A | N/A |
| PP Macro | 0.91 | 50 | 950 | 420 | 2.6 |

The alkali-resistance of the PE fibres was determined on a known type of fishing net for enabling a direct comparison of new and corresponding recycled fibres. The chosen net type was the "Braided polyethylene" as shown in Fig. 1. The alkali-conditioning was carried out in accordance with the procedure described in [4], with the fibres being immersed in a highly alkaline solution of 1M NaOH at 50 °C for up to 28 days. The alkali-cured fibres were analysed by SEM and direct tensile tests were

68  performed in accordance with ASTM C1557-14 [15] to evaluate the influence on the tensile properties.

69  Three different gauge lengths were tested: 20, 25 and 30 mm, by gluing the fibre to a piece of paper.

70  More details on the procedure can be found in [14].

71

72  **2.2  Mortar prisms**

73  The raw materials used for the mortar specimens were cement (CEM I 52.5 N), fine aggregates (sea sand

74  0-4 mm) and tap water. Prismatic mortar specimens measuring 40 x 40 x 160 mm$^3$, which were used for

75  the three-point bending test and subsequently the compressive test, were prepared in accordance with

76  [16]. Each batch consisted of three specimens with mixture proportions of 1.0 : 0.5 : 3.0 (cement : water :

77  fine aggregates).

78  The specimen preparation had the following steps: cement and sand were dry-mixed in a Hobart-type

79  paddle mixer; the mixture was hydrated by adding all water under mechanical stirring at slow speed

80  (corresponding to 140 rotations / min); fibres were added to the wet mixture followed by stirring at high

81  speed (corresponding to 285 rotations / min); the mixture was left to rest for 90 s, followed by stirring at

82  high speed for 60 s; prismatic samples were cast in steel moulds, vibrated in the moulds, covered and with

83  plastic sheet, which were demoulded after 24 hours and wet-cured for 27 days under laboratory

84  conditions until the day of testing. The principles for the casting and testing procedure are shown in Fig.

85  2.

86
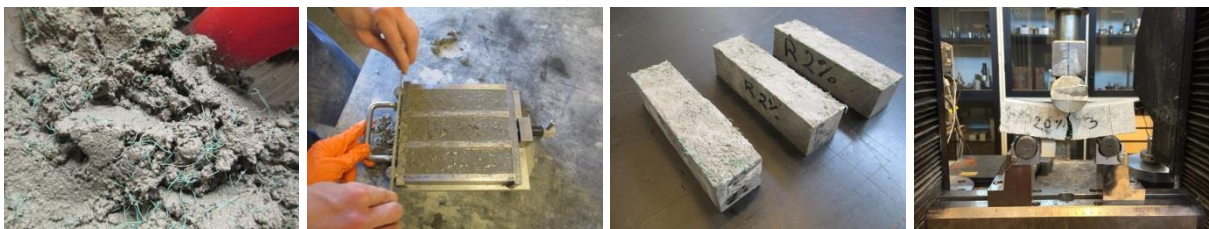


88  *Fig. 2. Mixing, casting, cured mortar prisms and three-point bending testing of mortar prisms*

89

90  One unreinforced control batch and eleven fibre reinforced batches of varying fibre content and type were

91  prepared. Eight specimens with R-PE fibre contents ranging from 0.17-1.33wt% were prepared and

92  tested. The specimens containing PP micro and macro fibres were prepared with fibre contents of 0.5wt%

93  and 0.5-1.0wt%, respectively. An R-PE fibre content of 1.33 wt% was the largest amount of fibres

94  possible to mix into the selected mortar matrix.

95

**2.3    Mechanical testing of mortar prisms**

97    Three-point bending tests of the prismatic specimens were performed in accordance with DS/EN 196-1-1

98    [16]. The clear span was 100 mm and the test setup is shown in Fig. 3. The test was performed in a

99    hydraulic displacement controlled testing machine, Instron 6022. A load was applied in a rate of 1

100    mm/min. The theoretical working curve for the three-point bending test is shown in Fig. 4.

101



102
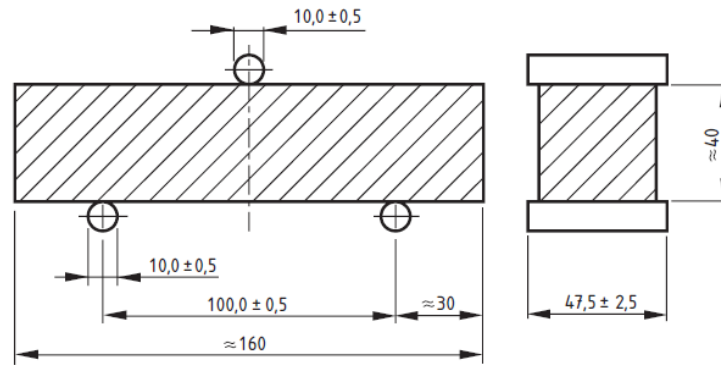
103    *Fig. 3. Three-point bending setup* [16]

104



105
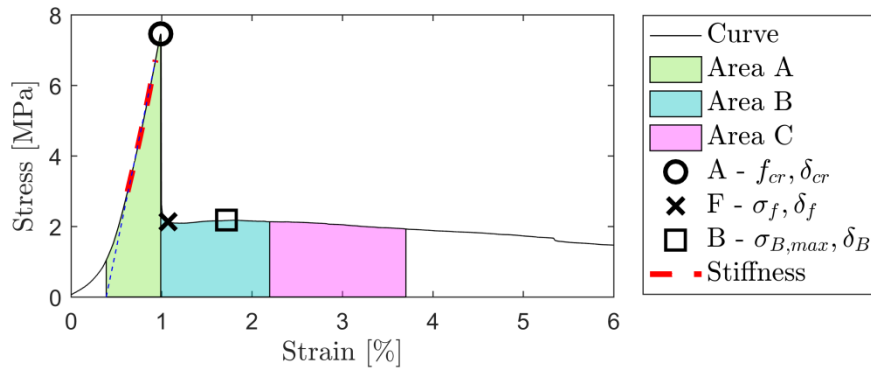
106    *Fig. 4. Theoretical working curve for three-point bending test*

107

108    The point where the first crack appears is denoted as point A, (the critical load $P_{cr}$, midspan deflection

109    $\delta_{cr}$). The flexural strength $f_{cr}$ of the uncracked material is calculated as follows [16]

$$f_{cr} = \frac{3\,P_{cr}\,L}{2\,a^3}$$ 
(Eq. 1)

110    Where $L = 100$ mm is the length of the clear span, and $a = 40$ mm is the side of the square section of the

111    prism. The strain is calculated from the midspan deflection by:

$$\varepsilon = \frac{6\,a\,\delta}{L^2} \times 100\%$$ 
(Eq. 2)

112  Where $\delta$ is the mid-span deflection. The stiffness of the uncracked material $E$ is calculated as the slope of

113  the linear part on the stress strain curve from $0.4\,f_{cr}$ to $0.9\,f_{cr}$ (marked with the red dotted line in Fig. 4).

114

115  Unreinforced mortar has a brittle failure when the first crack appears (Point A), whereas fibre reinforced

116  specimens have more ductile failure mode, thus a post-crack behaviour and the ability to absorb energy

117  when continuing the deflection [17]. The fibre efficiency factor (FEF) is the ratio between the maximum

118  stress of the uncracked matrix (point A) and the stress at which the fibres start working (point F). The

119  flexural toughness $T_{\delta cr}$, $T_{3\delta cr}$ and $T_{5.5\delta cr}$ are calculated as the area under the load-deflection curve, shown

120  as Area A, B, C, respectively. The procedures for calculating the toughness parameters, $T$, and toughness

121  indices, $I$, as described in the standard ASTM C1579 [18] have been followed.

$$Area_A = T_{\delta cr} = \int_0^{\delta_{cr}} P \; d\delta \qquad\qquad \text{(Eq. 3)}$$

$$Area_{A+B} = T_{3\delta cr} = \int_0^{3\cdot\delta_{cr}} P \; d\delta \qquad\qquad \text{(Eq. 4)}$$

$$Area_{A+B+C} = T_{5.5\delta cr} = \int_0^{5.5\cdot\delta_{cr}} P \; d\delta \qquad\qquad \text{(Eq. 5)}$$

122  $P$ is the load and $\delta$ the midspan displacement. The toughness index, $I$, is a measure of the improvement in

123  flexural toughness of the material from 0 till point B or C compared to the flexural toughness obtained the

124  first crack appears (point A). It is calculated as the ratio between $T_{\delta cr}$ and $T_{3\delta cr}$ or $T_{5.5\delta cr}$.

$$I_{A+B} = I_5 = \frac{T_{3\delta cr}}{T_{\delta cr}} \qquad\qquad \text{(Eq. 6)}$$

$$I_{A+B+C} = I_{10} = \frac{T_{5.5\delta cr}}{T_{\delta cr}} \qquad\qquad \text{(Eq. 7)}$$

125

126  The fibre influence on the flexural performance of the small-scale prisms is based on the above-

127  mentioned numbers for the mechanical performance of the fibre reinforced specimens.

128

129

## 3   RESULTS

### 3.1   Alkali-resistance of R-PE fibres

The alkali-resistance of new and recycled PE fibres from the type of fishing net "Braided polyethylene" was analysed by simulating the deterioration of the fibres in a highly alkaline environment such as cement-based materials. The SEM images in Fig. 5 illustrate examples of an unconditioned new fibre and a recycled fibre, and the same fibres immersed in the alkaline solution for 7 and 28 days, respectively. From the SEM images, it is observed that the recycled fibre was more influenced by the alkaline solution than the new fibres, since loose parts were sticking out from the fibre surface. However, no reduction in cross section area was seen during the 28 days of exposure.



*(a) New - Unconditioned*          *(b) New – 7 days in 1M NaOH*          *(c) New– 28 days in 1M NaOH*

*(d) Recycled - Unconditioned*          *(e) Recycled – 7 days in 1M NaOH*          *(f) Recycled – 28 days in 1M NaOH*
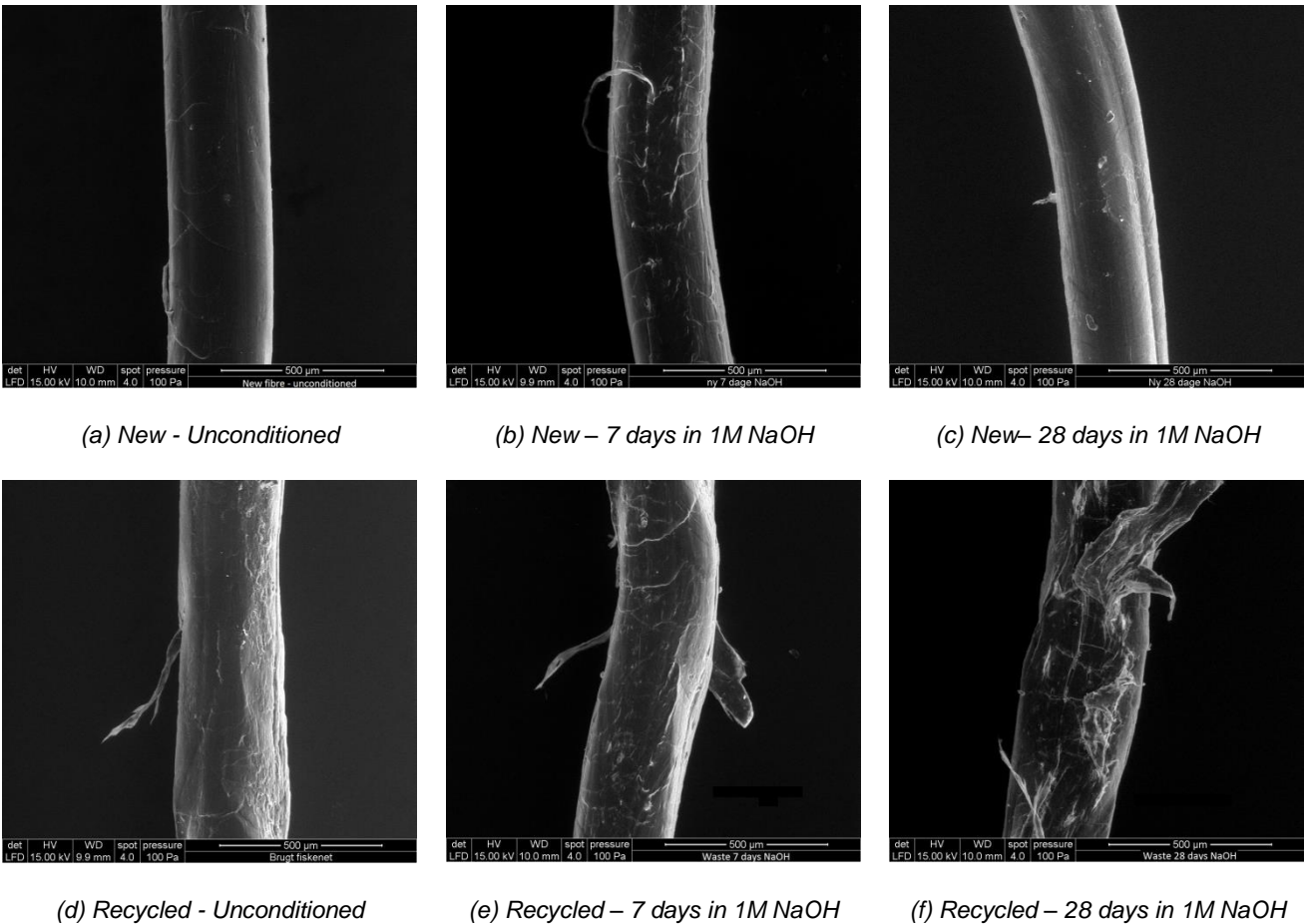
*Fig. 5. SEM images (300x) of new and recycled fibres from fishing nets of the type "Braided Polyethylene" immersed in a 1M NaOH solution for 28 days*

Regarding the tensile behaviour, fibres extracted from the fishing net "Braided polyethylene" were analysed. Examples of the stress-strain behaviour of N-PE and R-PE fibres are illustrated in Fig. 6. The

145   tensile test was again performed on unconditioned new (N) and recycled (R) fibres and alkali-conditioned

146   fibres of both types after 28 days immersion. Generally, it was found that fibres from the new nets had a

147   higher tensile strength and stiffness than fibres from corresponding recycled fishing nets. It was also

148   observed that the alkali-conditioning was not influencing the mechanical performance of the fibres to a

149   level that could be detected based on the performed tests. The maximum tensile strength was calculated as

150   the mean value for all tested gauge lengths (20, 25 and 30 mm). New unconditioned/alkali-conditioned

151   fibres achieved a tensile strength of 477/477 MPa, while the recycled fibres (unconditioned/alkali-

152   conditioned) had a tensile strength of 379/373 MPa. Thus no reduction in the tensile strength was

153   observed for the alkali-cured fibres. Good alkali-resistance of PE fibres was also reported by  previous

154   studies [17,19].

155



156
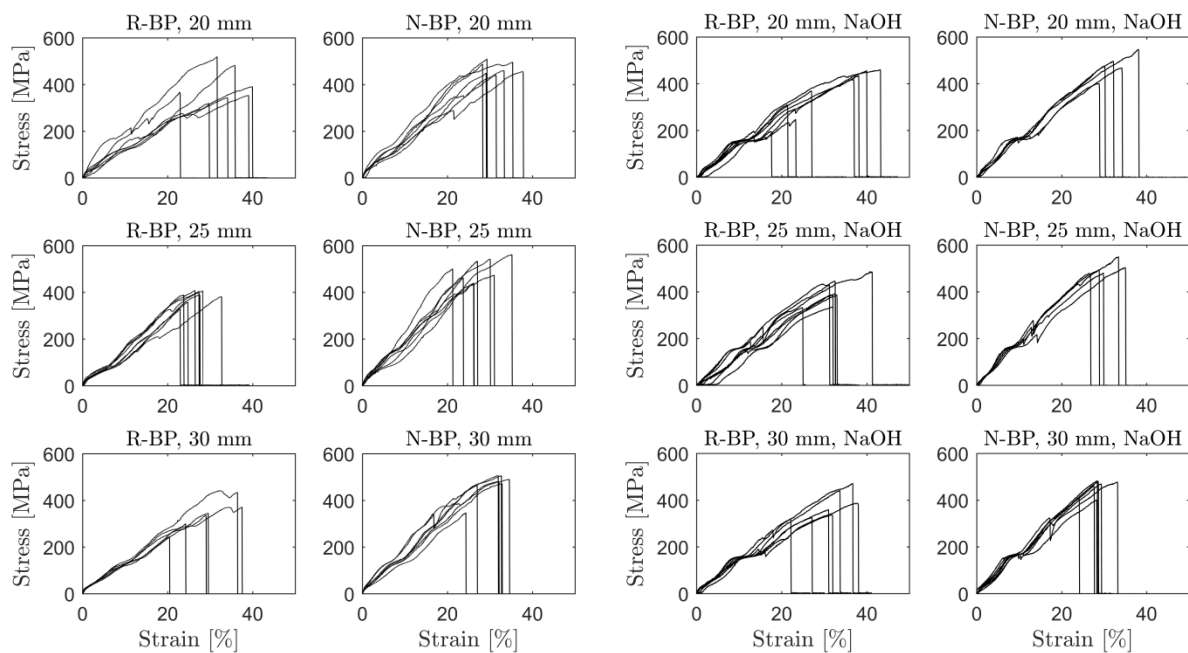
157   *Fig. 6. Tensile stress-strain behaviour of unconditioned and alkali-cured PE fibres from recycled (R) and*

158   *new (N) fishing nets of the type "Braided Polyethylene" (BP) from Euronete. Gauge lengths of 20-30 mm.*

159

160   **3.2   Three-point bending test of mortar prisms**

161   The results from the three-point bending test of mortar prisms after 28 days of curing are shown in Fig. 7.

162   The figure shows a control specimen, eight specimens with the addition of R-PE fibres varying from 0.17

163   wt% to 1.33 wt%, one specimen with 0.5wt% of PP micro fibres and two specimens with 0.5wt% and

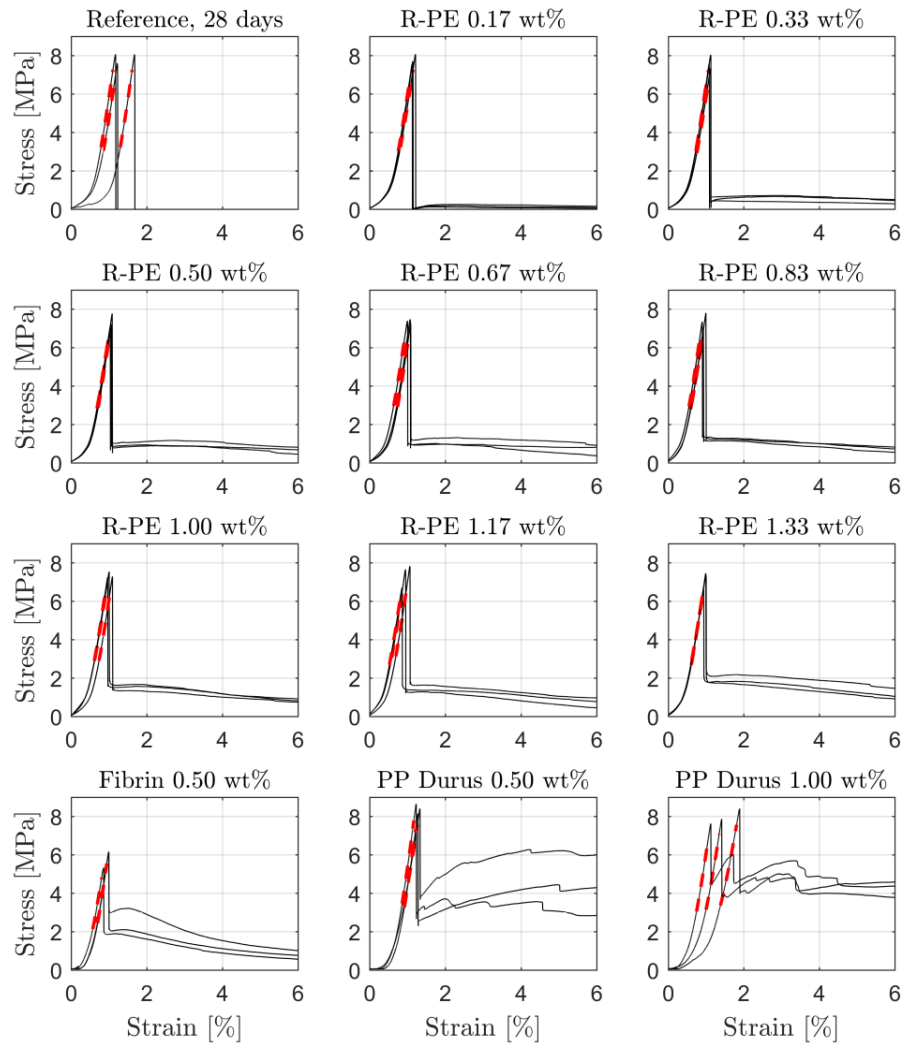164   1.0wt% of PP macro fibres.

165

*Fig. 7. Stress-strain behaviour of mortar prisms with addition of fibres*

Although the R-PE fibre samples contained fibres of different lengths, the shape of the stress-strain curves for equal fibre contents is very coinciding. The improvements in post-crack performance are shown as "the tail" on the stress-strain curve. Generally, it is observed that the post-crack performance of the specimens with R-PE fibres is rather poor, especially compared to the PP macro fibres, where good performance is found both with respect to the flexural strength and the post-crack performance. The addition of PP micro fibres also showed reasonable post-crack performance, while the flexural strength was negatively influenced by the addition of fibres. The large drop in stress observed for the specimens with R-PE fibres is considered to be a result of the low fibre stiffness and poor bonding between fibres and mortar.

178    The influence of the R-PE fibres on the mechanical properties of the prisms is shown in Fig. 8. The figure

179    illustrates the flexural strength of the uncracked and crack material, the stiffness of the uncracked

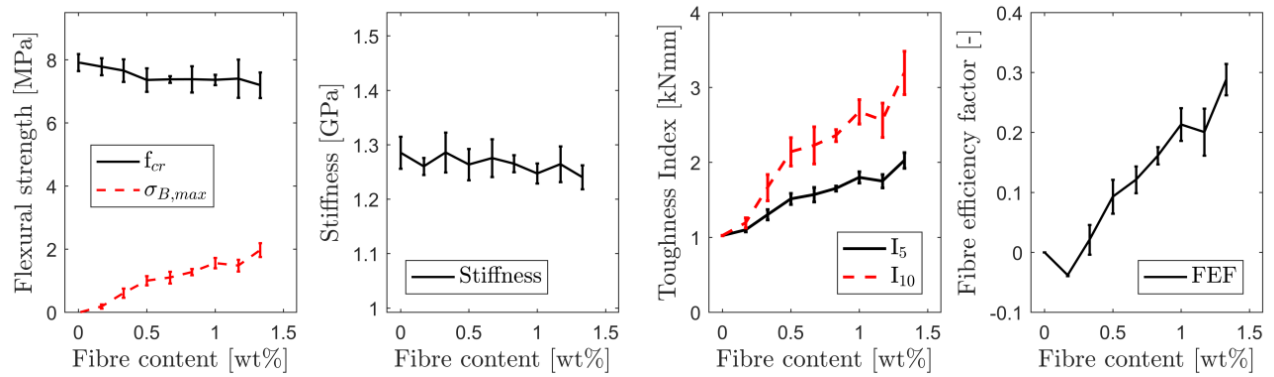180    material, the toughness indices and the fibre efficiency factor (FEF).

181



182

183    *Fig. 8. Influence of R-PE fibres on the mechanical properties of mortar prisms*

184

185    A small decrease in flexural strength and stiffness of the uncracked material is observed with the increase

186    in fibre content, while improvements are obtained by the increase in maximum post-crack strength,

187    toughness indices and FEF. Despite of these enhancements, the effect of the R-PE fibres is not considered

188    sufficient, since the maximum post-crack strength is only 27% of the first-crack strength at the maximum

189    fibre content of 1.33 wt%. Considering the toughness indices, these were found to be in the same range as

190    other studies on the use of waste plastic fibres in cement-based materials, e.g. [20].

191    Since the post-crack performance is improved with increasing fibre contents, it is assumed that the post-

192    crack performance could be improved by adding more fibres to the matrix. However, this would require a

193    change in the mix design and process, such as an increase in w/c ratio, since 1.35 wt% of fibres was the

194    maximum amount of fibres possible to mix properly into the mortar matrix for the given mix design. A

195    higher w/c-ratio would most likely result in a decrease in first-crack strength.

196

## 197   **4  Discussion**

198    The benefits of using waste fibres mechanically cut from discarded fish nets and trawls includes the low

199    amount of energy required for processing the fibres. Many types of fish nets and trawls, especially those

200    made of polyethylene, consist of either braided or twisted monofilament fibres, which are relatively easy

201    to separate and process to fibres applicable for fibre reinforcement of construction materials.

202

203 The R-PE fibres used in the present study had a straight shape, a smooth surface and a relatively low
204 stiffness ranging from 1.0-2.0 GPa. Other studies investigating the influence of fibre from different types
205 of waste plastics on the mechanical performance of cement-based materials, observed that other shapes
206 and materials of waste fibres resulted in properties superior to the ones found in this study. The different
207 fibre shapes and materials included fibres cut from waste polyethylene terephthalate (PET) bottles with
208 circular "O"-shapes or other deformed shaped [5,6,8,20,21], fibres from nylon carpets [22], and fibres of
209 waste fishing nets of nylon [4,7]. Some studies investigated the influence of fibres reprocessed from
210 different sources of waste plastics, for which it is possible to extrude fibres with exact geometries
211 [23,24]. However, this process would by more energy requiring.

212 Another application for the R-PE fibres could be as a preventative measure of plastic shrinkage cracking,
213 where a high elastic modulus is not a requirement and the tensile forces in the cement matrix are smaller.
214 Tests on this topic were carried out in a previous study by the authors [13].

215

216 **5  Conclusion**

217 The potential of using recycled polyethylene (R-PE) fibres mechanically cut from waste fishing nets was
218 presented in this study. Three-point bending tests were performed on mortar prisms in order to determine
219 the working curve and mechanical properties of fibre reinforced specimens as well as unreinforced
220 control specimens. Fibre contents from 0.17 to 1.33 wt% were examined. The results were compared to
221 specimens with the addition of commercially available PP fibres.

222 The following tendencies were observed:

223 ▪ The flexural strength and stiffness of the uncracked material was slightly decreasing with increasing
224   fibre content.

225 ▪ The post-crack toughness was increasing with increasing fibre content, which resulted in a less brittle
226   failure compared to the unreinforced specimens. However, the post-crack strength was very low
227   compared to the first-crack strength.

228 Tensile tests were carried out on fibres of a known type of fishing net in order to compare the degree of
229 deterioration of the fibres after being used for fishing operations. The alkali-resistance of the fibres were
230 also analysed based on SEM images and tensile tests.

231   ▪ A decrease in tensile strength was found between the new fibres and recycled fibres.

232   ▪ The fibres were seen to have good alkali-resistance and no decrease in tensile strength was
233     observed after immersing the fibres in a highly alkaline solution.

234

239    **7  References**

240    [1]    G. Macfadyen, T. Huntington, R. Cappell, Abandoned , lost or otherwise discarded fishing gear,

241           United Nations Environment Programme (UNEP);Food and Agriculture Organization of the

242           United Nations (FAO), Rome, 2009.

243    [2]    L. Gu, T. Ozbakkaloglu, Use of recycled plastics in concrete: A critical review, Waste Manag. 51

244           (2016) 19–42. doi:10.1016/j.wasman.2016.03.005.

245    [3]    R. Sharma, P.P. Bansal, Use of different forms of waste plastic in concrete - A review, J. Clean.

246           Prod. 112(1) (2016) 473–482. doi:10.1016/j.jclepro.2015.08.042.

247    [4]    S. Spadea, I. Farina, A. Carrafiello, F. Fraternali, Recycled nylon fibers as cement mortar

248           reinforcement, Constr. Build. Mater. 80 (2015) 200–209. doi:10.1016/j.conbuildmat.2015.01.075.

249    [5]    D. Foti, Use of recycled waste pet bottles fibers for the reinforcement of concrete, Compos. Struct.

250           96 (2013) 396–404. doi:10.1016/j.compstruct.2012.09.019.

251    [6]    L.A. Pereira De Oliveira, J.P. Castro-Gomes, Physical and mechanical behaviour of recycled PET

252           fibre    reinforced    mortar,    Constr.    Build.    Mater.    25    (2011)    1712–1717.

253           doi:10.1016/j.conbuildmat.2010.11.044.

254    [7]    S. Orasutthikul, D. Unno, H. Yokota, Effectiveness of recycled nylon fiber from waste fishing net

255           with respect to fiber reinforced mortar, Constr. Build. Mater. 146 (2017) 594–602.

256           doi:10.1016/j.conbuildmat.2017.04.134.

257    [8]    R.P. Borg, O. Baldacchino, L. Ferrara, Early age performance and mechanical characteristics of

258           recycled PET fibre reinforced concrete, Constr. Build. Mater. 108 (2016) 29–47.

259           doi:10.1016/j.conbuildmat.2016.01.029.

260    [9]    N. Pešić, S. Živanović, R. Garcia, P. Papastergiou, Mechanical properties of concrete reinforced

261           with recycled HDPE plastic fibres, Constr. Build. Mater. 115 (2016) 362–370.

262           doi:10.1016/j.conbuildmat.2016.04.050.

263    [10]   J.H.J. Kim, C.G. Park, S.W. Lee, S.W. Lee, J.P. Won, Effects of the geometry of recycled PET

264           fiber reinforcement on shrinkage cracking of cement-based composites, Compos. Part B Eng. 39.3

265           (2008) 442–450. doi:10.1016/j.compositesb.2007.05.001.

266    [11]   M. Serdar, A. Baričević, M. Jelčić Rukavina, M. Pezer, D. Bjegović, N. Štirmer, Shrinkage

267           Behaviour of Fibre Reinforced Concrete with Recycled Tyre Polymer Fibres, Int. J. Polym. Sci.

268    2015.3 (2015) 1–9. doi:10.1155/2015/145918.

269    [12]    B.S. Al-Tulaian, M.J. Al-Shannag, A.R. Al-Hozaimy, Recycled plastic waste fibers for reinforcing

270            Portland    cement    mortar,    Constr.    Build.    Mater.    127    (2016)    102–110.

271            doi:10.1016/j.conbuildmat.2016.09.131.

272    [13]    I.M.G. Bertelsen, L.M. Ottosen, G. Fischer, Quantitative analysis of the influence of synthetic

273            fibres on plastic shrinkage cracking using digital image correlation, Constr. Build. Mater. 199

274            (2019) 124–137. doi:10.1001/archinte.168.13.1371.

275    [14]    I.M.G. Bertelsen, L.M. Ottosen, Recycling of waste PE fishing nets as fibre reinforcement in

276            gypsum-based composites, Submitted. (n.d.).

277    [15]    ASTM C1557-14, C1557-14 Standard Test Method for Tensile Strength and Young ' s Modulus

278            of Fibers, (2014) 1–10. doi:http://doi.org/10.1520/C1557-14.

279    [16]    UNI/EN-196-1, Methods of testing cement – Part 1 : Determination of strength, (2005).

280    [17]    S. Yin, R. Tuladhar, F. Shi, M. Combe, T. Collister, N. Sivakugan, Use of macro plastic fibres in

281            concrete:    A    review,    Constr.    Build.    Mater.    93    (2015)    180–188.

282            doi:10.1016/j.conbuildmat.2015.05.105.

283    [18]    ASTM C1018-02, Standard Test Method for Flexural Toughness and First-Crack Strength of

284            Fiber-Reinforced Concrete ( Using Beam With, 04 (1998) 1–8. doi:10.1520/D3762-98.

285    [19]    Z. Zheng, D. Feldman, Synthetic fibre-reinforced concrete, Prog. Polym. Sci. 20 (1995) 185–210.

286            doi:10.1016/0079-6700(94)00030-6.

287    [20]    F. Fraternali, I. Farina, C. Polzone, E. Pagliuca, L. Feo, On the use of R-PET strips for the

288            reinforcement    of    cement    mortars,    Compos.    Part    B    Eng.    46    (2013)    207–210.

289            doi:10.1016/j.compositesb.2012.09.070.

290    [21]    D. Foti, Preliminary analysis of concrete reinforced with waste bottles PET fibers, Constr. Build.

291            Mater. 25 (2011) 1906–1915. doi:10.1016/j.conbuildmat.2010.11.066.

292    [22]    Y. Wang, A.-H. Zureick, B.-S. Cho, D.E. Scott, Properties of fibre reinforced concrete using

293            recycled fibres from carpet industrial waste, J. Mater. Sci. 29 (1994) 4191–4199.

294    [23]    S. Yin, R. Tuladhar, M. Combe, T. Collister, M. Jacob, A.R. Shanks, Y.I.N. Shi, T. Rabin, C.

295            Mark, C. Tony, J. Mohan, S. a Robert, S. Yin, R. Tuladhar, M. Combe, T. Collister, M. Jacob,

296            A.R. Shanks, Mechanical Properties of Recycled Plastic Fibres for Reinforcing Concrete, Fibre

297            Concr. (2013) 1–10.

298    [24]    S.B. Kim, N.H. Yi, H.Y. Kim, J.H.J. Kim, Y.C. Song, Material and structural performance

299            evaluation of recycled PET fiber reinforced concrete, Cem. Concr. Compos. 32 (2010) 232–240.

300            doi:10.1016/j.cemconcomp.2009.11.002.

301

The aim of the research presented in this PhD thesis was to discover new applications for discarded fishing nets as fibre reinforcement in construction materials. The main application was to use fibres in cementitious materials to control the formation of plastic shrinkage cracking. A digital image correlation (DIC) technique was applied to study the crack formation. A new approach for numerical post-processing of the DIC data enabled detailed and quantitative measures of the degree of surface cracking.